frontiers | Research Topics

# Immunological aspects of emerging and re-emerging zoonoses

**Edited by**
Wei Wang, Jingxin Li, Yuejin Liang and Wenping Gong

**Published in**
Frontiers in Immunology

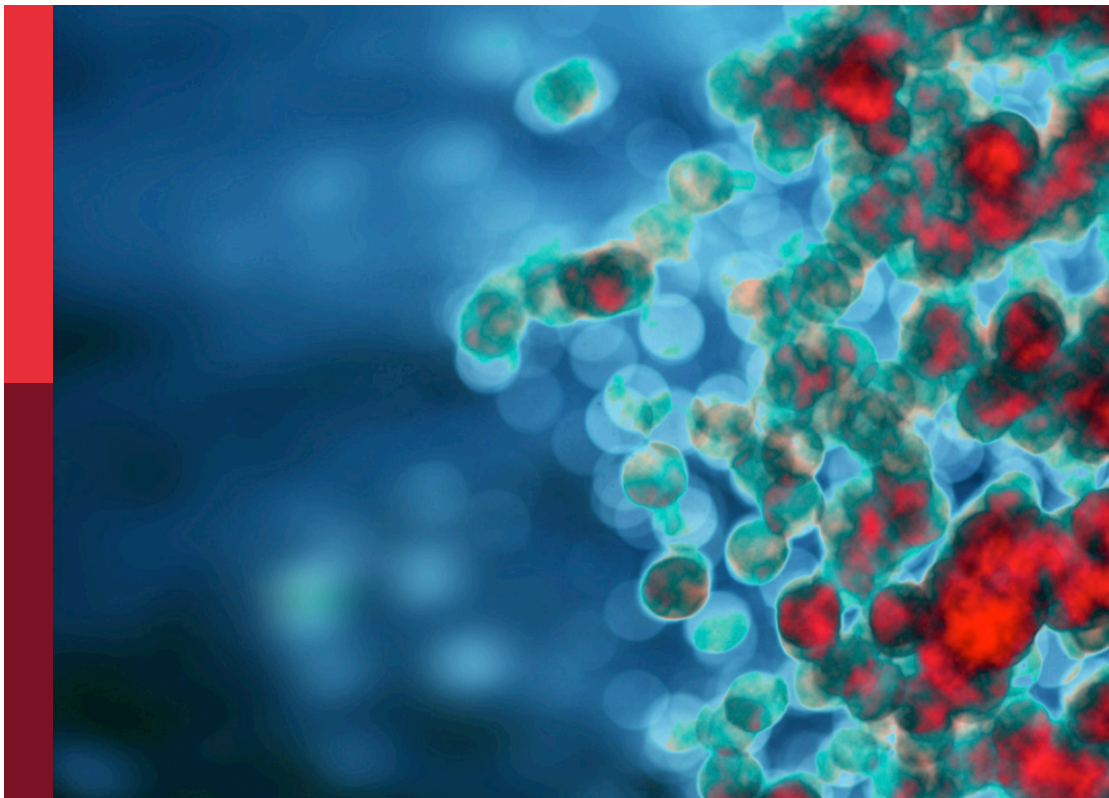

ISSN 1664-8714
ISBN 978-2-8325-4655-0
DOI 10.3389/978-2-8325-4655-0

## About Frontiers

Frontiers is more than just an open access publisher of scholarly articles: it is a pioneering approach to the world of academia, radically improving the way scholarly research is managed. The grand vision of Frontiers is a world where all people have an equal opportunity to seek, share and generate knowledge. Frontiers provides immediate and permanent online open access to all its publications, but this alone is not enough to realize our grand goals.

## Frontiers journal series

The Frontiers journal series is a multi-tier and interdisciplinary set of open-access, online journals, promising a paradigm shift from the current review, selection and dissemination processes in academic publishing. All Frontiers journals are driven by researchers for researchers; therefore, they constitute a service to the scholarly community. At the same time, the *Frontiers journal series* operates on a revolutionary invention, the tiered publishing system, initially addressing specific communities of scholars, and gradually climbing up to broader public understanding, thus serving the interests of the lay society, too.

## Dedication to quality

Each Frontiers article is a landmark of the highest quality, thanks to genuinely collaborative interactions between authors and review editors, who include some of the world's best academicians. Research must be certified by peers before entering a stream of knowledge that may eventually reach the public - and shape society; therefore, Frontiers only applies the most rigorous and unbiased reviews. Frontiers revolutionizes research publishing by freely delivering the most outstanding research, evaluated with no bias from both the academic and social point of view. By applying the most advanced information technologies, Frontiers is catapulting scholarly publishing into a new generation.

## What are Frontiers Research Topics?

Frontiers Research Topics are very popular trademarks of the *Frontiers journals series*: they are collections of at least ten articles, all centered on a particular subject. With their unique mix of varied contributions from Original Research to Review Articles, Frontiers Research Topics unify the most influential researchers, the latest key findings and historical advances in a hot research area.

Find out more on how to host your own Frontiers Research Topic or contribute to one as an author by contacting the Frontiers editorial office: frontiersin.org/about/contact

# Immunological aspects of emerging and re-emerging zoonoses

**Topic editors**

Wei Wang — Jiangsu Institute of Parasitic Diseases (JIPD), China
Jingxin Li — Jiangsu Provincial Center for Disease Control and Prevention, China
Yuejin Liang — University of Texas Medical Branch at Galveston, United States
Wenping Gong — Senior Department of Tuberculosis, The 8th Medical Center of PLA General Hospital, China

**Citation**

Wang, W., Li, J., Liang, Y., Gong, W., eds. (2024). *Immunological aspects of emerging and re-emerging zoonoses*. Lausanne: Frontiers Media SA. doi: 10.3389/978-2-8325-4655-0

# Table of contents

frontiers | Frontiers in Immunology

TYPE Editorial
PUBLISHED 06 March 2024
DOI 10.3389/fimmu.2024.1392382



OPEN ACCESS

EDITED AND REVIEWED BY
Pei-Hui Wang,
Shandong University, China

*CORRESPONDENCE
Wei Wang
wangweijipd@163.com
Wenping Gong
gwp891015@whu.edu.cn

RECEIVED 27 February 2024
ACCEPTED 29 February 2024
PUBLISHED 06 March 2024

CITATION
Wang W, Li J, Liang Y and Gong W (2024) Editorial: Immunological aspects of emerging and re-emerging zoonoses.
*Front. Immunol.* 15:1392382.
doi: 10.3389/fimmu.2024.1392382



# Editorial: Immunological aspects of emerging and re-emerging zoonoses

Wei Wang[1]*, Jingxin Li[2], Yuejin Liang[3] and Wenping Gong[4]*

[1]National Health Commission Key Laboratory on Parasitic Disease Prevention and Control, Jiangsu Provincial Key Laboratory on Parasites and Vector Control Technology, Jiangsu Institute of Parasitic Diseases, Wuxi, Jiangsu, China, [2]Jiangsu Provincial Medical Innovation Center, National Health Commission Key Laboratory of Enteric Pathogenic Microbiology, Jiangsu Provincial Center for Disease Control and Prevention, Nanjing, Jiangsu, China, [3]Department of Microbiology and Immunology, University of Texas Medical Branch, Galveston, TX, United States, [4]Senior Department of Tuberculosis, the Eighth Medical Center of Chinese People's Liberation Army (PLA) General Hospital, Beijing, China

KEYWORDS

**zoonoses, viral disease, immune response, immunodiagnostics, immunotherapeutics, COVID - 19**

Editorial on the Research Topic
Immunological aspects of emerging and re-emerging zoonoses

Zoonoses, a group of diseases that are transmitted between animals and humans, are considered as the most prevalent infections in humans (1). They present substantial global health threats and continue to pose significant challenges to both the scientific community and public health systems (2). Currently, approximately 60% of identified infectious diseases and 75% of emerging infectious diseases originate from zoonotic sources (3). Globally, zoonoses are estimated to be responsible for 2.5 billion cases of human illness and 2.7 million human deaths annually, with an additional 5 to 6 million individuals at risk of contracting zoonotic infections (4). Emerging and re-emerging zoonoses are therefore considered as major and global challenges for public health in terms of their profound health impacts and economic burdens (5). Recently, the One Health approach has been widely recommended to address the challenges of zoonoses (6, 7).

The current Research Topic consists of 9 publications including 6 original research articles and 3 review articles, covering immune responses, immunodiagnostics and immunotherapeutics of zoonoses, with the goal of improving the understanding of the immunological facets of emerging and re-emerging viral zoonoses in this changing world. This editorial aims to provide an overview of the contributing articles within this Research Topic and highlight their significance in advancing our understanding of zoonotic diseases.

Coronaviruses are a large family of RNA viruses that may infect both humans and animals (8). Coronavirus disease 2019 (COVID-19), caused by the coronavirus severe acute respiratory syndrome coronavirus 2 (SARS-CoV-2) (9), has been recognized as one of the deadliest infectious diseases in human history responsible for millions of human fatalities and trillions of economic losses (10, 11). A large number of studies have been therefore conducted with the aim to provide insights into the containment of the COVID-19 pandemic worldwide (12). In the current Research Topic, five articles focus on COVID-19. Jeon et al. found that increased interferon alpha 1 (IFNA1) and reduced interleukin (IL)-12p40 were closely linked to persistent hyperinflammation in COVID-19 pneumonia

patients. This suggests that the aberrant persistence of pulmonary and systemic inflammation might be associated with long COVID-19 sequelae. Serwanga et al. detected faster and stronger anti-SARS-CoV-2 spike-directed IgG, IgM, and IgA antibody responses in Ugandan asymptomatic COVID-19 patients compared to those with mild symptoms during acute infections. The Spike IgG antibody levels, peaking between 25 and 37 days and persisting for 28 months, exhibited significantly greater and more durable than nucleoprotein and receptor-binding domain (RBD) IgG antibody levels. In addition, they found a significantly positive correlation between Spike-and RBD-directed IgG antibody levels until 14 months of SARS-CoV-2 infections, indicating significant and persistent anti-spike immunity without RBD. Yang et al. reviewed the immune response features of immunodominant epitope-specific T cells targeting different SRAS-CoV-2 proteome structures following SRAS-CoV-2 infections and COVID-19 vaccination, analyzed the heterogenous phenotypic characteristics of SARS-CoV-2 specific T cells, and discussed the significant implications of cross-reactivity of human coronaviruses, SRAS-CoV-2 and variants of concern. Guan et al. generated two Chinese national standard candidates for anti-SARS-Cov-2 neutralizing antibody traced to the WHO International Standard according to the WHO manual for the establishment of national secondary standards. These candidates facilitate the development and potential application of COVID-19 vaccines in China. Abdelaziz and colleagues generated a multi-epitope vaccine (PanCoVac) that encoded the conserved T cell epitopes from all structural proteins of coronaviruses. This vaccine was *in vitro* processed and presented by HLA-A*0201, and immunization of NILV-PanCoVac (PanCoVac cloned into a non-integrating lentivirus vector at a single-low dose following infection with ancestral SARS-CoV-2) resulted in the absence of COVID-19-like symptoms and significantly reduced SARS-CoV-2 viral loads in lung specimens in Roborovski dwarf hamsters. This protective effect was observed at early stage (2 days post infection) after challenge and was not dependent on neutralizing antibodies, suggesting that PanCoVac may protect from severe disease caused by SARS-CoV-2 variants and future pathogenic coronaviruses. The great success of COVID-19 messenger RNA (mRNA) vaccines, as evidenced by the 2023 Nobel Prize in Physiology or Medicine (13), urges the research and development of novel RNA vaccines (14). Bai et al. summarized the discovery, synthesis, biological functions and metabolism of circular RNA (cirRNA), outlined the progress of cirRNA vaccine research, and provided an overview of production process and quality control of cirRNA vaccines.

Swine acute diarrhea syndrome coronavirus (SADS-CoV), belonging to the alpha coronavirus family, is a newly discovered, highly pathogenic coronavirus associated with acute diarrhea and mass piglet deaths (15). Huang et al. found that the nonstructural protein 5 of SADS-CoV remarkably suppressed Sendai virus (SEV)-induced production of IFN-β and inflammatory cytokines TNF-α, CXCL10, RIG-I, ISG15, RSAD2, ISG56, and IFIT3. In addition, SADS-CoV nsp5 was found to target and cleave mRNA-decapping enzyme 1a (DCP1A) via its protease activity to inhibit the IRF3 and NF-κB signaling pathways in order to decrease IFN-β and inflammatory cytokine production. Moreover, a form of DCP1A with a mutation in the glutamine 343 residue showed resistance to nsp5-mediated cleavage and exhibited enhanced capability in suppressing SADS-CoV infection compared to wild-type DCP1A, indicating the significance of SADS-CoV nsp5 as an interferon antagonist.

Mpox (formerly known as monkeypox) is a zoonotic viral disease caused by the mpox virus, primarily found in central and western Africa (16). Nevertheless, a sudden outbreak of mpox occurred, rapidly spreading across Europe, the Americas, and subsequently affecting all six WHO regions since May 2022 (17). To coordinate global efforts to address this challenge, WHO declared the mpox outbreak a public health emergency of international concern on July 23, 2022 in the context of the COVID-19 pandemic (18). In this Research Topic, Niu et al. summarized the origins and transmission routes of mpox virus, as well as insights into the epidemiology, pathophysiology, clinical manifestations, diagnosis, treatment and vaccines of mpox. This synthesis offers a detailed understanding of this disease.

Tick-borne encephalitis virus (TBEV) is a neurotropic flavivirus causing tick-borne encephalitis, which is associated with severe neurological disease, long-term neurological sequelae or death (19). Langat virus (LGTV), a naturally attenuated member of the TBEV complex, has been found to be lowly virulent in humans and shares a more than 80% amino acid homology with TBEV (20). Therefore, LGTV has been attempted as a live attenuated vaccine for prevention of TBEV infection (21, 22). In this Research Topic, Kubinski et al., found that LGTV infection induced both cross-reactive antibodies and T cells against TBEV in C57BL/6JOlaHsd (BL6) mice, and sera from LGTV-infected mice efficiently protected from developing severe tick-borne encephalitis, while adoptive transfer of T cells from LGTV-infected mice failed to provide this protection; additionally, histopathology of infected mouse brain specimens revealed a possible role of microglia and T cells in inflammatory processes within the brain.

While significant progress has been made in understanding immunological aspects of emerging and re-emerging zoonoses, several challenges and future directions remain. Firstly, in the context of viral zoonoses, including emerging variants, further investigations are needed to elucidate the complex interplay between viral pathogens and the immune system. Understanding the mechanisms of immune evasion employed by these viruses may inform the development of targeted countermeasures. Secondly, the global deployment of effective vaccines remains a priority. Research efforts are recommended to continue to focus on the development of safe and efficacious vaccines against zoonotic diseases, with an emphasis on rapid vaccine development platforms that respond promptly to emerging threats. Lastly, ongoing surveillance, comprehensive public health interventions, and international collaborations are essential for early detection, containment, and prevention of future zoonotic disease outbreaks.

In summary, this Research Topic offers a significant contribution to our understanding of the immunological aspects of emerging and re-emerging zoonoses. By elucidating the intricate mechanisms underlying host-pathogen interactions, immune responses, and immunopathology, these studies may provide insights into the development of effective preventive and control

interventions against emerging and re-emerging zoonoses. These publications have received 26,022 views and 7,034 downloads. We expect that the topic will help accelerate efforts toward the containment of emerging and re-emerging zoonoses.

## Author contributions

WW: Conceptualization, Funding acquisition, Resources, Writing – original draft. JL: Funding acquisition, Writing – review & editing. YL: Writing – review & editing. WG: Writing – review & editing.

## Funding

The author(s) declare that financial support was received for the research, authorship, and/or publication of this article. This study was supported by grants from National Natural Science Foundation of China (grant nos. 82341031, 82173584, and 82222062), National Natural Science Foundation of China and the Bill & Melinda Gates Foundation joint program (grant no. 7231101367/2023YFVA1002). Jiangsu Provincial Science Fund for Distinguished Young Scholars (grant no. BK20220064), Jiangsu Provincial Key Project of Science and Technology Plan (grant nos. BE2021738 and BE2023601), Wuxi Municipal Health Commission (grant no. Z202116) and Wuxi Municipal Department of Science and Technology (grant no. Y20212012).

## Acknowledgments

We would like to express our sincerest thanks to all authors that contributed to this Research Topic and the editorial office for their support during the publication of the Research Topic.

## Conflict of interest

The authors declare that the research was conducted in the absence of any commercial or financial relationships that could be construed as a potential conflict of interest.

## Publisher's note



## References

1. Rahman MT, Sobur MA, Islam MS, Ievy S, Hossain MJ, El Zowalaty ME, et al. Zoonotic diseases: Etiology, impact, and control. *Microorganisms*. (2020) 8:1405. doi: 10.3390/microorganisms8091405

2. Cao J, Jiang LB, Miller LH. *Decoding Infection and Transmissio*n: Deciphering the mystery of infectious diseases from data-based research. *Decod Infect Transm*. (2023) 1:100001. doi: 10.1016/j.dcit.2023.03.001

3. Recht J, Schuenemann VJ, Sánchez-Villagra MR. Host diversity and origin of zoonoses: The ancient and the new. *Anim (Basel)*. (2020) 10:1672. doi: 10.3390/ani10091672

4. Di Bari C, Venkateswaran N, Fastl C, Gabriël S, Grace D, Havelaar AH, et al. The global burden of neglected zoonotic diseases: Current state of evidence. *One Health*. (2023) 17:100595. doi: 10.1016/j.onehlt.2023.100595

5. Dong XP, Soong L. Emerging and re-emerging zoonoses are major and global challenges for public health. *Zoonoses*. (2021) 1:1. doi: 10.15212/ZOONOSES-2021-0001

6. He J, Guo Z, Yang P, Cao C, Xu J, Zhou X, et al. Social insights on the implementation of One Health in zoonosis prevention and control: a scoping review. *Infect Dis Poverty*. (2022) 11:48. doi: 10.1186/s40249-022-00976-y

7. Quaresma PF, Martins-Duarte ES, Soares Medeiros LC. Editorial: One Health approach in zoonosis: strategies to control, diagnose and treat neglected diseases. *Front Cell Infect Microbiol*. (2023) 13:1227865. doi: 10.3389/fcimb.2023.1227865

8. Cui J, Li F, Shi ZL. Origin and evolution of pathogenic coronaviruses. *Nat Rev Microbiol*. (2019) 17:181–92. doi: 10.1038/s41579-018-0118-9

9. Hu B, Guo H, Zhou P, Shi ZL. Characteristics of SARS-Cov-2 and COVID-19. *Nat Rev Microbiol*. (2021) 19:141–54. doi: 10.1038/s41579-020-00459-7

10. Fink G, Tediosi F, Felder S. Burden of Covid-19 restrictions: National, regional and global estimates. *EClinicalMedicine*. (2022) 45:101305. doi: 10.1016/j.eclinm.2022.101305

11. Richards F, Kodjamanova P, Chen X, Li N, Atanasov P, Bennetts L, et al. Economic burden of COVID-19: A systematic review. *Clinicoecon Outcomes Res*. (2022) 14:293–307. doi: 10.2147/CEOR.S338225

12. Sousa Neto AR, Carvalho ARB, Ferreira da Silva MD, Rêgo Neta MM, Sena IVO, Almeida RN, et al. Bibliometric analysis of global scientific production on COVID-19 and vaccines. *Int J Environ Res Public Health*. (2023) 20:4796. doi: 10.3390/ijerph20064796

13. Buggert M, Höglund P. The prize of prizes: mRNA research paving the way for COVID-19 vaccine success wins the Nobel Prize in Physiology or Medicine 2023. *Scand J Immunol*. (2023) 98:e13340. doi: 10.1111/sji.13340

14. Zhou W, Jiang L, Liao S, Wu F, Yang G, Hou L, et al. Vaccines' new era-RNA vaccine. *Viruses*. (2023) 15:1760. doi: 10.3390/v15081760

15. Gong L, Li J, Zhou Q, Xu Z, Chen L, Zhang Y, et al. A new bat-HKU2-like coronavirus in swine, Chin. *Emerg Infect Dis*. (2017) 23:1607–9. doi: 10.3201/eid2309.170915

16. Huang Y, Mu L, Wang W. Monkeypox: epidemiology, pathogenesis, treatment and prevention. *Signal Transduction Targeting Ther*. (2022) 7:373. doi: 10.1038/s41392-022-01215-4

17. Liu XN, Jiang X, Zhu Z, Sun LQ, Lu HZ. The novel monkeypox outbreak: What should we know and reflect on? *Zoonoses*. (2022) 2:20. doi: 10.15212/ZOONOSES-2022-0022

18. Taylor L. Monkeypox: WHO declares a public health emergency of international concern. *BMJ*. (2022) 378:o1874. doi: 10.1136/bmj.o1874

19. Phipps LP, Johnson N. Tick-borne encephalitis virus. *J Med Microbiol*. (2022) 71:1492. doi: 10.1099/jmm.0.001492

20. Gritsun TS, Nuttall PA, Gould EA. Tick-borne flaviviruses. *Adv Virus Res*. (2003) 61:317–71. doi: 10.1016/s0065-3527(03)61008-0

21. Rumyantsev AA, Goncalvez AP, Giel-Moloney M, Catalan J, Liu Y, Gao QS, et al. Single-dose vaccine against tick-borne encephalitis. *Proc Natl Acad Sci U S A*. (2013) 110:13103–8. doi: 10.1073/pnas.1306245110

22. Tsetsarkin KA, Maximova OA, Liu G, Kenney H, Teterina NL, Pletnev AG. Stable and highly immunogenic microRNA-targeted single-dose live attenuated vaccine candidate against tick-borne encephalitis constructed using genetic backbone of Langat virus. *mBio*. (2019) 10:e02904–18. doi: 10.1128/mBio.02904-18

frontiers | Frontiers in Immunology

TYPE Review
PUBLISHED 12 January 2023
DOI 10.3389/fimmu.2022.1091797



OPEN ACCESS

EDITED BY
Jingxin Li,
Jiangsu Provincial Center for Disease Control and Prevention, China

REVIEWED BY
Ardeshir Abbasi,
Tarbiat Modares University, Iran
Patompon Wongtrakoongate,
Mahidol University, Thailand
Zhigang Li,
Juntuo Biosciences Co., Ltd., China

*CORRESPONDENCE
Zhenglun Liang
lzhenglun@126.com
Qunying Mao
maoqunying@126.com

†These authors have contributed equally to this work and share first authorship

SPECIALTY SECTION
This article was submitted to Viral Immunology, a section of the journal Frontiers in Immunology

RECEIVED 07 November 2022
ACCEPTED 27 December 2022
PUBLISHED 12 January 2023

CITATION
Bai Y, Liu D, He Q, Liu J, Mao Q and Liang Z (2023) Research progress on circular RNA vaccines. *Front. Immunol.* 13:1091797. doi: 10.3389/fimmu.2022.1091797



# Research progress on circular RNA vaccines

Yu Bai[1,2,3†], Dong Liu[1,2,3†], Qian He[1,2,3], Jianyang Liu[1,2,3], Qunying Mao[1,2,3*] and Zhenglun Liang[1,2,3*]

[1]Division of Hepatitis and Enterovirus Vaccines, National Institutes for Food and Drug Control, Beijing, China, [2]NHC Key Laboratory of Research on Quality and Standardization of Biotech Products, National Institutes for Food and Drug Control, Beijing, China, [3]NMPA Key Laboratory for Quality Research and Evaluation of Biological Products, Institute of Biological Products, National Institutes for Food and Drug Control, Beijing, China

Owing to the success of linear mRNA coronavirus disease 2019 (COVID-19) vaccines, biopharmaceutical companies and research teams worldwide have attempted to develop more stable circular RNA (circRNA) vaccines and have achieved some preliminary results. This review aims to summarize key findings and important progress made in circRNA research, the *in vivo* metabolism and biological functions of circRNAs, and research progress and production process of circRNA vaccines. Further, considerations regarding the quality control of circRNA vaccines are highlighted herein, and the main challenges and problem-solving strategies in circRNA vaccine development and quality control are outlined to provide a reference for circRNA vaccine-related research.

KEYWORDS

**circular RNA vaccines, research progress, production process, quality control, outlook**

## 1 Introduction

Coronavirus disease 2019 (COVID-19) vaccines are currently the first vaccines to be rapidly and successfully developed and applied through multiple technological routes following the publication of a pathogenic sequence (1–4). These vaccines include inactivated vaccines, recombinant protein vaccines, adenovirus vector vaccine and mRNA-based vaccines, with the COVID-19 mRNA-based vaccines being the first-ever approved mRNA vaccines (5, 6). Currently, approximately 40 mRNA vaccines are undergoing clinical trials and 2 are commercially available. More than 4 billion doses of mRNA vaccines have been administered globally, accounting for approximately one-third of the total number of immunizations (7–9). mRNA vaccines not only induce high levels of humoral immunity, but also elicit relatively strong cellular immune responses (10–13). Owing to the rapidness and editability of the mRNA vaccine technology, it is suitable for use as a vaccine platform to tackle emerging infectious diseases (14, 15).

All of the aforementioned COVID-19 mRNA vaccines possess a linear structure. At present, modified linear mRNA molecules still have poor stability, which limits the amount of protein that can be expressed (16–19). Besides linear RNAs, circular RNAs (circRNAs) exist in nature. Such RNAs have a single-chain closed-loop circular structure formed by covalent bonds that results in greater stability *in vivo* compared with linear RNAs (20). circRNAs are also capable of protein encoding and translation, which confers potential for vaccine development (21). The successful development and application of COVID-19 mRNA vaccines have prompted researchers to explore the use of circRNAs for the development of higher-stability nucleic acid-based COVID-19 vaccines. Recently, several research teams successfully developed COVID-19 circRNA vaccines, which not only possess the advantages of linear mRNA vaccines, but also boast a greater stability at a range of temperatures and longer duration of protein expression than self-formulated linear mRNA vaccines (22–24). Accordingly, low doses of circRNA vaccines may be sufficient for eliciting strong immune responses (22, 23). Researchers have attempted to utilize the stability of circRNAs for the direct synthesis of chimeric antigen receptor (CAR) T cells through the introduction of CAR-expressing circRNA into T cells to avoid the tedious process of producing CAR-T cells through T cell isolation followed by engineering (25). Accordingly, some researchers believe that circRNA vaccines may serve as powerful tools for tackling future emerging major infectious diseases or other frequent viral diseases, such as hepatitis B virus (HBV), human herpes virus (HHV), Ebola virus (EBV), influenza A virus (IAV) and human papillomavirus (HPV), and may be developed into therapeutic vaccines for tumors (22–29). Biopharmaceutical companies and research teams worldwide have therefore diverted considerable attention and research efforts to the development of circRNA vaccines. In this review, we aimed to summarize the research progress and formulation process for circRNA vaccines and highlight the considerations and outstanding issues in the quality control of RNA vaccines to provide a reference for future circRNA vaccine-related research.

## 2 Discovery of circRNAs

In 1971, virus-like molecules that can invade plants and cause plant death were discovered by researchers in a study on potato spindle tuber disease and given the name "viroids." Unlike viruses, viroids are single molecules that lack a protein coat (25, 30). Sanger et al. first described viroids as single-stranded covalently closed circRNA molecules in 1976 (31). In 1979, Hsu and Coca-Prados discovered the presence of circRNA molecules without free flanking ends in HeLa cells using electron microscopy; this was the first reported observation of circRNA molecules in eukaryotic cells (32). The invention of the polymerase chain reaction (PCR) technique in 1985 led to a surge in research interest in linear RNA. As a result, only little attention was paid to circRNAs and some researchers believed that circRNAs were merely byproducts of linear RNAs; this led to the stagnation of circRNA-related research. In the early 1990s, sporadic studies identified and characterized circRNAs generated from endogenous RNAs (25). The published reports indicated that the non-polyadenylated RNA with scrambled exons produced from non-canonical splicing ("scrambled exons") are covalently closed circular RNAs, such as the specific circularization of *EST-1* gene transcripts (25, 33–36).

In the following years, a few studies proposed mechanisms by which these molecules could be generated, such as the hypothesis that inverted repeats are necessary for *Sry* circularization (37–39). And additional circular RNAs could be produced from the rat cytochrome P450 2C24 gene, the human cytochrome P450 gene and others (37, 38). In 2006, researchers discovered the presence of circular transcripts in *Drosophila melanogaster* (40). Beginning in about 2010, with the rapid development of RNA sequencing and bioinformatics techniques, studies involving the combined use of such techniques revealed the presence of diverse and highly conserved circRNAs in different organisms, such as humans, mice, plants, *Cryptococcus*, zebrafish, and protists, which led to an explosion in circRNA research (41–50). In 2015, circRNAs capable of protein encoding and translation were first reported (51). From 2017 onward, the extensive application of modern molecular biological experimental techniques to evaluate circRNAs enabled the validation of various circRNAs previously discovered through RNA sequencing and bioinformatics studies (52–57). In 2018, researchers successfully synthesized circRNAs capable of protein expression, which may be applied to vaccine development (58). In 2022, some research teams embarked on studies on COVID-19 circRNA vaccines and therapeutic vaccines for tumors or genetic diseases (Figure 1) (22, 23, 59, 60). With the continuous increase in the depth of circRNA research, circRNAs have been found to play important roles under certain physiological and pathological conditions, and are capable of protein expression, which might enable their incorporation into vaccines (61–64). Therefore, circRNAs have gradually become an area of great interest in molecular biology and other related fields of research (65, 66).

## 3 *In vivo* metabolism and functions of natural circRNAs

### 3.1 Synthesis of circRNAs

To date, RNAs have been recognized to be circularized *in vivo* by back-splicing and exon skipping, with back-splicing potentially being more prevalent owing to its seemingly more

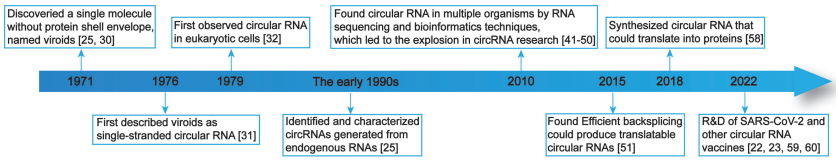


FIGURE 1
Key discoveries and advances in research on circRNAs.

frequent observations than exon skipping (67). RNA circularization by back-splicing refers to the inverse ligation of the downstream 5' splice donor site to the upstream 3' splice acceptor site after the emergence of breakpoints in RNA. Thereafter, certain intron sequences undergo alternative splicing, which ultimately leads to the generation of circRNA (21). Two widely accepted models of RNA circularization exist, lariat-driven circularization and direct back-splicing circularization. Lariat-driven circularization involves exon skipping events and intron escaping from debranching while direct back-splicing circularization involves *Cis*-elements-mediated and *Trans*-factors-mediated events. RNA circularization by exon skipping refers to the process in which circularization occurs following the splicing of exons together with introns (67). The published studies revealed that different breakpoint locations contribute to the diversity of circRNAs, and different types of circRNAs are generated by the random combination of exons, introns, intergenic regions, or non-transcribed regions through back-splicing (41, 67).

CircRNAs are generally classified into four main types based on differences in sequence combination: (1) Exonic circRNAs contain only exons, account for more than 80% of all identified circRNAs, and can be generated by lariat-driven circularization or direct back-splicing circularization. Base-pairing between the two flanking introns, which contain reverse complementary sequences, brings together a downstream 5′ ss and an upstream 3′ ss and facilitates back-splicing reactions to produce circular RNAs. (Figure 2A); (2) Exonic-intronic circRNAs, which are generated by exon-skipping circularization, harbor flanking intron sequences at the offside of core exons that should generally be spliced; therefore, exonic-intronic circRNAs are referred to as eiciRNAs or retained-intron circRNAs (Figure 2B); (3) Intronic circRNAs are also produced by a the intron escaping from debranching of lariat-derived mechanism relying on a consensus guanine (G)- and uracil (U)-rich domain near the 5′ splice site of pre-mRNA and a cytosine (C)-rich domain near the breakpoint. Intriguingly, the GU-rich domain can protect the C-rich domain from branching or degrading, thus generating stable circRNAs or so-called intron-derived circRNAs (Figure 2C); and (4) tRNA intronic circRNAs. For tRNA intronic circRNAs, pre-tRNAs are cleaved by the tRNA splicing endonuclease (TSEN) complex, and the exons and introns resulting from cleavage are ligated to form tRNA intronic circRNAs (Figure 2D) (41, 67–69).

According to the published studies, factors, such as sequence characteristics, protein regulators, and transcription stage, can affect the efficiency of back-splicing circularization (25, 41, 67). Indeed, beyond cis-elements, a number of RNA-binding proteins (RBPs) were found to actively modulate circular RNA biogenesis. Longer flanking intronic elements harboring several complementary or repeat sequences may contribute to higher circularization efficiency (25). Different splicing-associated proteins also exert different effects on circularization efficiency. For instance, adenosine deaminase acting on RNA-1 (ADAR1) suppresses RNA circularization (70).

## 3.2 Biological functions of circRNAs

According to several studies, circRNAs exist in various types of tissues in different species and possess multiple biological functions, such as the regulation of gene transcription and protein encoding (69, 71–74). CircRNAs also play important roles in the regulation of physiology and the occurrence, progression, and outcomes of a diverse range of diseases (75, 76).

### 3.2.1 Regulation of gene transcription

Researchers have reported that circRNAs can bind to the DNA of host genes to form DNA: RNA hybrids known as R-loops, which affect DNA replication, transcription, and post-damage repair. For instance, *circSEP3* (derived from exon 6 of *SEPALLATA3*) causes transcriptional termination through R-loop formation with *cSMARCA5* (derived from exon 15 of *SMARCA5*) (77). *circRHOT1* recruits Tat-interactive protein 60 kDa (TIP60) to the nuclear receptor subfamily 2 group F member 6 (*NR2F6*) promoter, thereby promoting cell proliferation, migration, and invasion in hepatocellular carcinoma through the induction of proto-oncogene expression (78).

### 3.2.2 "Sponging" effect

Natural circRNAs exhibit a "sponging" effect toward microRNAs (miRNAs). For instance, *circHIPK3* (derived from exon 2 of homeodomain interacting protein kinase 3 (*HIPK3*))

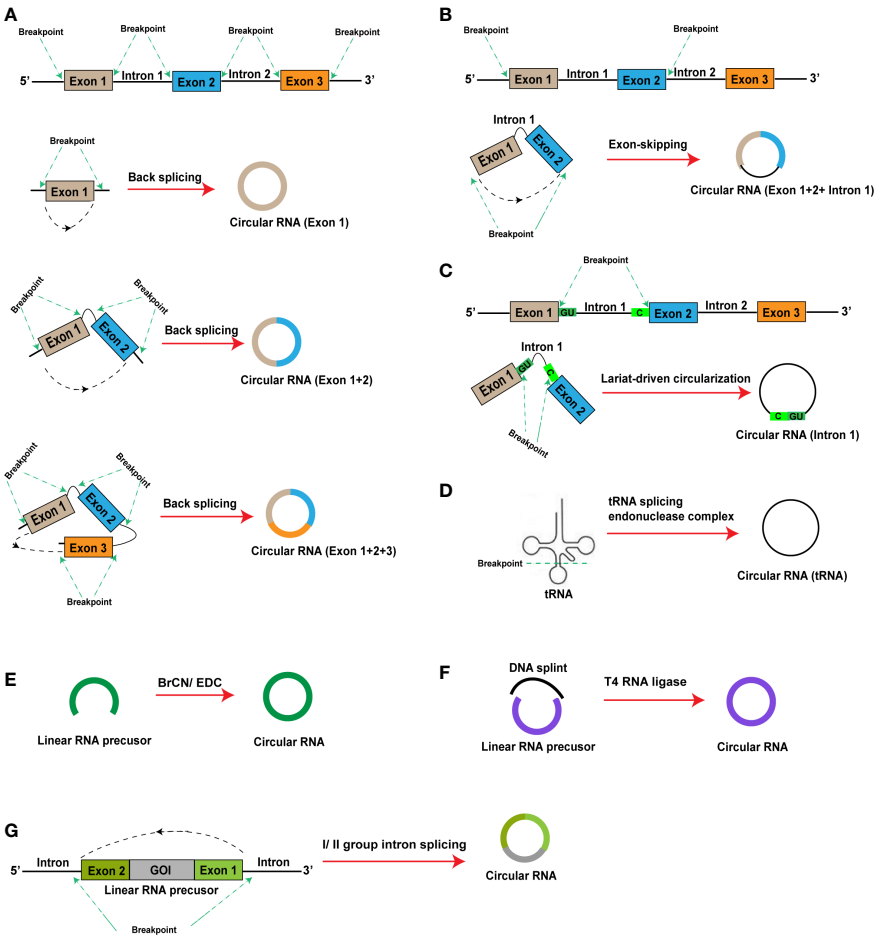


FIGURE 2
In vivo and in vitro (artificial) RNA circularization methods. **(A–D)** *In vivo* RNA circularization methods: **(A)** Exonic circRNA; **(B)** Exonic-intronic circRNA; **(C)** Intronic circRNA; **(D)** tRNA intronic circRNA; **(E, F)** *In vitro* (artificial) RNA circularization methods: **(E)** Chemical synthesis; **(F)** Ligation by T4 RNA ligase; **(G)** Intron self-splicing. BrCN, cyanogen bromide; EDC, 1-ethyl-3-(3-dimethylaminopropyl) carbodiimide; GOI, gene of interest.

can bind to *miR-124* and inhibit its activity, thereby preventing *miR-124* from inhibiting human cell proliferation (79); and *circHIPK2* regulates astrocyte activation by targeting *miR124-2HG* (80). Studies have indicated that circRNAs may exhibit a sponging effect toward proteins. Y-box binding protein-1 (Ybx1) is a transcription factor of many genes and its significant overexpression is associated with poor outcomes and the recurrence of various common tumors. According to researchers, *circNfix* can bind to Ybx1 and the E3 ubiquitin ligase, Nedd4l, which promotes their interactions and induces Ybx1 degradation (81).

### 3.2.3 Protein activation through complex formation

Many types of molecules in the host organism participate in the biological processes of host-virus interactions. A previous study revealed that the Epstein-Barr virus (EBV) produces the circRNA, *circBART2.2*, after infecting host cells, which can be recognized by the RIG-I receptor of the cells (82). Thereafter, RIG-I receptor activation occurs, enabling antiviral effects through subsequent activation of the downstream interferon signaling pathway. Another study found that circRNAs were not recognized by the RIG-I receptor after N6-methyladenosine (m6A) methylation, which serves as one of the mechanisms by which viruses evade host immune responses (83–85).

### 3.2.4 Protein translation

In 2015, the ability of circRNAs to encode and translate proteins was first discovered in the fruit fly. This key finding provided a theoretical basis for the subsequent development of circRNA vaccines (51, 67). Several studies have reported that circRNAs translate their encoding proteins *via* internal ribosomal entry site (IRES)-mediated or m6A-induced ribosome engagement site (MIRES)-mediated translation

initiation instead of 5' cap-dependent translation initiation (41, 67, 84). IRESs are RNA elements that recruit ribosomes to an internal region of mRNA for the initiation of translation, and can promote ribosome assembly and initiate translation through the recruitment of different trans-acting factors (21). IRESs are utilized for translation by many types of circRNAs, including *circMbl* and *circFGFR1 (*81). MIRES-mediated translation initiation involves the occurrence of m6A methylation at one or more sites in RNA, which enables the recruitment of eIF4G2 for the initiation of translation. For instance, *circE7*, which is encoded by human papillomaviruses (HPVs) and localized to the cytoplasm, contains m6A modifications and performs E7 oncoprotein translation (86). Another study reported that m6A modifications enhance IRES-mediated *circZNF609* translation efficiency (87).

## 3.3 CircRNA degradation

The stable closed-loop structure of circRNAs protects them from cleavage by exoribonucleases (67). Therefore, circRNAs are less easily degraded *via* routine RNA degradation pathways and are resistant to cleavage by the exoribonuclease RNase R in the short term (88). It is more stable than linear RNA, which is the natural advantage of circRNA vaccine development. Nevertheless, circRNAs are still degradable by certain means, including endonucleases. In a previous study, double-stranded RNA (dsRNA) or polyinosinic: polycytidylic acid (poly (I:C)) was found to activate the endonuclease, RNase L, *in vivo*, causing the global degradation of circRNAs (69). The ATP-dependent RNA helicase, upstream frameshift 1 (UPF1), and the endonuclease, G3BP1, can identify circRNAs with complex secondary structures and induce their degradation (67). circRNAs may undergo m6A modification, which is recognized by the m6A reader protein, HRSP12. Consequently, HRSP12 may interact with the RNase P/MRP endonuclease complex to induce circRNA degradation (89). Notably, circRNAs can be degraded by the endonuclease, RNase H, through targeting by specific primers and probes. The complementary binding of *miR-671* to the circRNA CDR1as sequence also induces AGO2-mediated circRNA degradation (52).

# 4 Research progress on circRNA vaccines

Prior to 2015, researchers had only observed the presence of non-protein-encoding circRNAs in organisms. The discovery of circRNAs capable of protein encoding and translation in the fruit fly in 2015 provided a theoretical basis for research and development of circRNA vaccines. With the continuous increase in the depth of circRNA-related research, three methods for the artificial preparation of circRNAs have emerged: (1) Chemical synthesis: cyanogen bromide (BrCN) or 1-ethyl-3-(3-dimethylaminopropyl) carbodiimide (EDC) induces covalent bond formation between the 5'-terminal phosphate and 3'-terminal hydroxyl groups of linear RNAs to produce circRNAs. The occurrence of side reactions, such as the formation of 2'-5' phosphodiester bonds during the circularization reaction, is a limitation of this approach. Further, chemical bonds in RNA oligomers are usually less effective than those in DNA analogs (Figure 2E); (2) Ligation by T4 RNA ligase: a linear RNA molecule can be circularized through the covalent bonding of a 5'-terminal monophosphate to a 3'-terminal hydroxyl group under the effects of T4 RNA ligase. However, the circularization reaction can only occur under conditions of a single phosphate at the 5' terminus. As RNA synthesized *in vitro* using T7 RNA polymerase contains a 5'-triphosphate terminus, two phosphate groups must be removed before circularization of the synthesized linear RNA. Presently, RNA 5' pyrophosphohydrolase (RppH) is used for the direct removal of the β and γ phosphates (Figure 2F); (3) Intron self-splicing: group I and II introns can perform RNase functions, enabling self-splicing of linear RNA molecules to form circRNAs without assistance from other enzymes (Figure 2G).

In 2015, researchers constructed a single exon minigene containing split GFP, and found that the pre-mRNA indeed produces translatable circRNA through efficient back-splicing in human and Drosophila cells (51). In 2018, researchers synthesized circRNAs encoding the enhanced green fluorescent protein (EGFP) using the group I intron splicing circularization method with IRES-mediated translation initiation. This synthesis led to the successful expression of EGFP in 293T cells. Surprisingly, the circRNAs could perform continuous expression for up to 168 h, whereas expression by self-formulated mRNAs only lasted for 48 h. Currently reported artificially synthesized protein-expressing circRNAs have mainly been produced through intron splicing or ligation by T4 RNA ligase, with the constituent elements being different for the two circularization methods (Figure 3) (58).

Wei et al. recently developed a circRNA vaccine against the original COVID-19 strain by adopting the group I intron splicing RNA circularization method with IRES-mediated translation initiation, and using lipid nanoparticles (LNPs) as delivery systems. In mice separately immunized with doses of 10 μg/animal and 50 μg/animal, the serum neutralizing antibody titers at 5 weeks post-boost were approximately $10^3$ and $10^5$, respectively, with relatively strong Th1 immune responses elicited by both doses. When a challenge experiment using the original viral strain was performed after monkeys had received two doses of the vaccine at a dose of 100 μg/animal, the immunization group was found to have a significant decrease in viral load in the lungs, degree of lung injury, and number of infiltrating inflammatory cells in the lungs. The technology

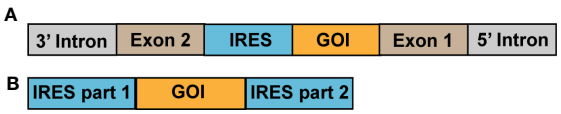


FIGURE 3
Methods currently used to formulate circRNA vaccines. **(A)** Circularization by intron splicing; **(B)** Ligation by T4 RNA ligase. GOI, gene of interest.

platform was subsequently utilized to generate a circRNA vaccine against the COVID-19 Delta variant, which was used for the immunization of mice at a dose of 10 μg/animal. At 7 weeks post-boost, the serum neutralizing antibody titer was approximately $10^4$ against the Delta variant, and reached approximately $10^{3.5}$ with the Omicron BA1 variant, thereby demonstrating the broad-spectrum activity of the vaccine. The formulated circRNA vaccine also had a greater stability than linear mRNA vaccines at 4°C, 25°C, and 37°C. Another COVID-19 circRNA vaccine prepared using the T4 RNA ligase method also displayed a certain level of immunogenicity in mice (22).

Seephetdee et al. adopted the group I intron splicing method for RNA circularization to formulate a COVID-19 circRNA vaccine using the spike (S) protein of the original COVID-19 strain as the antigen-binding construct and including multiple mutations (including K417N, L452R, T478K, E484K, N501Y, and D614G). Mice administered two immunizations of the vaccine at a dose of 5 μg/animal exhibited certain neutralizing activity against the Alpha, Beta, Delta, and Omicron variants and pseudoviruses. IFN-γ responses were also elicited in T cells (23).

Wang et al. formulated a COVID-19 circRNA vaccine using the group II intron splicing method for RNA circularization. When used for mice immunization, the vaccine elicited strong RBD-specific memory B cell responses and balanced Th1/Th2 cellular immune responses. The serum IgG titer of mice immunized with the circRNA vaccine was 10-fold that of mice immunized with a linear mRNA vaccine. Further, the circRNA vaccine exhibited good neutralizing activity against pseudo-SARS-CoV-2 and effectively blocked the binding of three types of receptor-binding domain (RBD) mutants (wild type, Delta, Omicron) to the hACE2 receptor on 293T cells. The COVID-19 circRNA vaccine could perform continuous expression in cells for 6 days, while expression by the self-formulated mRNA vaccine only lasted for 2 days (24).

The use of the T4 dt intron splicing method for RNA circularization causes the generation of "splicing scar" sequences, with different sequence lengths leading to different topological structures. A study revealed that differences in the constituent elements and compositions of circRNAs affected the translation efficiency, with vector topological structure, untranslated region (UTR), and IRES playing the most critical roles (26, 59). Through the experimental comparison of different splicing scar, 5'UTR, 3'UTR, and IRES sequences, the circRNA constructed using a 50 nt-long splicing scar sequence and the eIF4G-recruiting aptamer Apt-eIF4G sequence as the 5'UTR, full-length HBA1 sequence as the 3'UTR, and wild-type iCVB3 sequence as the IRES exhibited a considerable increase in translation efficiency and could perform continuous protein expression for up to 7 days in 293T cells. In contrast, the linear mRNA vaccine only achieved 3 days of continuous protein expression, with lower expression than that of the circRNA vaccine. The studies described above demonstrate that circRNA vaccines not only possess stronger immunogenicity, but also express proteins for a longer duration than self-formulated linear mRNA vaccines (90). Accordingly, stronger immune responses may be elicited by circRNA vaccines when administered at lower doses (22, 90).

The circRNA vaccines translated into proteins *via* IRES-mediated translation pathway. Similar to the linear mRNA vaccines, the circRNA vaccines are also translated into proteins in bodies to induce the robust humoral and effective cellular immunity, among which liposome and others could play the role in vaccine adjuvants. Some studies indicated that circRNA vaccines could continue to translate into proteins longer than the linear mRNA vaccines and even up to about 7 days (22, 58, 90). The mechanism might be that closed characteristics of circular RNAs theoretically prevent them from degradation by exonucleases that typically degrade linear RNAs from either 5′ or 3′ end (69). However, there is no research on how the circRNA vaccines degrades in bodies, and it may also be degraded *via* microRNA-mediated, m6A-mediated, RNase L-mediated, or other degradation pathways of biogenesis circRNAs.

Compare with peptide vaccines, inactivated virus vaccines and recombinant protein vaccines, circRNA vaccines could effectively induced the T cell immunity (22, 23). DNA vaccines have to come into the nucleus to be transcribed in mRNA, which leads to some risk for our bodies, whereas circRNA vaccines do not (1, 8). The published studies indicated that circRNA vaccines could continue to translate into proteins for a longer time compared with linear mRNA vaccines, suggesting that it has the better stability (24, 26, 90).

There are some obviously different between the circRNA and the linear mRNA vaccines. For example, the circRNAs and the linear RNAs have different degradation approaches *in vivo* (25, 67). In additional, the circRNA vaccines mainly uses the IRES mediated-translation pathway, while linear mRNA vaccines use the 5'cap (m7GpppN) structure mediated-translation pathway. Thus, the circRNA and the linear mRNA vaccines translate into proteins *via* different transcription initiation complexes involving in different initiation factors (91–94). The obvious difference is that the circRNA vaccines do not require any modification because the annular structure is not easily degraded by exoribonuclease, whereas the linear mRNA vaccines need the pseudouridine modification, the 5'cap structure and the 3'poly(A) structure (7, 8, 22, 24).

## 5 Overview of the circRNA vaccine production process

At present, the industrial production of circRNA vaccines is not mature, and most of them are in the stage of small-scale research. Reference can be made to the linear mRNA vaccine production process. The main differences are the cyclization process and the removal of associated impurities. Industrialized production of circRNA vaccines may be realized by the following process: (1) Synthesis of linear RNA molecules through *in vitro* transcription using plasmids as templates; (2) RNA circularization; and (3) Vaccine encapsulation using delivery systems, such as LNPs. Therefore, the acquisition of high-quality plasmids is of primary importance (90). The industrialized production process of plasmids is currently at a near-mature stage and consists of steps, such as fermentation, bacteria harvesting, lysis, clarification, ultrafiltration and concentration, and chromatographic purification. During the chromatographic purification step, the addition of different types of packing materials enables the removal of RNA, trace impurities, and endotoxins to obtain high-purity supercoiled plasmids. The obtained plasmids are subsequently subjected to single restriction endonuclease cleavage for linearization and chromatography for enzyme and salt removal. Linear RNA molecules are synthesized *via in vitro* transcription. Subsequently, the DNA template in the reaction products is removed using DNase I and the RNA product is purified by ultrafiltration. The linear RNA molecules are then subjected to circularization, which is a critical step in the circRNA vaccine preparation process. Currently, the intron splicing method holds the greatest promise for use as the circularization method in industrialized circRNA vaccine production as the addition of enzymes is not required. Ligation by T4 RNA ligase can also be used in industrialized circRNA production; however, its RNA circularization efficiency is significantly lowered during the circularization of RNA molecules with sequence length > 2000 bp. Furthermore, additional processes are required for the removal of T4 RNA ligase. By comprehensively considering various factors, ligation by T4 RNA ligase is identified to be less suitable for RNA circularization in industrialized production than intron splicing. Products of the circularization reaction include impurities, such as linear RNA precursors and spliced RNA sequences. The removal of linear RNA precursor molecules that had not been successfully circularized is a difficult problem faced by circRNA vaccine production due to the similarity of molecular weights between linear RNA precursors and the corresponding circRNA molecules. Researchers have reported the use of chromatography for the removal of linear RNA precursor molecules and other impurities from the circularization products (22). In the laboratory-scale production stage, high-performance liquid chromatography (HPLC) or RNase R digestion may be attempted for the removal of linear RNA precursors and other impurities (22, 24). However, RNase R is currently not suited for use in large-scale production due to its high cost. As the enhancement of RNA circularization efficiency leads to a reduction in impurity content, increasing circularization efficiency may be a feasible approach for the simplification of the purification process. A previous study demonstrated that RNA circularization efficiency could be effectively enhanced during the performance of circularization in a buffer solution with final concentrations of 50 mM Tris-HCl, 10 mM $MgCl_2$, and 1 mM DTT at a pH of 7.5 (58). Finally, the circRNAs are encapsulated in delivery systems, such as LNPs, and subsequently subjected to filling and capping to form the final vaccine product (Figure 4). Of note, the circRNA vaccine formulation process does not require the addition of a 5' cap and 3' poly(A) tail or the removal of enzymes from reaction products (22).

## 6 Considerations for the quality control of circRNA vaccines

Presently, two COVID-19 linear mRNA vaccines have already been marketed; however, the quality control processes for these vaccines are relatively mature. The World Health Organization (WHO) issued a guidance document on regulatory considerations regarding the evaluation of the quality, safety, and efficacy of messenger RNA vaccines for the prevention of infectious diseases (95–97). Further, the U.S. Pharmacopeial Convention (USP) developed the Analytical Procedures for mRNA Vaccine Quality, and the Center for Drug Evaluation (CDE) of the China National Medical Products Administration (NMPA) published the Guiding Principles on Pharmaceutical Research Techniques for Prophylactic COVID-19 mRNA Vaccines (trial) (98, 99). Considering the characteristics of circRNA vaccines, existing guidance documents for mRNA vaccines, other types of vaccines, and nucleic acid therapeutics may serve as reference for the formulation of circRNA vaccine quality control processes (Supplementary Material Table 1) (22, 24, 90, 96–103).

CircRNAs are dependent on IRES or m6A modifications for translation initiation. Owing to their unique closed-loop structures, circRNAs are resistant to degradation *via* routine pathways, which eliminates the need for 5' cap and 3' poly(A) tail structures in the RNA molecules used to formulate circRNA vaccines (22, 23). Therefore, 5' cap- and 3' poly(A) tail-related quality control is not required for circRNA vaccines.

Quality control items emerging from core quality attributes (CQAs) related to the unique characteristics of circRNA

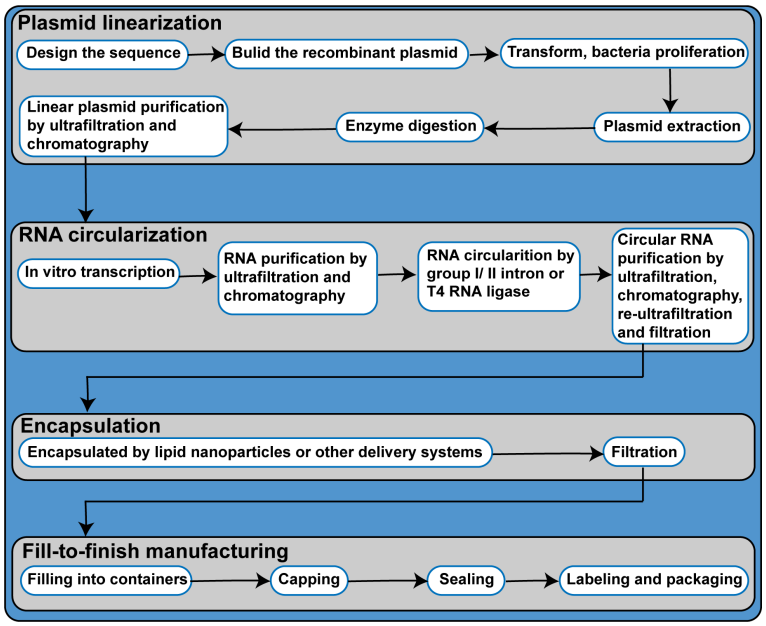


FIGURE 4
Process flow diagram of circRNA vaccine productions.

vaccines must be emphasized. Circularization rate is the most important CQA of circRNA vaccines and has been measured by capillary electrophoresis (CE) and high-performance liquid chromatography (HPLC) in previous studies (22, 24). The accuracy of circRNA sequences should also be measured based on sequencing methods. However, the process for circRNA vaccines differs from that of linear mRNA vaccines as circRNAs require endonuclease cleavage for loop opening prior to sequencing (22, 24). During the RNA circularization process, single-stranded RNA (intronic sequences) may become detached and a portion of the linear RNA precursors ultimately remain uncircularized. Researchers have reported the use of CE and HPLC for determining circRNA vaccine purity (22). If ligation by T4 RNA ligase is adopted for the preparation of circRNAs, quality control of the residual T4 RNA ligase content of the vaccine product must also be performed, which can be measured by the enzyme-linked immunosorbent assay (ELISA). When RNase R is used for the removal of linear RNA precursor molecules, quality control is also required for residual RNase R content, which can also be measured by ELISA. Currently, specific antigen-antibody binding methods, such as ELISA, are adopted to measure the residual double-stranded RNA (dsRNA) content of mRNA vaccines, with the anti-dsRNA J2 antibody being mainly used (104, 105). However, studies that aim to determine whether circRNAs can directly bind the anti-dsRNA J2 antibody or interfere with the binding of anti-dsRNA J2 antibody to dsRNA have not been reported. Therefore, sample applicability studies must be performed before the adoption of ELISA to measure the residual dsRNA content of circRNA vaccines (104–106).

## 7 Outlook of circRNA vaccines

CircRNA vaccines may serve as a powerful tool for tackling future emerging major infectious diseases or frequent viral diseases and may be developed into therapeutic vaccines for tumors. Biopharmaceutical companies and research teams worldwide have therefore diverted considerable attention and research efforts to the development of circRNA vaccines. Currently, research on circRNAs remains in the preclinical stage due to various issues in research and development, production, quality control, and safety. Recently, researchers proposed that a blueprint for quality by digital design (QbDD) to support rapid RNA vaccine process development, manufacturing and supply (107). Accordingly, the QbDD concept should be incorporated into circRNA vaccine development, production, and quality control (108). The development and validation of new circRNA vaccine-related methods should be based on specific requirements stipulated in the General Chapter <1220> “The Analytical Procedure Lifecycle” recently released by the USP and the ICH Q2 “Validation of Analytical Procedures” and Q14 “Analytical Procedure Development” draft guidelines published by the International Council for Harmonization of Technical Requirements for Pharmaceuticals for Human Use (ICH), for

which public comment is currently being sought. Further, an analytical target profile (ATP), risk analysis and identification, confirmation of CQAs, experimental design, process control, and in-use monitoring are required (108–113).

Future directions for the various aspects of circRNA vaccines are as follows:

Research and development: linear mRNA vaccines exhibit a "self-adjuvant" effect (4, 16, 106). The excess or deficiency of such effect is unfavorable for the induction of high levels of humoral immunity and effective cellular immunity. CircRNAs can activate the RIG-I and PKR cellular signal transduction pathways, which also provides a self-adjuvant effect (82, 88, 114–116). Therefore, the design and optimization of circRNA vaccines to activate the self-adjuvant effect to an appropriate degree are essential for enhancing vaccine efficacy. RNA circularization is a key stage in the circRNA vaccine formulation process, with circularization efficiency being a major determinant of vaccine production capacity, and high circularization efficiency being beneficial to the subsequent purification process (117). The design and optimization of the constituent elements and compositions of circRNA vaccines or development of novel RNA circularization methods are effective approaches for enhancing circularization efficiency. According to the published research, excessive RNA sequence length affects circularization efficiency. Therefore, during the design and optimization of target fragment length, care must be taken to avoid affecting the immunogenicity of the target protein or RNA circularization efficiency (90). CircRNA vaccines differ from mRNA vaccines as they possess a loop structure, and different target sequences may exhibit different conformations. Such characteristics of circRNAs may affect the RNA circularization efficiency and require adequate exploration during the research and development stage. Intron sequences play a key role in the RNA circularization reaction. Therefore, the optimization of intron sequences is a necessary step in the vaccine development stage (90). Exon length affects the efficiency of circularization by group I intron self-splicing, which also necessitates the optimization of exon sequence length during vaccine development. The selection of effective IRES structural elements is of great importance as it is a major determinant of protein translation by circRNA vaccines (24, 51, 58). Recently, it was reported that DeepCIP, the world's first CircRNA IRES prediction tool, could predict the IRES that are more suitable for CircRNAs, so that CircRNAs can be adapted to different scenarios, such as vaccines and antitumor therapy (118). CircRNAs require delivery systems for encapsulation to form vaccines. LNPs currently serve as the main delivery system for circRNAs. The development of targeted LNPs may potentially contribute to the enhancement of vaccine protection effects. Alternatively, research efforts can be devoted to the development of novel and more effective delivery systems that can replace LNPs. For instance, some earlier studies have explored the use of exosomes and ferritin as delivery systems (119, 120).

Production: Attempts can be made to optimize the reaction conditions to achieve enhanced circularization efficiency. Under laboratory conditions, a re-execution of the circularization step with circularized RNA contributes to higher circularization efficiencies. Therefore, the development of a recircularization process and the incorporation of such process into vaccine production can be attempted (58). The similarity in molecular weight between circRNAs and the corresponding linear RNA precursor molecules poses difficulties for the elimination of linear RNA precursors from the vaccine product during the purification process. Currently, chromatography is mainly adopted for purification; however, there is a lack of reports on whether its purification effects are sufficient to meet production needs.

Quality control: As mentioned earlier, the molecular weights of circRNAs are similar to those of the corresponding linear RNA precursor molecules. Consequently, the two types of RNA molecules exhibit close peak appearance times during CE or HPLC to determine the RNA circularization rate. Accordingly, it is difficult to effectively distinguish between the two (22, 24). Further optimization of experimental conditions should be performed to satisfy the requirements for measurement. National and regional reference standards for dsRNA may also be needed in the future, with factors, such as dsRNA base sequences, sequence length, number of phosphate groups at the 5'-terminus and base modifications taken into comprehensive consideration in the reference standard preparation process.

Safety: Organisms contain an abundance of circRNAs that play important roles in regulating gene transcription, expression, and cellular signal transduction pathways, with certain circRNAs capable of protein expression (80, 121). Whether exogenous circRNAs cause disruptions to the biological functions of naturally occurring circRNAs in the body is unknown. Residual linear RNA precursor molecules may cause stronger adverse reactions due to activating the excessive innate immune response. circRNA vaccines contain residual dsRNA content. As the occurrence of myocarditis after vaccination with mRNA vaccines has been reported to be associated with dsRNA residual in the vaccines (122), further research is required to ascertain whether circRNA vaccines may cause myocarditis.

## Author contributions

YB and ZL conceived the framework and main text of this review article. YB and DL wrote the draft. QM and ZL reviewed

the manuscript. QH and JL searched the literatures. All authors contributed to the article and approved the submitted version.

## Funding

This work was supported by CAMS Innovation Fund for Medical Sciences (2021-I2M-5-005).

## Conflict of interest

The authors declare that the research was conducted in the absence of any commercial or financial relationships that could be construed as a potential conflict of interest.

## Publisher's note



## Supplementary material

The Supplementary Material for this article can be found online at: https://www.frontiersin.org/articles/10.3389/fimmu.2022.1091797/full#supplementary-material

## References

1. He Q, Mao Q, Zhang J, Bian L, Gao F, Wang J, et al. COVID-19 vaccines: Current understanding on immunogenicity, safety, and further considerations. *Front Immunol* (2021) 12:669339. doi: 10.3389/fimmu.2021.669339

2. Mao Q, Xu M, He Q, Li C, Meng S, Wang Y, et al. COVID-19 vaccines: progress and understanding on quality control and evaluation. *Signal Transduct Target Ther* (2021) 6(1):199. doi: 10.1038/s41392-021-00621-4

3. Liu J, Mao Q, Wu X, He Q, Bian L, Bai Y, et al. Considerations for the feasibility of neutralizing antibodies as a surrogate endpoint for COVID-19 vaccines. *Front Immunol* (2022) 13:814365. doi: 10.3389/fimmu.2022.814365

4. Wang Q, Song Z, Yang J, He Q, Mao Q, Bai Y, et al. Transcriptomic analysis of the innate immune signatures of a SARS-CoV-2 protein subunit vaccine ZF2001 and an mRNA vaccine RRV. *Emerg Microbes Infect* (2022) 11(1):1145–53. doi: 10.1080/22221751.2022.2059404

5. Lamb YN. BNT162b2 mRNA COVID-19 vaccine: First approval. *Drugs* (2021) 81(4):495–501. doi: 10.1007/s40265-021-01480-7

6. Creech CB, Walker SC, Samuels RJ. SARS-CoV-2 vaccines. *Jama* (2021) 325 (13):1318–20. doi: 10.1001/jama.2021.3199

7. Fang E, Liu X, Li M, Zhang Z, Song L, Zhu B, et al. Advances in COVID-19 mRNA vaccine development. *Signal Transduct Target Ther* (2022) 7(1):94. doi: 10.1038/s41392-022-00950-y

8. Qin S, Tang X, Chen Y, Chen K, Fan N, Xiao W, et al. mRNA-based therapeutics: powerful and versatile tools to combat diseases. *Signal Transduct Target Ther* (2022) 7(1):166. doi: 10.1038/s41392-022-01007-w

9. *WHO coronavirus (COVID-19) dashboard* . Available at: https://www.who.int/redirect-pages/page/novel-coronavirus-(covid-19)-situation-dashboard.

10. Lozano-Ojalvo D, Camara C, Lopez-Granados E, Nozal P, Del Pino-Molina L, Bravo-Gallego LY, et al. Differential effects of the second SARS-CoV-2 mRNA vaccine dose on T cell immunity in naive and COVID-19 recovered individuals. *Cell Rep* (2021) 36(8):109570. doi: 10.1016/j.celrep.2021.109570

11. Apostolidis SA, Kakara M, Painter MM, Goel RR, Mathew D, Lenzi K, et al. Cellular and humoral immune responses following SARS-CoV-2 mRNA vaccination in patients with multiple sclerosis on anti-CD20 therapy. *Nat Med* (2021) 27(11):1990–2001. doi: 10.1038/s41591-021-01507-2

12. Sahin U, Muik A, Derhovanessian E, Vogler I, Kranz LM, Vormehr M, et al. COVID-19 vaccine BNT162b1 elicits human antibody and T(H)1 T cell responses. *Nature* (2020) 586(7830):594–9. doi: 10.1038/s41586-020-2814-7

13. Cafri G, Gartner JJ, Zaks T, Hopson K, Levin N, Paria BC, et al. mRNA vaccine-induced neoantigen-specific T cell immunity in patients with gastrointestinal cancer. *J Clin Invest* (2020) 130(11):5976–88. doi: 10.1172/jci134915

14. Whitley J, Zwolinski C, Denis C, Maughan M, Hayles L, Clarke D, et al. Development of mRNA manufacturing for vaccines and therapeutics: mRNA platform requirements and development of a scalable production process to support early phase clinical trials. *Transl Res* (2022) 242:38–55. doi: 10.1016/j.trsl.2021.11.009

15. Wang Y, Zhang Z, Luo J, Han X, Wei Y, Wei X. mRNA vaccine: a potential therapeutic strategy. *Mol Cancer* (2021) 20(1):33. doi: 10.1186/s12943-021-01311-z

16. Kobiyama K, Ishii KJ. Making innate sense of mRNA vaccine adjuvanticity. *Nat Immunol* (2022) 23(4):474–6. doi: 10.1038/s41590-022-01168-4

17. Dolgin E. The tangled history of mRNA vaccines. *Nature* (2021) 597 (7876):318–24. doi: 10.1038/d41586-021-02483-w

18. Voigt EA, Gerhardt A, Hanson D, Jennewein MF, Battisti P, Reed S, et al. A self-amplifying RNA vaccine against COVID-19 with long-term room-temperature stability. *NPJ Vaccines* (2022) 7(1):136. doi: 10.1038/s41541-022-00549-y

19. Oberli MA, Reichmuth AM, Dorkin JR, Mitchell MJ, Fenton OS, Jaklenec A, et al. Lipid nanoparticle assisted mRNA delivery for potent cancer immunotherapy. *Nano Lett* (2017) 17(3):1326–35. doi: 10.1021/acs.nanolett.6b03329

20. Liu CX, Chen LL. Circular RNAs: Characterization, cellular roles, and applications. *Cell* (2022) 185:2016–34. doi: 10.1016/j.cell.2022.04.021

21. Zhou WY, Cai ZR, Liu J, Wang DS, Ju HQ, Xu RH, et al. Metabolism, functions and interactions with proteins. *Mol Cancer* (2020) 19(1):172. doi: 10.1186/s12943-020-01286-3

22. Qu L, Yi Z, Shen Y, Lin L, Chen F, Xu Y, et al. Circular RNA vaccines against SARS-CoV-2 and emerging variants. *Cell* (2022) 185(10):1728–1744 e16. doi: 10.1016/j.cell.2022.03.044

23. Seephetdee C, Bhukhai K, Buasri N, Leelukkanaveera P, Lerdwattanasombat P, Manopwisedjaroen S, et al. A circular mRNA vaccine prototype producing VFLIP-X spike confers a broad neutralization of SARS-CoV-2 variants by mouse sera. *Antiviral Res* (2022) 204:105370. doi: 10.1016/j.antiviral.2022.105370

24. Chen C, Wei H, Zhang K, Li Z, Wei T, Tang C, et al. A flexible, efficient, and scalable platform to produce circular RNAs as new therapeutics. *bioRxiv preprint server Biol* (2022). doi: 10.1101/2022.05.31.494115

25. Patop IL, Wust S, Kadener S. Past, present, and future of circRNAs. *EMBO J* (2019) 38(16):e100836. doi: 10.15252/embj.2018100836

26. Qi Y, Han W, Chen D, Zhao J, Bai L, Huang F, et al. Engineering circular RNA regulators to specifically promote circular RNA production. *Theranostics* (2021) 11(15):7322–36. doi: 10.7150/thno.56990

27. Bai Y, Lian P, Li J, Zhang Z, Qiao J. The active GLP-1 analogue liraglutide alleviates H9N2 influenza virus-induced acute lung injury in mice. *Microb Pathog* (2021) 150:104645. doi: 10.1016/j.micpath.2020.104645

28. He Q, Bai Yu, Yang J, Lu S, Mao Q, Gao F, et al. B.1.351 SARS-CoV-2 variant exhibits higher virulence but LessViral shedding than that of the ancestral strain in YoungNonhuman primates. *Microbiol Spectr* (2022) 10(5):e0226322. doi: 10.1128/spectrum.02263-22

29. Bian L, Bai Yu, Gao F, Liu M, He Q, Wu X, et al. Effective protection of ZF2001 against the SARS-CoV-2 delta variant in lethal K18-hACE2 mice. *Virol J* (2022) 19(1):86. doi: 10.1186/s12985-022-01818-x

30. Tsagris EM, Martinez de Alba AE, Gozmanova M, Kalantidis K. Viroids. *Cell Microbiol* (2008) 10(11):2168–79. doi: 10.1111/j.1462-5822.2008.01231.x

31. Sanger GKHL, Riesner D, Gross HJ, Kleinschmidt AK. Viroids are single-stranded covalently closed circular RNA molecules existing as highly base-pairedrod-like structures. *Proc NatI. Acad Sci* (1976) 73(11):3852–6. doi: 10.1073/pnas.73.11.3852

32. Hsu MT, Coca-Prados M. Electron microscopic evidence for the circular form of RNA in the cytoplasm of eukaryotic cells. *Nature* (1979) 280(5720):339–40. doi: 10.1038/280339a0

33. Ge LQ, Huang B, Jiang YP, Gu HT, Xia T, Yang GQ, et al. Carboxylesterase precursor (EST-1) mediated the fungicide jinggangmycin-suppressed reproduction of sogatella furcifera (Hemiptera: Delphacidae). *J economic entomology* (2017) 110 (5):2199–206. doi: 10.1093/jee/tox201

34. Cocquerelle C, Mascrez B, Hetuin D, Bailleul B. Mis-splicing yields circular RNA molecules. *FASEB J* (1993) 7(1):155–60. doi: 10.1096/fasebj.7.1.7678559

35. Capel B, Swain A, Nicolis S, Hacker A, Walter M, Koopman P, et al. Circular transcripts of the testis-determining gene sry in adult mouse testis. *Cell* (1993) 73 (5):1019–30. doi: 10.1016/0092-8674(93)90279-y

36. Cocquerelle C, Daubersies P, Majerus MA, Kerckaert JP, Bailleul B. Splicing with inverted order of exons occurs proximal to large introns. *EMBO J* (1992) 11 (3):1095–8. doi: 10.1002/j.1460-2075.1992.tb05148.x

37. Dubin RA, Kazmi MA, Ostrer H. Inverted repeats are necessary for circularization of the mouse testis sry transcript. *Gene* (1995) 167(1-2):245–8. doi: 10.1016/0378-1119(95)00639-7

38. Zaphiropoulos PG. Exon skipping and circular RNA formation in transcripts of the human cytochrome p-450 2C18 gene in epidermis and of the rat androgen binding protein gene in testis. *Mol Cell Biol* (1997) 17(6):2985–93. doi: 10.1128/mcb.17.6.2985

39. Pasman Z, Been MD, Garcia-Blanco MA. Exon circularization in mammalian nuclear extracts. *RNA* (1996) 2(6):603–10.

40. Houseley JM, Garcia-Casado Z, Pascual M, Paricio N, O'Dell KM, Monckton DG, et al. Noncanonical RNAs from transcripts of the drosophila muscleblind gene. *J Hered* (2006) 97(3):253–60. doi: 10.1093/jhered/esj037

41. Zhang Y, Yang L, Chen LL. Characterization of circular RNAs. *Methods Mol Biol* (2021) 2372:179–92. doi: 10.1007/978-1-0716-1697-0_16

42. Salzman J, Gawad C, Wang PL, Lacayo N, Brown PO. Circular RNAs are the predominant transcript isoform from hundreds of human genes in diverse cell types. *PloS One* (2012) 7(2):e30733. doi: 10.1371/journal.pone.0030733

43. Memczak S, Jens M, Elefsinioti A, Torti F, Krueger J, Rybak A, et al. Circular RNAs are a large class of animal RNAs with regulatory potency. *Nature* (2013) 495 (7441):333–8. doi: 10.1038/nature11928

44. Zhang Y, Zhang XO, Chen T, Xiang JF, Yin QF, Xing YH, et al. Circular intronic long noncoding RNAs. *Mol Cell* (2013) 51(6):792–806. doi: 10.1016/j.molcel.2013.08.017

45. Jeck WR, Sharpless NE. Detecting and characterizing circular RNAs. *Nat Biotechnol* (2014) 32(5):453–61. doi: 10.1038/nbt.2890

46. Zhang XO, Wang HB, Zhang Y, Lu X, Chen LL, Yang L. Complementary sequence-mediated exon circularization. *Cell* (2014) 159(1):134–47. doi: 10.1016/j.cell.2014.09.001

47. Tagawa T, Kopardé VN, Ziegelbauer JM. Identifying and characterizing virus-encoded circular RNAs. *Methods* (2021) 196:129–37. doi: 10.1016/j.ymeth.2021.03.004

48. Bozzoni I. Widespread occurrence of circular RNA in eukaryotes. *Nat Rev Genet* (2021) 22(9):550–1. doi: 10.1038/s41576-021-00375-3

49. Cooper S, Wadsworth ES, Ochsenreiter T, Ivens A, Savill NJ, Schnaufer A. Assembly and annotation of the mitochondrial minicircle genome of a differentiation-competent strain of trypanosoma brucei. *Nucleic Acids Res* (2019) 47(21):11304–25. doi: 10.1093/nar/gkz928

50. Huo L, Zhang P, Li C, Rahim K, Hao X, Xiang B, et al. Genome-wide identification of circRNAs in pathogenic basidiomycetous yeast cryptococcus neoformans suggests conserved circRNA host genes over kingdoms. *Genes* (2018) 9(3):118. doi: 10.3390/genes9030118

51. Wang Y, Wang Z. Efficient backsplicing produces translatable circular mRNAs. *RNA* (2015) 21(2):172–9. doi: 10.1261/rna.048272.114

52. Chen YG, Kim MV, Chen X, Batista PJ, Aoyama S, Wilusz JE, et al. Sensing self and foreign circular RNAs by intron identity. *Mol Cell* (2017) 67(2):228–238.e5. doi: 10.1016/j.molcel.2017.05.022

53. Jakobi T, Dieterich C. Computational approaches for circular RNA analysis. *Wiley Interdiscip Rev RNA* (2019) 10(3):e1528. doi: 10.1002/wrna.1528

54. Pandey PR, Munk R, Kundu G, De S, Abdelmohsen K, Gorospe M. Methods for analysis of circular RNAs. *Wiley Interdiscip Rev RNA* (2020) 11(1):e1566. doi: 10.1002/wrna.1566

55. Abe BT, Wesselhoeft RA, Chen R, Anderson DG, Chang HY. Circular RNA migration in agarose gel electrophoresis. *Mol Cell* (2022) 82(9):1768–1777 e3. doi: 10.1016/j.molcel.2022.03.008

56. Kuznetsova I, Rackham O, Filipovska A. Investigating mitochondrial transcriptomes and RNA processing using circular RNA sequencing. *Methods Mol Biol* (2021) 2192:43–57. doi: 10.1007/978-1-0716-0834-0_4

57. Verboom K, Everaert C, Bolduc N, Livak KJ, Yigit N, Rombaut D, et al. SMARTer single cell total RNA sequencing. *Nucleic Acids Res* (2019) 47(16):e93. doi: 10.1093/nar/gkz535

58. Wesselhoeft RA, Kowalski PS, Anderson DG. Engineering circular RNA for potent and stable translation in eukaryotic cells. *Nat Commun* (2018) 9(1):2629. doi: 10.1038/s41467-018-05096-6

59. Crunkhorn S. Improving circular RNA protein yields. *Nat Rev Drug Discovery* (2022) 21(9):636. doi: 10.1038/d41573-022-00129-8

60. *Orna therapeutics, orna therapeutics raises $221 million series b financing to advance circular RNA platform and accelerate programs to the clinic* (Accessed August 16, 2022).

61. Yang Q, Li F, He AT, Yang BB. Circular RNAs: Expression, localization, and therapeutic potentials. *Mol Ther* (2021) 29(5):1683–702. doi: 10.1016/j.ymthe.2021.01.018

62. Wawrzyniak O, Zarębska Ż, Kuczyński K, Gotz-Więckowska A, Rolle K. Protein-related circular RNAs in human pathologies. *Cells* (2020) 9(8):1841. doi: 10.3390/cells9081841

63. Solé C, Lawrie CH. Circular RNAs and cancer: Opportunities and challenges. *Adv Clin Chem* (2020) 99:87–146. doi: 10.1016/bs.acc.2020.02.008

64. Li D, Yang Y, Li ZQ, Li LC, Zhu XH. Circular RNAs: from biogenesis and function to diseases. *Chin Med J* (2019) 132(20):2457–64. doi: 10.1097/cm9.0000000000000465

65. Singh M, Dwibedy SLL, Biswal SR, Muthuswamy S, Kumar A, Kumar S, et al. A novel and potential regulator in pathophysiology of schizophrenia. *Metab Brain Dis* (2022) 37(5):1309–16. doi: 10.1007/s11011-022-00978-7

66. Ebermann C, Schnarr T, Müller S. Recent advances in understanding circular RNAs. *F1000Research* (2020) 9:F1000. doi: 10.12688/f1000research.25060.1

67. Kristensen LS, Andersen MS, Stagsted LVW, Ebbesen KK, Hansen TB, Kjems J. The biogenesis, biology and characterization of circular RNAs. *Nat Rev Genet* (2019) 20(11):675–91. doi: 10.1038/s41576-019-0158-7

68. Chen X, Yang T, Wang W, Xi W, Zhang T, Li Q, et al. Circular RNAs in immune responses and immune diseases. *Theranostics* (2019) 9(2):588–607. doi: 10.7150/thno.29678

69. Zhou M, Xiao MS, Li Z, Huang C. New progresses of circular RNA biology: from nuclear export to degradation. *RNA Biol* (2021) 18(10):1365–73. doi: 10.1080/15476286.2020.1853977

70. Omata Y, Okawa M, Haraguchi M, Tsuruta A, Matsunaga N, Koyanagi S, et al. RNA Editing enzyme ADAR1 controls miR-381-3p-mediated expression of multidrug resistance protein MRP4 *via* regulation of circRNA in human renal cells. *J Biol Chem* (2022) 298(8):102184. doi: 10.1016/j.jbc.2022.102184

71. Chen LL. The expanding regulatory mechanisms and cellular functions of circular RNAs. *Nat Rev Mol Cell Biol* (2020) 21(8):475–90. doi: 10.1038/s41580-020-0243-y

72. Li I, Chen YG. Emerging roles of circular RNAs in innate immunity. *Curr Opin Immunol* (2021) 68:107–15. doi: 10.1016/j.coi.2020.10.010

73. Xu X, Zhang J, Tian Y, Gao Y, Dong X, Chen W, et al. CircRNA inhibits DNA damage repair by interacting with host gene. *Mol Cancer* (2020) 19(1):128. doi: 10.1186/s12943-020-01246-x

74. Xiao MS, Ai Y, Wilusz JE. Biogenesis and functions of circular RNAs come into focus. *Trends Cell Biol* (2020) 30(3):226–40. doi: 10.1016/j.tcb.2019.12.004

75. Huang A, Zheng H, Wu Z, Chen M, Huang Y. Circular RNA-protein interactions: functions, mechanisms, and identification. *Theranostics* (2020) 10 (8):3503–17. doi: 10.7150/thno.42174

76. Di Timoteo G, Rossi F, Bozzoni I. Circular RNAs in cell differentiation and development. *Dev (Cambridge England)* (2020) 147(16):dev182725. doi: 10.1242/dev.182725

77. Conn VM, Hugouvieux V, Nayak A, Conos SA, Capovilla G, Cildir G, et al. A circRNA from SEPALLATA3 regulates splicing of its cognate mRNA through r-loop formation. *Nat Plants* (2017) 3:17053. doi: 10.1038/nplants.2017.53

78. Wang L, Long H, Zheng Q, Bo X, Xiao X, Li B. Circular RNA circRHOT1 promotes hepatocellular carcinoma progression by initiation of NR2F6 expression. *Mol Cancer* (2019) 18(1):119. doi: 10.1186/s12943-019-1046-7

79. Zheng Q, Bao C, Guo W, Li S, Chen J, Chen B, et al. Circular RNA profiling

reveals an abundant circHIPK3 that regulates cell growth by sponging multiple miRNAs. *Nat Commun* (2016) 7:11215. doi: 10.1038/ncomms11215

80. Huang R, Zhang Y, Han B, Bai Y, Zhou R, Gan G, et al. Circular RNA HIPK2 regulates astrocyte activation *via* cooperation of autophagy and ER stress by targeting MIR124-2HG. *Autophagy* (2017) 13(10):1722–41. doi: 10.1080/15548627.2017.1356975

81. Ding C, Yi X, Wu X, Bu X, Wang D, Wu Z, et al. Exosome-mediated transfer of circRNA CircNFIX enhances temozolomide resistance in glioma. *Cancer Lett* (2020) 479:1–12. doi: 10.1016/j.canlet.2020.03.002

82. Ge J, Wang J, Xiong F, Jiang X, Zhu K, Wang Y, et al. Epstein-Barr Virus-encoded circular RNA CircBART2.2 promotes immune escape of nasopharyngeal carcinoma by regulating PD-L1. *Cancer Res* (2021) 81(19):5074–88. doi: 10.1158/0008-5472.CAN-20-4321

83. Wu J, Guo X, Wen Y, Huang S, Yuan X, Tang L, et al. N6-methyladenosine modification opens a new chapter in circular RNA biology. *Front Cell Dev Biol* (2021) 9:709299. doi: 10.3389/fcell.2021.709299

84. Wang X, Ma R, Zhang X, Cui L, Ding Y, Shi W, et al. Crosstalk between N6-methyladenosine modification and circular RNAs: current understanding and future directions. *Mol Cancer* (2021) 20(1):121. doi: 10.1186/s12943-021-01415-6

85. Chen YG, Chen R, Ahmad S, Verma R, Kasturi SP, Amaya L, et al. N6-methyladenosine modification controls circular RNA immunity. *Mol Cell* (2019) 76 (1):96–109.e9. doi: 10.1016/j.molcel.2019.07.016

86. Tornesello ML, Faraonio R, Buonaguro L, Annunziata C, Starita N, Cerasuolo A, et al. The role of microRNAs, long non-coding RNAs, and circular RNAs in cervical cancer. *Front Oncol* (2020) 10:150. doi: 10.3389/fonc.2020.00150

87. Legnini I, Di Timoteo G, Rossi F, Morlando M, Briganti F, Sthandier O, et al. Circ-ZNF609 is a circular RNA that can be translated and functions in myogenesis. *Mol Cell* (2017) 66(1):22–37.e9. doi: 10.1016/j.molcel.2017.02.017

88. Wesselhoeft RA, Kowalski PS, Parker-Hale FC, Huang Y, Bisaria N, Anderson DG, et al. And can extend translation duration in vivo. *Mol Cell* (2019) 74(3):508–520.e4. doi: 10.1016/j.molcel.2019.02.015

89. Park OH, Ha H, Lee Y, Boo SH, Kwon DH, Song HK, et al. Endoribonucleolytic cleavage of m(6)A-containing RNAs by RNase P/MRP complex. *Mol Cell* (2019) 74(3):494–507.e8. doi: 10.1016/j.molcel.2019.02.034

90. Chen R, Wang SK, Belk JA, Amaya L, Li Z. Angel cardenas, et al., engineering circular RNA for enhanced protein production. *Nat Biotechnol* (2022). doi: 10.1038/s41587-022-01393-0

91. Merrick WC, Pavitt GD. Protein synthesis initiation in eukaryotic cells. *Cold Spring Harb Perspect Biol* (2018) 10(12):a033092. doi: 10.1101/cshperspect.a033092

92. Johnson AG, Grosely R, Petrov AN, Puglisi JD. Dynamics of IRES-mediated translation. *Philos Trans R Soc Lond B Biol Sci* (2017) 372(1716):20160177. doi: 10.1098/rstb.2016.0177

93. Dave P, George B, Sharma DK, Das S. Polypyrimidine tract-binding protein (PTB) and PTB-associated splicing factor in CVB3 infection: an ITAF for an ITAF. *Nucleic Acids Res* (2017) 45(15):9068–84. doi: 10.1093/nar/gkx519

94. Gharbi J, Ben M'hadheb-Gharbi M, Souii A. Impaired binding of standard initiation factors eIF3b, eIF4G and eIF4B to domain V of the live-attenuated coxsackievirus B3 Sabin3-like IRES–alternatives for 5'UTR-related cardiovirulence mechanisms. *Diagn Pathol* (2013) 8:161. doi: 10.1186/1746-1596-8-161

95. Verdecia M, Kokai-Kun JF, Kibbey M, Acharya S, Venema J, Atouf F. COVID-19 vaccine platforms: Delivering on a promise? *Hum Vaccin Immunother* (2021) 17(9):2873–93. doi: 10.1080/21645515.2021.1911204

96. WHO Expert Committee on Biological Standardization. *Annex 3 evaluation of the quality, safety and efficacy of messenger RNA vaccines for the prevention of infectious diseases- regulatory considerations*. WHO (2021).

97. World Health Organization. *Evaluation of the quality, safety and efficacy of RNA-based*. WHO (2020).

98. United States Pharmacopeial Convention. *Analytical procedures for mRNA vaccine quality*. The United States Pharmacopeial Convention (2022).

99. Center for Drug Evaluation of China. *Technical guidelines for pharmaceutical research on mRNA vaccines for the prevention of 2019 novel coronavirus (Trial)*. Center for Drug Evaluation of China (2020).

100. EUROPEAN MEDICINES AGENCY. *EMA-consideration on core requirements for RMPs of COVID-19 vaccines*. European Medicines Agency (2022).

101. Food and Drug Administration. *Q&A for spikevax (COVID-19 vaccine mRNA)*. European Medicines Agency (2022).

102. Food and Drug Administration. *Q&A for comirnaty (COVID-19 vaccine mRNA)*. Food and Drug Administration (2022).

103. EUROPEAN MEDICINES AGENCY *EMA-reflection paper on the regulatory requirements for vaccines intended to provide protection against variant strain(s) of SARS-CoV-2*. European Medicines Agency (2021).

104. Oberstra J, Schonborn J, Breyel1 E, Tittgen J, Schumacher J, Lukacs N. Monoclonal antibodies to double-stranded RNA as probes. *Nucleic Acids Res* (1991) 19(11):2993. doi: 10.1093/nar/19.11.2993

105. Bonin M, Oberstraß JÜRgen, Lukacs N, Ewert K, Oesterschulze E, Kassing R, et al. Determination of preferential binding sites for anti-dsRNA antibodies on double-stranded RNA by scanning force microscopy. *Rna* (2000) 6(4):563–70. doi: 10.1017/s1355838200992318

106. Sorensen EW, Nelson J, Mintri S, Rabideau AE, Zheng W, Besin G, et al. Impact of mRNA chemistry and manufacturing process on innate immune activation. *Sci Adv* (2020) 6:eaaz6893. doi: 10.1126/sciadv.aaz6893

107. Zoltán Kis Simon D, Kontoravdi C, Shah N. A blueprint for quality by digital design to support rapid RNA vaccine process development, manufacturing & supply. *accine Insights* (2022) 1(4):219–33. doi: 10.18609/vac.2022.33

108. Daniel S, Kis Z, Kontoravdi C, Shah N. Quality by design for enabling RNA platform production processes. *Trends Biotechnol* (2022) 40(10):1213–28. doi: 10.1016/j.tibtech.2022.03.012

109. Damase TR, Sukhovershin R, Boada C, Taraballi F, Pettigrew RI, Cooke JP. The limitless future of RNA therapeutics. *Front Bioeng Biotechnol* (2021) 9:628137. doi: 10.3389/fbioe.2021.628137

110. Wadman M. The overlooked superpower of mRNA vaccines. *Science* (2021) 373(6554):479. doi: 10.1126/science.373.6554.479

111. Stuart LM. In gratitude for mRNA vaccines. *N Engl J Med* (2021) 385 (15):1436–8. doi: 10.1056/NEJMcibr2111445

112. Topol EJ. Messenger RNA vaccines against SARS-CoV-2. *Cell* (2021) 184 (6):1401. doi: 10.1016/j.cell.2020.12.039

113. Kumar A, Blum J, Thanh Le T, Havelange N, Magini D, Yoon IK. The mRNA vaccine development landscape for infectious diseases. *Nat Rev Drug Discovery* (2022) 21(5):333–4. doi: 10.1038/d41573-022-00035-z

114. Liu CX, Guo SK, Nan F, Xu YF, Yang L, Chen LL. RNA Circles with minimized immunogenicity as potent PKR inhibitors. *Mol Cell* (2022) 82(2):420–434.e6. doi: 10.1016/j.molcel.2021.11.019

115. Kariko K, Buckstein M, Ni H, Weissman D. Suppression of RNA recognition by toll-like receptors: the impact of nucleoside modification and the evolutionary origin of RNA. *Immunity* (2005) 23(2):165–75. doi: 10.1016/j.immuni.2005.06.008

116. Paramasivam A, Vijayashree Priyadharsini J. Novel insights into m6A modification in circular RNA and implications for immunity. *Cell Mol Immunol* (2020) 17(6):668–9. doi: 10.1038/s41423-020-0387-x

117. Flemming A. The enigma of circular RNA. *Nat Rev Immunol* (2019) 19 (6):351. doi: 10.1038/s41577-019-0173-0

118. Zhou Y, Wu J, Yao S, Xu Y, Zhao W, Tong Y, et al. DeepCIP: a multimodal deep learning method for the prediction of internal ribosome entry sites of circRNAs. *bioRxiv preprint server Biol* (2022). doi: 10.1101/2022.10.03.510726

119. Packer M, Gyawali D, Yerabolu R, Schariter J, White P. A novel mechanism for the loss of mRNA activity in lipid nanoparticle delivery systems. *Nat Commun* (2021) 12(1):6777. doi: 10.1038/s41467-021-26926-0

120. Azarpanah H, Farhadloo M, Vahidov R, Pilote L. Vaccine hesitancy: evidence from an adverse events following immunization database, and the role of cognitive biases. *BMC Public Health* (2021) 21(1):1686. doi: 10.1186/s12889-021-11745-1

121. Han J, Li S, Feng Y, He Y, Hong W, Ye Z. A novel circular RNA (hsa_circ_0059930)-mediated miRNA-mRNA axis in the lipopolysaccharide-induced acute lung injury model of MRC-5 cells. *Bioengineered* (2021) 12 (1):1739–51. doi: 10.1080/21655979.2021.1916276

122. Singh B, Kaur P, Cedeno L, Brahimi T, Patel P, Virk H, et al. COVID-19 mRNA vaccine and myocarditis. *Eur J Case Rep Internal Med* (2021) 8(7):2681. doi: 10.12890/2021_002681

frontiers | Frontiers in Immunology

TYPE Original Research
PUBLISHED 27 January 2023
DOI 10.3389/fimmu.2023.1101808



OPEN ACCESS

EDITED BY
Wei Wang,
Jiangsu Institute of Parasitic Diseases (JIPD), China

REVIEWED BY
Rajesh Valanparambil,
Emory University, United States
Shetty Ravi Dyavar,
Adicet Bio, Inc, United States
Hemalatha Babu,
Emory University, United States

*CORRESPONDENCE
Woong-Yang Park
woongyang@gmail.com
Yeon-Sook Kim
idalicekim@gmail.com
Nam-Hyuk Cho
chonh@snu.ac.kr

†These authors have contributed equally to this work and share first authorship

SPECIALTY SECTION
This article was submitted to Viral Immunology, a section of the journal Frontiers in Immunology

RECEIVED 18 November 2022
ACCEPTED 09 January 2023
PUBLISHED 27 January 2023

CITATION
Jeon K, Kim Y, Kang SK, Park U, Kim J, Park N, Koh J, Shim M-S, Kim M, Rhee YJ, Jeong H, Lee S, Park D, Lim J, Kim H, Ha N-Y, Jo H-Y, Kim SC, Lee J-H, Shon J, Kim H, Jeon YK, Choi Y-S, Kim HY, Lee W-W, Choi M, Park H-Y, Park W-Y, Kim Y-S and Cho N-H (2023) Elevated IFNA1 and suppressed IL12p40 associated with persistent hyperinflammation in COVID-19 pneumonia.
*Front. Immunol.* 14:1101808.
doi: 10.3389/fimmu.2023.1101808



# Elevated IFNA1 and suppressed IL12p40 associated with persistent hyperinflammation in COVID-19 pneumonia

Kyeongseok Jeon[1,2†], Yuri Kim[1†], Shin Kwang Kang[3†], Uni Park[1,2†], Jayoun Kim[4], Nanhee Park[4], Jaemoon Koh[5], Man-Shik Shim[3], Minsoo Kim[2], Youn Ju Rhee[3], Hyeongseok Jeong[6], Siyoung Lee[7], Donghyun Park[7], Jinyoung Lim[8], Hyunsu Kim[8], Na-Young Ha[9], Hye-Yeong Jo[10], Sang Cheol Kim[10], Ju-Hee Lee[10], Jiwon Shon[11], Hoon Kim[11,12], Yoon Kyung Jeon[5], Youn-Soo Choi[2], Hye Young Kim[2], Won-Woo Lee[1,2], Murim Choi[2], Hyun-Young Park[13], Woong-Yang Park[7,8*], Yeon-Sook Kim[6*] and Nam-Hyuk Cho[1,2,14,15,16*]

[1]Department of Microbiology and Immunology, Seoul National University College of Medicine, Seoul, Republic of Korea, [2]Department of Biomedical Sciences, Seoul National University College of Medicine, Seoul, Republic of Korea, [3]Department of Thoracic and Cardiovascular Surgery, Chungnam National University School of Medicine, Deajon, Republic of Korea, [4]Medical Research Collaborating Center, Seoul National University Hospital, Seoul, Republic of Korea, [5]Department of Pathology, Seoul National University College of Medicine, Seoul, Republic of Korea, [6]Department of Internal Medicine, Chungnam National University School of Medicine, Deajon, Republic of Korea, [7]Geninus Inc., Seoul, Republic of Korea, [8]Samsung Genome Institute, Samsung Medical Center, Seoul, Republic of Korea, [9]Chungnam National University Hospital, Biomedical Research Institute, Deajon, Republic of Korea, [10]Division of Healthcare and Artificial Intelligence, Department of Precision Medicine, Korea National Institute of Health, Korea Disease Control and Prevention Agency, Cheongju, Republic of Korea, [11]Department of Biohealth Regulatory Science, School of Pharmacy, Sungkyunkwan University, Suwon-si, Gyeonggi-do, Republic of Korea, [12]Biopharmaceutical Convergence Major, School of Pharmacy, Sungkyunkwan University, Suwon-si, Gyeonggi-do, Republic of Korea, [13]Department of Precision Medicine, Korea National Institute of Health, Korea Disease Control and Prevention Agency, Cheongju, Republic of Korea, [14]Institute of Endemic Diseases, Medical Research Center, Seoul National University, Seoul, Republic of Korea, [15]Seoul National University Bundang Hospital, Seongnam, Gyeonggi-do, Republic of Korea, [16]Wide River Institute of Immunology, Seoul National University, Hongcheon, Gangwon-do, Republic of Korea

**Introduction:** Despite of massive endeavors to characterize inflammation in COVID-19 patients, the core network of inflammatory mediators responsible for severe pneumonia stillremain remains elusive.

**Methods:** Here, we performed quantitative and kinetic analysis of 191 inflammatory factors in 955 plasma samples from 80 normal controls (sample n = 80) and 347 confirmed COVID-19 pneumonia patients (sample n = 875), including 8 deceased patients.

**Results:** Differential expression analysis showed that 76% of plasmaproteins (145 factors) were upregulated in severe COVID-19 patients comparedwith moderate patients, confirming overt inflammatory responses in severe COVID-19 pneumonia patients. Global correlation analysis of the plasma factorsrevealed two core inflammatory modules, core I and II, comprising mainly myeloid cell and lymphoid cell compartments, respectively, with enhanced impact in a severity-

dependent manner. We observed elevated IFNA1 and suppressed IL12p40, presenting a robust inverse correlation in severe patients, which was strongly associated with persistent hyperinflammation in 8.3% of moderate pneumonia patients and 59.4% of severe patients.

**Discussion:** Aberrant persistence of pulmonary and systemic inflammation might be associated with long COVID-19 sequelae. Our comprehensive analysis of inflammatory mediators in plasmarevealed the complexity of pneumonic inflammation in COVID-19 patients anddefined critical modules responsible for severe pneumonic progression.

KEYWORDS

COVID-19, SARS-CoV-2, pneumonia, inflammation, IFNa, IL-12p40

# Introduction

Coronavirus disease 2019 (COVID-19), caused by respiratory infection with severe acute respiratory syndrome coronavirus 2 (SARS-CoV-2), has spread worldwide with a disastrous impact on humankind. Currently, there have been more than 607 million infections globally, leading to over six million deaths due to acute respiratory distress syndrome (ARDS) as of September 2022 (https://covid19.who.int/). The pathogenesis of SARS-CoV-2-induced pneumonia is rather heterogeneous depending on clinical stage and may occur in two phases. First, the initial viral phase is characterized by viral replication resulting in direct virus-mediated tissue damage. Second, the extent of this damage response may sequentially determine the complex immunopathogenesis causing a local and systemic inflammatory response that can persist even after viral clearance (1, 2). Therefore, an optimal combination of antiviral and anti-inflammatory therapies may be required to prevent severe pneumonic progression and disease mortality in a stage- and severity-dependent manner (3). Further studies incorporating the impact of direct viral damage and sequential immunopathogenesis might be required to identify the best targets for early intervention and severity-specific treatment of COVID-19 since we have a limited understanding of key driving initiators of severe pulmonary inflammation and long COVID syndrome, also known as post-acute sequelae of SARS-CoV-2 infection.

In this study, we performed extensive quantitation of 191 proteins involved in various innate and adaptive immune responses and inflammation in plasma samples collected longitudinally from 347 confirmed COVID-19 pneumonia patients with well-defined clinical information and an additional 80 uninfected normal subjects. Plasma proteomics may reflect the integrated landscape of pulmonary and systemic inflammation in COVID-19 patients. Systemic analysis of kinetic changes and correlation according to disease stage and severity may also hold the promise of revealing causal relationships among the various inflammatory mediators. In addition, we confirmed their primary cellular sources based on single cell RNA (scRNA) sequencing data sets from lung autopsy and respiratory specimens. These results enabled us to define key inflammatory modules of molecular and cellular components involved in severe pneumonic progression, deduce their functional and causal relationship with stronger correlation power, and provide important insights into underlying mechanisms of driving effectors in severe COVID-19 patients in the context of relevant clinical outcomes. Therefore, our study may present key prognostic predictors required for biomarker development of effective therapeutics as well as advanced criteria for selecting patients for intensive care.

# Materials and methods

## Study design, patient information, and ethics statement

We enrolled 80 uninfected volunteers without respiratory disease and 347 SARS-CoV-2 PCR-positive patients admitted to Chungnam National University Hospital (Daejon, Republic of Korea), Seoul Medical Center (Seoul, Republic of Korea), and Samsung Medical Center (Seoul Republic of Korea). COVID-19 patients were categorized based on WHO severity definitions (https://covid19.who.int/) (4). General information on the baseline characteristics of the study participants included in this study are summarized in Table 1. Peripheral blood was collected in ethylenediaminetetraacetic acid (EDTA) tubes during hospitalization and centrifuged to collect plasma within 24 h after collection. Then, plasma samples were stored at -80°C before analysis. Lung autopsy samples were obtained from six deceased COVID-19 patients. Experiments conformed to the Declaration of Helsinki principles, and written informed consent was obtained from all donors or their legal guardians prior to the study. The clinical research was approved by the institutional review boards of Chungnam National University Hospital (IRB no.: CNUH 2020-12-002-008), Seoul Medical Center (IRB no.: SEOUL 2021-02-016), Samsung Medical Center (IRB no.: SMC-2021-03-160), Seoul National University Hospital (IRB no.: C-1509-103-705), and the Korea National Institute of Health (IRB no.: 2020-09-03-C-A).

## Multiplex immunoassay of plasma proteins

To identify the differentially regulated plasma factors depending on COVID-19 disease severity, 350 plasma factors (Supplementary Table

TABLE 1 Demographics and baseline characteristics of COVID-19 patients.

| Variables | Normal Control (N = 80) | COVID-19 | | | p-value*** |
|---|---|---|---|---|---|
| | | Total (N = 347) | Moderate (N = 315) | Severe (N = 32) | |
| | | WHO severity | Grade 4 (N = 280) | Grade 6-9 (N = 24) | |
| | | | Grade 5 (N = 35) | Grade 10 (N = 8) | |
| Sex, N (%) | | | | | 0.791 |
| male | 40 (50.0%) | 188 (54.0%) | 171 (54.1%) | 17 (53.1%) | |
| female | 40 (50.0%) | 159 (46.0%) | 144 (45.9%) | 15 (46.9%) | |
| Age, year | | | | | <0.0001 |
| mean ± SD. | 45.6 ± 16.9 | 53.5 ± 17.6 | 52.0 ± 17.3 | 68.1 ± 13.5 | |
| range | 21-78 | 19-92 | 19-92 | 36-91 | |
| BMI, kg/m2 | | | | | 0.091 |
| mean ± SD. | 24.0 ± 3.6 | 24.2 ± 3.9 | 24.2 ± 3.9 | 23.4 ± 4.3 | |
| range | 17.0-31.0 | 12.4-39.4 | 12.4-39.4 | 15.9-31.2 | |
| Comorbidity, N (%) | | | | | |
| Hypertension | 18 (22.5%) | 113 (32.7%) | 94 (29.9%) | 19 (59.4%) | 0.0012 |
| Diabetes | 7 (8.8%) | 78 (22.5%) | 60 (19.1%) | 18 (56.3%) | <0.0001 |
| Cardiovascular ds. | 2 (2.5%) | 21 (6.1%) | 16 (5.1%) | 7 (21.9%) | 0.1814 |
| Respiratory ds. | 0 (0.0%) | 14 (4.0%) | 10 (3.2%) | 4 (12.5%) | 0.0159 |
| Kidney ds. | 0 (0.0%) | 13 (3.8%) | 11 (3.5%) | 2 (6.3%) | 0.1474 |
| Other chronic ds.* | 1 (1.3%) | 31 (9.0%) | 26 (8.3%) | 5 (15.6%) | <0.0001 |
| Treatment, N (%) | | | | | |
| Antibiotics | | 56 (16.2%) | 44 (14.0%) | 12 (37.5%) | |
| Antiviral drugs | | 44 (12.7%) | 23 (7.3%) | 19 (59.4%) | |
| Corticosteroids | | 73 (21.1%) | 43 (13.7%) | 30 (93.8%) | |
| Other therapies** | | 101 (29.2%) | 93 (29.6%) | 8 (25%) | |
| Time from onset to O2 therapy, Days | | | | | |
| mean ± SD. | | 7.1 ± 4.0 | 7.4 ± 3.6 | 6.7 ± 4.4 | |
| range | | 1-18 | 1-18 | 1-18 | |

*neoplasia, chronic liver ds., or dementia.
**Immune plasma, monoclonal antibodies, anticoagulant, or Pyramax.
***One-way ANOVA was used to estimate p-values for significant difference in demographic features among normal control, moderate, and severe groups.

S1) from 20 plasma samples (10 from 3 moderate patients and 10 from 5 severe patients) were screened by quantitative immunoassays using a total of 21 multiplex panels according to the manufacturers' instructions *via* a multiplex assay service (Koma Biotech., Seoul, Republic of Korea). Four types of commercially available kits were used for measurement (Supplementary Table S1). The MILLIPLEX MAP Human Complement Magnetic Bead Panel 2 (Millipore, Burlington, MA, USA) included C1q, C3, C3b/iC3b, C4, complement factor B, complement factor H, and properdin. The MILLIPLEX MAP Human Sepsis Magnetic Bead Panel 3 (Millipore) included elastase 2, lactoferrin, NGAL, resistin, and thrombospondin-1. Magnetic Luminex Performance Assay multiplex kits (R&D Systems, Inc. Minneapolis, MN, USA) were used for TGF-β1-3. Magnetic Luminex Screening Assay multiplex kits (R&D systems, Inc.) included all the other factors measured in this study. Assay plates were read with a Luminex 100/200TM analyzer (ThermoFisher, Waltham, MA, USA). For quantification for each factor, the supplied standard proteins were used, and a standard curve was drawn by the best fit algorithm using MasterPlex QT 2010 software (MiraiBio, Hitachi, CA, USA). We used detection limit values of non-detected factors below the detection range (Supplementary Table S2). Based on the screening results, 191 plasma factors were selected for further studies (Supplementary Tables S3).

## Lung tissue preparation, H&E staining, and scRNA sequencing

Lung autopsy samples obtained from deceased patients were immediately fixed in 10% formalin or immersed in RNAlater solution (ThermoFisher) for paraffin embedding or scRNA

sequencing, respectively. Paraffin-embedded lung tissue samples were prepared as previously reported (5). Briefly, the tissues that were fixed overnight were dehydrated and defatted by immersing in ethanol and xylene sequentially and treated with melted paraffin (58-60°C). Paraffin-embedded tissues were cut at a thickness of 4 μm and stained with hematoxylin and eosin (H&E). Lung pathology was evaluated and analyzed by two experienced pathologists under a light microscope (BX-53, Olympus, Tokyo, Japan). For scRNA sequencing, lung tissues were dissociated into single cells by chopping with a blade and were incubated in RPMI1640 containing 1 mg/ml Collagenase IV (ThermoFisher) and 0.1 mg/ml DNase I (Worthington, Columbus, OH, USA) at 37°C for 30 min. Lung single cells were filtered by nylon mesh and 70 μm cell strainers (Falcon) and centrifuged at 1,000 x *g* for 5 min. After RBC lysis, cell counts and viability were measured with a Countess 3 Automated Cell Counter (ThermoFisher), and 20,000 live cells were used to generate gel beads-in-emulsion (GEMs) by using the Chromium Single Cell 5' Library and Gel Bead Kits v.1 and a Chromium Controller (10x Genomics) according to the manufacturer's instructions, as we previously reported (6). After GEM-RT incubation and cDNA amplification, the cDNA quality and concentration were analyzed and calculated using an Agilent Bioanalyzer (Agilent Technologies, Santa Clara, CA, USA), and scRNA sequencing was performed using the NextSeq 550 platform (Illumina, San Diego, CA, USA).

## Bioinformatics of scRNA-seq and statistical analysis

The raw sequencing data for scRNA-seq were processed with CellRanger (version 3.1.0) (7). Reads were aligned to the combined genome of human (GRCh38, Ensembl) and SARS-CoV-2 (ASM985889v3, NCBI). The feature-barcode matrices were generated using the CellRanger count. The cells of the feature-barcode matrices were filtered by the numbers of expressed genes and the mitochondrial-to-total gene count ratio. The filtered feature-barcode matrices were used to create Seurat (version 4.1.1) objects (8). The Seurat objects were normalized using the SCTransform algorithm. To align the cells originating from different samples, 3,000 highly variable genes from each sample were selected. Anchors representing a similar biological state across samples based on the overlap in their nearest neighbors were sought, and samples were aligned based on the top 20 canonical correlation vectors. The aligned samples were scaled, and principal component analysis (PCA) was conducted. The cells were clustered by unsupervised clustering (0.2 resolution) and visualized by UMAP. To identify marker genes, upregulated genes in each cluster relative to the other clusters were selected on the basis of the Wilcoxon rank sum test implemented in Seurat FindAllMarkers function with >0.25 log fold change compared with other clusters and a Bonferroni-adjusted $P < 0.05$. By manual inspection, the 17 different clusters were assigned to 13 cell types.

Unsupervised clustering of samples, patients, or plasma factors was performed using the *k*-means algorithm. The optimum number of clusters was determined by using silhouette coefficient analysis in NBClust and factoextra packages (R package Version 1.0.7.). Before data visualization, each feature was scaled and centered as a z score using the scale function in R software. Multiple group comparisons were performed using the two-tailed Mann–Whitney test or Kruskal–Wallis test. Spearman's correlation test was performed using the corrplot package in R software. For visualization, heatmaps and dot plots were generated using the ComplexHeatmap (9) and ggplot2 packages, respectively. Correlation plots were generated with the corrplot package by only showing correlations with $p < 0.05$ and ordered by hierarchical clustering. Core I and core II in the global correlation network are indicated based on hierarchical clustering results in the correlation plot.

## Gene ontology and pathway enrichment analysis

Plasma factors were considered to be expressed differentially if there were significant differences ($p < 0.05$) in comparison among the NC group, moderate group (grades 4 and 5), and severe group (grades 6~10). These differentially expressed proteins were subjected to gene set enrichment analysis to assess the biological function related to COVID-19 severity. Enrichment analysis of GO biological pathways and hallmark gene sets was performed using the clusterProfiler (10) and enrichR (11) packages of R statistical software (R core team, 2020), respectively. Enriched terms were visualized using ggplot2 (12).

## Linear mixed model analyses

Demographic and baseline characteristics were expressed as the mean with standard deviation and range for continuous variables and frequencies with percentages for categorical variables. Differences among group severities in plasma factors were assessed with independent samples *t* test or Wilcoxon rank sum test according to their normality. In addition, if the results of group comparison were statistically significant, pairwise multiple comparison with Bonferroni correction was applied. We performed hierarchical clustering with all plasma factors to distinguish biologically distinct subgroups with a distance-based algorithm. A linear mixed model was used to investigate the periodically measured plasma factor changes over time, adjusting for age and sex. Statistical analysis was conducted using SAS 9.4 software (SAS system for Windows, version 9.4; SAS Institute, Cary, NC, USA) and the R package (version 4.2.1, R Core Team, 2020; R: A language and environment for statistical computing. R Foundation for Statistical Computing, Vienna, Austria. URL https://www.R-project.org/).

## Quantitation of viral loads

Real-time reverse transcription-polymerase chain reaction (RT–PCR) assays for the detection of SARS-CoV-2 were performed according to the manufacturer's instructions (Kogenebiotech, Seoul, Republic of Korea) (5). Total RNA was obtained from nasopharyngeal and throat swab (upper respiratory tract) and sputum (lower respiratory tract) samples. Primer sets targeting the E and RdRP genes of SARS-CoV-2 were used with a cutoff cycle threshold (Ct) value higher than 38 cycles.

10.3389/fimmu.2023.1101808

# Results

## Patient characteristics

The baseline characteristics of the confirmed COVID-19 patients included in this study are summarized in Table 1 and Figure 1A. The uninfected normal control (NC) group included 80 sex- and age-matched individuals who provided 80 plasma specimens. A total of 347 hospitalized patients with confirmed COVID-19 pneumonia participated in our cohort and were classified based on WHO clinical grading (grade 4-10: 4, moderate disease without oxygen therapy; 5, moderate COVID-19 with oxygen therapy by mask or nasal prongs; 6, severe disease treated with noninvasive ventilation or high flow oxygen; 7, severe disease with intubation and mechanical ventilation [$pO_2/FiO_2 \geq 150$ or $SpO_2/FiO_2 \geq 200$]; 8, severe disease with mechanical ventilation [$pO_2/FiO_2 < 150$ or $SpO_2/FiO_2 < 200$] or

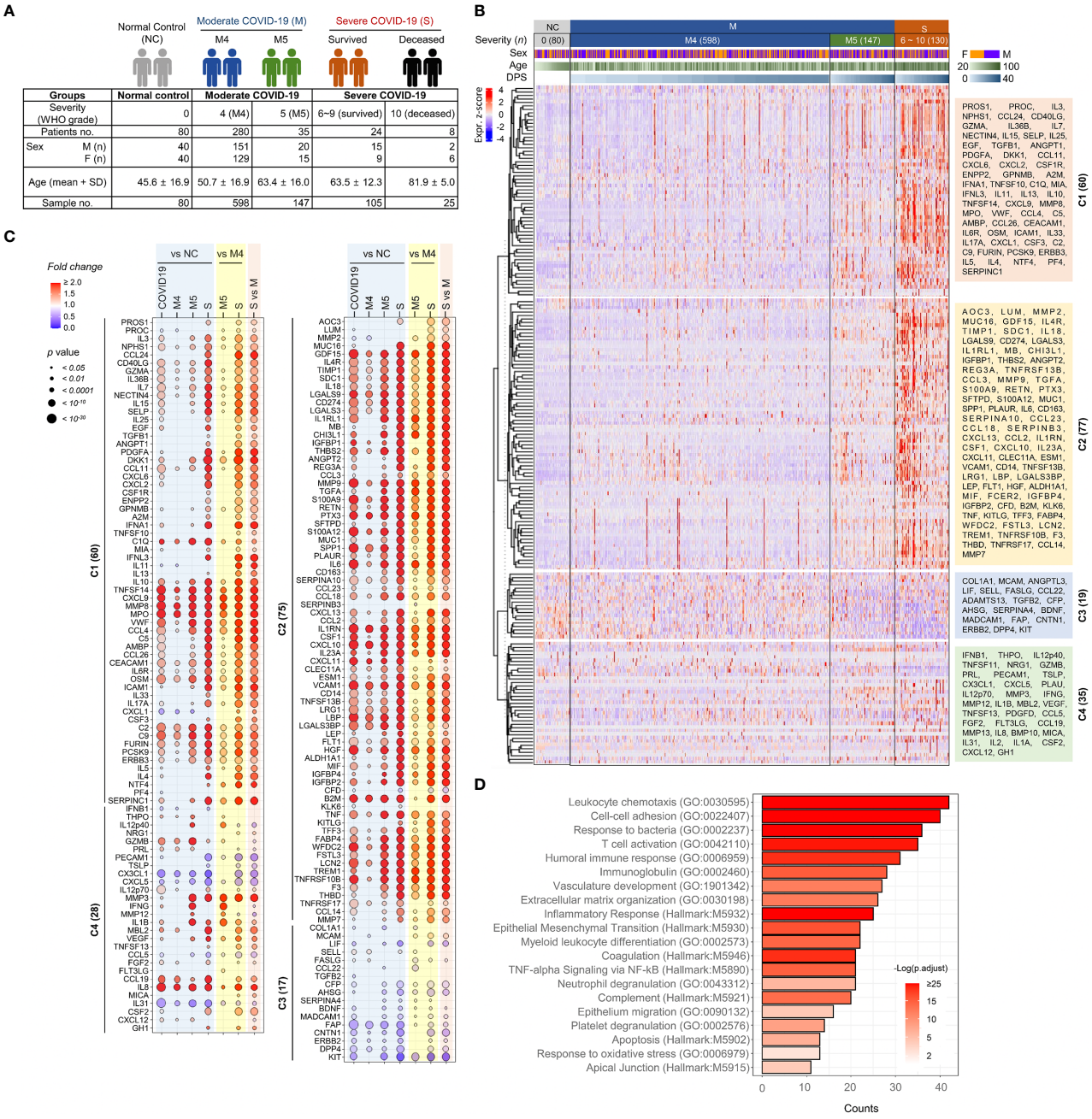


| Groups | Normal control | Moderate COVID-19 | | Severe COVID-19 | |
|---|---|---|---|---|---|
| Severity (WHO grade) | 0 | 4 (M4) | 5 (M5) | 6~9 (survived) | 10 (deceased) |
| Patients no. | 80 | 280 | 35 | 24 | 8 |
| Sex M (n) | 40 | 151 | 20 | 15 | 2 |
| Sex F (n) | 40 | 129 | 15 | 9 | 6 |
| Age (mean + SD) | 45.6 ± 16.9 | 50.7 ± 16.9 | 63.4 ± 16.0 | 63.5 ± 12.3 | 81.9 ± 5.0 |
| Sample no. | 80 | 598 | 147 | 105 | 25 |

FIGURE 1
Overt inflammatory responses associated with severe COVID-19 pneumonia. **(A)** Overview of the study cohort. **(B)** Unsupervised hierarchical clustering of 191 plasma factors measured by multiplexed immunoassay presented four separated clusters, C1-C4. The plasma samples are arranged according to COVID-19 severity (M: moderate pneumonia, S: severe pneumonia) and the collection days post-symptom onset (DPS). Eighty plasma samples collected from uninfected volunteers (NCs) are also included. The heatmap shows z scores and clustering determined using correlation and average linkage. **(C)** Bubble plots show the relative fold change in the average level of each plasma factor in comparison with indicated patient groups. The statistical significance in difference among the subject groups was calculated with the Mann–Whitney test or Kruskal–Wallis test. **(D)** Gene Ontology (GO) and hallmark gene set-based enrichment analyses of differentially regulated plasma proteins among NCs and COVID-19 patients present representative biological processes and the number of counts with statistical significance.

vasopressors; 9, severe COVID-19 treated with mechanical ventilation [$pO_2/FiO_2$ < 150] and vasopressors, dialysis, or extracorporeal membrane oxygenation; and 10, deceased patients) (https://covid19.who.int/) (4). The moderate group with grade 4 (M4) or 5 (M5) COVID-19 included 280 and 35 patients, respectively. The severe COVID-19 group with grades 6 to 10 (S6 ~ S10) included 32 patients, with 8 deceased patients due to fatal ARDS. The NC, moderate, and severe COVID-19 groups had similar proportions of male and female patients, but the age distribution in the severe group (mean ± S.D.: 68.1 ± 13.5) was older than those in the NC (45.6 ± 16.9) and moderate groups (52.0 ± 17.3). The severe group presented a significantly higher proportion of comorbidities, such as hypertension and diabetes, than the NC and moderate groups (Table 1). All patients were recruited before July 2021 and were not immunized with the COVID-19 vaccine before infection.

First, we investigated the potential association of disease severity with viral loads in respiratory secretions (13). The overall viral loads in the upper (nasopharyngeal swab specimens) and lower (sputum specimens) respiratory tract samples were not significantly different between the moderate and severe groups (Supplementary Figure S1A-C). When we assessed the potential effect of age on viral dynamics, overall viral loads tended to be similar among the patient groups regardless of age (old: ≥60, young: <60) and severity (Supplementary Figure S1C), even though older patients in the M4 group showed significantly higher viral loads than older patients in the severe group, especially based on lower respiratory tract specimens.

## Overt inflammatory responses associated with severe COVID-19 pneumonia

To screen plasma factors differentially regulated according to the disease severity of COVID-19, we performed quantitative immunoassays using 21 multiplex panels detecting 350 plasma factors that are functionally associated with various types of inflammation and immune responses (Supplementary Table S1). In the pilot test, 20 plasma samples (10 from 3 moderate patients and 10 from 5 severe patients) collected after symptom onset were analyzed (Supplementary Table S2), and we selected 191 plasma factors (Supplementary Table S3), namely, 60 factors showing significant differences between the samples from the moderate and severe groups in the initial screening and 131 plasma proteins potentially associated with pulmonary and systemic inflammation reported in previous studies (14–19). Plasma samples were longitudinally collected from 347 COVID-19 patients 1~6 times at 3~7-day intervals. Quantitative analysis of the 191 selected factors in 955 plasma specimens from 80 NCs ($n$=80 plasma samples) and 347 COVID-19 patients ($n$=875 plasma samples) was performed, and the results are summarized in Figure 1B. Unbiased hierarchical clustering of the Z-score trajectories of all the plasma factors demonstrated four clearly separated major clusters (C1 ~ C4). C1 and C2 were generally elevated in severe patients when compared to NCs and moderate patients, whereas the C3 group tended to be decreased in severe patients (Figure 1C). The C1 factors showed more persistent responses, but the C2 factors tended to be decreased gradually at later stages. The C4 group factors presented heterogeneous responses with fluctuations depending on disease severity and course. A comparison of the overall mean values of the plasma factors among the NC and patient groups revealed that 180 factors were significantly and differentially regulated (Figure 1C). A comparison of the mean values between the NC and COVID-19 groups revealed that 153 plasma factors were significantly and differentially regulated (128 factors upregulated and 25 factors downregulated in COVID-19 patients). When we performed linear mixed model analysis to assess significant differences among the severity groups after adjusting for the age and sex of the patients to further confirm the specific association of the plasma factors with disease severity (Supplementary Table S4), 167 factors showed significant differences between the NC and COVID-19 groups and their time-dependent trajectories, even after adjusting for age and sex. Differential expression analysis between the moderate and severe COVID-19 groups indicated that 169 factors were significantly upregulated (145 factors) or downregulated (24 factors) in plasma from severe COVID-19 patients compared to moderate pneumonia patients (Figure 1C). Even though most of the differentially expressed plasma factors were gradually increased or decreased depending on disease severity, it is noteworthy that several factors, including IL12p40, GZMB, IFNG, MMP12, and IL1B, were significantly upregulated in the M5 group compared with the NC, M4, or severe COVID-19 groups (Figure 1C).

The 180 differentially regulated plasma factors in the NC and COVID-19 groups were subjected to Gene Ontology enrichment and hallmark gene set enrichment analyses (20, 21). Even though our quantitative assay was based on selected panels mainly related to immune responses and inflammation, relative enrichment of specific pathways was observed (Figure 1D). These included pathways primarily involved in leukocyte chemotaxis, cell–cell adhesion, response to bacterial molecules, T-cell activation, humoral immune response, vascular development, extracellular matrix organization, and epithelial-mesenchymal transition.

The kinetic responses of 170 plasma proteins showing significant differences among the NC, M4, M5, and severe groups are presented in Supplementary Figure S2. Kinetic changes in representative factors involved in the enriched functional pathways showed significant differences among the patient groups, as summarized in Figure 2. For example, a type I interferon, IFNA1, presenting a significantly higher response in severe COVID-19 patients, surged during the early phase of symptom onset and gradually declined, whereas IFNL3, a type III interferon, which was also significantly elevated in the severe group compared with the moderate group, gradually increased in severe patients during disease progression (Figure 2B). Other plasma factors involved in inflammation (IL6, IL10, IL13, MPO, and LBP), endothelial activation and coagulation (THBD, F3, VWF, PROS1, and MMP8), T-cell homeostasis and activation (IL7, IL15, IL18, IL4, and IL23A), and humoral response (IL4R, IL1RL1, IL33, TNFSF13B, and C9) were also significantly upregulated with various kinetic responses (Figures 2D–G). These overt inflammatory responses associated with severe disease progression were concomitantly presented with elevated tissue damage responses, such as vascular development (HGF, ENPP2, CHI3L1, THBS2, and ANGPT2), extracellular matrix organization (MMP2, MMP3, MMP9, PTX3, and SPP1), and epithelial mesenchymal transition (TGFB1, PLAUR, IGFBP2, IGFBP4, and SDC1) (Figures 2H–J), suggesting the complexity of dysregulated systemic inflammation potentially initiated from severe pulmonary insults by SARS-CoV-2 infection (5, 22, 23).

10.3389/fimmu.2023.1101808

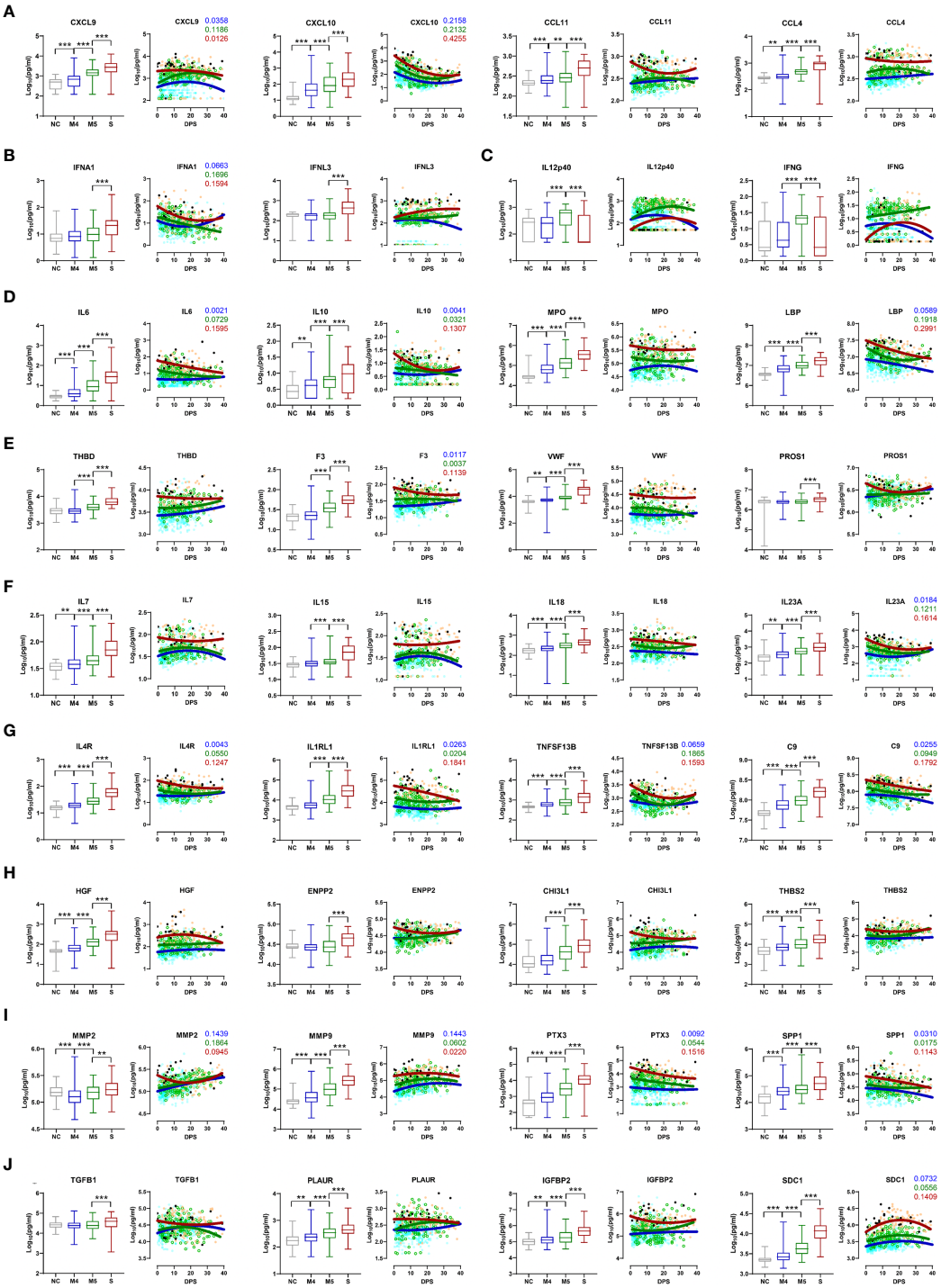


FIGURE 2
Kinetic changes in representative plasma factors differentially regulated among NCs and COVID-19 patients. Kinetic responses of representative inflammatory factors involved in leukocyte chemotaxis **(A)**, type I and III interferon response **(B)**, Th1 cytokines **(C)**, general inflammation **(D)**, endothelial activation and coagulation **(E)**, T-cell homeostasis and activation **(F)**, humoral response **(G)**, vascular development **(H)**, extracellular matrix organization **(I)**, and epithelial–mesenchymal transition **(J)**. The overall protein level of an indicated factor in plasma is compared among the NC and patient groups with the Kruskal–Wallis test (left panels) and their kinetic responses according to days post-symptom onset (DPS) (right panels). Solid lines indicate nonlinear regression. R squared values are colored accordingly if the value of any regression is above 0.1. Gray: NC, blue: M4 group, green: M5 group, red: severe group, and black dots for fatal cases. $^{**}p < 0.01$, $^{***}p < 0.001$.

## Cellular sources of plasma factors in the inflamed lungs of COVID-19 patients

Histopathologic examination of the lungs of patients who died due to COVID-19 revealed variable phases of diffuse alveolar damage from the acute exudative phase to the proliferative and fibrotic phases (Supplementary Figure S3). The pathologic findings from the lungs included diffuse interstitial thickening, fibrosis, granulation tissue formation and lymphoplasma cell infiltration with reactive type II pneumocyte hyperplasia and hyaline membrane formation in the alveolar wall. Occasional foci of macrophages, neutrophil infiltration with seromucinous fluid or hemorrhage in alveolar spaces were also observed. Focal pulmonary microthrombi or large vessel thrombi were identified in some patients.

SARS-CoV-2 RNA was barely detected in our autopsy samples by scRNA sequencing analysis, and 13 cell types were identified and manually annotated (Supplementary Figure S4, S5A). Macrophages were the predominant inflammatory cells, ranging from 47.9% to 78.7% of lung-infiltrating leukocytes. T cells were the second most dominant cell type, comprising 4.2% to 28.1%, and neutrophils accounted for 7.4~14.5% of the pulmonary leukocytes. NK and NKT cells represented approximately 5.2% and 1.9% of the pulmonary leukocytes, respectively, and B cells accounted for ~ 1.1% (Supplementary Figure S5B). We also observed that 0.7~3.0% of the leukocytes were mast cells in the lung autopsy samples from the patients who died. Some notable differences between the NC and fatal COVID-19 lungs were a relative decrease in NK cells in the patients (0.5–9.7%, mean=5.7%) *vs.* controls (mean: 16.1%) as well as an increase in macrophages (47.9–78.7%, mean=59.4%) and NKT cells (0.2–4.5%, mean=1.9%) in COVID-19 patients *vs.* controls (mean=43.7% and 0.4% for macrophages and NKT cells, respectively), even though the differences were not statistically significant. To further examine the respiratory leukocyte population in COVID-19 patients, we utilized two public scRNA data sets based on analyses of respiratory samples (nasopharyngeal and bronchoalveolar lavage fluid samples) (Supplementary Figure S6A) (24, 25). These included 9 NC sets and 36 COVID-19 samples from 28 patients (11 moderate and 17 severe patients, including 4 fatal cases). The relative proportions of specific leukocyte populations in the combined data set from COVID-19 patients revealed remarkable reductions in NK (moderate: 12.8%, severe: 2.6%) and T (moderate: 11.3%, severe: 5.1%) cell populations in the severe COVID-19 group compared to the moderate COVID-19 group (Supplementary Figure S6B). In contrast, neutrophils were increased in severe patients (30.1%) compared with moderate patients (19.5%). In addition, NKT cells (moderate: 5.5%, severe: 6.9%), B cells (moderate: 2.6%, severe: 3.7%), and macrophages (moderate: 48.2%, severe: 51.6%) were slightly increased in the severe group compared with the moderate group.

When we examined transcriptional expression of the plasma factors in the scRNA data sets to identify the cellular sources of the plasma proteins, we detected 180 transcripts among 191 factors in the scRNA data sets from our lung autopsy samples or previously deposited respiratory samples (24, 25). RNA transcripts for 124 plasma factors were detected in more than 10% of a specific cellular type and are summarized in Supplementary Figure S5C, S6C.

## Global correlation map of 191 plasma proteins in COVID-19 patients

To assess the potential associations of all 191 quantified proteins with each other in COVID-19 patient plasma, we generated a global correlation map (Figure 3). This consists of the pairwise correlation of 191 plasma factors in 875 patient samples (36,481 correlation coefficients) that were subjected to unsupervised hierarchical clustering (Figure 3A). This approach revealed 14,801 significantly ($p < 0.05$) correlated pairs showing either positive (12,584 pairs) or negative (2,217 pairs) correlations (Figure 3B). Among the significantly correlated pairs, 195 pairs presented robust positive correlation (Spearman's $r \geq 0.7$), and 2,745 pairs displayed moderate positive correlation ($0.7 >$ Spearman's $r \geq 0.4$), whereas only 37 pairs showed moderate negative correlation ($-0.7 <$ Spearman's $r \leq -0.4$). Based on the correlation coefficients and the number of significant correlators of each plasma factor displaying absolute Spearman's $r \geq 0.4$, we generated a global correlation map including 159 proteins (Figure 3C). We also annotated the primary cellular sources of each factor, as shown in Supplementary Figure S5C, S6C. The global correlation map presenting robust correlation (Spearman's $r \geq 0.7$ in red lines) highlighted two core modules, cores I and II. The core I module comprised 23 plasma factors mainly derived from macrophages (PTX3, MMP8, MPO, TIMP1, CD274, IL6, IL1RN, TREM1, CXCL9, LGALS3, and MMP9), neutrophils (PTX3, S100A9, MMP8, MPO, TIMP1, CD274, IL1RN, TREM1, MMP9, and S100A12), epithelial cells (WFDC2, GDF15, SDC1, TNFRSF10B, F3, LGALS3, LCN2, and FSTL3), and endothelial cells (IL6, FSTL3, and THBD) (Figure 3C). The core II module included 12 proteins primarily expressed in epithelial cells (IL7, IL36B, NECTIN4, and CXCL6), NK(T) and T cells (GZMA, CD40LG, and IL3), and fibroblasts (CCL11) (Figure 3C). The core I and II components displayed robust and multiple correlations with each other and significant correlations with approximately 170 factors on average, suggesting a strong and wide functional relationship. In addition, several core I factors, such as TIMP1, CD274, and IL6, were strongly correlated with LRG1 and LBP derived from epithelial cells and macrophages, respectively, as well as complement factors C2 and C9. Components of core II also strongly correlated with PDGFA, CXCL2, and TGFB1, which were primarily expressed in alveolar epithelial cells and T cells, respectively. Notably, CCL4 derived from NKT and T cells showed a strong positive correlation with several components of the core I and core II networks, suggesting a connective role between both inflammatory networks (Figure 3C).

We next examined changes in patterns of the correlation network in each severity group to assess the impact of plasma factors according to COVID-19 severity (Figure 4 and Supplementary Figure S7). The total number of significant correlation pairs with absolute Spearman's $r \geq 0.4$ gradually increased in a severity-dependent manner, and the severe group presented 3,121 correlated pairs, whereas the M4 group and M5 group had 1,576 and 2,086 significant correlated pairs, respectively, suggesting stronger and more diverse functional associations of the plasma factors during more severe disease progression (Supplementary Figure S7B). The global correlation map of the M4 and M5 groups (moderate pneumonia) with the robust correlated pairs (absolute Spearman's $r \geq 0.7$) included 39 and

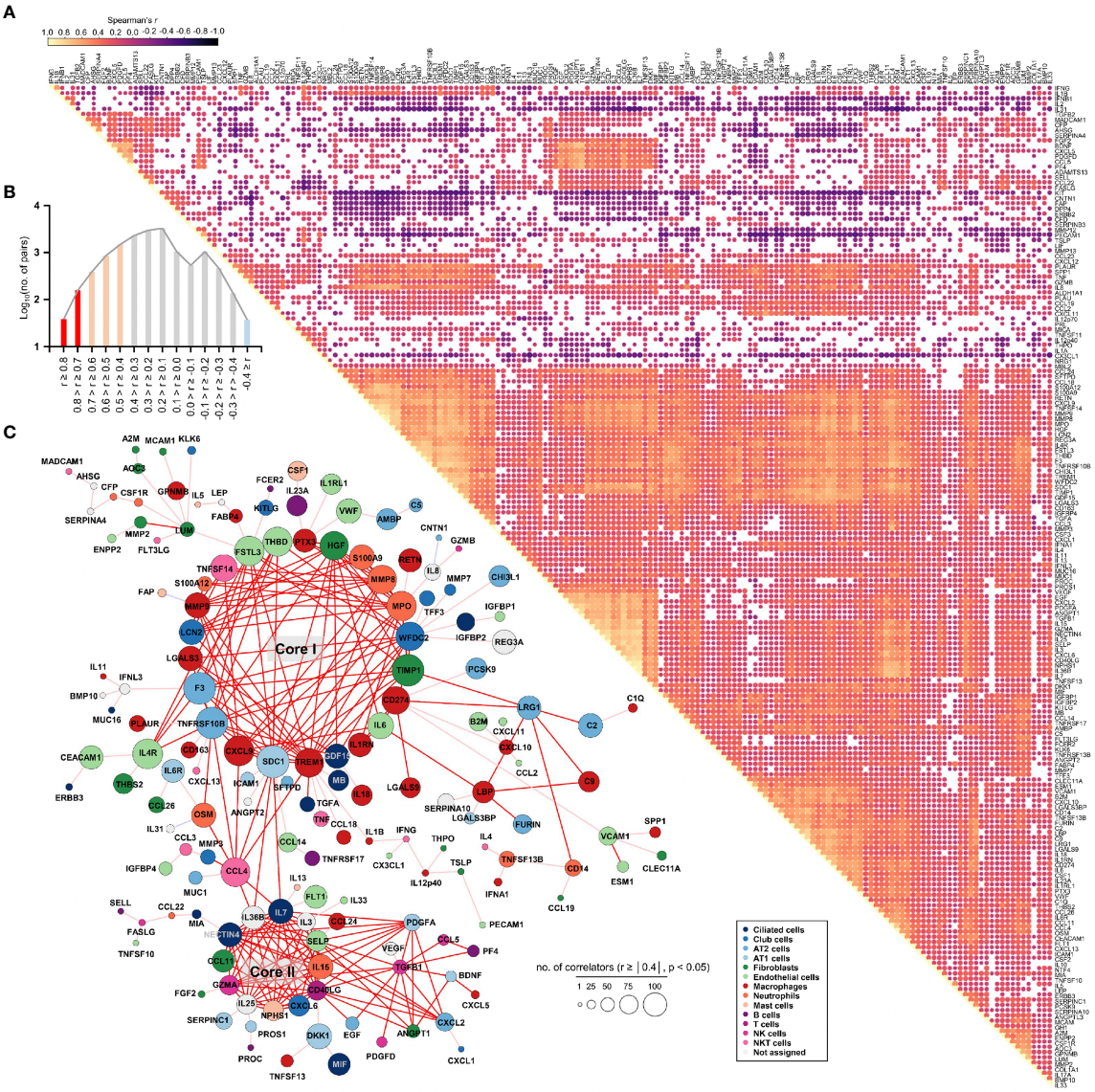


FIGURE 3
Global correlation map of 191 plasma proteins from COVID-19 pneumonia patients. **(A)**, Correlation matrix across all time points of 191 plasma factors from COVID-19 patients. Only significant correlations ($p < 0.05$) are represented as dots. Spearman's correlation coefficients from comparisons of protein measurements within the same specimen are visualized by color intensity. **(B)** Distribution of the number of significant correlation pairs ($p < 0.05$). Red (robust positive correlation): Spearman's $r \geq 0.7$, orange (moderate positive correlation): 0.7 > Spearman's $r \geq 0.4$, and sky blue (moderate negative correlation): -0.7 < Spearman's $r \leq -0.4$. There was no robust negative correlation pair (Spearman's $r \leq -0.7$). **(C)** Global correlation map of 159 proteins based on the correlation coefficients and the number of significant correlators of each plasma factor displaying an absolute Spearman's $r \geq 0.4$. The circle size is proportionally adjusted depending on the number of significant correlators, and the color code of each component is determined based on primary cellular source (see Supplementary Figure S5C, S6C). All the correlation pairs with Spearman's $r \geq 0.7$ are linked by a red line. If the absolute r value of maximum correlation was more than 0.4 but less than 0.7, only the best correlator is linked by either a pink line (positive corr.) or a sky blue line (negative corr.).

66 proteins, respectively (Figures 4A, B). The severe group presented 72 factors with robust correlations, and the number of significantly (absolute Spearman's $r \geq 0.4$) correlated pairs of robust correlators ($n$=1,975) was drastically increased when compared with those of the M4 ($n$=710) and M5 ($n$=1,191) groups (Figure 4C and Supplementary Figure S7B). We observed that the number of robust correlators in the core I module in the M5 ($n$=17) and severe ($n$=16) groups was higher than that in the M4 group ($n$=9). In contrast, the robust correlators in the core II module seemed to be rather conserved regardless of disease severity, but the number of significantly correlated pairs (absolute Spearman's $r \geq 0.4$) was increased, especially those of CXCL6, IL15, GZMA, and NECTIN4. These results suggest that pneumonic progression requiring oxygen supply (M5 and severe groups) might be facilitated by more diverse inflammatory mediators in the core I module, whereas critical pneumonic commitment requiring intensive respiratory care (severe group) may be associated with enhanced impact on other mediators by the members of the core II module. Additionally, several factors, such as ENPP2, C5, FASLG, VWF, IFNA1, and CSF1, newly appeared as robust positive correlators strongly associated with more diverse plasma factors in the severe group than in the moderate group (Figure 4C), also indicating their enhanced impact on other plasma factors during severe pneumonic

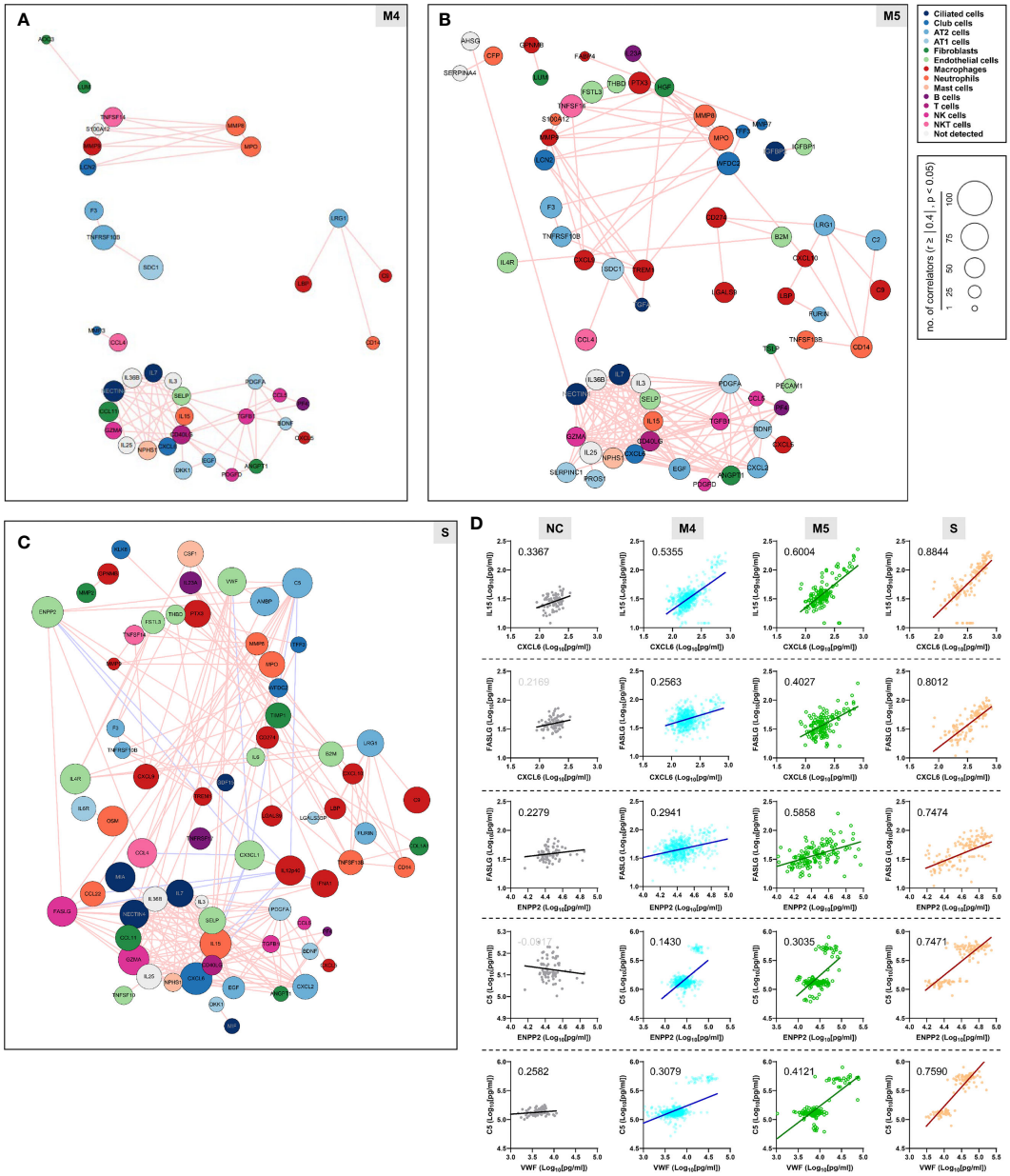


FIGURE 4
Enhanced correlation in quantity and quality among the plasma factors according to COVID-19 severity. Correlation maps of plasma proteins displaying robust correlation power (absolute Spearman's $r \geq 0.7$) in plasma samples from moderate **(A)** M4 and **(B)** M5 and severe patients **(C)** S are presented. The circle size is proportionally adjusted depending on the number of significant correlators (absolute Spearman's $r \geq 0.4$), and the color code of each component is determined based on primary cellular source. All the correlated pairs with a Spearman's $r \geq 0.7$ are linked by either pink (positive corr.) or sky blue lines (negative corr.). **(D)** Representative correlation plots of the indicated plasma factors which show enhanced correlation power in quantity and quality according to COVID-19 severity. Spearman's *r* value for each plot is presented.

progression in COVID-19 patients. Consistently, we observed a gradual increase in correlation power among the top correlators, such as IL-15, CXCL6, FASLG, ENPP2, C5, and VWF, in the severe group as the disease severity was aggravated (Figure 4D). Furthermore, we noticed that IL12p40 and CX3CL1 displayed strong positive correlations with each other but showed robust negative correlations with other inflammatory mediators, such as C5, ENPP2, CCL22, FASLG, CCL4, VWF, IL15, and CXCL6, in the severe patient group (Figure 4C, 5, and Supplementary Figure S8). The degree of negative correlation of IL12p40 and CX3CL1 with inflammatory factors gradually increased depending on COVID-19 severity (Figure 5A, B), suggesting that suppression of IL12p40 and CX3CL1 might be associated with enhanced inflammatory responses driving critical pneumonic progression in patients. In addition, IL12p40 was the top negative correlate of IFNA1 in the severe group, and their inverse correlation was gradually enhanced according to COVID-19 severity (Figures 5C, D). IFNA1 also presented a robust positive correlation with CCL11, FASLG, and IL23A in severe patients, and their correlation power was gradually enhanced as COVID-19 severity increased.

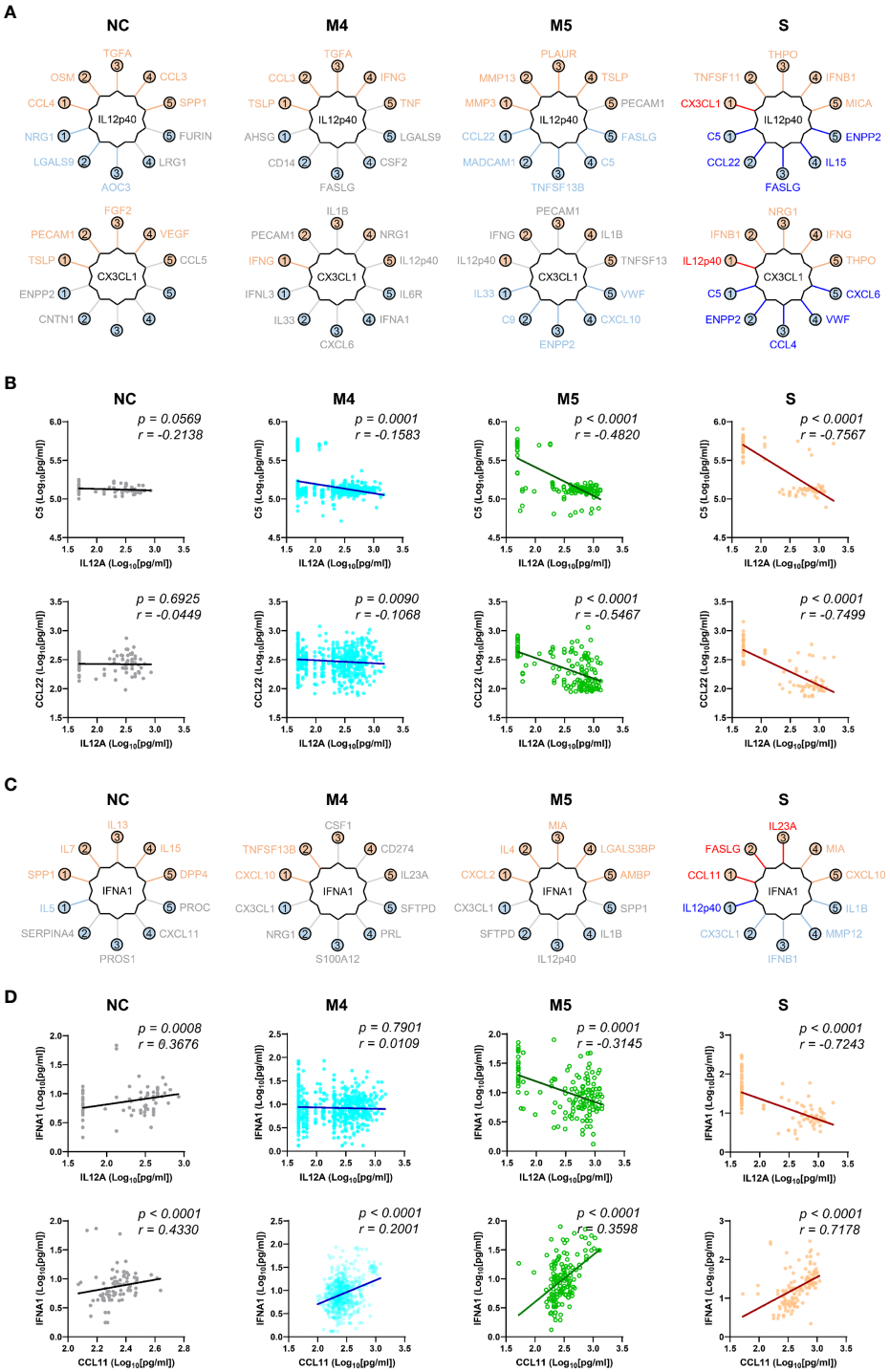


FIGURE 5
Robust inverse correlation of IL12p40 and CX3CL1 with various inflammatory mediators and IFNA1 in severe COVID-19 patients. **(A)** Top 5 positive and negative correlators of IL12p40 and CX3CL1 in NC and COVID-19 patients with various disease severities (M4 and M5: moderate pneumonia, S: severe pneumonia). Upper factors are the best 5 positive correlators and lower mediators are the best 5 negative correlators of IL12p40 and CX3CL1. The color of each factor is annotated according to the value of their correlation coefficient; red and blue: robust correlation with absolute Spearman's $r \geq 0.7$, orange and sky blue: moderate correlation with 0.7 > absolute Spearman's $r \geq 0.4$, and gray: no significant correlation ($p > 0.05$). **(B)** Representative correlation plots of IL12p40 with C5 (upper panels) and CCL22 (lower panels). Spearman's *r* and *p* value for each plot are presented. **(C)** Top 5 positive and negative correlators of IFNA1 in NC and COVID-19 patients with various disease severities (M4 and M5: moderate pneumonia, S: severe pneumonia). Color code of each factor is applied as in **(A, D)**. Representative correlation plots of IFNA1 with IL12p40 (upper panels) and CCL11 (lower panels). Spearman's *r* and *p* value for each plot are presented.

## Association of elevated IFNA1 and suppressed IL12p40 with hyperinflammation in COVID-19 pneumonia

When we examined the plasma factors in the plasma samples or patient data sets with average values from the moderate patients by principal component analysis (PCA) and unbiased clustering, there were two separate groups, MG1 ($n$=289, 91.7%) and MG2 ($n$=26, 8.3%) (Figures 6A, C, and Supplementary Figure S9). Interestingly, MG2 patient samples presented consistent elevation of a group of plasma factors regardless of plasma collection time (Supplementary Figure S9A). Even though this does not clearly differentiate the disease severity, MG2 patients tended to present significantly higher levels of inflammatory mediators than MG1 patients (Figure 6E) and associated with more severe COVID-19 than MG1 patients (Figure 6F). Comparison of the mean values between MG1 and MG2 patients revealed that 155 plasma factors were significantly and differentially regulated (145 factors upregulated and 10 factors downregulated in MG2 patients) (Supplementary Table S5). Among them, MMP8 (7.8-fold), CXCL1 (7.0-fold), PTX3 (6.4-fold), VWF (5.0-fold), C1Q (4.9-fold), CXCL10 (4.8-fold), TNFSF14 (4.7-fold), EGF (4.6-fold), MPO (4.6-fold), PDGFA (4.6-fold), CSF1 (4.6-fold), SERPINC1 (4.6-fold), and CSF3 (4.3-fold) in MG2 patients compared to MG1 patients were upregulated by more than four times on average (Figure 6C). In addition, IFNA1 was significantly elevated in MG2 patients by 2.8-fold compared with MG1 patients. In contrast, IL12p40 (0.3-fold), KIT (0.3-fold), and CX3CL1 (0.3-fold) were significantly suppressed in MG2 patients compared with MG1 patients by more than 60% on average (Figure 6C).

PCA and blinded clustering of the plasma samples or patient data sets with average values of the plasma factors from the severe group also defined two patient groups, SG1 ($n$=13, 40.6%) and SG2 ($n$=19, 59.4%) (Figures 6B, D, and Supplementary Figure S10). The average z-score distribution of plasma factors in SG2 patients was significantly higher than that in SG1 patients, indicating more robust inflammatory responses in SG2 patients than in SG1 patients (Figure 6E). It is notable that the average z-score distribution in MG2 patients was even higher than that of SG1 patients, indicating that a proportion of moderate patients (MG2) could present even higher inflammatory responses than SG1 patients despite their lower clinical severity (Figure 6E). Nevertheless, we observed no significant difference in disease severity (Figure 6F) and patient age between the two severe patient groups (Figure 6G). A comparison of the mean values between SG1 and SG2 patients revealed that 102 plasma factors were significantly differentially regulated (85 factors upregulated and 17 factors downregulated in SG2 patients) (Supplementary Table S5). Among them, CXCL10 (4.3-fold), VWF (4.2-fold), PTX3 (3.7-fold), EGF (3.6-fold), CSF1 (3.6-fold), C5 (3.6-fold), REG3A (3.3-fold), CCL22 (3.3-fold), and IFNA1 (3.1-fold) in SG2 patients compared to SG1 patients were upregulated by more than three times on average. In contrast, IL12p40 (0.1-fold), THPO (0.2-fold), IFNG (0.3-fold), CX3CL1 (0.3-fold), KIT (0.3-fold), MMP12 (0.4-fold), and MICA (0.4-fold) were significantly suppressed in SG2 patients compared with SG1 patients by more than 60% on average (Figure 6D). Nonetheless, 14 factors, namely, IL18, WFDC2, HGF, VCAM1, ANGPT2, GDF15, IL1RL1, MUC16, TGFA, CCL23, MMP7, SPP1, PLAUR, and LGALS3, were consistently and significantly elevated in the severe patients (SG1 and SG2) compared with the moderate patients (MG1 and MG2) (Supplementary Table S5). Notably, the majority of these factors were mainly derived from respiratory epithelial cells (IL18, WFDC2, GDF15, MUC16, TGFA, MMP7, and LGALS3) and macrophages (IL18, SPP1, PLAUR, CCL23, and LGALS3) (Figure 3C; Supplementary Figure S5C , S6C).

# Discussion

The main target of SARS-CoV-2 in gas exchange units is type II alveolar cells, which serve as progenitor cells for type I cells and provide homeostatic repair mechanisms after injury. Hence, direct viral damage to type II cells can significantly impair respiratory function, often leading to severe pneumonic progression (26). Higher viral loads may not be critically associated with severe disease, as demonstrated by our current and previous studies (13, 27). Moreover, when we compared viral loads and kinetics in respiratory samples from our COVID-19 cohort and more pathogenic MERS-CoV-infected patients (mortality: 20.4%) during the 2015 Korean outbreak (Supplementary Figure S1D, E) (28), viral loads of SARS-CoV-2 in respiratory specimens generally peaked upon symptom onset and rapidly declined thereafter, whereas MERS-CoV loads peaked 4-10 days after symptom onset. There was no significant difference in overall viral loads and kinetics in COVID-19 patients depending on age and disease severity, but the viral loads of MERS-CoV were significantly higher among non-survivors than among survivors. Viral kinetics display more persistent replication with a clear delay in the peak response approximately 12-14 days after symptom onset in deceased MERS patients with older age (Supplementary Figure S1D, E) (28). Viral kinetics in pathogenic SARS-CoV-1 infections (mortality: ~10%) also show a peak response approximately 10 days after symptom onset (29). These results clearly indicate that more pathogenic CoVs, such as SARS-CoV-1 and MERS-CoV, present more sustained viral replication in the respiratory tracts of severe patients, with peak responses at approximately the second week after symptom onset, and the higher viral loads tend to be correlated with disease severity and patient age. In contrast, viral loads of SARS-CoV-2 peaking upon symptom onset declined rapidly as the disease and inflammation progressed regardless of disease severity and patient age, strongly suggesting that the degree of pathogenic inflammatory response seems to be determined primarily by host factors rather than higher viral loads.

Although previous studies have already reported massive proteomic analysis in sera or plasma from COVID-19 patients by mass spectrometry or proximity extension assays (16, 17, 30–34), our current study used highly sensitive and multiplexed immunoassays to measure precise concentration ranges in plasma. In addition, our cohort included a relatively large patient size, focused only on pneumonic patients with well-defined clinical scores and stages, and analyzed the majority of inflammatory factors associated with pulmonary and systemic inflammation reported in previous studies (14–19). In differential expression analysis between the moderate and severe COVID-19 groups, 169 factors out of 191 proteins were significantly upregulated (145 factors) or downregulated (24 factors) in plasma from severe patients compared to moderate

10.3389/fimmu.2023.1101808

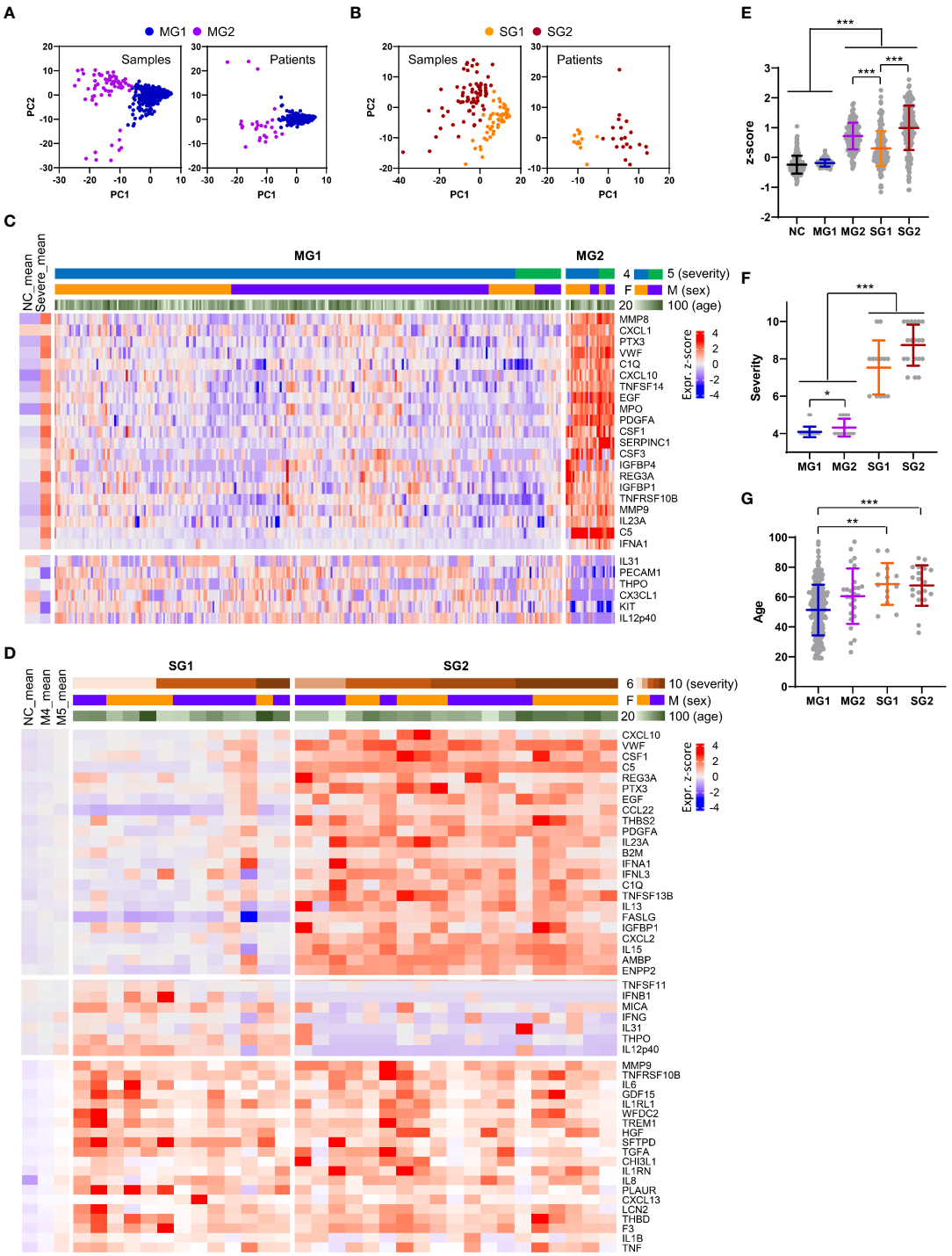


FIGURE 6
Heterogeneity of inflammatory responses in COVID-19 pneumonia patients. **(A, B)** PCA of plasma proteins in moderate (MG1 and MG2, **(A)** and severe (SG1 and SG2, 9B) COVID-19 patients. Each dot represents 1 plasma sample or the mean value of a single patient. **(C)** Z-score heatmap with unsupervised clustering of the mean concentrations of plasma factors defines the MG1 and MG2 groups of moderate COVID-19 patients. Representative plasma proteins differentially expressed between the MG1 and MG2 groups were selected and presented. The average z scores of the NCs (NC_mean) and severe patients (severe_mean) are shown in the left panel. **(D)** Z-score heatmap with unsupervised clustering of the mean concentration of plasma factors defines the SG1 and SG2 groups of severe COVID-19 patients. Representative plasma proteins differentially expressed between the SG1 and SG2 groups or significantly elevated in both severe groups when compared to the moderate groups were selected and presented. The average z scores of the NCs (NC_mean) and moderate patients (M4_mean and M5_mean) are shown in the left panel. **(E)** Distribution of the mean z scores of 191 factors in the NC group, moderate groups (MG1 and MG2), and severe groups (SG1 and SG2). **(F)** Distribution of disease severity in the moderate groups (MG1 and MG2) and severe groups (SG1 and SG2). **(G)** Age distribution in the moderate groups (MG1 and MG2) and severe groups (SG1 and SG2). Statistical significance among the patient groups was calculated with the Kruskal–Wallis test (**$p < 0.01$, ***$p < 0.001$).

patients (Figure 1C). These include a type I interferon, IFNA1, mainly derived from activated macrophages, and various inflammatory features of hyperinflammatory responses (IL6, IL10, IL13, MPO, and LBP), chemokine responses (CXCL10, CXCL9, CXCL11, IL-8, CCL4, CXCL13, CXCL2, CCL11, CXCL6, CCL2, CCL26, CCL19, CCL18, CCL24, CCL14, PF4, and CCL23), endothelial activation and coagulation (THBD, F3, VWF, PROS1, and MMP8), T-cell homeostasis and activation (IL7, IL15, IL18, IL4, and IL23A), and humoral responses (IL4R, IL1RL1, IL33, TNFSF13B, and C9) as well as elevated tissue damage responses, including vascular development (HGF, ENPP2, CHI3L1, THBS2, and ANGPT2), extracellular matrix organization (MMP2, MMP3, MMP9, PTX3, and SPP1), and epithelial mesenchymal transition (TGFB1, PLAUR, IGFBP2, IGFBP4, and SDC1). These results suggest the complexity and acute initiation of dysregulated systemic inflammation induced by SARS-CoV-2 infection in patients with severe COVID-19. In addition, our extensive correlation analysis of the plasma factors together with scRNA sequencing data from lung autopsy and respiratory samples further defined two core inflammatory modules, cores I and II, and their primary cellular sources (Figure 3C). The core I components were mainly contributed by activated macrophages, neutrophils, epithelial cells, and endothelial cells, whereas the core II network was primarily linked to activated epithelial cells, NK(T) cells, and T cells. The quantity and quality of correlation power tended to be increased in the core I and core II networks in a severity-dependent manner (Figure 4), suggesting enhanced complexity and functional interactions among leukocytes and pulmonary parenchymal cells as viral pneumonia progresses (1, 2, 17, 25, 35). Considering the enhanced infiltration of neutrophils, macrophages, and NKT cells into inflamed lung tissue but reduced NK- and T-cell responses in severe COVID-19 patients compared with moderate patients (Supplementary Figure S5B, S6B), our current data implied a differential role of innate and adaptive immune cells in pathological changes during disease progression *via* specific expression and interactions among the key players of both core modules. Of note, a substantial increase in the correlation power and expression level of the core II network members involved in NKT-cell homeostasis and effector function promoting both humoral and cell-mediated immunity (36–38) may support the pathogenic role of the NKT-cell population in severe inflammation, although the specific contribution of their subpopulations to COVID-19 is still controversial and needs to be verified (39). Moreover, the core I and II modules were further associated with complement activation (5, 40) and aberrant TGFB response (41), respectively, observed in severe COVID-19 patients. Several inflammatory mediators, such as ENPP2, C5, FASLG, VWF, and CSF1, additionally presented a more robust correlation with the core inflammatory networks in the severe group (Figure 4C), and these factors were reported as independent significant indicators of severe COVID-19 in previous studies (1, 5, 42–44). We also observed that the plasma levels of several proteins mainly derived from respiratory epithelial cells (IL18, WFDC2, GDF15, MUC16, TGFA, MMP7, and LGALS3) and macrophages (IL18, SPP1, PLAUR, CCL23, and LGALS3) were capable of distinguishing moderate and severe COVID-19 significantly and consistently regardless of the overall inflammatory status of the patients (Supplementary Table S5); hence, the damaging response of pulmonary epithelial cells and dysregulated macrophage activation might be critical determinants of severe pneumonic progression.

Interestingly, we noticed that IL12p40 and CX3CL1 displayed strong positive correlations with each other but showed robust negative correlations with several core inflammatory modules, mainly in the severe patient group (Figure 4C). In addition, molecular signatures of cell-mediated immunity, such as IL12p40, IFNG, and GZMB, in the M5 group were specifically and significantly higher than those in the NC, M4, and severe groups (Figure 1C and 2C), suggesting their protective and pathogenic roles in moderate pneumonia. An elevated IFNA1 response displayed a strong negative correlation with IL12p40 and CX3CL1, whereas it presented a robust positive correlation with CCL11, FASLG, and IL23A, especially in severe COVID-19 patients (Figure 5). This also suggested that an aberrant type I IFN response during the acute phase of SARS-CoV-2 infection may be associated with immune dysregulation and disease progression in severe COVID-19 patients requiring extensive respiratory support. Indeed, our current data using sensitive immunoassays of the plasma of pneumonic COVID-19 patients support the pathogenic role of an acute surge in the IFNA1 response, at least in a proportion of severe pneumonia patients and COVID-19 patients who died, even though the specific role of type I and III interferons in severe COVID-19 progression is still controversial (45, 46). One of the striking features is the heterogeneous phenotype of hyperinflammation associated with the strong inverse correlation of IL12p40 and IFNA1 observed in both moderate and severe COVID-19 pneumonia patients (Figure 5 and 6). Given that IL12p40 is a common subunit of IL12p70 (heterodimer of IL12p35 and IL12p40) and IL23 (heterodimer of IL23p19 and IL12p40) (47), it is also intriguing to see significant upregulation of both IL12p70 and IL23 in severe patients than in moderate subjects (Figure 1C). In addition, IL12p40 presented significant negative correlation with both IL12p70 and IL23 (IL23p19) in COVID-19 patients (Supplementary Figure S11). Differential expression of these cytokine subunits may be due to heterogeneity of their primary cellular resources (IL12p40 from macrophages, IL12p35 and IL23p19 from non-hematopoietic epithelial cells or endothelial cells, see Figure S5 and S6) and heterodimeric interactions among various IL12 family cytokine subunits (47) during COVID-19 inflammation. Even though the heterodimeric subunits of IL-12 and IL23 are known to be simultaneously co-expressed in activated myeloid cells, they can also assemble to form functionally active heterodimers after secretion from different cell types *via* alternate two-cell pathway (48). Further study on regulation mechanisms governing the differential expression of various IL12 family cytokine subunits might be required to define their specific role in COVID-19 inflammation. Nonetheless, enhanced IFNA1 and a suppressed IL12p40 response strongly associated with persistent and overt inflammatory responses were detected even in a proportion of moderate pneumonia patients (8.3%, MG2) and in more than half (59.4%, SG2) of severe COVID-19 patients. Therefore, this unexpected reciprocal correlation of IFNA1 and IL12p40, mainly expressed in macrophages (Figure 4C), might also be strongly associated with the heterogeneity of dysregulated inflammation in pneumonic COVID-19 patients. Given that the severity of illness during acute COVID-19 is significantly but partially associated with long COVID-19 syndrome or post-acute COVID-19 (49), further follow-up studies on the potential linkage of post-acute COVID-19 with the overt inflammatory response

associated with an inverse correlation of higher IFNA1 and lower IL12p40 are needed. A recent review on long COVID-19 after breakthrough SARS-CoV-2 infection also suggested that vaccination before infection confers only partial protection in the post-acute phase of the disease and emphasized the need for continued optimization of strategies against post-acute syndrome even for people with breakthrough infection (50).

A limitation of our study is the inclusion of plasma samples rather biased toward moderate pneumonia cases (sample *n*=745) than severe pneumonia cases (sample *n*=130), and all these samples were obtained from unvaccinated patients with primary SARS-CoV-2 infection. The patients were also treated with various combinations of antiviral drugs and corticosteroids depending on disease severity during hospitalization. Therefore, further validation with a larger scale of plasma specimens from clinically variable COVID-19 patients, even after vaccination or reinfection, is needed.

## Data availability statement

The datasets presented in this study can be found in online repositories. The names of the repository/repositories and accession number(s) can be found in the article/Supplementary Material.

## Ethics statement

The clinical research was approved by the institutional review boards of Chungnam National University Hospital (IRB no.: CNUH 2020-12-002-008), Seoul Medical Center (IRB no.: SEOUL 2021-02-016), Samsung Medical Center (IRB no.: SMC-2021-03-160), Seoul National University Hospital (IRB no.: C-1509-103-705), and the Korea National Institute of Health (IRB no.: 2020-09-03-C-A). The patients/participants provided their written informed consent to participate in this study.

## Author contributions

W-YP, Y-SK, H-YP and N-HC designed this research. KJ, YK, SK, UP, JK, NP, JK, N-YH, M-SS, MK, YR, HJ, SL, DP, JL, HK, SK, J-HL, JS, HK, YJ, MC, H-YP, W-YP, Y-SK and N-HC collect human specimens, performed experiments, and analyzed the datasets. KJ, JayK, JS, HK, YJ, MC, and N-HC organized and presented the results. KJ, YK, UP, JaeK, YJ, MC, and N-HC contributed to the writing of the draft. JayK, HK, YJ, Y-SC, HK, W-WL, MC, and N-HC reviewed and revised the manuscript. All authors listed have made a substantial, direct, and intellectual contribution to the work and approved it for publication.

## Funding

This work was supported by grants from the Korea National Institute of Health Infrastructural Research Program (4800–4861–312–210–13), operation of data center for national biomedical data resources (2021-NI-017-00), the National Research Foundation (NRF) funded by the Ministry of Science and ICT (2021M3A9I2080490), 2022 Joint Research Project of Institutes of Science and Technology (to NHC), and the Basic Science Research Program through the National Research Foundation of Korea funded by the Ministry of Education (2022R1A6A3A1307317). KJ and UP received a scholarship from the BK21-plus education program provided by the National Research Foundation of Korea.

## Acknowledgments

We thank all the participants and the healthcare workers at Chungnam National University Hospital, Seoul Medical Center, and Samsung Medical Center for help and support.

## Conflict of interest

SL, DP and W-YP are employed by Geninus Inc.

The remaining authors declare that the research was conducted in the absence of any commercial or financial relationships that could be construed as a potential conflict of interest.

## Publisher's note



## Supplementary material

The Supplementary Material for this article can be found online at: https://www.frontiersin.org/articles/10.3389/fimmu.2023.1101808/full#supplementary-material

## References

1. Merad M, Blish CA, Sallusto F, Iwasaki A. The immunology and immunopathology of COVID-19. *Science.* (2022) 375(6585):1122–7. doi: 10.1126/science.abm8108

2. Paludan SR, Mogensen TH. Innate immunological pathways in COVID-19 pathogenesis. *Sci Immunol* (2022) 7(67):eabm5505. doi: 10.1126/sciimmunol.abm5505

3. Robinson PC, Liew DFL, Tanner HL, Grainger JR, Dwek RA, Reisler RB, et al. COVID-19 therapeutics: Challenges and directions for the future. *Proc Natl Acad Sci U S A.* (2022) 119(15):e2119893119. doi: 10.1073/pnas.2119893119

4. WHO Working Group on the Clinical Characterisation Management of COVID-Infection. A minimal common outcome measure set for COVID-19 clinical research. *Lancet Infect Dis* (2020) 20(8):e192–e7.

5. Kim DM, Kim Y, Seo JW, Lee J, Park U, Ha NY, et al. Enhanced eosinophil-mediated inflammation associated with antibody and complement-dependent pneumonic insults in critical COVID-19. *Cell Rep* (2021) 37(1):109798. doi: 10.1016/j.celrep.2021.109798

6. Lee T, Kim Y, Kim HJ, Ha NY, Lee S, Chin B, et al. Acute surge of atypical memory and plasma b-cell subsets driven by an extrafollicular response in severe COVID-19. *Front Cell Infect Microbiol* (2022) 12:909218. doi: 10.3389/fcimb.2022.909218

7. Zheng GX, Terry JM, Belgrader P, Ryvkin P, Bent ZW, Wilson R, et al. Massively parallel digital transcriptional profiling of single cells. *Nat Commun* (2017) 8:14049. doi: 10.1038/ncomms14049

8. Hao Y, Hao S, Andersen-Nissen E, Mauck WM3rd, Zheng S, Butler A, et al. Integrated analysis of multimodal single-cell data. *Cell.* (2021) 184(13):3573–87 e29. doi: 10.1016/j.cell.2021.04.048

9. Gu ZG, Eils R, Schlesner M. Complex heatmaps reveal patterns and correlations in multidimensional genomic data. *Bioinformatics.* (2016) 32(18):2847–9. doi: 10.1093/bioinformatics/btw313

10. Yu GC, Wang LG, Han YY, He QY. clusterProfiler: an r package for comparing biological themes among gene clusters. *Omics.* (2012) 16(5):284–7. doi: 10.1089/omi.2011.0118

11. Chen EY, Tan CM, Kou Y, Duan Q, Wang Z, Meirelles GV, et al. Enrichr: interactive and collaborative HTML5 gene list enrichment analysis tool. *BMC Bioinf* (2013) 14:128. doi: 10.1186/1471-2105-14-128

12. Ginestet C. ggplot2: Elegant graphics for data analysis. *J R Stat Soc Ser A.* (2011) 174:245. doi: 10.1111/j.1467-985X.2010.00676_9.x

13. Kim Y, Cheon S, Jeong H, Park U, Ha NY, Lee J, et al. Differential association of viral dynamics with disease severity depending on patients' age group in COVID-19. *Front Microbiol* (2021) 12:712260. doi: 10.3389/fmicb.2021.712260

14. Arunachalam PS, Wimmers F, Mok CKP, Perera R, Scott M, Hagan T, et al. Systems biological assessment of immunity to mild versus severe COVID-19 infection in humans. *Science.* (2020) 369(6508):1210–20. doi: 10.1126/science.abc6261

15. Shen B, Yi X, Sun Y, Bi X, Du J, Zhang C, et al. Proteomic and metabolomic characterization of COVID-19 patient sera. *Cell.* (2020) 182(1):59–72 e15.

16. Demichev V, Tober-Lau P, Lemke O, Nazarenko T, Thibeault C, Whitwell H, et al. A time-resolved proteomic and prognostic map of COVID-19. *Cell Syst* (2021) 12(8):780–94.e7.

17. Filbin MR, Mehta A, Schneider AM, Kays KR, Guess JR, Gentili M, et al. Longitudinal proteomic analysis of severe COVID-19 reveals survival-associated signatures, tissue-specific cell death, and cell-cell interactions. *Cell Rep Med* (2021) 2 (5):100287. doi: 10.1016/j.xcrm.2021.100287

18. Abers MS, Delmonte OM, Ricotta EE, Fintzi J, Fink DL, De Jesus AAA, et al. An immune-based biomarker signature is associated with mortality in COVID-19 patients. *JCI Insight* (2021) 6(1):e144455. doi: 10.1172/jci.insight.144455

19. Gutmann C, Takov K, Burnap SA, Singh B, Ali H, Theofilatos K, et al. SARS-CoV-2 RNAemia and proteomic trajectories inform prognostication in COVID-19 patients admitted to intensive care. *Nat Commun* (2021) 12(1):3406. doi: 10.1038/s41467-021-23494-1

20. Gene Ontology Consortium. The gene ontology resource: enriching a GOld mine. *Nucleic Acids Res* (2021) 49(D1):D325–D34. doi: 10.1093/nar/gkaa1113

21. Liberzon A, Birger C, Thorvaldsdottir H, Ghandi M, Mesirov JP, Tamayo P. The molecular signatures database (MSigDB) hallmark gene set collection. *Cell Syst* (2015) 1 (6):417–25. doi: 10.1016/j.cels.2015.12.004

22. Wong LR, Perlman S. Immune dysregulation and immunopathology induced by SARS-CoV-2 and related coronaviruses - are we our own worst enemy? *Nat Rev Immunol* (2022) 22(1):47–56. doi: 10.1038/s41577-021-00656-2

23. Tay MZ, Poh CM, Renia L, MacAry PA, Ng LFP. The trinity of COVID-19: Immunity, inflammation and intervention. *Nat Rev Immunol* (2020) 20(6):363–74. doi: 10.1038/s41577-020-0311-8

24. Liao M, Liu Y, Yuan J, Wen Y, Xu G, Zhao J, et al. Single-cell landscape of bronchoalveolar immune cells in patients with COVID-19. *Nat Med* (2020) 26(6):842–4. doi: 10.1038/s41591-020-0901-9

25. Chua RL, Lukassen S, Trump S, Hennig BP, Wendisch D, Pott F, et al. COVID-19 severity correlates with airway epithelium-immune cell interactions identified by single-cell analysis. *Nat Biotechnol* (2020) 38(8):970–9. doi: 10.1038/s41587-020-0602-4

26. Bridges JP, Vladar EK, Huang H, Mason RJ. Respiratory epithelial cell responses to SARS-CoV-2 in COVID-19. *Thorax.* (2022) 77(2):203–9. doi: 10.1136/thoraxjnl-2021-217561

27. Dadras O, Afsahi AM, Pashaei Z, Mojdeganlou H, Karimi A, Habibi P, et al. The relationship between COVID-19 viral load and disease severity: A systematic review. *Immun Inflammation Dis* (2022) 10(3):e580. doi: 10.1002/iid3.580

28. Yang JS, Yoo MG, Lee HJ, Jang HB, Jung HD, Nam JG, et al. Factors associated with viral load kinetics of middle east respiratory syndrome coronavirus during the 2015 outbreak in Republic of Korea. *J Infect Dis* (2021) 223(6):1088–92. doi: 10.1093/infdis/jiaa466

29. Peiris JS, Chu CM, Cheng VC, Chan KS, Hung IF, Poon LL, et al. Clinical progression and viral load in a community outbreak of coronavirus-associated SARS pneumonia: A prospective study. *Lancet.* (2003) 361(9371):1767–72. doi: 10.1016/S0140-6736(03)13412-5

30. Messner CB, Demichev V, Wendisch D, Michalick L, White M, Freiwald A, et al. Ultra-high-throughput clinical proteomics reveals classifiers of COVID-19 infection. *Cell Syst* (2020) 11(1):11–24.e4. doi: 10.1016/j.cels.2020.05.012

31. Al-Nesf MAY, Abdesselem HB, Bensmail I, Ibrahim S, Saeed WAH, Mohammed SSI, et al. Prognostic tools and candidate drugs based on plasma proteomics of patients with severe COVID-19 complications. *Nat Commun* (2022) 13(1):946. doi: 10.1038/s41467-022-28639-4

32. Geyer PE, Arend FM, Doll S, Louiset ML, Winter SV, Muller-Reif JB, et al. High-resolution serum proteome trajectories in COVID-19 reveal patient-specific seroconversion. *EMBO Mol Med* (2021) 13(8):e14167. doi: 10.15252/emmm.202114167

33. Shu T, Ning W, Wu D, Xu J, Han Q, Huang M, et al. Plasma proteomics identify biomarkers and pathogenesis of COVID-19. *Immunity.* (2020) 53(5):1108–22 e5. doi: 10.1016/j.immuni.2020.10.008

34. Gisby J, Clarke CL, Medjeral-Thomas N, Malik TH, Papadaki A, Mortimer PM, et al. Longitudinal proteomic profiling of dialysis patients with COVID-19 reveals markers of severity and predictors of death. *Elife.* (2021) 10:e64827. doi: 10.7554/eLife.64827.sa2

35. Szabo PA, Dogra P, Gray JI, Wells SB, Connors TJ, Weisberg SP, et al. Longitudinal profiling of respiratory and systemic immune responses reveals myeloid cell-driven lung inflammation in severe COVID-19. *Immunity.* (2021) 54(4):797–814 e6. doi: 10.1016/j.immuni.2021.03.005

36. Kumar A, Suryadevara N, Hill TM, Bezbradica JS, Van Kaer L, Joyce S. Natural killer T cells: An ecological evolutionary developmental biology perspective. *Front Immunol* (2017) 8:1858. doi: 10.3389/fimmu.2017.01858

37. Stock P, Lombardi V, Kohlrautz V, Akbari O. Induction of airway hyperreactivity by IL-25 is dependent on a subset of invariant NKT cells expressing IL-17RB. *J Immunol* (2009) 182(8):5116–22. doi: 10.4049/jimmunol.0804213

38. Middendorp S, Nieuwenhuis EE. NKT cells in mucosal immunity. *Mucosal Immunol* (2009) 2(5):393–402. doi: 10.1038/mi.2009.99

39. Koay HF, Gherardin NA, Nguyen THO, Zhang W, Habel JR, Seneviratna R, et al. Are NKT cells a useful predictor of COVID-19 severity? *Immunity* (2022) 55(2):185–7. doi: 10.1016/j.immuni.2022.01.005

40. Ma LN, Sahu SK, Cano M, Kuppuswamy V, Bajwa J, McPhatter J, et al. Increased complement activation is a distinctive feature of severe SARS-CoV-2 infection. *Sci Immunol* (2021) 6(59):eabh2259. doi: 10.1126/sciimmunol.abh2259

41. Witkowski M, Tizian C, Ferreira-Gomes M, Niemeyer D, Jones TC, Heinrich F, et al. Untimely TGFbeta responses in COVID-19 limit antiviral functions of NK cells. *Nature.* (2021) 600(7888):295–301. doi: 10.1038/s41586-021-04142-6

42. Nikitopoulou I, Fanidis D, Ntatsoulis K, Moulos P, Mpekoulis G, Evangelidou M, et al. Increased autotaxin levels in severe COVID-19, correlating with IL-6 levels, endothelial dysfunction biomarkers, and impaired functions of dendritic cells. *Int J Mol Sci* (2021) 22(18):10006. doi: 10.3390/ijms221810006

43. Andre S, Picard M, Cezar R, Roux-Dalvai F, Alleaume-Butaux A, Soundaramourty C, et al. T Cell apoptosis characterizes severe covid-19 disease. *Cell Death Differ* (2022) 29 (8):1486–99. doi: 10.1038/s41418-022-00936-x

44. Quartuccio L, Fabris M, Sonaglia A, Peghin M, Domenis R, Cifu A, et al. Interleukin 6, soluble interleukin 2 receptor alpha (CD25), monocyte colony-stimulating factor, and hepatocyte growth factor linked with systemic hyperinflammation, innate immunity hyperactivation, and organ damage in COVID-19 pneumonia. *Cytokine.* (2021) 140:155438. doi: 10.1016/j.cyto.2021.155438

45. Kim YM, Shin EC. Type I and III interferon responses in SARS-CoV-2 infection. *Exp Mol Med* (2021) 53(5):750–60. doi: 10.1038/s12276-021-00592-0

46. Schreiber G. The role of type I interferons in the pathogenesis and treatment of COVID-19. *Front Immunol* (2020) 11:595739. doi: 10.3389/fimmu.2020.595739

47. Floss DM, Moll JM, Scheller J. IL-12 and IL-23-Close relatives with structural homologies but distinct immunological functions. *Cells.* (2020) 9(10):2184. doi: 10.3390/cells9102184

48. Gerber AN, Abdi K, Singh NJ. The subunits of IL-12, originating from two distinct cells, can functionally synergize to protect against pathogen dissemination in vivo. *Cell Rep* (2021) 37(2):109816. doi: 10.1016/j.celrep.2021.109816

49. Nalbandian A, Sehgal K, Gupta A, Madhavan MV, McGroder C, Stevens JS, et al. Post-acute COVID-19 syndrome. *Nat Med* (2021) 27(4):601–15. doi: 10.1038/s41591-021-01283-z

50. Al-Aly Z, Bowe B, Xie Y. Long COVID after breakthrough SARS-CoV-2 infection. *Nat Med* (2022) 28(7):1461–7. doi: 10.1038/s41591-022-01840-0

frontiers | Frontiers in Immunology

TYPE Original Research
PUBLISHED 14 February 2023
DOI 10.3389/fimmu.2023.1107639



OPEN ACCESS

EDITED BY
Jingxin Li,
Jiangsu Provincial Center for Disease Control and Prevention, China

REVIEWED BY
Giada Mattiuzzo,
Medicines and Healthcare products Regulatory Agency, United Kingdom
Lihua Hou,
Acadamy of Military Medical Sciences (AMMS), China

*CORRESPONDENCE
Jifeng Hou
houjf@nifdc.org.cn
Zhenglun Liang
lzhenglun@126.com
Miao Xu
xumiao@nifdc.org.cn

†These authors have contributed equally to this work and share first authorship

SPECIALTY SECTION
This article was submitted to Viral Immunology, a section of the journal Frontiers in Immunology

RECEIVED 25 November 2022
ACCEPTED 24 January 2023
PUBLISHED 14 February 2023

CITATION
Guan L, Mao Q, Tan D, Liu J, Zhang X, Li L, Liu M, Wang Z, Cheng F, Cui B, He Q, Wang Q, Gao F, Wang Y, Bian L, Wu X, Hou J, Liang Z and Xu M (2023) Establishment of national standard for anti-SARS-Cov-2 neutralizing antibody in China: The first National Standard calibration traceability to the WHO International Standard.
*Front. Immunol.* 14:1107639.
doi: 10.3389/fimmu.2023.1107639



# Establishment of national standard for anti-SARS-Cov-2 neutralizing antibody in China: The first National Standard calibration traceability to the WHO International Standard

Lidong Guan[1,2,3†], Qunying Mao[1,2,3†], Dejiang Tan[1,2,3†], Jianyang Liu[1,2,3], Xuanxuan Zhang[1,2,3], Lu Li[1,2,3], Mingchen Liu[1,2,3], Zhongfang Wang[4], Feiran Cheng[1,2,3], Bopei Cui[1,2,3], Qian He[1,2,3], Qingzhou Wang[1,2,3], Fan Gao[1,2,3], Yiping Wang[1,2,3], Lianlian Bian[1,2,3], Xing Wu[1,2,3], Jifeng Hou[1,2,3*], Zhenglun Liang[1,2,3*] and Miao Xu[1,2,3*]

[1]Institute of Biological Products, National Institutes for Food and Drug Control, Beijing, China, [2]National Health Commission Key Laboratory of Research on Quality and Standardization of Biotech Products, National Institutes for Food and Drug Control, Beijing, China, [3]National Medical Products Administration Key Laboratory for Quality Research and Evaluation of Biological Products, Institute of Biological Products, National Institutes for Food and Drug Control, Beijing, China, [4]Guangzhou Laboratory, Guangzhou, China

Neutralizing antibody (NtAb) levels are key indicators in the development and evaluation of severe acute respiratory syndrome coronavirus-2 (SARS-CoV-2) vaccines. Establishing a unified and reliable WHO International Standard (IS) for NtAb is crucial for the calibration and harmonization of NtAb detection assays. National and other WHO secondary standards are key links in the transfer of IS to working standards but are often overlooked. The Chinese National Standard (NS) and WHO IS were developed by China and WHO in September and December 2020, respectively, the application of which prompted and coordinated sero-detection of vaccine and therapy globally. Currently, a second-generation Chinese NS is urgently required owing to the depletion of stocks and need for calibration to the WHO IS. The Chinese National Institutes for Food and Drug Control (NIFDC) developed two candidate NSs (samples 33 and 66–99) traced to the IS according to the WHO manual for the establishment of national secondary standards through a collaborative study of nine experienced labs. Either NS candidate can reduce the systematic error among different laboratories and the difference between the live virus neutralization (Neut) and pseudovirus neutralization (PsN) methods, ensuring the accuracy and comparability of NtAb test results among multiple labs and methods, especially for samples 66–99. At present, samples 66–99 have been approved as the second-generation NS, which is the first NS calibrated tracing to the IS with 580 (460–740) International Units (IU)/mL and 580 (520–640) IU/mL by Neut and PsN, respectively. The use of standards improves the reliability and

comparability of NtAb detection, ensuring the continuity of the use of the IS unitage, which effectively promotes the development and application of SARS-CoV-2 vaccines in China.

KEYWORDS

**international standard (IS), national standard (NS), COVID-19, neutralizing antibody (NtAb), traceability, live virus neutralization assay (Neut), pseudovirus neutralization assay (PsN)**

# 1 Introduction

The coronavirus disease 2019 (COVID-19) outbreak has caused over 620 million confirmed infections worldwide and at least 6.5 million deaths (1). To effectively prevent and control the COVID-19 epidemic, the research and development of the COVID-19 vaccine was rapidly conducted at an unprecedented global scale and investment. Currently, 198 vaccines are in the preclinical stage, 169 have entered clinical trials, and 43 have been approved for market application or emergency use (2, 3). Over 12 billion vaccine doses have been administered worldwide (1). Thirteen vaccines have been approved for market application or emergency use in China, and over 3.4 billion vaccine doses have been administered (3, 4). However, owing to the continuous emergence of variants of concern (VOC) and their immune escape ability, vaccine research and development has shifted from the original prototype strain vaccine to the multi-conjugate, multivalent, broad-spectrum, and pan-coronavirus vaccines with prototype strains as one of the components (5–11).

The level of neutralizing antibodies (NtAb) is an important indicator of vaccine effectiveness (12–14) and a key indicator in the study of treatment and population seroepidemiology. The accuracy, comparability, and reliability of the test results are of great significance for vaccine development, production, and application (15). At present, the commonly used detection methods mainly include the live virus neutralization (Neut) and pseudovirus neutralization (PsN) methods (16–18). Between them, the traditional Neut method is the internationally recognized gold standard, but it requires the use of live virus and live cells, which needs to be carried out in a level three biosafety laboratory, and is greatly affected by many influencing factors, such as the detection of virus strains, cells, other living matrices, and personal subjective judgment (19). Although the PsN method has a short detection cycle, high biological safety, and objective detection results, it also requires using live cells and artificially constructed pseudovirus (19). Importantly, it is difficult to compare the effectiveness of vaccines in different clinical trials due to the use of different testing methods and laboratories, which has become a key challenge in the management of the COVID-19 pandemic for the World Health Organization (WHO) and regulatory agencies worldwide. Especially in the case of the global development of COVID-19 vaccines with the use of multi-technology routes, involvement of multiple centers, rapid synchronous development, and clinical evaluation (20), the timely establishment of accurate and reliable NtAb standards for COVID-19 vaccines is of great importance.

Therefore, China's NIFDC and WHO invited experts to establish the first National Standard (NS) for the COVID-19 neutralizing antibody (No. 280034-202001) and the first WHO International Standard (IS) for anti-SARS-CoV-2 immunoglobulin (Coded: 20/136) in September and December 2020, respectively (21, 22). The NtAb potencies were 1000 units/mL and 1000 International Units (IU)/mL, respectively. These two standards were expected to guarantee and promote the effective evaluation of COVID-19 vaccines, which was known to be the principal role of the WHO and Chinese national regulations in the prevention and control of the COVID-19 epidemic. At present, the inventory of the first NS in China is about to be depleted. To meet the needs of vaccine research, development, and application in China, and trace the Chinese national standards to IU and ensure the unity of IU worldwide, the research and development of the new generation of standards is imminent. In 2021, the Chinese National Institutes for Food and Drug Control (NIFDC) in conjunction with other companies and institutes prepared two candidates using the convalescent plasma and immunoglobulin of patients with COVID-19 collected before April 2021, respectively. After homogeneity and stability research, nine relevant laboratories in China were invited to conduct a collaborative calibration study, and a NS with calibrated tracing to IS was established. This study describes the results of cooperative calibration and traceability of the Chinese NS to the IS, to provide uniform and coordinated global standards for the promotion of vaccine research, development, production, and application in China.

# 2 Materials and methods

## 2.1 Materials and ethics statement

Thirteen plasma samples from COVID-19 convalescent patients collected before April 2021 and one batch anti-SARS-CoV-2 immunoglobulin (Lot: 20200905) were generously provided by Sinopharm Wuhan Plasma derived Biotherapies Co., Ltd. All donors gave informed consent for the use of their plasma.

## 2.2 Production and tests of the candidates

Candidate 1 (Lot:202102) was a frozen preparation of a pool of plasma from 13 individuals infected with one of the early 2021 SARS-CoV-2 isolates. After heat-inactivation for 30 min at 56°C and

defibrination, the pooled plasma was aseptically aliquoted in glass DIN ampoules, each containing 0.2 mL, which were sealed and cryopreserved at −35°C. The Candidate 1 preparation was also tested for markers of known blood-borne virus infections (HBsAg, HIV-1/HIV-2 antibody, HCV antibody, and syphilis antibody) and was found to be negative.

Candidate 2 is a freeze-dried preparation of anti-SARS-CoV-2 immunoglobulin, which was prepared by the company according to the immunoglobulin manufacturing process (Lot: 20200905). It was aseptically aliquoted in glass DIN ampoules, each containing 0.5 mL, and lyophilized, sealed, and cryopreserved at −35°C.

The absolute NtAb titers of candidates 1 and 2 were 1650 and 566 detected by the PsN method, respectively, with good homogeneity (geometric coefficient of variation [GCV] between samples: 24% and 33%, respectively). The stabilities of the two candidates were assessed using an accelerated thermal degradation study. The ampoules of the two candidates were stored at different temperatures: −35 (baseline), +4, +20, and +37°C for two weeks and one month. The potencies relative to the −35°C baseline were calculated. Real-time data on the degradation of candidate 1 and 2 samples showed no loss of potency for up to a month and performed well in terms of stability (Supplementary Figure 1).

## 2.3 Collaborative calibration study

### 2.3.1 Samples and virus

The collaborative study sample consisted of 10 samples, as summarized in Supplementary Table 1 (coded 10, 11, 22, 33, 44, 55, 66, 77, 88 and 99, respectively). Sample 11 was the first WHO International Standard for anti-SARS-CoV-2 immunoglobulin (coded 20/136), purchased from NIBSC (20). Sample 22 was the first national standard of China for anti-SARS-CoV-2 immunoglobulin (Lot 280034-202001) and was stored in our unit (19). Sample 99 was a duplicate of sample 66 (candidate 1). Sample 33 (candidate 2; Lot: 20200905) was provided by NIFDC. Samples 10 and 44 were SARS-CoV-2-negative healthy human serum. Samples 55 and 77 were convalescent sera from two donors infected with SARS-CoV-2 provided by the Boya Biopharmaceutical Group Co., Ltd., with lower or higher titers, respectively. Sample 88 was a pool of sera from COVID-19 recovered patients collected in Guangzhou Laboratory with sequence-confirmed infection with the Delta variant.

The methods used by the participants were in-house Neut, and PsN assays. The PsN assay used a non-replicative vesicular stomatitis virus (VSV)-based pseudotype virus provided by the NIFDC and commercial company.

### 2.3.2 Participants

Nine laboratories with NtAb detection experience agreed to participate in the study, including Jiangsu Provincial Center for Disease Control And Prevention, Sinovac Life Science Co., Ltd., Guangzhou Laboratory, Institute of Medical Biology, Chinese Academy of Medical Sciences, Wuhan Institute of Biological Products Co., Ltd., Institute of Biotechnology, Academy of Military Medical Sciences, Beijing Institute of Biological Products Co., Ltd., the Division of HIV/acquired immunodeficiency syndrome (AIDS) and Sexually Transmitted Virus Vaccines, and the Division of Blood Products, NIFDC. All laboratories were referred to by a code number from one to nine, randomly allocated.

### 2.3.3 Collaborative calibration study

The NIFDC organized this collaborative study. Participants were requested to test the study samples using their established methods, including Neut and PsN assays, for the detection of antibodies against the wild-type (WT) SARS-CoV-2 and Delta variant.

The Neut assay, for the detection of anti-SARS-CoV-2 antibodies, is a cytopathic effect-based microneutralization assay (23). The PsN method was performed according to Nie et al. (24). The participants were asked to perform three independent assays for each challenged strain on different days. At least eight dilutions were suggested for each assay for each sample, and at least four wells were set for each dilution in parallel.

## 2.4 Statistical methods

The raw data were submitted to the NIFDC. The end-point titer of each sample was calculated from the 50% inhibitory dilutions ($ID_{50}$) provided by the participants using the NIFDC biostats software. To be calibrated by the WHO IS, the relative potency of each sample against the WHO IS was calculated by taking the end-point titer ratio of sample/WHO IS in same assay and multiplying assigned value of the first WHO IS (1000 IU/mL). All log-transformed data were analyzed using a probit model. Model fit was assessed using analysis of variance. Variabilities between laboratories and assays are expressed using GCV. The calculation and analysis software used included Microsoft Excel 2016 (Microsoft corporation, USA, 2016), NIFDC Biostat 1.0 (NIFDC, China,2019), and JMP 13(SAS Institute, Cary, NC, 1989-2016).

# 3 Results

## 3.1 Collaborative calibration and feedback data

Nine Chinese labs with experience in testing SARS-CoV-2 NtAb, including two national vaccine quality control laboratories, one national laboratory, one disease prevention and control agency, four vaccine manufacturers, and one research institute participated in this collaborative calibration study. All labs returned results according to requirements. The Neut method was adopted by six laboratories, and the PsN method was adopted by four laboratories. In each method, three independent and effective tests were performed on all samples using the WT and Delta strains, respectively.

The geometric mean titer (GMT) results for all samples from the nine laboratories are presented in Figure 1. The assay results for all laboratories showed the same trend. All the results of the negative samples (Nos. 10 and 44) were negative, and the coincidence rate was 100%. Among the eight positive samples, negative results for samples 55 and 77 were found among some Neut-Delta detection assays from three laboratories. The 2/3, 3/3, and 3/3 negative results for sample 55 were obtained in Lab4, Lab8, and Lab6, respectively. The 2/3 negative results for sample 77 were obtained in Lab4. The remaining six

10.3389/fimmu.2023.1107639

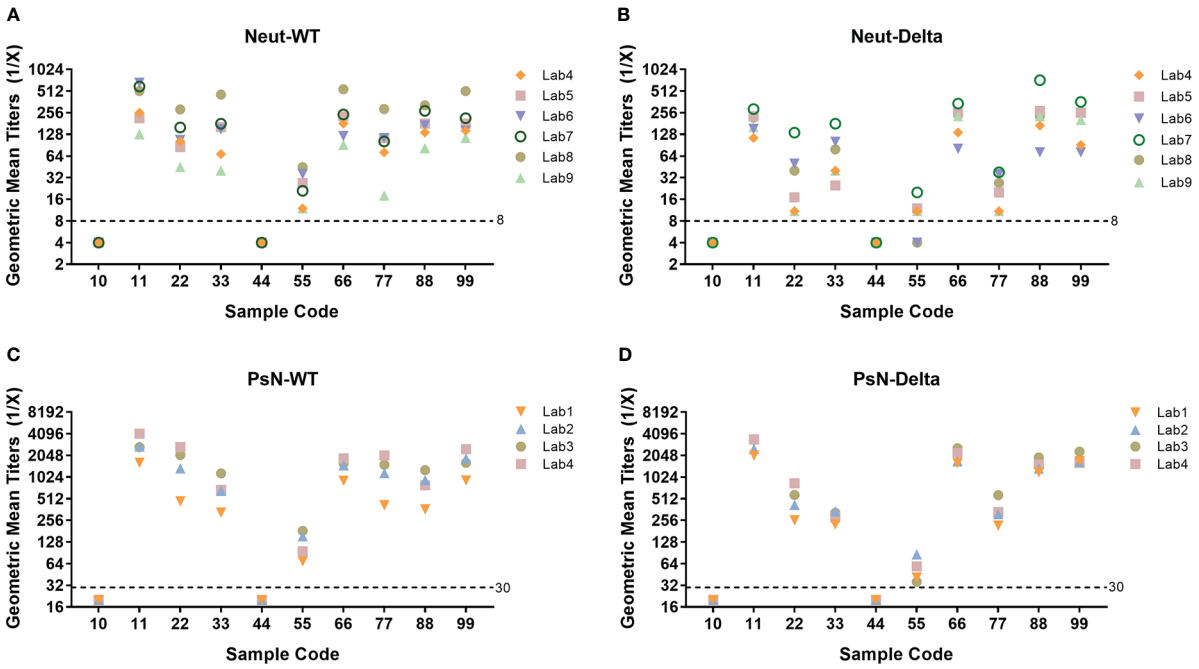


FIGURE 1
Neutralizing antibody (NtAb) geometric mean titers (GMT) of all collaborative calibration study samples across all participants. **(A)** Live virus neutralization assay (Neut), WT strain; **(B)** Neut assay, Delta variant; **(C)** Pseudovirus neutralization assay (PsN), WT strain; **(D)** PsN assay, Delta variant. Nine laboratories with experience in testing SARS-CoV-2 NtAbs participated in this collaborative calibration study. The Neut method was adopted by six laboratories, and the PsN method was adopted by four laboratories. In each laboratory, three independent and effective tests were performed on all samples using the WT and Delta strains, respectively. All laboratories returned results according to requirements.

samples tested positive. Statistical analysis showed that all the data met the validity of the model. In total, 480 results using the Neut method (WT, Delta) and PsN method (WT, Delta) were analyzed using the Grubbs test. All the results had no outliers at the 5% significance level; therefore, all data were included in the subsequent analyses.

## 3.2 Intra-assay and inter-assay variability

The relative potencies of the coded duplicate samples of candidate standard 1 (samples 66 and 99) were used to assess intra-assay variability and are shown in Supplementary Figure 2. For the Neut assay, relative potencies ranged between 0.5 and 2.0 in 93% of cases challenged with both the WT and Delta strains, with the exception of one result in Lab5 and Lab9 (each challenged with the WT strain) and one result in Lab4 and Lab5 (each challenged with the Delta strain). For PsN, the relative potencies ranged between 0.5 and 2.0 in 100% of cases challenged with both the WT and Delta strains. The results showed a good level of intra-assay precision among the participating laboratories, with better precision in the PsN method (Supplementary Figure 2).

Inter-assay variability, as illustrated by the between-assay GCVs in Supplementary Table 2, ranged from 0% to 105.7% (4.0-fold difference in the results obtained for sample 33 by Lab6) for the Neut assay challenged with the WT strain, and ranged from 0% to 163.3% (5.3-fold difference in the results obtained for sample 33 by Lab8) for the Neut assay challenged with the Delta strain. For the PsN assay, the inter-assay variability ranged from 3.2% (1.1-fold difference in the results obtained for sample 66 by Lab3) to 78.6% (3.1-fold difference in the results obtained for sample 55 by Lab3) when challenged by WT, and from 5.3% (1.1-fold difference in the results obtained for sample 66 by Lab1) to 79.5% (3.1-fold difference in the results obtained for sample 33 by Lab3) when challenged with the Delta strain, respectively. Good inter-assay variability was found for both the Neut and PsN assays among the participating laboratories. Better intra-assay variability was also found in the PsN method compared with that in the Neut method, consistent with the performance of these methods.

## 3.3 Collaborative calibration results

The test results of each laboratory of the two candidate standards (samples 33 and 66–99) were subjected to statistical and frequency distribution analyses. As shown in Figure 2, when challenged with the WT strain, the GMTs of the Neut method for samples 33 and 66–99 were 133 (86–205) and 194 (157–238), respectively. The GMT of the PsN method were 641 (468–878) and 1512 (1287–1776), respectively. The frequency distribution shows that the peak pattern of samples 66–99 is more symmetrical and sharper than that of sample 33. Statistically, both were normally distributed (P>0.05).

When challenged with the Delta strain, the GMTs of the Neut method for samples 33 and 66–99 were 62 (41–94) and 186 (152–227), respectively, whereas those of the PsN method were 289 (227–368) and 1889 (1695–2106), respectively. Statistically, the results of samples 33 and 66–99 were also normally distributed (P>0.05), but the result distribution peak of the Neut method challenged with the Delta strain was not as symmetric and sharp as that of the WT strain.

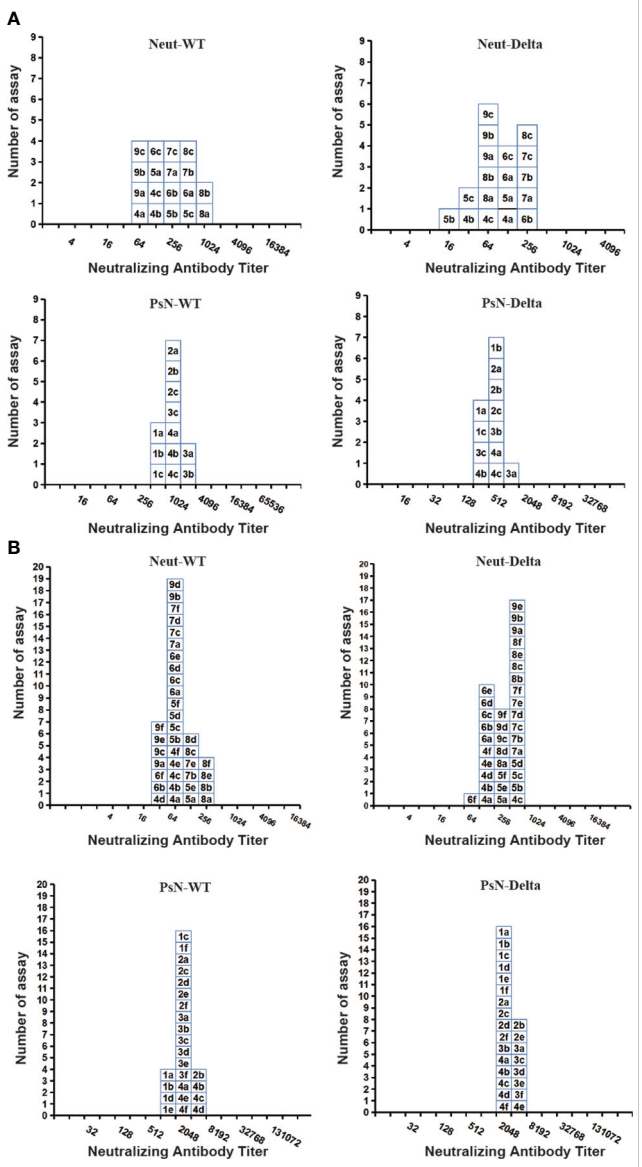


FIGURE 2
Histograms showing the distribution of the endpoint titer ($ID_{50}$) for two candidate national standards (samples 33 and 66–99) across laboratories. **(A)** Sample 33, **(B)** Samples 66–99. Each box represents the endpoint titer for each assay, labelled with the laboratory code number (1–9), and followed by one independent assay (a–f), indicating the assays. The live virus neutralization assay (Neut) and pseudovirus neutralization assay (PsN) results using the wild-type (WT) strain or Delta variant are shown side by side.

### 3.3.1 Inter-laboratory variability

To assess the effect of test results calibrated by samples 33 and 66–99 from different laboratories, the neutralization relative titers (RT) for each sample were expressed relative to samples 33 and 66–99 in each assay, respectively.

For the neutralizing results detected using the WT strain, the GCV of the endpoint titer for each sample between all participants were 64–148% and 36–115% in the Neut and PsN methods, respectively (Table 1). Relative to sample 33, the GCV of RT/33 among all participants decreased to 34–94% and 12–55% using the Neut and PsN methods, respectively. Relative to samples 66–99, the GCV of RT/66–99 among all participants decreased to 29–88% and 7–54%, respectively. Samples 33 and 66–99 effectively reduced the variability among different laboratories. Samples 66–99 were more effective than sample 33 in reducing the inter-laboratory GCV and could reduce the difference in the detection of all samples (including Delta convalescent serum, sample 88).

For the neutralizing results detected using the Delta variant, the GCV of the endpoint titer among all participants were 33–167% and 18–65% in the Neut and PsN methods, respectively (Table 1). Relative to sample 33, the GCV of RT/33 for all participants decreased to 57–149% and 19–55% for the Neut and PsN methods, respectively. Relative to sample 66–99, the GCV of RT/66–99 for all participants decreased to 38–175% and 5–69%, respectively. It is suggested that when challenged with the Delta variant, the use of samples 33 and 66–99 can only reduce the detection difference of some samples and even lead to an increase in the inter-laboratory difference of most samples. The results indicate that the two candidates are not suitable for the Neut and PsN methods using the Delta variant.

### 3.3.2 Inter-method variability

To assess the effects of candidates 33 and 66–99 on different detection methods, the correlation between the two methods before and after calibration, and the GMT ratio (GMT Neut method/GMT PsN method) were analyzed.

#### 3.3.2.1 Correlation

First, as shown in Figure 3, the endpoint titers, RT/33, and RT/66–99 were used to express the detection results challenged by WT strain. The correlation P values of the Neut and PsN methods were 0.0103, 0.0175, and 0.0246, and the r values were 0.8728, 0.8898, and 0.8690, respectively. When challenged with the Delta variant, the correlation P values of the endpoint titers, RT/33, and RT/66–99 were 0.0125, 0.0278, and 0.0363, respectively, whereas the r values were 0.8626, 0.8607, and 0.8402, respectively. The results expressed by the endpoint titers showed that there was a significant correlation between the results of the two methods ($P < 0.05$) whether it is the WT strain or Delta variant, and the r values were between 0.86 and 0.87, both of which were well correlated. When samples 33 or 66–99 were used to calibrate the methods, the P value between the two methods was still <0.05, and the r value was between 0.84 and 0.89. This result indicates that the calibration does not change the correlation between the Neut and PsN methods, and that the correlation is still good.

#### 3.3.2.2 GMT difference

To visualize the difference in GMT between the two methods, the GMT Rate of Neut/PsN (Rate $_{N/P}$) for each sample was calculated for WT and Delta strain detection, respectively (Table 2). When the WT strain was used, the Rate N/P of the endpoint titer was a 4.3–12.4-fold difference between the Neut and PsN methods. After calibration of samples 33 and 66–99, the Rate $_{N/P}$ decreased to 0.9–2.6- and 0.6–1.6-fold, respectively. When the Delta variant was used, the Rate $_{N/P}$ of the endpoint titer was 4.0–16.7-fold between Neut and PsN method. Calibrated by samples 33 and 66–99, the Rate N/P dropped to 0.7–3.6- and 0.4–1.6-fold, respectively. This indicates that regardless of the WT or Delta variant, the application of samples 33 and 66–99 effectively reduced the variability between the Neut and PsN methods, especially for samples 66–99.

10.3389/fimmu.2023.1107639

TABLE 1 Geometric Coefficients of Variation (%, GCV) of endpoint titer and relative titers against sample 33 or samples 66–99 across all participants.

| Challenge Virus | Assay type | %, GCV | Sample Code | | | | | | | |
|---|---|---|---|---|---|---|---|---|---|---|
| | | | *11* | *22* | *33* | *55* | *66* | *77* | *88* | *99* |
| WT | Neut | Endpoint | 93 | 86 | 132 | 74 | 86 | 148 | 64 | 70 |
| | | RT/33 | 94 | 47 | / | 48 | 55 | 34 | 49 | 54 |
| | | RT/66–99 | 88 | 29 | 55 | 53 | / | 80 | 31 | / |
| | PsN | Endpoint | 46 | 115 | 67 | 56 | 36 | 100 | 70 | 52 |
| | | RT/33 | 51 | 55 | / | 27 | 39 | 49 | 12 | 51 |
| | | RT/66–99 | 7 | 54 | 39 | 51 | / | 42 | 43 | / |
| Delta | Neut | Endpoint | 40 | 167 | 107 | 33 | 69 | 73 | 111 | 90 |
| | | RT/33 | 95 | 57 | / | 88 | 142 | 71 | 149 | 148 |
| | | RT/66–99 | 43 | 175 | 143 | 50 | / | 110 | 38 | / |
| | PsN | Endpoint | 28 | 65 | 20 | 48 | 25 | 50 | 23 | 18 |
| | | RT/33 | 23 | 55 | / | 43 | 24 | 35 | 19 | 22 |
| | | RT/66–99 | 18 | 54 | 24 | 69 | / | 27 | 5 | / |

Green represents lower GCV of relative titers than that of endpoint titers, and red represents higher GCV of relative titers than that of endpoint titers.
To assess the suitability of samples 33 and 66–99, the neutralization relative titers (RT) for each sample were calculated relative to samples 33 and 66–99 in each assay. The GCV of the endpoint titer, RT/33, and RT/66–99 among all participants was statistically analyzed to reflect variability between different laboratories. WT, wild-type; PsN, pseudovirus neutralization assay; Neut, live virus neutralization assay.

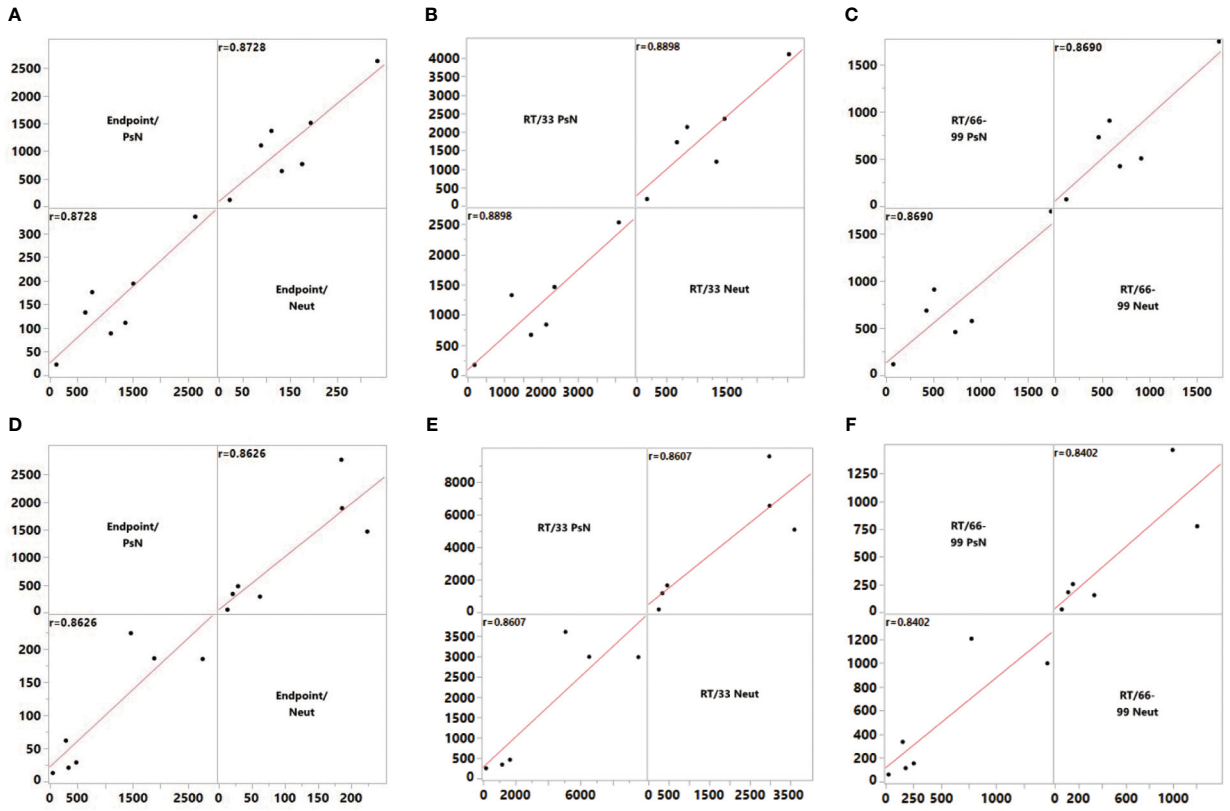


FIGURE 3
Correlation of endpoint titer and RT/33 and RT/66–99 between the pseudovirus neutralization assay (PsN) and live virus neutralization assay (Neut) methods. **(A)** Endpoint titer, wild-type (WT) strain, **(B)** Titers relative to 33, WT strain, **(C)** Titers relative to 66–99, WT strain, **(D)** Endpoint titer, Delta Variant, **(E)** Titers relative to 33, Delta Variant, **(F)** Titers relative to 66–99, Delta Variant. To assess the level of agreement between the PsN and Neut methods, correlations were estimated using the Row-wise method. Correlation coefficients were calculated using the endpoint titer and the titer relative to samples 33 and 66–99.

10.3389/fimmu.2023.1107639

TABLE 2 Endpoint titer, RT/33, RT/66–99 between the Neut and PsN assays.

| Challenge Virus | Samples code | Endpoint titer | | | RT/33 | | | RT/66–99 | | |
|---|---|---|---|---|---|---|---|---|---|---|
| | | Neut assay | PsN assay | Neut/PsN | Neut assay | PsN assay | Neut/PsN | Neut assay | PsN assay | Neut/PsN |
| WT strain | 11 | 335 | 2632 | 7.8 | 2530 | 4105 | 1.6 | 1732 | 1741 | 1.0 |
| | 22 | 111 | 1367 | 12.3 | 839 | 2133 | 2.5 | 574 | 905 | 1.6 |
| | 33 | 133 | 641 | 4.8 | / | / | / | 684 | 424 | 0.6 |
| | 55 | 23 | 117 | 5.1 | 172 | 182 | 1.1 | 118 | 74 | 0.6 |
| | 66–99 | 194 | 1512 | 7.8 | 1461 | 2358 | 1.6 | / | / | / |
| | 77 | 89 | 1103 | 12.4 | 670 | 1721 | 2.6 | 459 | 730 | 1.6 |
| | 88 | 176 | 764 | 4.3 | 1326 | 1192 | 0.9 | 908 | 506 | 0.6 |
| Delta Variant | 11 | 185 | 2765 | 14.9 | 2980 | 9573 | 3.2 | 997 | 1464 | 1.5 |
| | 22 | 29 | 478 | 16.7 | 461 | 1654 | 3.6 | 154 | 253 | 1.6 |
| | 33 | 62 | 289 | 4.7 | / | / | / | 335 | 153 | 0.5 |
| | 55 | 13 | 52 | 4.0 | 252 | 180 | 0.7 | 60 | 25 | 0.4 |
| | 66–99 | 186 | 1889 | 10.2 | 2988 | 6539 | 2.2 | / | / | / |
| | 77 | 21 | 337 | 15.9 | 341 | 1168 | 3.4 | 114 | 179 | 1.6 |
| | 88 | 224 | 1467 | 6.6 | 3600 | 5077 | 1.4 | 1205 | 776 | 0.6 |

Green represents lower values of RT/33 or RT/66–99 between the Neut and PsN assays than that of the endpoint titer.
To visualize the difference in GMT between the two methods, the GMT Rate of Neut/PsN (Rate N/P) for each sample was calculated for WT and Delta detection, respectively. WT, wild-type; PsN, pseudovirus neutralization assay; Neut, live virus neutralization assay.

When challenged with the WT or Delta variant, samples 66–99 reduced the Rate N/P between the two methods to 0.6–1.6-fold or 0.4–1.6-fold. The results confirmed the consistency and comparability of the test results between the Neut and PsN methods.

## 3.4 Calibration to the WHO IS

### 3.4.1 Candidate standards

In this study, the endpoint titers of samples 33 and 66–99 were converted to IU relative to the endpoint titer of the WHO IS. All experimental data were analyzed for normality and homogeneity of variance. The results showed that the IU data of samples 66–99 were all distributed normally using the Neut and PsN methods. There was no significant difference in the geometric mean between the two methods (P=0.9733), but the dispersion degree of the Neut method was greater than that of the PsN method (Figure 4A). According to the weighted statistical analysis, the calibrated value of samples 66–99 traceability to WHO IS was 580 (460–740) IU/mL and 580 (520–640) IU/mL in the Neut and PsN methods, respectively. Nevertheless, a significant difference in the geometric mean of sample 33 was found between the two methods (P=0.0314, Figure 4B), which led to the assignment not being merged. Therefore, the calibrated values for sample 33 were 400 (320–490) IU/mL and 240 (190–310) IU/mL for the Neut and PsN methods, respectively.

### 3.4.2 First Chinese NS for SARS-CoV-2 NtAb

As the first NS in China was established before the WHO IS, it was not traceable to the first-generation international standard through collaborative calibration. At the same time, to clarify the quantitative value relationship between the NS and the first generation of NS established, the first NS was also traceable to the WHO IS based on this collaborative calibration. After the sample 22 results were converted to IU by the WHO IS, there was also a significant difference between the two methods (P=0.0239, Figure 4C), and the values could not be combined. Therefore, the weighted method was adopted for statistical analysis. The traceability values of sample 22 were 330 (280–390) IU/mL and 520 (410–660) IU/mL for the Neut and PsN methods, respectively.

# 4 Discussion

In December 2020, the WHO Expert Committee on Biological Standardization (ECBS) approved the first WHO International Standard for anti-SARS-CoV-2 immunoglobulin (20/136, 250 IU/ampoule) (22). To harmonize the wide range of methods used globally, a pool of convalescent plasma from 11 COVID-19 patients (NIBSC code 20/136) was evaluated as a candidate IS in a collaborative study. The results showed that 20/136 could effectively demonstrate a decrease in %GCV value among laboratories using different methods, thus addressing the lack of standards for many methods worldwide, and providing a globally unified value for the harmonization and coordination of the detection of COVID-19 antibodies. However, owing to the wide variety of viral targets and classes of immunoglobulin for binding antibodies, an IU could not be assigned for the first WHO IS. The standard was recommended as a comparator; to avoid confusion between the quantification of binding

and neutralizing activity, the binding antibody unit (BAU) was introduced (16, 25). At the same time, owing to the extensive demand for IS, the WHO also encourages and supports countries or regions worldwide to develop and apply secondary standards, which not only ensures that the limited IS can be used to maintain the stability and sustainability of quantity traceability but also meets the great demand for vaccines and the related research and development of drugs worldwide. For this purpose, the "WHO manual for the preparation of reference materials for use as secondary standards in antibody testing", and the "WHO manual for the establishment of national and other secondary standards for antibodies against infectious agents focusing on SARS-CoV2" were issued, which raise the requirements for the development of standards, collaborative calibration, statistical analysis, and assignment, and guide the development and application of national secondary standards systematically globally (26).

As early as September 2020, the Chinese NIFDC established the first generation of China's national NtAb standard (NS-1st, No. 280034-202001, 1000 U/mL) before the establishment of the WHO IS, which was prepared from Chinese COVID-19 convalescent plasma (19). Collaborative calibration was carried out by 11 laboratories, including the national quality control laboratory, which confirmed that the first generation of NS could effectively reduce the differences in NtAb detection among laboratories, achieving improvements in the accuracy and comparability of NtAb detection among different laboratories and products. The establishment of this standard has played a key role in ensuring the research and development of vaccines and antibodies in China. However, at that time, it could not be traced back to the WHO IS.

For this reason, in 2021, as one of the national quality control laboratories in China and the WHO CC, the NIFDC prepared two candidate standards (lot No. 1 and lot No. 2: CS from COVID-19

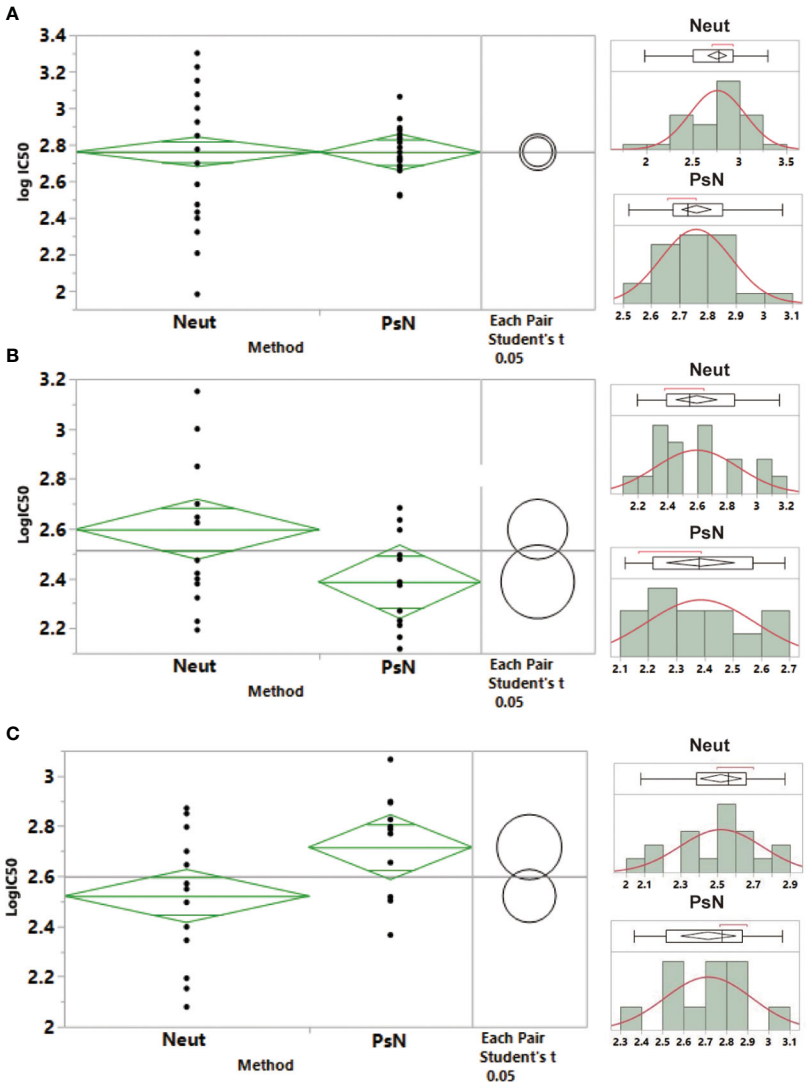


FIGURE 4
Statistical analysis for the neutralizing antibody potencies of samples 66–99, 33, and 22, and calibration to the international standard. **(A)** Samples 66–99; **(B)** Sample 33; **(C)** Sample 22. A normal distribution analysis of the neutralizing antibody potencies of samples 66–99, 33, and 22 was carried out. One-way analysis of variance was used to analyze the variance between the live virus neutralization assay (Neut) and pseudovirus neutralization assay (PsN).

convalescent plasma or immunoglobulin, respectively) in accordance with the WHO guidelines and the requirements for the development of reference materials in the Chinese Pharmacopoeia (25–29). This collaborative study included nine laboratories with extensive experience in COVID-19-NtAb detection in China. In total, 10 samples, including three candidate standards (batch number 2 and repeatedly set batch number 1), one first NS, two negative healthy human sera, two WT convalescent sera with different titers, and one Delta convalescent serum, were jointly calibrated to the first WHO IS. The results showed that samples 66–99 could effectively reduce the difference between laboratory tests of all samples (including Delta sera) for the WT strains. The GCV value of the Neut method and the PsN method reduced from 64–148% and 36–115% to 29–88% and 7–54%, respectively. At same time, under the premise of ensuring a good correlation between the Neut and PsN methods ($P < 0.05$, $r = 0.8690$ for WT; $P < 0.05$, $r = 0.8402$ for Delta), the difference between these two methods could also reduce significantly by standardization with samples 66-99. The ratio for the GMT Neut/PsN method decreased to 0.6–1.6 fold different and 0.4–1.6 fold different from 4.3–12.4 times and 4.0–16.7 times on challenge with the WT strain and Delta variant, respectively. It has been indicated that samples 66–99 can significantly reduce the difference between Neut and PsN methods, and effectively ensure the consistency and comparability of the detection results.

Measurement traceability is the core of reference for material development. To ensure the accuracy and reliability of the measurement value, the WHO specifically documented in the preparation manual of secondary standards and clearly proposed that the calibration value of the secondary standard should include measurement uncertainty (MU), which can be expressed by the 95% confidence limit, and MU should contain requirements for method specificity (27, 28). According to the WHO's requirements, the test results of samples 66–99 in each test were calibrated to IU/mL according to the test results of the WHO IS in the same test, and the distribution and mean value tests were conducted using the X fitting Y modeling, showing that there was no significant difference ($P=0.9733$) between the two methods for sample 66–99, but the dispersion degree was different. Following statistical analysis, the values were 580 (460–740) IU/mL and 580 (520–640) IU/mL for the Neut and PsN methods, respectively. However, there was a significant difference between the two methods in terms of the first NS (sample 22) in China ($P=0.0239$). The assigned values were 330 (280–390) IU/mL and 520 (410–660) IU/mL. The candidate standards and the first-generation NS were traced to the WHO IS with methodically specific research based on statistical analysis at this collaborative calibration, which not only ensures the traceability accuracy and reliability of secondary standards but also clarifies the quantity relationship between new standards and the first NS, ensuring the smooth connection of new standards.

In summary, the secondary standards established by regions or countries are key to ensuring the correct application of WHO IS for practical NtAb detection. Calibration accuracy and property consistency with WHO IS are key to ensuring that the quantity value of the WHO IS is correctly transferred to the working standard, so that the WHO IS can play an accurate role. However, the development of secondary standards is usually ignored and there are few specific research reports on the calibration and traceability of antibodies. According to the "WHO manual for the preparation of reference materials for use as secondary standards in antibody testing" and the "WHO manual for the establishment of national and other secondary standards for antibodies against infectious agents focusing on SARS-CoV2", the first national standard traceable to the WHO IS, which is the China NS (No. 280034-202102, sample 66-99), was established through collaborative calibration with 580 (460–740) IU/mL and 580 (520–640) IU/mL, respectively, and will be used for the quantitative detection of COVID-19 NtAb (Neut and PsN method). This standard effectively reduced the inter-laboratory detection error of all samples for the WT strain. More importantly, through collaborative calibration research, it was verified that it can significantly reduce the system error between the two methods for the first time without affecting their correlation, suggesting that the application of this standard can effectively ensure comparability and consistency of the detection results between the two methods. As a national quality control laboratory, the NIFDC has also established a robust and reliable COVID-19 NtAb analysis method based on the analytical quality by design (AQbD) and entire life cycle concepts, which can effectively reduce the random error of detection method. The combined application of this method and the secondary standard can achieve the goal of ensuring accurate, comparable, and stable detection of COVID-19 NtAb, and build a scientific foundation for effectively overcoming the challenge of comparing the effectiveness of the COVID-19 vaccine among WHO and regulators around the world. Unfortunately, this standard did not significantly reduce inter-laboratory differences in the Delta strain. Meanwhile, the Omicron and other VOC were not included in this research because of time constraints. In the future, we will pay more attention to the research on the WHO IS, continue research on secondary reference materials for NtAb against Omicron and new emerging VOC variants, and provide sufficient, reliable, and traceable WHO IS reference materials for the research of new vaccines and immune strategies.

## Data availability statement

The original contributions presented in the study are included in the article/Supplementary Material. Further inquiries can be directed to the corresponding authors.

## Author contributions

Conceptualization, ZL, MX, and JH; methodology, LG, QM, and DT; formal analysis: JL, XZ, LL, ML, ZW, FC, BC, QH, QW, FG, YW, LB, and XW; writing—original draft preparation, LG and QM; writing, review, and editing, ZL; supervision, DT and MX; funding acquisition, MX. All authors contributed to the article and approved the submitted version.

## Funding

This research was funded by the Emergency Key Program of Guangzhou Laboratory (Grant No. EKPG21-30-1) and the CAMS Innovation Fund for Medical Sciences (Grant No. 2021-I2M-5-005).

## Acknowledgments

We thank Jiangsu Provincial Center for Disease Control and Prevention, Sinovac Life Science Co., Ltd., Guangzhou Laboratory, Institute of Medical Biology, Chinese Academy of Medical Sciences, Wuhan Institute of Biological Products Co., Ltd., Institute of Biotechnology, Academy of Military Medical Sciences, Beijing Institute of Biological Products Co., Ltd., Division of HIV/acquired immunodeficiency syndrome (AIDS) and Sexually Transmitted Virus Vaccines and the Division of Blood Products, and the NIFDC for taking part in this collaborative calibration study. We thank Sinopharm Wuhan Plasma-derived Biotherapies Co., Ltd. for kindly providing the human plasma and immunoglobulin samples. We thank Boya Biopharmaceutical Group Co., Ltd. for providing collaborative calibration samples 55 and 77. We thank Guangzhou Laboratory for providing sera from recovered COVID-19 patients, which were collected during sequence-confirmed infection with the Delta variant.

## Conflict of interest

The authors declare that the research was conducted in the absence of any commercial or financial relationships that could be construed as a potential conflict of interest.

## Publisher's note



## Supplementary material

The Supplementary Material for this article can be found online at: https://www.frontiersin.org/articles/10.3389/fimmu.2023.1107639/full#supplementary-material

## References

1. World Health Organization. *WHO coronavirus (COVID-19) dashboard* (2022). Available at: https://covid19.who.int/ (Accessed November 15, 2022).

2. World Health Organization. *COVID-19 vaccine tracker and landscape* (2022). Available at: https://www.who.int/publications/m/item/draft-landscape-of-covid-19-candidate-vaccines (Accessed November 15, 2022).

3. *COVID-19 vaccine tracker* (2022). Available at: https://covid19.trackvaccines.org/ (Accessed November 15, 2022).

4. National Health Commission of the Peoples's Republic of China. (2022). Available at: http://www.nhc.gov.cn/xcs/zhengcwj/202212/acd8ba68d934488983909e81642dc337.shtml (Accessed December 14, 2022).

5. Davies NG, Abbott S, Barnard RC, Jarvis CI, Kucharski AJ, Munday JD, et al. Estimated transmissibility and impact of SARS-CoV-2 lineage B.1.1.7 in England. *Science* (2021) 372:eabg3055. doi: 10.1126/science.abg3055

6. Campbell F, Archer B, Laurenson-Schafer H, Jinnai Y, Konings F, Batra N, et al. Increased transmissibility and global spread of SARS-CoV-2 variants of concern as at June 2021. *Euro Surveill* (2021) 26:2100509. doi: 10.2807/1560-7917.ES.2021.26.24.2100509

7. Cao Y, Wang J, Jian F, Xiao T, Song W, Yisimayi A, et al. Omicron escapes the majority of existing SARS-CoV-2 neutralizing antibodies. *Nature* (2022) 602:657–63. doi: 10.1038/s41586-021-04385-3

8. Su S, Wang Q, Jiang S. Facing the challenge of viral mutations in the age of pandemic: developing highly potent, broad-spectrum, and safe COVID-19 vaccines and therapeutics. *Clin Transl Med* (2021) 11:e284. doi: 10.1002/ctm2.284

9. Dolgin E. Pan-coronavirus vaccine pipeline takes form. *Nat Rev Drug Discovery* (2022) 21:324–6. doi: 10.1038/d41573-022-00074-6

10. Xu K, Gao P, Liu S, Lu S, Lei W, Zheng T, et al. Protective prototype-beta and delta-omicron chimeric RBD-dimer vaccines against SARS-CoV-2. *Cell* (2022) 185:2265–78.e14. doi: 10.1016/j.cell.2022.04.029

11. US Food and Drug Administration. *Coronavirus (COVID-19) update: FDA authorizes moderna, pfizer-BioNTech bivalent COVID-19 vaccines for use as a booster dose* (2022). Available at: https://www.fda.gov/news-events/press-announcements/coronavirus-covid-19-update-fda-authorizes-moderna-pfizer-biontech-bivalent-covid-19-vaccines-use (Accessed June 20, 2022).

12. Khoury DS, Cromer D, Reynaldi A, Schlub TE, Wheatley AK, Juno JA, et al. Neutralizing antibody levels are highly predictive of immune protection from symptomatic SARS-CoV-2 infection. *Nat Med* (2021) 27:1205–11. doi: 10.1038/s41591-021-01377-8

13. Feng S, Phillips DJ, White T, Sayal H, Aley PK, Bibi S, et al. Correlates of protection against symptomatic and asymptomatic SARS-CoV-2 infection. *Nat Med* (2021) 27:2032–40. doi: 10.1038/s41591-021-01540-1

14. Liu J, Mao Q, Wu X, He Q, Bian L, Bai Y, et al. Considerations for the feasibility of neutralizing antibodies as a surrogate endpoint for COVID-19 vaccines. *Front Immunol* (2022) 13:814365. doi: 10.3389/fimmu.2022.814365

15. Wang Y. Standardised neutralising antibody assays are needed for evaluating COVID-19 vaccines. *EBiomedicine* (2021) 73:103677. doi: 10.1016/j.ebiom.2021.103677

16. World Health Organization. *WHO/BS.2020.2403 development of the WHO international standard and reference panel for anti-SARS-CoV-2 antibody* (2020). Available at: https://www.who.int/publications/m/item/WHO-BS-2020.2403 (Accessed November 18, 2020).

17. Riepler L, Rössler A, Falch A, Volland A, Borena W, von Laer D, et al. Comparison of four SARS-CoV-2 neutralization assays. *Vaccines (Basel)* (2020) 9:13. doi: 10.3390/vaccines9010013

18. Bewley KR, Coombes NS, Gagnon L, McInroy L, Baker N, Shaik I, et al. Quantification of SARS-CoV-2 neutralizing antibody by wild-type plaque reduction neutralization, microneutralization and pseudotyped virus neutralization assays. *Nat Protoc* (2021) 16:3114–40. doi: 10.1038/s41596-021-00536-y

19. Banga Ndzouboukou JL, Zhang YD, Fan XL. Recent developments in SARS-CoV-2 neutralizing antibody detection methods. *Curr Med Sci* (2021) 41:1052–64. doi: 10.1007/s11596-021-2470-7

20. Guan L, Yu Y, Wu X, Nie J, Zhang J, Wang Z, et al. The first Chinese national standards for SARS-CoV-2 neutralizing antibody. *Vaccine* (2021) 39:3724–30. doi: 10.1016/j.vaccine.2021.05.047

21. Lurie N, Saville M, Hatchett R, Halton J. Developing covid-19 vaccines at pandemic speed. *N Engl J Med* (2020) 382:1969–73. doi: 10.1056/NEJMp2005630

22. World Health Organization. First WHO international standard for anti-SARS-CoV-2 immunoglobulin; and first WHO international reference panel for anti-SARS-CoV-2 immunoglobulin. In: *WHO expert committee on biological standardization: seventy-second and seventy-third report*. Geneva, Switzerland: World Health Organization (2021). p. 66–8.

23. Li YP, Liang ZL, Gao Q, Huang LR, Mao QY, Wen SQ, et al. Safety and immunogenicity of a novel human enterovirus 71 (EV71) vaccine: a randomized, placebo-controlled, double-blind, phase I clinical trial. *Vaccine* (2012) 30:3295–303. doi: 10.1016/j.vaccine.2012.03.010

24. Nie J, Li Q, Wu J, Zhao C, Hao H, Liu H, et al. Establishment and validation of a pseudovirus neutralization assay for SARS-CoV-2. *Emerg Microbes Infect* (2020) 9:680–6. doi: 10.1080/22221751.2020.1743767

25. World Health Organization. Proposed second WHO international standard for anti-SARS-CoV-2 immunoglobulin. In: *WHO expert committee on biological standardization [seventy-fourth report]*. Geneva, Switzerland: World Health Organization (2021). p. 61–3.

26. World Health Organization. WHO manual for the establishment of national and other secondary standards for antibodies against infectious agents focusing on SARS-CoV2. In: *WHO expert committee on biological standardization [seventy-fifth report]*. Geneva, Switzerland: World Health Organization (2022). p. 1–74.

27. World Health Organization. *WHO manual for the establishment of national and other secondary standards for vaccines* (2011). Available at: https://www.who.int/publications/i/item/WHO-IVB-11.03 (Accessed June 20, 2022).

28. World Health Organization. Recommendations for the preparation, characterization and establishment of international and other biological reference standards. In: *WHO expert committee on biological standardization [fifty-fifth report]*. Geneva, Switzerland: World Health Organization (2004).

29. Chinese pharmacopoeia commission. *Vol. III. pharmacopeia of the people's republic of China*. Beijing, China: China Medical Science Press (2020) p. 23–4.

frontiers | Frontiers in Immunology

TYPE Original Research
PUBLISHED 28 February 2023
DOI 10.3389/fimmu.2023.1134371



OPEN ACCESS

EDITED BY
Yuejin Liang,
University of Texas Medical Branch at Galveston, United States

REVIEWED BY
Benjamin Gabriel,
University of Pennsylvania, United States
Karin Stiasny,
Medical University of Vienna, Austria

*CORRESPONDENCE
Chittappen Kandiyil Prajeeth
prajeeth.chittappen.kandiyil@tiho-hannover.de

†These authors share first authorship

‡These authors share senior authorship

SPECIALTY SECTION
This article was submitted to Viral Immunology, a section of the journal Frontiers in Immunology

RECEIVED 30 December 2022
ACCEPTED 13 February 2023
PUBLISHED 28 February 2023

CITATION
Kubinski M, Beicht J, Zdora I, Saletti G, Kircher M, Petry-Gusmag M, Steffen I, Puff C, Jung K, Baumgärtner W, Rimmelzwaan GF, Osterhaus ADME and Prajeeth CK (2023) Cross-reactive antibodies against Langat virus protect mice from lethal tick-borne encephalitis virus infection.
*Front. Immunol.* 14:1134371.
doi: 10.3389/fimmu.2023.1134371



# Cross-reactive antibodies against Langat virus protect mice from lethal tick-borne encephalitis virus infection

Mareike Kubinski[1†], Jana Beicht[1†], Isabel Zdora[2,3†], Giulietta Saletti[1], Magdalena Kircher[4], Monique Petry-Gusmag[1], Imke Steffen[1,5], Christina Puff[2], Klaus Jung[4], Wolfgang Baumgärtner[2,3], Guus F. Rimmelzwaan[1], Albert D. M. E. Osterhaus[1‡] and Chittappen Kandiyil Prajeeth[1*‡]

[1]Research Center for Emerging Infections and Zoonoses, University of Veterinary Medicine Hannover, Foundation, Hannover, Germany, [2]Department of Pathology, University of Veterinary Medicine Hannover, Foundation, Hannover, Germany, [3]Center of Systems Neuroscience, Hannover Graduate School for Neurosciences, Infection Medicine, and Veterinary Sciences (HGNI), Hannover, Germany, [4]Institute for Animal Breeding and Genetics, University of Veterinary Medicine Hannover, Foundation, Hannover, Germany, [5]Institute for Biochemistry, University of Veterinary Medicine Hannover, Foundation, Hannover, Germany

**Introduction:** Naturally attenuated Langat virus (LGTV) and highly pathogenic tick-borne encephalitis virus (TBEV) share antigenically similar viral proteins and are grouped together in the same flavivirus serocomplex. In the early 1970s, this has encouraged the usage of LGTV as a potential live attenuated vaccine against tick-borne encephalitis (TBE) until cases of encephalitis were reported among vaccinees. Previously, we have shown in a mouse model that immunity induced against LGTV protects mice against lethal TBEV challenge infection. However, the immune correlates of this protection have not been studied.

**Methods:** We used the strategy of adoptive transfer of either serum or T cells from LGTV infected mice into naïve recipient mice and challenged them with lethal dose of TBEV.

**Results:** We show that mouse infection with LGTV induced both cross-reactive antibodies and T cells against TBEV. To identify correlates of protection, Monitoring the disease progression in these mice for 16 days post infection, showed that serum from LGTV infected mice efficiently protected from developing severe disease. On the other hand, adoptive transfer of T cells from LGTV infected mice failed to provide protection. Histopathological investigation of infected brains suggested a possible role of microglia and T cells in inflammatory processes within the brain.

**Discussion:** Our data provide key information regarding the immune correlates of protection induced by LGTV infection of mice which may help design better vaccines against TBEV.

KEYWORDS

**TBEV, immunity, cross-reactivity, LGTV, CNS**

# 1 Introduction

Flaviviruses are closely related RNA viruses that are capable of causing a spectrum of life-threatening diseases in humans. These include arthropod-borne disease-causing viruses such as tick-borne encephalitis virus (TBEV), dengue virus (DENV), Zika virus (ZIKV), Japanese encephalitis virus (JEV), yellow fever virus (YFV) and West Nile virus (WNV) (1). The single positive-stranded genomic RNA of flaviviruses encodes a single polyprotein which is cleaved into three structural proteins (capsid (C), envelope (E) and membrane (M)) and seven non-structural proteins (NS1, NS2A, NS2B, NS3, NS4A, NS4B and NS5) (2). Natural infection and vaccination with currently licensed inactivated whole TBEV vaccines evoke potent host immune responses against viral antigens. Interestingly, immune responses against flaviviruses were shown to cross-react with closely and distantly related viruses within this family (1, 3, 4). Cross-reactive immunity can either be protective or may contribute to disease enhancement (5–8). Serological analysis has identified antigenically related flaviviruses and grouped them into distinct serocomplexes (9). For instance, sera from individuals vaccinated against TBEV were shown to neutralize naturally attenuated Langat virus (LGTV), Kyasanur forest disease virus, Alkhurma virus and Powassan virus reminiscent of their grouping into the TBEV serocomplex (3). TBEV and LGTV share greater than 80% amino acid identity in the E protein (10). In humans, TBEV infections are mostly asymptomatic or lead to mild symptoms such as fever and headache. However, after several weeks, some patients develop tick-borne encephalitis (TBE) which may be life-threatening and lead to lifelong disabilities. In the early 1970s, LGTV was used as a candidate live-attenuated vaccine against TBEV infection in certain highly endemic areas of Russia. This was considered highly effective until encephalitis incidence of about 1:10000 was reported among vaccinees (10, 11). Consequently, the use of LGTV-based live vaccines has been discontinued. Currently, two formalin-inactivated whole TBEV vaccines (European strains) are used in Europe (12, 13). For effective prevention of TBE, manufacturers recommend administration of booster doses at three to five year intervals. However, data presented in a recent report suggests that these vaccines are still effective even when the booster intervals are extended to 10 years (14). Nevertheless, vaccine failures and breakthroughs have been reported in endemic areas and is a serious matter of concern (14–18). In contrast, the ability of live viral vaccines to induce both humoral- and cell-mediated immune responses, is highly appreciated. To further explore the potential of future candidate live attenuated TBE vaccines, a better understanding of the cross-immunity against TBEV induced by LGTV infection is important. In the present study, we dissected the contributions of cross-reactive antibodies and T cells in providing protection against lethal TBEV infection by adoptively transferring either serum or T cells from LGTV infected donor mice into naïve recipient mice. To this end, we have monitored disease progression, virus replication and histopathology in organs of mice challenged with TBEV upon LGTV infection.

# 2 Material and methods

## 2.1 Ethical statement

All animal experiments were conducted in strict compliance with European guidelines (EU directive on animal testing 2010/63/EU) and German Animal Welfare Law. The study protocol was approved by the Lower Saxony State Office for Consumer Protection and Food Safety (approval no. 33.8-42502-04-19/3259).

## 2.2 Mice

Female, 4-10 weeks old C57BL/6JOlaHsd (BL6) mice were purchased from Envigo RMS GmbH and were housed under pathogen-free conditions at the animal facility of the University of Veterinary Medicine Hannover, Foundation, in individually ventilated cages type Sealsafe Plus GM500 or IsoCage N Biocontainment system (Tecniplast) for the entire duration of the experiment. All mice were subjected to two weeks of habituation and acclimatization before they were taken into the experiments. Sterilized food pellets and water were provided *ad libitum*.

## 2.3 Viruses and cell culture

LGTV strain TP21 was obtained from Helmholtz Centre for Infection Research, Department of Molecular Immunology, Brunswick, Germany. Viral stocks were generated in VeroE6 cells and infectious virus titer was determined according to method described by Reed and Muench and expressed as tissue culture infectious dose 50% (TCID50) (19). TBEV strain Neudoerfl was provided by the Department of Microbiology of the German Armed Forces, Munich, Germany. Virus propagation and determination of titer by TCID50 assay were done in A549 cells. VeroE6 cells were grown in Eagle's minimum essential medium (EMEM, Sigma-Aldrich) supplemented with 10% fetal bovine serum (FBS), 1% penicillin/streptomycin (Pen/Strep), 1% GlutaMAX™ and 20 mM HEPES. A549 cells were cultured in F-12 Nut Mix (1X) + GlutaMAX-I (Gibco™) containing 10% FBS, 1% Pen/Strep, 1% GlutaMAX™ and 20 mM HEPES. Cells were stored at 37°C/5% $CO_2$. All cell lines and viral stocks were tested negative for mycoplasma.

## 2.4 LGTV immunogenicity study

Six- to eight-week-old BL6 mice (n=6 per group) were inoculated subcutaneously (s.c.) with $1.4x10^4$ TCID50 LGTV TP21 in 100 µl PBS or PBS only. At 28 days post infection (dpi), mice were bled by retrobulbar sinus puncture under isoflurane induced anesthesia and blood was collected in MiniCollect® CAT Serum Sep Clot Activator tubes (Greiner Bio-One GmbH). To obtain sera, blood was kept for 30 min at room temperature (RT)

and centrifuged at 3000x*g* for 10 min. Subsequently, mice were euthanized by cervical dislocation and spleens were collected. Single-cell suspensions from mouse spleens were prepared by using cell strainers and erythrocyte lysis was performed using ACK Lysing buffer (Gibco™). Subsequently, cells were resuspended in RPMI 1640 (1X) (Gibco™) + 10% FBS + 1% Pen/Strep + 5 mM ß-mercaptoethanol (R10F) for further use.

## 2.5 Adoptive transfer experiments

Donor mice (n=5 per group) were immunized by administering PBS or LGTV as described above. At 28 dpi, sera and spleens were collected from these mice. Sera from respective groups were pooled before transferring into naïve recipient mice. Similarly, splenocytes from each group were pooled and $CD3^+$ T cells were isolated using the autoMACS® Pro Separator (Miltenyi Biotec B.V. & Co. KG) with the mouse Pan T Cell Isolation Kit II (Miltenyi Biotec B.V. & Co. KG). Ten to twelve weeks old naïve recipient mice (n=5 per group) either received 200 µl of serum or $2.53x10^7$ $CD3^+$ T cells intraperitoneally (i.p.). After 4 h, recipient mice were challenged s.c. with $5.4x10^3$ TCID50 TBEV Neudoerfl (100 µl). Following TBEV challenge infection, mice were monitored daily for a period of 16 dpi. Mice that developed clinical signs were given certain scores as per the information provided in the scoring sheet (Supplementary Table S1). Based on the clinical score attained, the humane endpoint (HEP) was determined and those mice that reached HEP were sacrificed. All other mice were monitored until 16 dpi (study endpoint) and subsequently euthanized. At sacrifice, serum was collected as described above. Left hemisphere of the brain, spinal cord and spleen were collected in PBS, homogenized with a stainless-steel bead by using the TissueLyser II (Qiagen) with 30 Hz for 1 min and stored at -80°C.

## 2.6 Virus neutralization assay

LGTV and TBEV virus neutralizing antibody titers (VNT) in serum of control and LGTV infected mice were determined by using virus neutralization assay (VNA) on VeroE6 and A549 cells, respectively, with 80% confluence. Sera was heat-inactivated for 30 min at 56°C and 2-fold serial dilutions were prepared in infection medium (same as growth medium but with 2% FBS). Serum dilutions were mixed with 100 TCID50 of LGTV TP21 or TBEV Neudoerfl and incubated for 1 h at 37°C/5% $CO_2$. Serum-virus mix was added to VeroE6 or A549 cells and incubated at 37°C/5% $CO_2$. Read-out based on presence/absence of cytopathic effect (CPE) was done after 5-6 days. VNT100 was determined as the reciprocal of the highest serum dilution where no CPE was visible.

## 2.7 Luciferase immunoprecipitation systems assay

Luciferase immunoprecipitation systems (LIPS) assay was performed as described previously (20). Briefly, supernatants containing TBEV-specific fusion proteins (C, prM, E-DIII, NS1, NS3-DIII, NS4b) or fusion protein without insert (secNLuc, control) were incubated with 1:100 dilution of heat-inactivated mouse serum. Luminescence was measured using the microplate reader infinite 200Pro (Tecan) with Tecan i-control software (version 2.0.10.0, Tecan). Average of triplicate measurements was determined and data was expressed as $\log_{10}$ relative light units (RLU). Luminescence values higher than the average of negative samples plus five-times the standard deviation are considered positive.

## 2.8 *Ex vivo* restimulation of splenocytes

Short peptide oligomers (15-mers with 11 amino acid overlaps) spanning the entire C, E, NS1, NS3 and NS5 proteins of TBEV Neudoerfl (UniProtKB: P14336) were synthesized (≥ 75% purity, GenScript Biotech Corp). Lyophilized peptides were reconstituted in DMSO (Hybri-Max™, Sigma-Aldrich) and peptide pools were generated as described in Supplementary Table S2. Concentration of each peptide in the pool was adjusted to 10 µg/ml and was used at final concentration of 1 µg/ml. Splenocytes ($0.5\text{-}1x10^6$ cells/well) were restimulated with respective peptide pools. Negative controls were treated with DMSO or R10F. Positive controls were treated with mixture of 30 ng/ml Phorbol 12-myrisate 13-acetate (PMA; Cayman Chemical) and 0.5 µg/ml Ionomycin (Cayman Chemical).

## 2.9 IFN-γ ELISpot assay

Splenocytes ($5x10^5$ splenocytes/well) restimulated as described above were tested for IFN-γ producing cells using mouse IFN-γ ELISpot Plus kit (Mabtech). For positive control (PMA/ionomycin stimulation), only $5x10^4$ splenocytes/well were used. The assay was carried out according to manufacturer's instructions. Following overnight incubation with respective peptide pools at 37°C/5% $CO_2$, plates were stained, developed and scanned using the ImmunoSpot® S6 Ultimate Reader (Cellular Technology Limited). ImmunoSpot® software (version 7.0.20.1, Cellular Technology Limited) was used for counting spots and data analysis. IFN-γ spots per $10^6$ splenocytes were calculated and duplicate measurements were averaged. After subtraction of negative control, data were shown as IFN-γ spot-forming cells (SFC)/$10^6$ splenocytes.

## 2.10 Flow cytometry analysis

Following restimulation of splenocytes with respective peptide pools (as described above) for 6 h at 37°C/5% $CO_2$, T cells were further characterized by performing intracellular cytokine staining and flow cytometry. To block cytokine secretion from activated T cells, Brefeldin A (10 µg/ml, Sigma-Aldrich) was added to the medium for the final 4 h of restimulation. Cells were stained with LIVE/DEAD™ Fixable Near-IR Dead Cell Stain Kit for 633 or 635 nm excitation (Invitrogen™) for 20 min in the dark. Fc blocking

was done with anti-Mouse CD16-CD32 (Clone: 93) for 15 min at RT. Surface staining using anti-Ms CD3e FITC (Clone: 145-2C11), anti-Ms CD4 PE (Clone RM4-5) and anti-Ms CD8a PerCP-Cyanine5.5 (Clone: 53-6.7) was done for 20 min at 4°C in the dark. After fixation and permeabilization with BD Cytofix/Cytoperm™ (BD Biosciences) for 20 min at 4°C in the dark, intracellular staining using anti-Ms IFN- γ APC (Clone: XMG1.2) and anti-hu/ms Granzyme B BV421 (Clone: QA18A28, BioLegend®) was performed for 30 min at 4°C in the dark. Finally, cells were resuspended in PBS and acquired by BD LSR Fortessa X-20 (BD Biosciences) using BD FACSDiva (version 9.0, BD Biosciences). All antibodies were purchased from eBioSciences™ (Invitrogen™) unless otherwise stated. Data analysis was performed by FlowJo™ software (version 10.8.1, BD Biosciences).

## 2.11 Determination of infectious virus titers

A 1:10 serial dilution of serum or organ homogenate (free of cell debris) was prepared in A549 infection medium (same as growth medium but with only 2% FBS) and transferred to approximately 80% confluent A549 cells. After 5-6 days at 37°C/5% $CO_2$, TCID50 values for individual samples were determined by CPE-based read-out as described above. Detection limit for each organ titration was defined as lowest homogenate dilution ($10^1$) divided by the average of respective organ weights.

## 2.12 RNA isolation and real time quantitative reverse transcription PCR

Total RNA of serum (pre-diluted 1:10 in A549 medium) or organ homogenate (free of cell debris) was isolated using QIAmp® Viral RNA Mini Kit (Qiagen) according to manufacturer's manual. For detection of TBEV RNA, real time quantitative reverse transcription (RT)-PCR using One-Step RT-PCR Kit (Qiagen) was performed based on the protocol established by Schwaiger and Cassinotti (21) with few modifications. To determine TBEV RNA copies, a dilution row of TBEV Neudoerfl RNA standard was used. The standard was kindly provided by Stefanie Becker (Institute for Parasitology and Research Center for Emerging Infections and Zoonoses at University of Veterinary Medicine Hannover, Foundation). As negative control, AVE buffer instead of sample was used. Real time quantitative RT-PCR was performed in duplicates using AriaMx Real-time PCR System (Agilent Technologies) with Agilent Aria software (version 1.5, Agilent Technologies). Cq values were converted into $\log_{10}$ TBEV copies/ml or gram tissue, respectively, according to the standard curve.

## 2.13 Histology

For histopathological analysis, the right hemisphere of the brain and the gastrointestinal tract were collected and fixed in ROTI®Histofix 4% (4% formaldehyde, Roth) for a minimum of 48 h. Two longitudinal sections of the brain and representative sections of duodenum, jejunum, ileum, caecum, colon and rectum of all mice were embedded in paraffin wax followed by cutting 2-3 µm thick sections using a microtome. Sections were stained with hematoxylin and eosin (H&E).

## 2.14 Histological evaluation

H&E stained sections of brain and intestine were analyzed using a semiquantitative scoring system. Ten different regions of the brain including olfactory bulb, cerebral cortex, basal forebrain, hippocampus, thalamus, hypothalamus, midbrain, pons, medulla and cerebellum were investigated applying six scoring categories. Scores were generated for each evaluable brain region separately. Meninges, perivascular as well as vascular inflammation, vascular lesions including perivascular edema, hemorrhage and fibrinoid necrosis, microgliosis characterized by hyperplasia and/or hypertrophy of microglia/macrophages as well as cellular necrosis characterized by karyorrhexis, karyolysis, pyknosis and triangularly shaped, hyperosinophilic and shrunken neurons were evaluated using a scoring system detailed in Supplementary Table S3. Duodenum, jejunum, ileum, caecum, colon and rectum were scored using five different categories. Hypercellularity/inflammatory infiltrates within the *lamina propria* of the *tunica mucosa* were evaluated. Additionally, *plexus submucosus* and *plexus myentericus* ganglia were each scored regarding necrosis of ganglion neurons characterized by karyorrhexis, karyolysis and pyknosis, hyperosinophilia and shrinkage of neurons as well as inflammatory infiltrates/hypercellularity (for detailed scoring system see Supplementary Table S4).

## 2.15 Immunohistochemistry

Immunohistochemistry (IHC) was performed as described previously (22) applying the avidin-biotin-peroxidase (ABC) complex method and using antibodies for the detection of TBEV (anti-TBEV E protein clone 1493, Matthias Niedrig, mouse monoclonal), T cells (anti-CD3, Agilent Dako, Cat.No. A0452, rabbit polyclonal), B-lymphocytes (anti-CD45R, BD Bioscience, Cat.No. 553085, rat monoclonal), microglia/macrophages (anti-ionized calcium-binding adapter molecule 1 (Iba1), Wako Chemicals, 019-19741, polyclonal rabbit) and astrocytes (anti-glial fibrillary acidic protein (GFAP), Dako Cytomation, Cat.No. Z0334, rabbit polyclonal). Briefly, sections of brain and intestine were dewaxed and rehydrated in a graded series of alcohol. For anti-CD3, anti-CD45R and anti-Iba1 antibodies, antigen retrieval was achieved by boiling sections in citrate buffer (pH = 6) in a microwave (800W) prior to blocking of unspecific binding sites. For anti-TBEV and anti-GFAP antibodies, no pretreatment was necessary. After overnight incubation of primary antibodies, sections were incubated with the respective biotinylated secondary antibodies for 45 min. The staining was visualized using chromogen 3,3'-diaminobenzidine tetrahydrochloride (DAB) and counterstaining of nuclei with Mayer's hematoxylin (Roth C.GmbH & Co KG).

## 2.16 Immunohistochemical evaluation

The immunohistochemical stains of brain and intestine with TBEV, CD3, CD45R, Iba1 and GFAP were analyzed using a semiquantitative scoring scheme. No infiltration with CD45R-positive B-lymphocytes and no altered staining for GFAP were evident and therefore not included in further analyses. Detection and distribution of TBEV-positive cells, CD3-positive T cells, and Iba1-positive microglia/macrophages in the brain and intestinal tissue sections were evaluated using the scoring system detailed in Supplementary Table S5.

## 2.17 Statistical analysis

The immunogenicity and survival data were analyzed using GraphPad Prism software (version 9.0.0, GraphPad Software Inc.). For comparison of VNT100, LIPS and ELISpot data unpaired t-test was used. Survival data are shown as Kaplan-Meier curves and were analyzed by log rank test. Histopathological and IHC scorings were analyzed using R (version 4.2, www.r-project.org) and described using mean (median, minimum, maximum) per experimental group. The effects of transfer group ($CD3^+$, Serum), treatment (control, LGTV) as well as the interaction of group and treatment were first analyzed using non-parametric ANOVA (23). In case of significant effects in the ANOVA, subsequent pairwise comparisons between experimental groups were performed using Wilcoxon rank sum tests. Raw p-values from the Wilcoxon tests were adjusted for multiple testing within sets of scores related to the same organ region using the method of Bonferroni-Holm. A *p-value* <0.05 was considered significant

# 3 Results

## 3.1 Infection of mice with LGTV induces cross-reactive antibodies against TBEV

Previously we have shown that s.c. administration of LGTV protects mice against subsequent lethal challenge infection with TBEV (24). In the present study, we aimed at defining the correlates of protection induced by LGTV acting against TBEV. Sera collected from control and LGTV infected mice at 28 dpi were tested for the presence of virus neutralizing (VN) antibodies against LGTV and TBEV. As expected, high titers of LGTV-neutralizing antibodies were observed in LGTV infected mice (Figure 1A). Interestingly, the

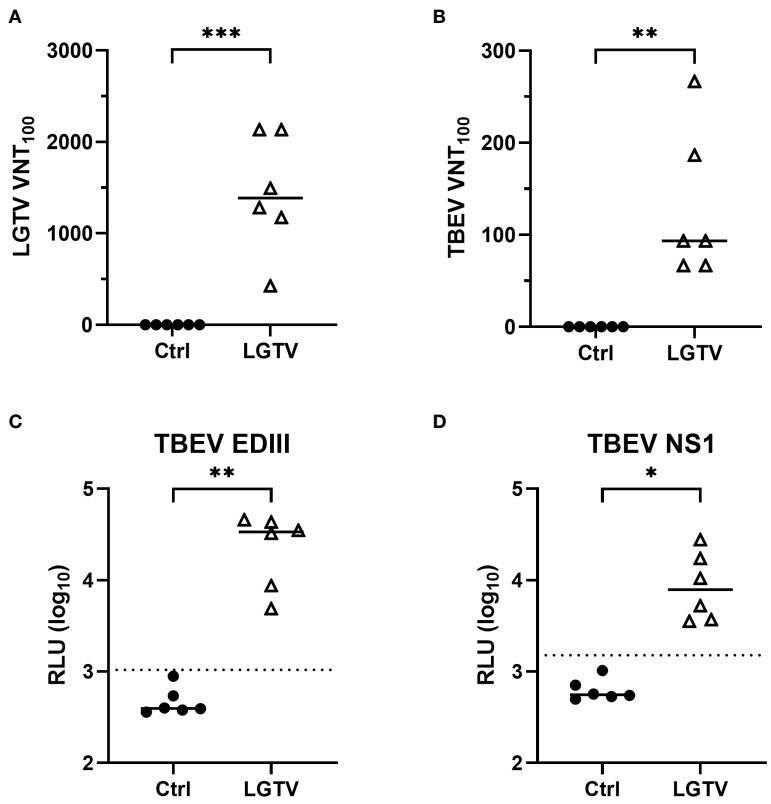


FIGURE 1
TBEV cross-reactive antibodies in the serum of LGTV immunized mice. Serum collected from control (•) or LGTV (Δ) infected mice (n=6) were tested for their ability to block the infection of **(A)** LGTV (p = 0.0003) and **(B)** TBEV (p = 0.0029) in VeroE6 and A549 cells, respectively. The graphs show the titer at which 100% virus neutralization is achieved ($VNT_{100}$). LIPS assay with 1:100 dilution of serum detected antibodies against **(C)** domain III of the TBEV E protein (p = 0.0029) and **(D)** TBEV NS1 protein (p = 0.0214). Luciferase activity was measured in three independent experiments and is displayed as mean values of $log_{10}$ RLU. Luminescence values higher than the average of negative samples plus five-times the standard deviation (dotted line) are considered positive. Median is shown in all graphs. *p<0.05, **p<0.01 and ***p<0.001.

10.3389/fimmu.2023.1134371

same sera also displayed considerable neutralizing activity against TBEV, although the VN titers were 10-fold lower than those to LGTV (Figure 1B). Using LIPS assay, we could demonstrate the presence of cross-reactive antibodies against domain III of TBEV E and NS1 proteins (Figures 1C, D).

## 3.2 LGTV specific T cells cross-react with TBEV antigens

As for antibodies induced by LGTV infection, the LGTV infection induced T cell response and its cross-reactivity to TBEV antigens were analyzed. To this end, we restimulated splenocytes from control and LGTV infected mice with 15-mer synthetic peptide pools of C, E, NS1, NS3 and NS5 proteins of TBEV. These peptide pools were designed with 11 amino acid overlaps, hence ensuring that none of the $CD4^+$ and $CD8^+$ T cell epitopes were missed out. Frequencies of IFN-γ producing effector T cells were determined using IFN-γ ELISpot. A high frequency of T cells that specifically cross-reacted with epitopes within E, NS3 and NS5 proteins of TBEV was observed (Figure 2A). As indicated in Figure 2A, the most prominent response was observed upon restimulation with the peptide pool that encompasses the amino acid (aa) sequence 205-419 of NS3 and the C terminal region (aa673-903) of the NS5 protein. Furthermore, flow cytometric evaluation of splenocytes revealed that $CD4^+$ T cells were the major source of IFN-γ producing cells more prominently in response to $NS3_{205-419}$ and $NS5_{673-903}$ restimulation (Figure 2B). Nevertheless, we could not detect $CD8^+$ T cell effectors in response to the TBEV peptides restimulation.

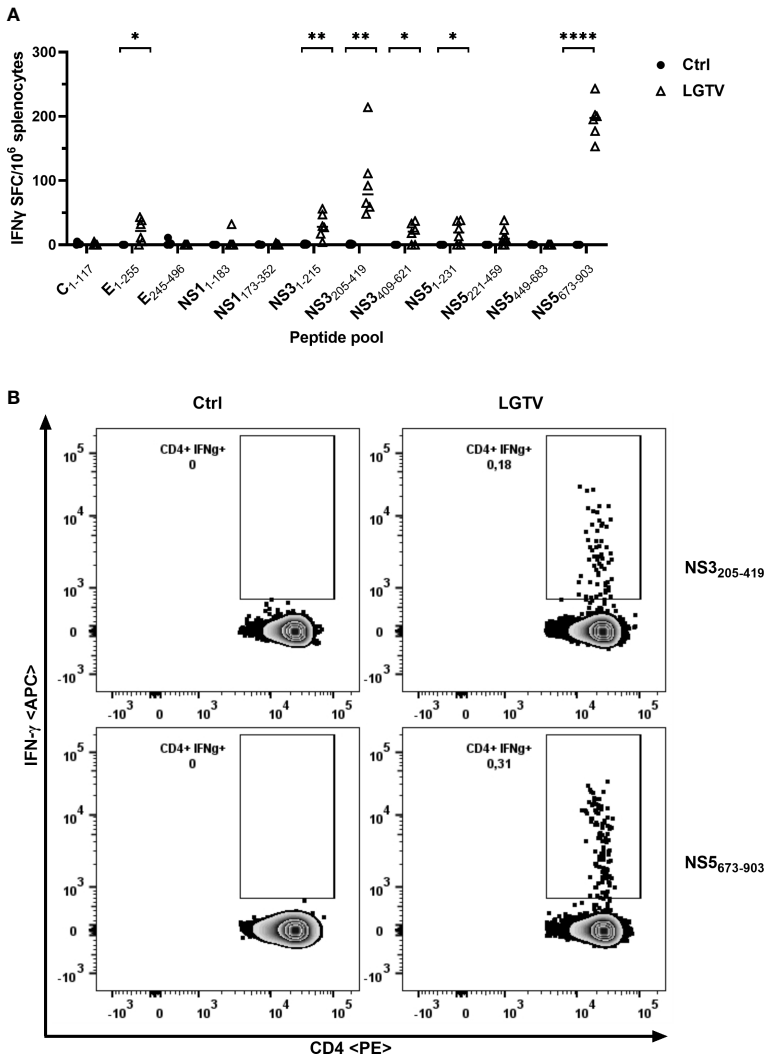


FIGURE 2
T cells induced by LGTV cross-react with TBEV antigenic peptides. **(A)** Splenocytes collected from control (•) or LGTV (Δ) infected mice (n=6) were restimulated with TBEV-specific peptide pools and the frequency of IFN-γ producing cells were determined using IFN-γ ELISpot assay. For statistical analysis, unpaired t-test was used ($E_{1-255}$: p = 0.0168; $NS3_{1-215}$: p = 0.0038; $NS3_{205-419}$: p = 0.003; $NS3_{409-621}$: p = 0.0178; $NS5_{1-231}$: p = 0.023; $NS5_{673-903}$: p <0.0001) and the median is shown. **(B)** Flow cytometric analysis of splenocytes restimulated with TBEV peptide pools. Representative FACS plots gated on live $CD3^+$ $CD4^+$ T cells show IFN-γ in LGTV infected mice in response to TBEV $NS3_{205-419}$ and $NS5_{673-903}$ peptide pool restimulation. *p<0.05, **p<0.01 and ****p<0.0001.

## 3.3 Serum from LGTV protects mice against TBEV challenge

We demonstrated that LGTV infected mice developed VN antibodies that cross-react with TBEV. To determine if the cross-reactive antibodies confer protection to mice against lethal TBEV challenge, we adoptively transferred sera collected from control or LGTV infected mice into naïve BL6 mice prior to TBEV exposure (Figure 3; Supplementary Figures S1A, B).

Body weight loss and development of clinical signs were assessed daily and mice were sacrificed when the HEP was reached. Following TBEV challenge, the majority of mice (4 out of 5) that had received control sera continuously lost weight (Figure 4A) starting from 6 dpi and did not recover thereafter (Figure 4C). As the disease progressed, they displayed piloerection, decreased activity, kyphosis and signs of abdominal discomfort. These mice reached the HEP between 8-12 dpi and were subsequently sacrificed. Major HEP determinant in most cases was body weight loss reaching 20%. The one surviving mouse in this group did not display any clinical signs of disease and remained healthy until 16 dpi, which was the study endpoint. Contrarily, four out of five mice from the group that received sera from LGTV infected donors were completely protected and remained healthy without any visible clinical signs until 16 dpi (Figures 4B, C). Only one mouse in this group started losing weight at around 11 dpi and reached the HEP at 13 dpi with severe signs of disease characterized by extreme body weight loss, dulled fur with slightly hunched back, reduced activity and neurological signs manifested as spinal ataxia. Additionally, virus burden and distribution in the serum, spleen, spinal cord and brain was determined in these mice. No infectious virus was found in serum and spleen in any of these mice, suggesting absence of viremia at the time of sacrifice (Figure 4D). However, high TBEV infectivity titers were detected in the brain and spinal cord of all mice that reached the HEP including the one mouse that received serum from LGTV infected donors. TCID50 results confirm absence of infectious TBEV in brain and spinal cord of the remaining four healthy recipient mice from the LGTV serum group and one survivor from the control group (Figure 4D). Detection of viral genome copies by real time quantitative RT-PCR also yielded similar results with the exception of one survivor in the LGTV serum recipient group where infectious TBEV was not detected in TCID50 analysis but low levels of viral RNA (~$10^5$ copies/gram tissue) could be found in the brain but not in the spinal cord (Supplementary Figure S2). Similarly, viral genome copies but

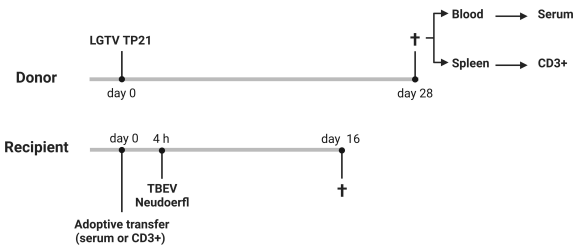


FIGURE 3
Schematic representation of adoptive transfer experiments. 6-8 weeks old control or LGTV infected donor mice (n=5) were sacrificed at 28 dpi and the sera and spleens were collected. 200 µl of pooled serum or 2.53x$10^7$ $CD3^+$ T cells from control or LGTV infected mice were administered i.p. into 10-12 weeks old naïve recipient mice (n=5). After 4 h, these mice were challenged with TBEV Neudoerfl (created with BioRender.com).

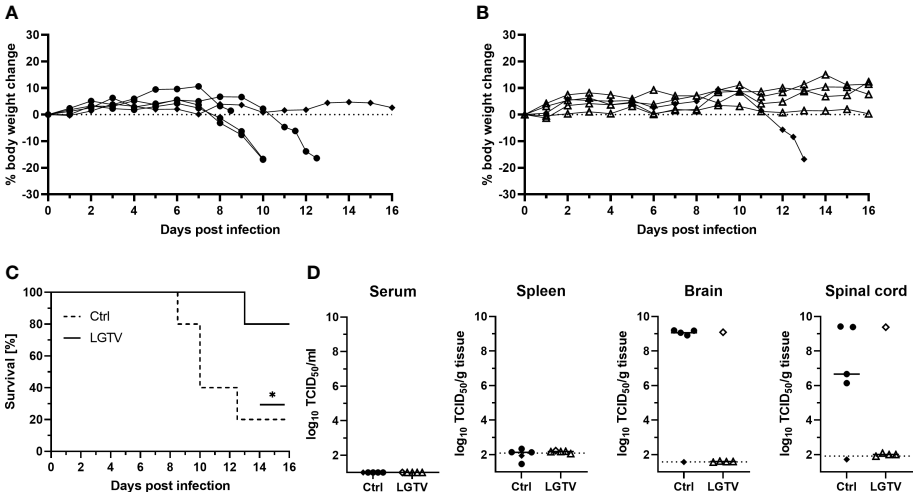


FIGURE 4
Immune serum from LGTV infected mice protects mice against subsequent TBEV challenge infection. Serum pooled from the respective group was i.p. injected into recipient mice (n=5). Following TBEV challenge infection, body weight of mice that received **(A)** control serum or **(B)** LGTV immune serum was monitored over a period of 16 dpi. Mice were taken out of experiment when the HEP was reached. **(C)** Survival curve plotted for the recipient mice that received control serum (dotted line) or serum from LGTV infected mice (solid line). Significant difference was analyzed by log rank test ($p = 0.033$). **(D)** TCID50 was performed on serum and tissue homogenates to determine the viral load in serum, spleen, brain and spinal cord of control (•) or LGTV (Δ) serum recipients collected at the day of sacrifice. Median values are shown. Mice that differed in their clinical state from other mice in the control and LGTV serum recipient group are highlighted as rhombus shaped symbols. *$p<0.05$.

not infectious virus could be detected in spleen and brain of the only survivor of the control serum recipient group. Overall, the results further confirm that LGTV antibodies cross-react with TBEV antigens and efficiently protect mice from lethal TBEV infection.

## 3.4 T cells from LGTV infected mice did not confer protection against TBEV challenge

To further investigate the contribution of T cells induced by LGTV infection in protecting mice against TBEV infection, we adoptively transferred $CD3^+$ T cells sorted from the spleens of either control or LGTV infected mice into naïve recipient mice prior to TBEV challenge (Figure 3; Supplementary Figure S1C). Purity of transferred T cells was determined by flow cytometry before transfer and was approximately 97% (Supplementary Figure S3). To ensure that the frequency of T cells actual reflected our previously published vaccination-challenge experiments, we transferred T cells isolated from five donor mice into five recipient mice. Unexpectedly, all mice that received T cells either from controls or from LGTV infected donors developed severe illness and succumbed to infection between 10-13 dpi (Figure 5C). Irrespective of the source of transferred T cells, the recipient mice displayed weight loss starting 7 dpi and never recovered thereafter (Figures 5A, B). Furthermore, the viral load in the brain and spinal cord between these two recipient groups was similar (Figure 5D, Supplementary Figure S2B) suggesting the inability of T cells to control the ongoing infection in the absence of serum antibodies.

## 3.5 Histopathological changes of the central nervous system

The most striking histopathological changes observed in H&E stained brain sections of affected mice comprised cellular necrosis, microgliosis, perivascular inflammation and vasculitis in the brain parenchyma mostly confined to the grey matter and including the leptomeninx (Figures 6A-G). ANOVA for these parameters resulted in significant interaction effects, meaning the effect of LGTV treatment was inverse for $CD3^+$ and serum transfer. After multiple testing adjustment, this interaction effect remained only significant for "H&E brain cerebral cortex cellular necrosis" (Supplementary Table S6). Affected brains displayed neuronal and glial necrosis characterized by shrunken and hypereosinophilic cells with karyorrhectic, karyolytic and pyknotic nuclei. Areas of necrosis were accompanied by an increased number of activated microglia/macrophages and T cells as well as neuronophagia. In addition, inflammatory infiltrates were predominantly found perivascularly and consisted mostly of lymphocytes, macrophages and scattered neutrophils. Additionally, a fibrinoid, non-leukocytoclastic vasculitis of small to medium sized blood vessels characterized by loss of vascular wall integrity with an infiltration of the destructed vascular wall with inflammatory cells was noticed.

All brain regions were scored according to the semiquantitative scoring scheme (Supplementary Table S3) and revealed similar findings. Therefore, three representative, consistently affected brain regions (olfactory bulb, cerebral cortex and hippocampus) were selected for more detailed analysis. Since statistical significances displayed high variations across brain regions and parameters, focus was set on these brain regions. Statistical scores as

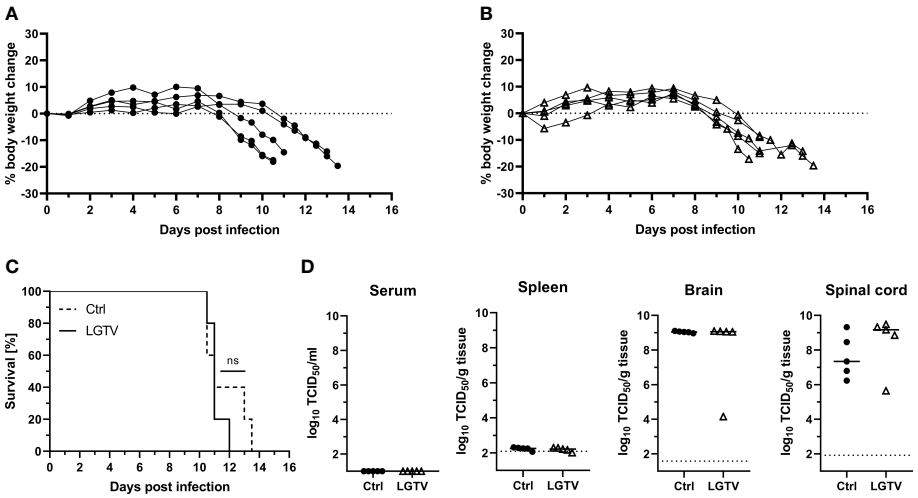


FIGURE 5
T cells from LGTV infected mice do not protect mice against subsequent TBEV challenge infection. $CD3^+$ T cells purified from control or LGTV infected mice (n=5) were i.p. administered into naïve recipient mice (n=5). Following TBEV challenge infection, body weight of mice that received T cells of **(A)** control or **(B)** LGTV infected mice was monitored over a period of 16 dpi. Mice were taken out when they reached the HEP. **(C)** Survival curve plotted for the recipient mice that received control $CD3^+$ T cells (dotted line) or $CD3^+$ T cells from LGTV infected mice (solid line). Significant difference was analyzed by log rank test (p = 0.4389). **(D)** TCID50 was performed on serum and tissue homogenates to determine the viral load in serum, spleen, brain and spinal cord of control (•) or LGTV (Δ) $CD3^+$ T cell recipients collected at the day of sacrifice. Median values are shown.

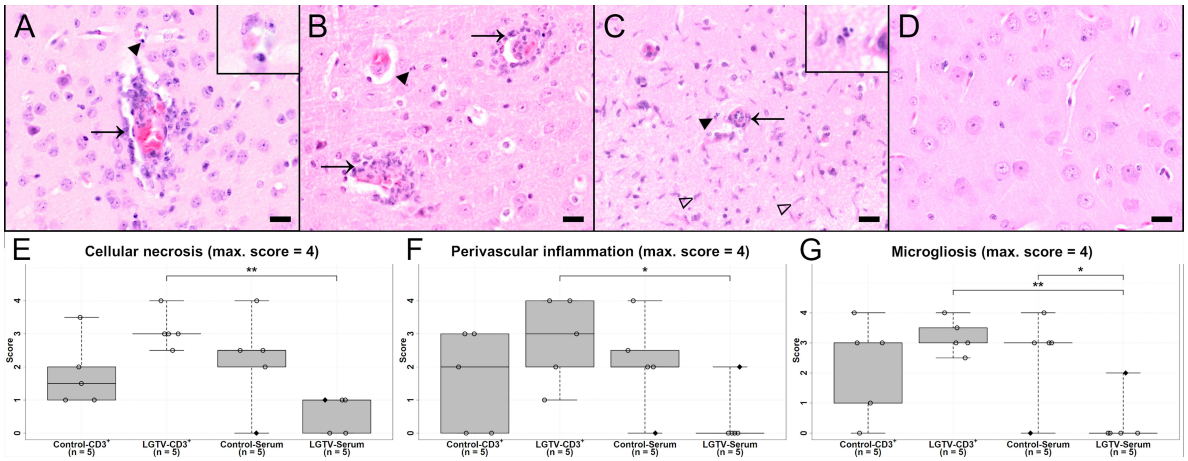


FIGURE 6
H&E stained sections of cerebral cortex of one representative mouse from each group **(A)** $CD3^+$ T cell transfer from control donors; **(B)** $CD3^+$ T cell transfer from LGTV infected donors; **(C)** serum transfer from control donors; **(D)** serum transfer from LGTV infected donors. In **(A–C)** signs of inflammation with infiltration of damaged blood vessels with inflammatory cells (arrow, **(A)**, **(B)**), perivascular inflammation as well as cell necrosis (arrowhead and inserts) and microgliosis (blank arrowhead, **(C)**) are visible. In the cerebral cortex of the mouse that had received serum from LGTV infected donors, no histopathological changes are observed **(D)**. Scale bars: 20 µm. **(E–G)** display box plots of the scoring values for "cellular necrosis" **(E)**, "perivascular inflammation" **(F)** and "microgliosis" **(G)** of cerebral cortex for each experimental group. Significant differences detected by pairwise Wilcoxon rank-sum tests after non-parametric ANOVA and multiple testing adjustment are indicated by asterisks (* $p < 0.05$; ** $p < 0.01$). Mice that differed in their clinical state from other mice in the control and LGTV serum recipient group are highlighted as rhombus shaped dots in the box plots.

well as significant values for cerebral cortex and scoring categories including H&E and immunohistochemical evaluation are depicted in Figure 6; Supplementary Figure S4, S5 and Supplementary Table S6.

In H&E stained sections, mice of the control-$CD3^+$, LGTV-$CD3^+$ and control-serum groups displayed more severe histopathological changes within the brain than mice that had received serum from LGTV infected donors (Figure 6; Supplementary Figure S4). Significant differences within the olfactory bulb for the scoring categories microgliosis, cellular necrosis and vascular inflammation were observed (Supplementary Figures S4A, C). The scores related to cellular necrosis differed significantly between the LGTV-$CD3^+$ and the LGTV-serum group (Supplementary Figure S4A; $p = 0.008$) as well as the control-$CD3^+$ and the LGTV-serum group (Supplementary Figure S4A; $p = 0.018$). A significant difference for microgliosis was detected between LGTV-$CD3^+$ and LGTV-serum group (Supplementary Figure S4C; $p = 0.008$). Vascular inflammation scores differed significantly between control-serum and LGTV-serum group ($p = 0.048$). Within the cerebral cortex, mice from the LGTV-serum group displayed significantly lower scores for cellular necrosis of cerebral cortex than mice from the LGTV-$CD3^+$ group (Figure 6E; $p = 0.008$). Furthermore, scores of the LGTV-serum group for microgliosis of cerebral cortex were significantly lower in comparison to LGTV-$CD3^+$ ($p = 0.008$) and control-serum group (Figure 6G; $p = 0.048$). Perivascular inflammation of cerebral cortex scores were significantly different between LGTV-$CD3^+$ group and LGTV-serum group (Figure 6F; $p = 0.024$). Overall, lowest scores were achieved by the group that had received serum from LGTV infected donors, although one mouse that presented clinical signs from this group displayed histopathological lesions in the brain (Figures 6E-G). In the hippocampus, a significant difference for microgliosis was observed between LGTV-$CD3^+$ group and LGTV-serum group (Supplementary Figure S4F; $p = 0.008$).

IHC using an antibody directed against the TBEV E protein Figures 7A, D, G, J) revealed the presence of high virus burden in the brain of all mice that succumbed to TBEV infection (15/20) irrespective of their treatment regimen (Figures 7A, D, G; Supplementary Figures S5A, D). TBEV antigen was mostly found in the cytoplasm of cells that appeared to be neurons according to distribution and morphology. This is consistent with previous findings (24). In four mice from the LGTV infected serum recipient group, no TBEV E protein was detected immunohistochemically. The only diseased mouse in this group where the histopathological changes were evident also showed positive immunoreactivity for TBEV E protein in the brain (Figure 7M). This is supported by statistical analysis. Scores of IHC-TBEV in the olfactory bulb differed significantly between the control-$CD3^+$ and the LGTV-serum group (Supplementary Figure S5A; $p = 0.018$). Additionally, the cerebral cortex ANOVA yielded that IHC-TBEV scores were significantly higher in $CD3^+$ T cell recipients than in serum recipients. Specifically, TBEV-IHC scores of the LGTV-serum group were significantly lower than scores of mice from LGTV-$CD3^+$ group (Figure 7M; $p = 0.024$).

IHC for CD3 (Figures 7B, E, H, K) revealed that $CD3^+$ T cells were infiltrating the perivascular space as well as the vascular wall of affected brains (Figures 7B, E, H). The olfactory bulb showed significant differences for CD3 immunoreactivity between control-$CD3^+$ and LGTV-serum group ($p = 0.036$), between LGTV-$CD3^+$ and LGTV-serum group ($p = 0.008$) and control-serum and LGTV-serum group (Supplementary Figure S5B; $p = 0.024$). Furthermore, IHC-CD3 scores in the cerebral cortex of the

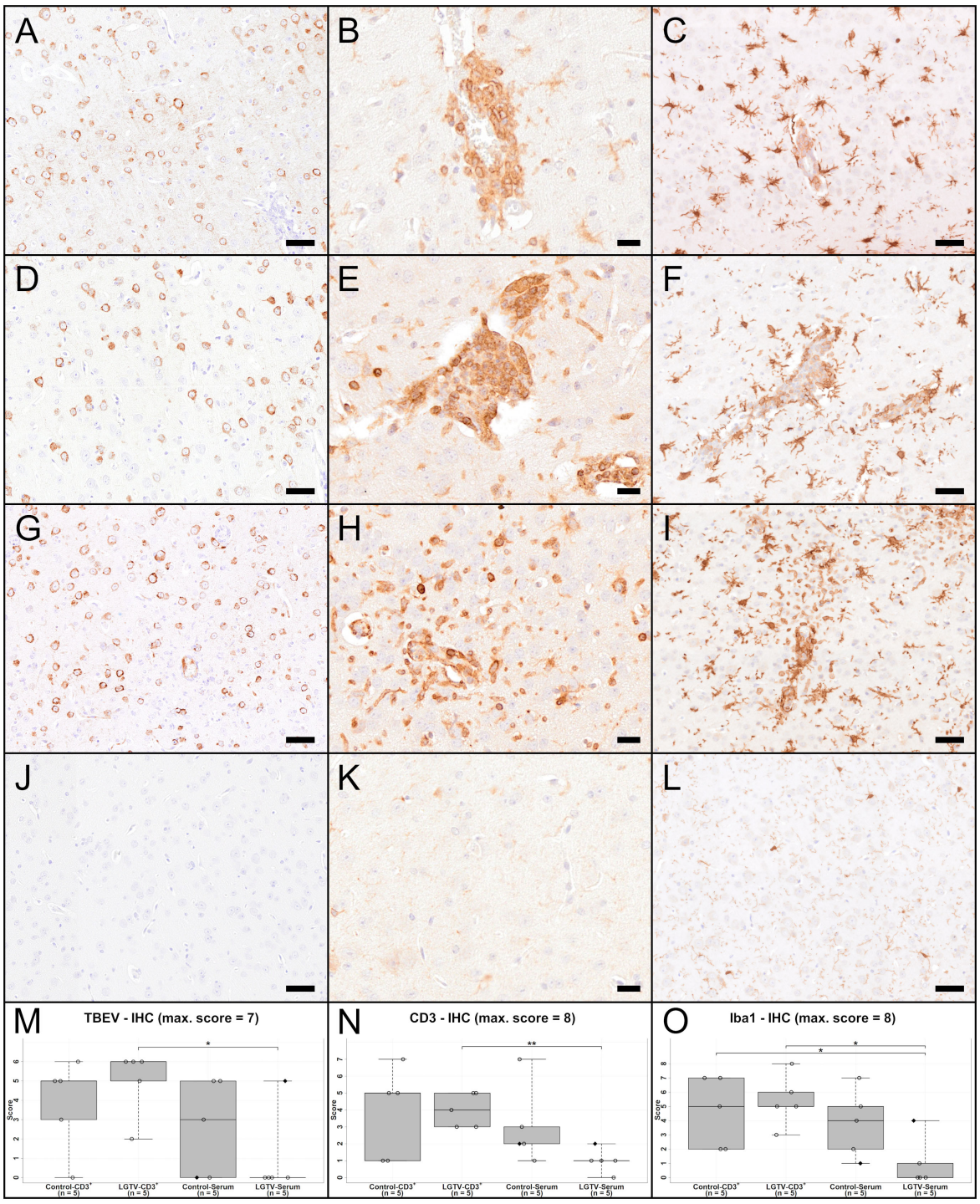


FIGURE 7
IHC of cerebral cortex for TBEV **(A, D, G, J)**, T cell marker CD3 **(B, E, H, K)** and microglia/macrophage marker Iba1 **(C, F, I, L)** of one representative mouse from each group **(A–C)**: $CD3^+$ T cell transfer from control donors; **(D–F)**: $CD3^+$ T cell transfer from LGTV infected donors; **(G–I)**: serum transfer from control donors; **(J–L)**: serum transfer from LGTV infected donors). TBEV E protein is detectable in the cytoplasm of neurons in all mice **(A, D, G)** except the mouse in the serum transfer group from LGTV infected donor mice **(J)**. CD3-positive T cells are detectable in the vascular wall as well as the perivascular space of affected mice **(B, E, H)**, while no immunoreaction is visible in the mouse of the serum transfer from LGTV infected donor mice **(K)**. There is distinct increase in staining intensity and number of Iba1-positive microglia/macrophages indicating activation and proliferation of microglia and/or proliferation/infiltration of macrophages in affected mice **(C, F, I)** in comparison to the mouse of the serum transfer group from LGTV infected donor mice in which microglia are normal-sized with fine processes **(L)**. Scale bar **(A, D, G, J, C, F, I, L)**: 50 µm; scale bar **(B, E, H, K)**: 20 µm. **(M–O)** display box plots of the scoring values of IHC for TBEV (TBEV-IHC; **(M)**, IHC for CD3 (Iba1-IHC; **(N)** and IHC for microglia/macrophages marker Iba1 (Iba1-IHC; **(O)** of cerebral cortex for each experimental group. Significant differences detected by pairwise Wilcoxon rank-sum tests after non-parametric ANOVA and multiple testing adjustment are indicated by asterisks (* $p < 0.05$; ** $p < 0.01$). Mice that differed in their clinical state from other mice in the control and LGTV serum recipient group are highlighted as rhombus shaped symbols in the box plots.

LGTV-serum group were significantly lower than scores of mice from LGTV-CD3$^+$ group (Figure 7N; p = 0.008).

IHC for the microglia/macrophage marker Iba1 (Figures 7C, F, I, J) confirmed the presence of assumed microgliosis in brains with histopathological changes described above characterized by increased staining intensity and increased numbers of microglia/macrophages (Figures 7C, F, I, Supplementary Figures S5C, F). Statistical analysis revealed that IHC-Iba1 (vascular/perivascular + parenchymal) scores in the cerebral cortex of the LGTV-serum group were significantly lower than scores of mice from the LGTV-CD3$^+$ group (Figure 7O; p = 0.016) and of mice from the control-CD3$^+$ group (Figure 7O; p = 0.032).

## 3.6 Severe gastrointestinal pathology observed post TBEV challenge

Significant body weight loss (> 20%) following TBEV challenge was a prominent characteristic in all mice that reached the HEP. Analysis of H&E stained sections from duodenum, jejunum, ileum, caecum, colon and rectum revealed ganglioneuritis of the *myenteric* and *submucosal plexus* of varying degree in all groups except the LGTV-serum recipient group (Figure 8). Neurons in injured ganglia displayed signs of neuronal necrosis and furthermore, an infiltration with inflammatory cells and/or hyperplasia of resident immune cells was observed. After evaluation and scoring of all intestinal regions, ileum, caecum and colon displayed consistent alterations in affected mice and were therefore analyzed in more detail. Statistical results of the H&E as well as IHC scorings of the region caecum are shown in Figures 8E, F, 9M-O; Supplementary Figures S6, S7 and Supplementary Table S6. In detail, statistical significances of ileum for *plexus myentericus* hypercellularity/inflammation were observed between control-CD3$^+$ and control-serum group (p = 0.048) and control-serum and LGTV-serum group (Supplementary Figures S6A, B; p = 0.008).

Accordingly, TBEV E protein was detected by IHC in the intestine of all groups (Figures 9A, D, G) except the LGTV-serum group (Figure 9J). Viral antigen was localized cytoplasmically in neurons of the *plexus myentericus* and *submucosus*. Specifically, IHC-TBEV scores in the caecum of the LGTV-serum group were significantly lower than scores of mice from the control-CD3$^+$ group (Figure 9M; p = 0.048). IHC-TBEV scores of ileum and colon are displayed in Supplementary Figures S7A, D.

IHC for the T cell marker CD3 revealed an infiltration of affected ganglia with T cells in control-CD3$^+$, LGTV-CD3$^+$ and control-serum mice (Figures 9B, E, H) and lacking infiltration in LGTV-serum mice (Figure 9K). Significant differences for CD3-IHC of ileum were detected for *plexus myentericus* between control-CD3$^+$ and LGTV-serum group (p = 0.024) as well as control-serum and LGTV-serum group (p = 0.008) and for *plexus submucosus* between control-serum and LGTV-serum group (Supplementary Figure S7B; p = 0.024). In the caecum (Figure 9N), significant differences for CD3-IHC scores in both *plexus submucosus* and in the *plexus myentericus* were observed between control-CD3$^+$ and LGTV-serum group (p = 0.008) as well as control-serum and LGTV-serum group (Supplementary Figure S7E; p = 0.048).

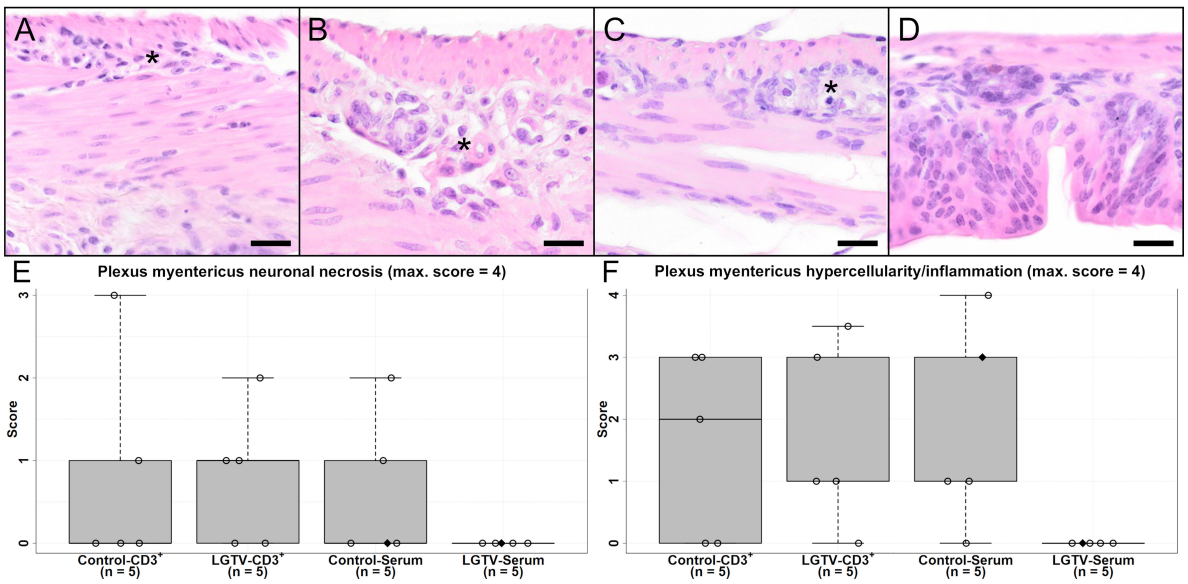


FIGURE 8
H&E stained sections of caecum of one representative mouse from each group **(A)** CD3$^+$ T cell transfer from control donors; **(B)** CD3$^+$ T cell transfer from LGTV infected donors; **(C)** serum transfer from control donors; **(D)** serum transfer from LGTV infected donors). The *plexus myentericus* displays varying degrees of ganglioneuritis in **(A–C)** (asterisk). No histopathological changes in the *plexus myentericus* of the mouse from the serum transfer of LGTV infected donor group **(D)** are detectable. Scale bars: 20 µm. **(E, F)** display box plots of the scoring values for *plexus myentericus* neuronal necrosis **(E)** and *plexus myentericus* hypercellularity/inflammation **(F)** of caecum for each group. Mice that differed in their clinical state from other mice in the control and LGTV serum recipient group are highlighted as rhombus shaped symbols in the box plots.

10.3389/fimmu.2023.1134371

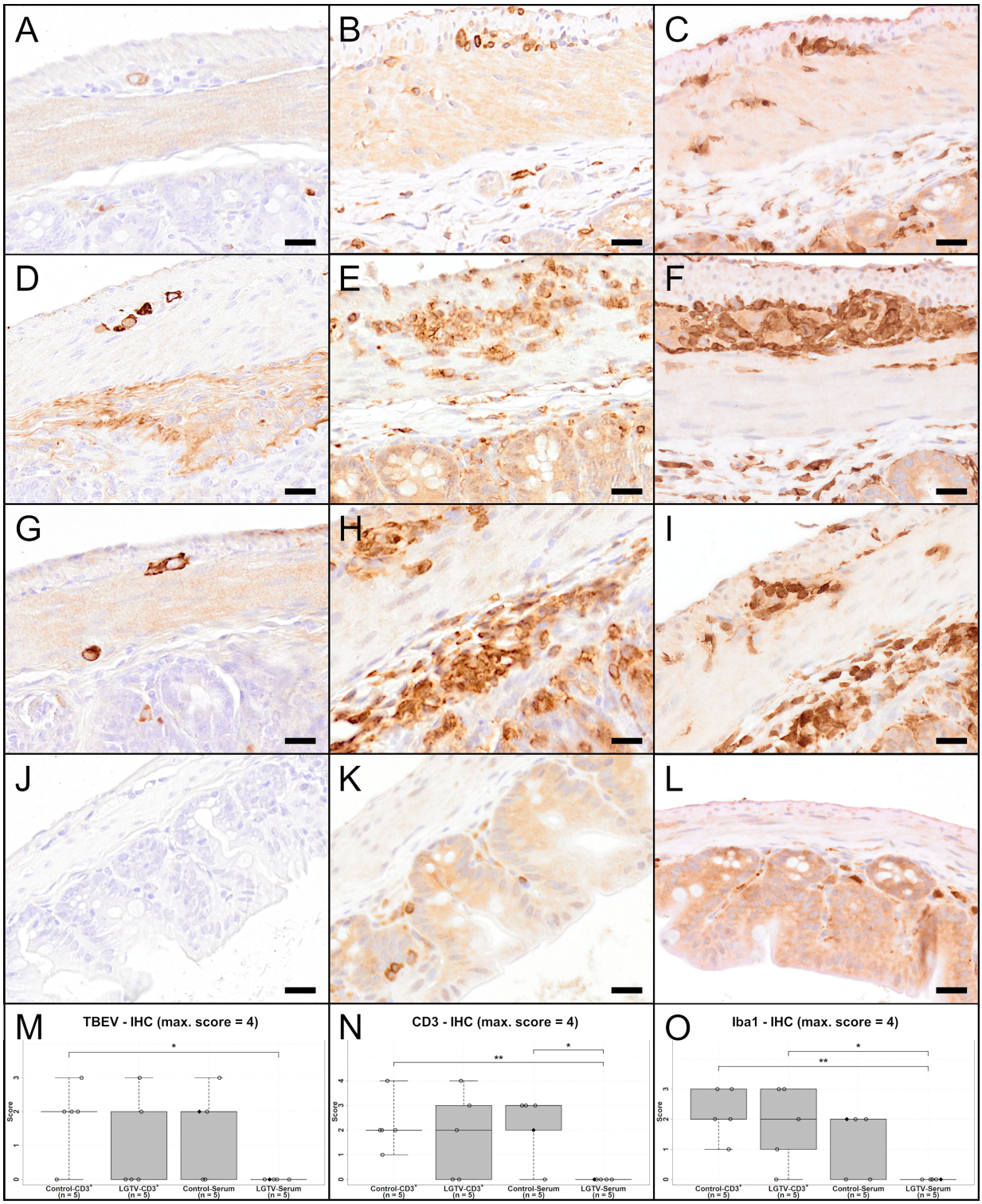


FIGURE 9
IHC of caecum for TBEV **(A, D, G, J)**, T cell marker CD3 **(B, E, H, K)** and microglia/macrophage marker Iba1 **(C, F, I, L)** of one representative mouse from each group **(A–C)** $CD3^+$ T cell transfer from control donors; **(D–F)** $CD3^+$ T cell transfer from LGTV infected donors; **(G–I)** serum transfer from control donors; **(J–L)** serum transfer from LGTV infected donors). TBEV E protein is detectable in the cytoplasm of neurons in the *plexus myentericus* and *submucosus* in all mice **(A, D, G)** except the ones in the group of the serum transfer from LGTV infected donor mice **(J)**. Ganglioneuritis in affected mice is characterized by CD3-positive T cell infiltration in both plexus **(B, E, H)**. No CD3-immunoreaction in the plexus of the serum transfer from LGTV infected donor mice is detectable **(K)**. In addition, an infiltration of plexus with Iba1-positive macrophages in affected mice **(C, F, I)** in comparison to mice of the group serum transfer from LGTV infected donor mice is detectable **(L)**. Scale bars: 20 µm. **(M–O)** display box plots of the scoring values of IHC for TBEV (IHC-TBEV; **(M)**, IHC for CD3 (IHC-CD3; **(N)** and IHC for macrophage marker Iba1 (Iba1-IHC; **(O)**. Significant differences detected by pairwise Wilcoxon rank-sum tests after non-parametric ANOVA and multiple testing adjustment are indicated by asterisks (* $p < 0.05$; ** $p < 0.01$). Mice that differed in their clinical state from other mice in the control and LGTV serum recipient group are highlighted as rhombus shaped symbols in the box plots.

Additionally, there was an infiltration/increased number of Iba1-positive cells (Figures 9C, F, I, J) with significant differences of Iba1-IHC scores in the *plexus myentericus* of ileum between control-CD3$^+$ and LGTV-serum group ($p = 0.008$), LGTV-CD3$^+$ and LGTV-serum group ($p = 0.048$) and control-serum and LGTV-serum group (Supplementary Figure S7C; $p = 0.048$). In the *plexus myentericus* of caecum, significant differences between control-CD3$^+$ and LGTV-serum group ($p = 0.008$) as well as LGTV-CD3$^+$ and LGTV-serum group ($p = 0.048$) were observed (Figure 9O). The Iba1-IHC scores of colon differed significantly in the *plexus myentericus* between control-serum and LGTV-serum group ($p = 0.008$) and in the *plexus submucosus* between LGTV-CD3$^+$ and LGTV-serum group (Supplementary Figure S7F; $p = 0.048$).

The fact that mice displaying ganglioneuritis together with detection of TBEV E protein within neurons of ganglia and inflammatory cell infiltration with T cells could represent another factor leading to severe TBEV-associated disease in addition to CNS pathology.

## 4 Discussion

Using a mouse model of TBEV infection, we demonstrated that effectors of adaptive immunity induced upon LGTV infection are cross-reactive with TBEV. Nevertheless, only transfer of serum but not T cells from LGTV infected donor mice into naïve recipient mice protected against disease induced by subsequent TBEV challenge. Our study defines antibodies as a major correlate of protection induced by LGTV infection that protects against TBEV infection and prevents the mice from developing severe disease.

Although safety concerns have been associated with LGTV immunization in the past, as it is not fully apathogenic to humans, it still indicates potential for live-attenuated virus vaccines against TBE. Pre-existing immunity can either positively or negatively influence the outcome of subsequent infection with a heterologous flavivirus (1, 5, 7, 25, 26). Therefore, immune correlates induced by LGTV infection in providing either protective immunity or predisposing for more severe pathogenesis of TBEV infection needs to be further investigated.

A close antigenic relationship among flaviviruses allows antibodies induced against one virus to recognize and react with similar epitopes of another virus. Although, cross-reactivity is more pronounced among closely related members, there is evidence that this can also happen among distantly related flavivirus. For instance, a phylogenetic tree based on the amino acid sequence of the E protein shows that TBEV is closely related to other tick-borne virus such as Powassan virus and is distantly related to mosquito-borne ZIKV and DENV. Yet, antibodies induced against TBEV has been shown to cause slight enhancement of ZIKV infection *in vitro* (4). Similarly, serology of human cohorts vaccinated against TBEV and YFV show cross-neutralizing antibodies against Louping ill virus, WNV and DENV (27). Furthermore, it has been shown that immunity to YFV impairs the antibody response (5). Phillpotts and colleagues screened several mouse antibodies raised against closely related flaviviruses, including LGTV, and demonstrated antibody-dependent enhancement (ADE) of TBEV infectivity *in vitro* (28). Similarly, cross-reactive antibodies induced by ZIKV may also lead to enhancement of DENV infection (29). Since ADE to heterologous infections is not uncommon among flavivirus infections, we explored the effects of LGTV induced cross-reactive antibodies on TBEV infection.

It was encouraging to see that four among five mice that passively received immune serum from LGTV infected mice were completely protected and did not show any signs of disease or increased virus burden in the organs following lethal TBEV challenge. However, qPCR detected small amount of viral RNA in one of the four survivors from the LGTV serum recipient groups. This is in accordance with our previous work where we also found TBEV in the brain despite of protective immunity induced by prior LGTV infection (24). It is likely that virus that escapes immune detection in the periphery, enters and replicates within the CNS before the resident glial cells combined with infiltrating immune cells clear the infection. In contrast, viral RNA was detected in the spleen as well as in the brain of the only surviving mice in the control serum recipient group hinting at ineffective viral clearance from the periphery. Furthermore, histopathological examination did not show severe pathological lesions in the brain or gastrointestinal tract of surviving mice. Only one mouse of the LGTV serum group displayed histopathological lesions in the brain as well as TBEV-positive immunoreactivity. However, this mouse did not show significant pathological lesions within the gastrointestinal tract (Figures 9E, F) and no TBEV-immunopositive reaction was observed (Figures 9M). TBEV neutralizing antibody titers in sera collected from LGTV infected mice were significantly lower as compared to LGTV neutralization titers. However, this was sufficient to block infection and prevent mice from developing TBEV induced disease. Further screening of immune sera to determine the specificity of these antibodies revealed that a significantly high proportion of these antibodies is directed against the epitopes located in domain III of the TBEV E glycoprotein and the NS1 protein. This is in line with other studies showing that type specific anti-E and anti-NS1 antibodies contribute to protection in experimental models of TBEV and other flavivirus infections (30–33). Therefore, it is noteworthy that anti-E and anti-NS1 antibodies induced by LGTV infection may also be contributing to cross-protective immunity against TBEV. Currently, it is unclear if cross-reactive antibodies to other viral proteins such as C, prM, NS3 and NS4 are also induced by LGTV as our LIPS screening was not able to detect them in the immune sera (data not shown).

Like antibodies, T cell cross-reactivity for flaviviral antigens has also been reported (34). Nevertheless, there is evidence that the proportion of such cross-reactive T cells may be lower than what is known for antibodies (35). Interestingly, we also observed that T cells from LGTV infected mice recognized and responded to TBEV antigens. Hence, we speculated that this translated into protective immunity as shown for other flavivirus infections (8, 36). For instance, CD4$^+$ and CD8$^+$ T cells primed against DENV are capable of protecting mice against ZIKV infection (26, 37). Similar cross-reactive immunity is also seen in humans vaccinated against JEV and YFV, whose T cells responded to DENV antigens (38). Nevertheless, in our experiments adoptive transfer of T cells from LGTV infected donor mice failed to protect

naïve recipient mice from subsequent challenge with TBEV. Upon further characterization by flow cytometry, we found that IFN-γ producing cells in response to NS3 and NS5 peptide pools restimulation were $CD4^+$ T cells. We could not detect any effector $CD8^+$ T cell response (IFN-$\gamma^+$ and/or granzyme $B^+$) to any given peptide pool restimulation. These observations are interesting and could partly explain the inefficiency of T cell transfer from LGTV infected mice to provide protection. Antigen-specific CD8+ T cells are among the key effectors of cell-mediated antiviral immunity as they recognize infected cells and prevent subsequent virus replication. Their role is especially significant for intracellular pathogens like viruses, which establish themselves in tissues and are less accessible to antibodies (39). In the T cell recipient mice, the absence of specific antibodies combined with the inability of LGTV infection to prime for TBEV cross-reactive $CD8^+$ T cell responses may have been responsible for the failure to prevent TBEV spread into the CNS.

On the other hand, the effectors of $CD4^+$ T cells activate antiviral mechanisms by other cells and may play a significant role in viral clearance. Nevertheless, in CNS with less immune activity, increased presence of T cells can also be detrimental and contribute to neural tissue damage. Although we did not observe differences in the onset and clinical progression of disease between recipient mice that received T cells from control or LGTV infected donors, histopathological observations indicate pronounced microgliosis and cellular necrosis in all affected mice. Furthermore, presence of T cells in the vascular and perivascular regions possibly hint at their contribution in pathological neuroinflammatory processes in the CNS.

Another previously described key feature of this TBEV infection model is gastrointestinal pathology in majority of affected mice (40). This is most likely a consequence of ganglioneuritis in the *plexus myentericus* and *submucosus* leading to dysfunctionality of the gastrointestinal tract. Although histopathological evaluations show increased presence of T cells in these areas, it is rather inconclusive whether T cells contribute to neuronal necrosis. It must be noted that mice start showing weight loss around 6 dpi which also gives time to prime endogenous T cell repertoire. This may be the reason why no significant differences were observed between mice recipient of control serum, control $CD3^+$ T cells and LGTV $CD3^+$ T cells.

Based on the information obtained from this and a previous study (24), we conclude that LGTV-specific antibodies that recognize TBEV antigens are main contributors of protection. On the other hand, T cells in the absence of antibody-mediated virus control may contribute to pathological changes. This could be vital information for the future design of live vaccines against TBEV and other closely related flavivirus infections.

## Data availability statement

The raw data supporting the conclusions of this article will be made available by the authors, without undue reservation.

## Ethics statement

The animal study was reviewed and approved by Lower Saxony State Office for Consumer Protection and Food Safety.

## Author contributions

Conceptualization: CKP, AO, and GR. Methodology: JB, MKu, GS, MP-G, CKP, IZ, and CP. Formal analysis: JB, MKu, CKP, IZ, CP, WB, and MKi. Investigation: JB, MKu, CKP, IZ, CP, WB, and MKi. Resources: IS, IZ, CP, and WB. Writing—original draft preparation: JB, MKu, CKP, and IZ. Writing—review and editing: IZ, GS, MKi, MP-G, IS, CP, KJ, WB, GR, AO. Visualization: JB, MKu, CKP, and IZ. Supervision: CKP, AO, GR. Funding acquisition: AO, GR, and WB. All authors contributed to the article and approved the submitted version.

## Funding

This research was funded by the Federal Ministry of Education and Research within the TBENAGER grant for AO. Parts of this work were funded by the Alexander von Humboldt Foundation in the framework of the Alexander von Humboldt Professorship endowed by the German Federal Ministry of Education and Research to GR and the Deutsche Forschungsgemeinschaft (DFG, German Research Foundation) - 398066876/GRK 2485/1. This Open Access publication was funded by the Deutsche Forschungsgemeinschaft (DFG, German Research Foundation) - 491094227 "Open Access Publication Funding" and the University of Veterinary Medicine Hannover, Foundation.

## Acknowledgments

We would like to thank Julia Friese, Julia Baskas, Caroline Schütz, Jana-Svea Harre and Petra Grünig for excellent technical support.

## Conflict of interest

The authors declare that the research was conducted in the absence of any commercial or financial relationships that could be construed as a potential conflict of interest.

## Publisher's note

# Supplementary material

The Supplementary Material for this article can be found online at: https://www.frontiersin.org/articles/10.3389/fimmu.2023.1134371/full#supplementary-material

SUPPLEMENTARY FIGURE 1
TBEV cross-reactive antibodies and T cells of adoptively transferred serum and T cells. Pooled sera from control or LGTV infected donor mice (n=5) were tested for their ability to block the infection of **(A)** LGTV and **(B)** TBEV in VeroE6 and A549 cells, respectively. The graphs show the titer at which 100% virus neutralization is achieved (VNT100). **(C)** Splenocytes obtained from individual control (•) or LGTV (Δ) infected donor mice (n=5) were restimulated with TBEV-specific peptide pools and the frequency of IFN-γ producing cells was determined using ELISpot assay. The median is shown.

SUPPLEMENTARY FIGURE 2
Viral load in the organs of serum and T cell recipient mice that were challenged with TBEV. Real time quantitative RT-PCR was performed on total RNA isolated from serum and tissue homogenates collected at day of sacrifice of recipient mice which either received **(A)** serum or **(B)** $CD3^+$ T cells from control (•) or LGTV (Δ) infected donor mice and were subsequently challenged with TBEV. The median is shown. Mice that differed in their clinical state from other mice in the control and LGTV serum recipient group are highlighted as rhombus shaped symbols

SUPPLEMENTARY FIGURE 3
Purity of adoptively transferred $CD3^+$ T cell pools. Flow cytometric analysis of purified $CD3^+$ T cells from control (upper panel) and LGTV (lower panel) donor groups prior to adoptive transfer to recipient mice. FACS plots are gated on live $CD3^+$ T cells.

SUPPLEMENTARY FIGURE 4
Box plots of the hematoxylin and eosin (H&E) scoring values for "cellular necrosis" **(A, D)**, "perivascular inflammation" **(B, E)** and "microgliosis" **(C, F)** of olfactory bulb **(A-C)** and hippocampus **(D-F)** for each experimental group. Significant differences detected by pairwise Wilcoxon rank-sum tests after non-parametric ANOVA are indicated by asterisks (* $p < 0.05$; ** $p < 0.01$; *** $p < 0.001$). Mice that differed in their clinical state from other mice in the control and LGTV serum recipient group are highlighted as rhombus shaped symbols in the box plots.

SUPPLEMENTARY FIGURE 5
Box plots of the scoring values of immunohistochemistry for TBEV **(A, D)**, T cell marker CD3 **(B, E)** and microglia/macrophage marker Iba1 **(C, F)** of olfactory bulb **(A-C)** and hippocampus **(D-F)** for each experimental group. Significant differences detected by pairwise Wilcoxon rank-sum tests after non-parametric ANOVA are indicated by asterisks (* $p < 0.05$; ** $p < 0.01$; *** $p < 0.001$). Mice that differed in their clinical state from other mice in the control and LGTV serum recipient group are highlighted as rhombus shaped symbols in the box plots.

SUPPLEMENTARY FIGURE 6
Box plots of the hematoxylin and eosin (H&E) scoring values for "plexus myentericus neuronal necrosis" **(A, C)** and "plexus myentericus hypercellularity" **(B, D)** of ileum **(A, B)** and colon **(C, D)** for each experimental group. Significant differences detected by pairwise Wilcoxon rank-sum tests after non-parametric ANOVA are indicated by asterisks (* $p < 0.05$; ** $p < 0.01$; *** $p < 0.001$). Mice that differed in their clinical state from other mice in the control and LGTV serum recipient group are highlighted as rhombus shaped symbols in the box plots.

SUPPLEMENTARY FIGURE 7
Box plots of the scoring values of immunohistochemistry for TBEV **(A, D)**, T cell marker CD3 **(B, E)** and microglia/macrophage marker Iba1 **(C, F)** of ileum **(A-C)** and colon **(D-F)** for each experimental group. Significant differences detected by pairwise Wilcoxon rank-sum tests after non-parametric ANOVA are indicated by asterisks (* $p < 0.05$; ** $p < 0.01$; *** $p < 0.001$). Mice that differed in their clinical state from other mice in the control and LGTV serum recipient group are highlighted as rhombus shaped symbols in the box plots.

# References


1. Rathore APS, St. John AL. Cross-reactive immunity among flaviviruses. *Front Immunol* (2020) 11:1–9. doi: 10.3389/fimmu.2020.00334

2. Kubinski M, Beicht J, Gerlach T, Volz A, Sutter G, Rimmelzwaan GF. Tick-borne encephalitis virus: A quest for better vaccines against a virus on the rise. *Vaccines* (2020) 8(3):1–45. doi: 10.3390/vaccines8030451

3. McAuley AJ, Sawatsky B, Ksiazek T, Torres M, Korva M, Lotrič-Furlan S, et al. Cross-neutralisation of viruses of the tick-borne encephalitis complex following tick-borne encephalitis vaccination and/or infection. *NPJ Vaccines* (2017) 2(1):1–10. doi: 10.1038/s41541-017-0009-5

4. Duehr J, Lee S, Singh G, Foster GA, Krysztof D, Stramer SL, et al. Tick-borne encephalitis virus vaccine-induced human antibodies mediate negligible enhancement of zika virus infection InVitro and in a mouse model. *mSphere* (2018) 3(1):1–10. doi: 10.1128/mSphereDirect.00011-18

5. Bradt V, Malafa S, von Braun A, Jarmer J, Tsouchnikas G, Medits I, et al. Pre-existing yellow fever immunity impairs and modulates the antibody response to tick-borne encephalitis vaccination. *NPJ Vaccines* (2019) 4(1):1–11. doi: 10.1038/s41541-019-0133-5

6. Katzelnick LC, Gresh L, Halloran ME, Mercado JC, Kuan G, Gordon A, et al. Antibody-dependent enhancement of severe dengue disease in humans. *Science* (2017) 358(6365):929–32. doi: 10.1126/science.aan6836

7. Regla-Nava JA, Elong Ngono A, Viramontes KM, Huynh A-T, Wang Y-T, Nguyen A-VT, et al. Cross-reactive dengue virus-specific CD8(+) T cells protect against zika virus during pregnancy. *Nat Commun* (2018) 9(1):3042. doi: 10.1038/s41467-018-05458-0

8. Saron WAA, Rathore APS, Ting L, Ooi EE, Low J, Abraham SN, et al. Flavivirus serocomplex cross-reactive immunity is protective by activating heterologous memory CD4 T cells. *Sci Adv* (2018) 4(7):1–14. doi: 10.1126/sciadv.aar4297

9. Calisher CH, Karabatsos N, Dalrymple JM, Shope RE, Porterfield JS, Westaway EG, et al. Antigenic relationships between flaviviruses as determined by cross-neutralization tests with polyclonal antisera. *J Gen Virol* (1989) 70(Pt 1):37–43. doi: 10.1099/0022-1317-70-1-37

10. Gritsun TS, Lashkevich VA, Gould EA. Tick-borne encephalitis. *Med Ther Pediatr* (2003) 18(3):145–51. doi: 10.1016/S0166-3542(02)00206-1

11. Cornelius ADA, Hosseini S, Schreier S, Fritzsch D, Weichert L, Michaelsen-Preusse K, et al. Langat virus infection affects hippocampal neuron morphology and function in mice without disease signs. *J Neuroinflamm* (2020) 17(1):278. doi: 10.1186/s12974-020-01951-w

12. Lehrer AT, Holbrook MR. Tick-borne encephalitis vaccines. *J Bioterror Biodef* (2011) 01(01):003–. doi: 10.4172/2157-2526.S1-003

13. Chernokhaeva LL, Rogova YV, Kozlovskaya LI, Romanova LI, Osolodkin DI, Vorovitch MF, et al. Experimental evaluation of the protective efficacy of tick-borne encephalitis (TBE) vaccines based on European and far-Eastern TBEV strains in mice and in vitro. *Front Microbiol* (2018) 9(JUL):1–12. doi: 10.3389/fmicb.2018.01487

14. Schmidt AJ, Altpeter E, Graf S, Steffen R. Tick-borne encephalitis (TBE) in Switzerland: Does the prolongation of vaccine booster intervals result in an increased risk of breakthroughs? *J Travel Med* (2022) 29(2):1–6. doi: 10.1093/jtm/taab158

15. Andersson CR, Vene S, Insulander M, Lindquist L, Lundkvist Å, Günther G. Vaccine failures after active immunisation against tick-borne encephalitis. *Vaccine* (2010) 28(16):2827–31. doi: 10.1016/j.vaccine.2010.02.001

16. Lotric-Furlan S, Avšič-Županc T, Strle F. Tick-borne encephalitis after active immunization. *Int J Med Microbiol* (2008) 298(Suppl 1):309–13. doi: 10.1016/j.ijmm.2008.03.006

17. Hansson KE, Rosdahl A, Insulander M, Vene S, Lindquist L, Gredmark-Russ S, et al. Tick-borne encephalitis vaccine failures: A 10-year retrospective study supporting the rationale for adding an extra priming dose in individuals starting at age 50 years. *Clin Infect Dis* (2020) 70(2):245–51. doi: 10.1093/cid/ciz176

18. Dobler G, Kaier K, Hehn P, Böhmer MM, Kreusch TM, Borde JP. Tick-borne encephalitis virus vaccination breakthrough infections in Germany: A retrospective analysis from 2001 to 2018. *Clin Microbiol Infect* (2020) 26(8):1090.e7–1090.e13. doi: 10.1016/j.cmi.2019.12.001

19. Reed LJ, Muench H. A simple method of estimating fifty per cent endpoints. *Am J Epidemiol* (1938) 27(3):493–7. doi: 10.1093/oxfordjournals.aje.a118408

20. Könenkamp L, Ziegler U, Naucke T, Groschup MH, Steffen I. Antibody ratios against NS1 antigens of tick-borne encephalitis and West Nile viruses support differential flavivirus serology in dogs. *Transbound Emerg Dis* (2022) 69(5):e2789–99. doi: 10.1111/tbed.14630

21. Schwaiger M, Cassinotti P. Development of a quantitative real-time RT-PCR assay with internal control for the laboratory detection of tick borne encephalitis virus (TBEV) RNA. *J Clin Virol* (2003) 27(2):136–45. doi: 10.1016/S1386-6532(02)00168-3

22. Leitzen E, Raddatz BB, Jin W, Goebbels S, Nave K-A, Baumgärtner W, et al. Virus-triggered spinal cord demyelination is followed by a peripheral neuropathy resembling features of Guillain-Barré syndrome. *Sci Rep* (2019) 9(1):4588. doi: 10.1038/s41598-019-40964-1

23. Akritas MG, Arnold SF, Brunner E. Nonparametric hypotheses and rank statistics for unbalanced factorial designs. *J Am Stat Assoc* (1997) 92(437):258–65. doi: 10.1080/01621459.1997.10473623

24. Petry M, Palus M, Leitzen E, Mitterreiter JG, Huang B, Kröger A, et al. Immunity to TBEV related flaviviruses with reduced pathogenicity protects mice from disease but not from TBEV entry into the CNS. *Vaccines* (2021) 9(3):1–14. doi: 10.3390/vaccines9030196

25. Salgado R, Hawks SA, Frere F, Vázquez A, Huang CY-H, Duggal NK. West Nile Virus vaccination protects against usutu virus disease in mice. *Viruses* (2021) 13(12):1–13. doi: 10.3390/v13122352

26. Wen J, Wang Y-T, Valentine KM, Dos Santos Alves RP, Xu Z, Regla-Nava JA, et al. CD4(+) T cells cross-reactive with dengue and zika viruses protect against zika virus infection. *Cell Rep* (2020) 31(4):107566. doi: 10.1016/j.celrep.2020.107566

27. Mansfield KL, Horton DL, Johnson N, Li L, Barrett ADT, Smith DJ, et al. Flavivirus-induced antibody cross-reactivity. *J Gen Virol* (2011) 92(12):2821–9. doi: 10.1099/vir.0.031641-0

28. Phillpotts RJ, Stephenson JR, Porterfield JS. Antibody-dependent enhancement of tick-borne encephalitus virus infectivity. *J Gen Virol* (1985) 66(8):1831–7. doi: 10.1099/0022-1317-66-8-1831

29. Fowler AM, Tang WW, Young MP, Mamidi A, Viramontes KM, McCauley MD, et al. Maternally acquired zika antibodies enhance dengue disease severity in mice. *Cell Host Microbe* (2018) 24(5):743–750.e5. doi: 10.1016/j.chom.2018.09.015

30. Li Y, Counor D, Lu P, Duong V, Yu Y, Deubel V. Protective immunity to Japanese encephalitis virus associated with anti-NS1 antibodies in a mouse model. *Virol J* (2012) 9:135. doi: 10.1186/1743-422X-9-135

31. Jacobs SC, Stephenson JR, Wilkinson GWG. Protection elicited by a replication-defective adenovirus vector expressing the tick-borne encephalitis virus non-structural glycoprotein NS1. *J Gen Virol* (1994) 75(9):2399–402. doi: 10.1099/0022-1317-75-9-2399

32. Salat J, Mikulasek K, Larralde O, Formanova PP, Chrdle A, Haviernik J, et al. Tick-borne encephalitis virus vaccines contain non-structural protein 1 antigen and may elicit NS1-specific antibody responses in vaccinated individuals. *Vaccines* (2020) 8(1):1–13. doi: 10.20944/preprints202002.0136.v1

33. Martina BEE, van den Doel P, Koraka P, van Amerongen G, Spohn G, Haagmans BL, et al. A recombinant influenza a virus expressing domain III of West Nile VirusInduces protective immune responses against influenza and West Nile virus. *PloS One* (2011) 6(4):1–8. doi: 10.1371/journal.pone.0018995

34. Grifoni A, ORourke PH, de Silva AD, Costa PR, Durbin A, Diehl SA, et al. Flavivirus induced T cell cross-reactivity. *Am J Trop Med Hyg* (2018) 99(4):227–2289. doi: 10.1128/jvi.00089-20

35. Grifoni A, Voic H, Dhanda SK, Kidd CK, Brien JD, Buus S, et al. T Cell responses induced by attenuated flavivirus vaccination are specific and show limited cross-reactivity with other flavivirus species. *J Virol* (2020) 94(10):1–19. doi: 10.1128/JVI.00089-20

36. Wang R, Gao N, Li Y, Fan D, Zhen Z, Feng K, et al. Cross-protection against four serotypes of dengue virus in mice conferred by a zika DNA vaccine. *Front Cell Infect Microbiol* (2019) 9:147. doi: 10.3389/fcimb.2019.00147

37. Wen J, Shresta S. T Cell immunity to zika and dengue viral infections. *J Interferon Cytokine Res* (2017) 37(11):475–9. doi: 10.1089/jir.2017.0106

38. Turtle L, Tatullo F, Bali T, Ravi V, Soni M, Chan S, et al. Cellular immune responses to live attenuated Japanese encephalitis (JE) vaccine SA14-14-2 in adults in a JE/Dengue Co-endemic area. *PloS Negl Trop Dis* (2017) 11(1):e0005263. doi: 10.1371/journal.pntd.0005263

39. Shrestha B, Pinto AK, Green S, Bosch I, Diamond MS. CD8+ T cells use TRAIL to restrict West Nile virus pathogenesis by controlling infection in neurons. *J Virol* (2012) 86(17):8937–48. doi: 10.1128/JVI.00673-12

40. Boelke M, Puff C, Becker K, Hellhammer F, Gusmag F, Marks H, et al. Enteric ganglioneuritis, a common feature in a subcutaneous tbev murine infection model. *Microorganisms* (2021) 9(4). doi: 10.3390/microorganisms9040875

frontiers | Frontiers in Immunology

TYPE Review
PUBLISHED 10 March 2023
DOI 10.3389/fimmu.2023.1146196



OPEN ACCESS

EDITED BY
Jingxin Li,
Jiangsu Provincial Center for Disease Control and Prevention, China

REVIEWED BY
Yun Shi,
Sichuan University, China
Chao Wu,
Nanjing Drum Tower Hospital, China

*CORRESPONDENCE
Zhongfang Wang
wangzhongfang@gird.cn
Nanshan Zhong
nanshan@vip.163.com
Yunhui Zhang
yunhuizhang3188@126.com

†These authors have contributed equally to this work and share first authorship

SPECIALTY SECTION
This article was submitted to Viral Immunology, a section of the journal Frontiers in Immunology

RECEIVED 17 January 2023
ACCEPTED 01 March 2023
PUBLISHED 10 March 2023

CITATION
Yang G, Wang J, Sun P, Qin J, Yang X, Chen D, Zhang Y, Zhong N and Wang Z (2023) SARS-CoV-2 epitope-specific T cells: Immunity response feature, TCR repertoire characteristics and cross-reactivity.
*Front. Immunol.* 14:1146196.
doi: 10.3389/fimmu.2023.1146196



# SARS-CoV-2 epitope-specific T cells: Immunity response feature, TCR repertoire characteristics and cross-reactivity

Gang Yang[1,2,3†], Junxiang Wang[4†], Ping Sun[1], Jian Qin[3], Xiaoyun Yang[2,4], Daxiang Chen[2,4], Yunhui Zhang[3*], Nanshan Zhong[1,2,4*] and Zhongfang Wang[2,4*]

[1]Faculty of Life Science and Technology, Kunming University of Science and Technology, Kunming, China, [2]Guangzhou Laboratory, Guangzhou, China, [3]Department of Pulmonary and Critical Care Medicine, The First People's Hospital of Yunnan Province, Kunming, China, [4]State Key Laboratory of Respiratory Disease & National Clinical Research Center for Respiratory Disease, Guangzhou Institute of Respiratory Health, The First Affiliated Hospital of Guangzhou Medical University, Guangzhou Medical University, Guangzhou, China

The devastating COVID-19 pandemic caused by SARS-CoV-2 and multiple variants or subvariants remains an ongoing global challenge. SARS-CoV-2-specific T cell responses play a critical role in early virus clearance, disease severity control, limiting the viral transmission and underpinning COVID-19 vaccine efficacy. Studies estimated broad and robust T cell responses in each individual recognized at least 30 to 40 SARS-CoV-2 antigen epitopes and associated with COVID-19 clinical outcome. Several key immunodominant viral proteome epitopes, including S protein- and non-S protein-derived epitopes, may primarily induce potent and long-lasting antiviral protective effects. In this review, we summarized the immune response features of immunodominant epitope-specific T cells targeting different SRAS-CoV-2 proteome structures after infection and vaccination, including abundance, magnitude, frequency, phenotypic features and response kinetics. Further, we analyzed the epitopes immunodominance hierarchy in combination with multiple epitope-specific T cell attributes and TCR repertoires characteristics, and discussed the significant implications of cross-reactive T cells toward HCoVs, SRAS-CoV-2 and variants of concern, especially Omicron. This review may be essential for mapping the landscape of T cell responses toward SARS-CoV-2 and optimizing the current vaccine strategy.

KEYWORDS

**SARS-CoV-2, T cell immunity, epitopes, TCR repertoire, cross-reactivity**

# 1 Introduction

Severe acute respiratory syndrome coronavirus 2 (SARS-CoV-2) and multiple emerging variants or subvariants have caused a persistent global coronavirus disease 2019 (COVID-19) pandemic over the past three years, particularly devastating to elderly patients with underlying diseases, and resulting in more than 6 million COVID-19-related deaths (1–3). A characteristic feature of COVID-19 is that the clinical manifestations vary widely in the population, with some individuals presenting as asymptomatic or mildly infected, while others become severe respiratory failure or even death, but the mechanisms underlying this major difference have not been fully elucidated (4, 5). Recent evidence demonstrated that asymptomatic COVID-19 individuals have highly multifunctional SARS-CoV-2-specific T cell responses (6, 7), and coordinated and robust CD4+ and CD8+ T cell immunity are associated with milder disease (8). It is therefore obvious that T cells mediated protective immunity plays a critical role in controlling SARS-CoV-2 infection, which relies on CD4+ T cells to secrete a series of cytokines to support B cell-mediated antibody responses and promote the function of innate immune cells, while CD8+ T cells mediate direct antiviral function through killing infected host cells by a variety of mechanisms (9, 10).

Activated T cells targeting different SARS-CoV-2 antigen proteins were reported to be detected in up to 70% of acute and convalescent COVID-19 individuals (11, 12). The magnitude of CD4+ and CD8+ T cell response is closely related to almost all SARS-CoV-2 proteins, but a few virus antigens [spike, nucleocapsid, Membrane, non-structural proteins (nsp) 3, nsp4, nsp12, nsp13, open reading frame (ORF)3a, ORF8] cover 80% of T cell responses, suggesting a distinct immunodominant pattern (13). However, previous studies involving T cell responses toward total viral proteins rather than single epitopes after natural infection or vaccination may underestimate or even obscure the T cell immune characteristics (14). Recent studies of identification and characterization of SARS-CoV-2-specific T cell epitopes covered the most prevalent human leukocyte antigen (HLA) allelic variants worldwide (14–38), reporting that CD4+ and CD8+ T cell responses in each individual recognize at least 30 to 40 SARS-CoV-2 antigen epitopes (13), and different epitopes-specific T cell responses associate with COVID-19 disease severity and clinical outcome (23). These studies mainly used multiple methodologies such as enzyme-linked immunospot (ELISpot), intracellular cytokine staining (ICS), activation induced marker (AIM) and multimer staining for epitope identification, and single-cell RNA or T cell receptor (TCR) sequencing analysis for more detailed epitope-specific T cell information. Those critical studies provided the outstanding opportunity for a deeper understanding of SARS-CoV-2 immunodominant epitopes-specific T cells with the responses abundance, magnitude, frequency, phenotypic feature, kinetics, biological functions, TCR repertoire characteristics and immunodominance hierarchy (Table 1), and were thus focused and included in this review, while the literature only involving epitope identification and validation without more comprehensive and in-depth analysis was not the focus.

Thus far, hundreds of COVID-19 vaccines are known to be under development or have been approved to fight the pandemic. Some of these vaccines have proven to effectively reduce disease severity and mortality, suggesting a central role for vaccine-induced T cell immunity in protecting against severe tissue damage (43, 44). However, the continuous emergence of SARS-CoV-2 variants and subvariants poses a great challenge to current COVID-19 vaccine strategies (45). Those vaccines primarily focus on the SARS-CoV-2 spike glycoprotein that is highly immunogenic but susceptible to mutations in viral variants, resulting in greatly compromised protection from neutralizing antibody responses (46). Fortunately, the SARS-CoV-2 immunodominant epitope regions recognized by T cells and B cells have only minimal overlap, and awareness of this is particularly critical in vaccine design (13, 47). Hence, future vaccine strategies should cover more conserved immunodominant T cell epitopes, which are less affected by mutations and thus can induce broader and more efficient cross-protection against future SARS-CoV-2 variants and subvariants (48). Considering these challenges, this review focuses on characterizing the SARS-CoV-2 epitopes-specific T cells response feature and analyzing their TCR repertoire characteristics and cross-reactivity, which are essential for mapping the landscape of T cell responses mediated by SARS-CoV-2 and optimizing the current vaccine strategy.

# 2 SARS-CoV-2 structure and its T cell epitope

SARS-CoV-2 is a positive-sense RNA virus with large genome approximately of 29,903 nucleotides in length (49). The SARS-CoV-2 genome consists of 12 open reading frames (ORF) and encodes 16 non-structural proteins (NSP1-16), 9 accessory proteins (ORF3a-10) and 4 structural proteins including spike (S), envelope (E), membrane (M) and nucleocapsid (N) (Figure 1) (50). The M, S and E proteins on the surface of SARS-CoV-2 are embedded in the lipid bilayer membrane, while the internal N protein encapsulates viral RNA. Specifically, the S glycoprotein, composed of the S1 subunit and S2 subunit, is the main structure that mediates virus entry into host cells. It recognizes and binds to the cell surface receptor angiotensin-converting enzyme 2 (ACE2) through the receptor binding domain (RBD) to mediate membrane fusion reaction (51). The M protein can interact with multiple viral proteins and is a critical structural component for coronavirus assembly and formation (52). The E protein is the smallest structural protein and plays multiple roles in SARS-CoV-2 pathogenesis, virus packaging and release (53). The N protein directly binds to the viral RNA genome and assembles it into a ribonucleoprotein complex by synergizing with the M protein (54). In addition to structural protein components, 16 non-structural proteins remain essential in the life replication cycle of SARS-CoV-2. These nsps include various important enzymes and transcription factors such as viral protease nsp5, RNA-dependent RNA polymerase (RdRp) nsp12, helicase nsp13 and so forth (55). The 3' end of the SARS-CoV-2 genome also encodes 9 accessory proteins including ORF3a, ORF3b, ORF6, ORF7a, ORF7b, ORF8,

**TABLE 1** Summary of SARS-CoV-2 immunodominant epitopes information.

| Epitope Abbreviation | Peptide Source | Sequence | Known HLA restriction | Classification | Conservation (to Omicron) | Detailed information of epitope-specific T cells | | | | | Reference |
|---|---|---|---|---|---|---|---|---|---|---|---|
| | | | | | | Frequency or Magnitude | phenotype in convalescents/vaccinees | TCR reportoiese | Infection or Vaccination | Kinetics following vaccination | |
| N105-113 | Nucleocapsid | SPRWYFYYL | HLA-B*07:02 | CD8 | Conservative | $6.88\times10^{-4}$ in COVID-19 patients; $3.00\times10^{-5}$ in unexposed individuals | $T_{cm}$ | Highly diverse; Bias use of the TRBV27 and longer CDR3β loops | Infection | / | (15, 16, 19, 25, 39, 40) |
| N322-330 | Nucleocapsid | MEVTPSGTWL | HLA-B*40:01; HLA-B*44:03 | CD8 | Conservative | $3.6\times10^{-5}$ in early convalescent individuals; $1\times10^{-5}$ in late convalescent individuals | Not mentioned | TRBV27/TRBJ1-4 | Infection | / | (16, 20) |
| N361-369 | Nucleocapsid | KTFPPTEPK | HLA-A11:01; HLA-B44:01; HLA-A03:01 | CD8 | Conservative | elicit T cell responses in 75% of COVID-19 convalescent individuals | Not mentioned | Public CDR3β motif ASSRAGTGYNEQF and ASSPSVYFEVSGANVLT | Infection | / | (20, 21, 35, 41) |
| S269-277 | Spike | YLQPRTFLL | HLA-A*02:01 | CD8 | Conservative | $1.65\times10^{-6}$ in healthy individuals; $1.44\times10^{-5}$ in COVID-19 acute and $1.28\times10^{-5}$ in convalescent patients | $T_{naive}$ and $T_{scm}$ dominant naïve memory T cell | ①TRAV12-1/TRAJ43, with public CVVNXXDMRF motif ②TRAV12-2/TRAJ30, with public CAVNXDDKIIF motif ③TRBV7-9 | Infection and vaccination | Three epitopes specific CD8+T cells elicited by BNT162b2 peak frequency of ~$3.6\times10^{-4}$ and maintaining full function for at least 80-120 days | (17, 20, 25, 37, 42) |
| S1208–1216 | Spike | QYIKWPWYI | HLA-A*24:02 | CD8 | Conservative | $7.71\times10^{-5}$ in convalescent patients; $9.50\times10^{-6}$ in healthy individuals | diverse $T_{cm}$, $T_{scm}$, $T_{emra}$ and $T_{naive}$ | Highly diverse | Infection and vaccination | | (18, 20, 22, 25) |
| S448–456 | Spike | NYNYLYRLF | HLA-A*24:02 | CD8 | Conservative | $6.3\times10^{-5}$ in convalescent patients; $8.44\times10^{-6}$ in healthy individuals | diverse $T_{cm}$, $T_{scm}$, $T_{emra}$ and $T_{naive}$ | TRBV2/TRBJ2-7; with public CDR3β motif XXXGYEQYF | Infection and vaccination | | (18, 22, 25) |
| S751–767 | Spike | NLLLQYGS FCTQLNRAL | HLA-DRB1*15:01 | CD4 | N440K mutation | $1.36\times10^{-4}$ in early convalescent patient; $3.8\times10^{-5}$ in the late convalescent phase | $T_{cm}$ and cTfh | bias use of TRVB24-1, TRVB20-1 and TRBV6-1, with a highly public CDR3β motif CSARRGTEAFF | vaccination | ①Two epitopes specific CD4+ T cells in peripheral blood occur as early as day 7 after primary BNT162b2 vaccination and peak at days 7-14 after the second dose, maintaining for at least 200 days. ②DP04/S167-specific Tfh cell responses in lymph nodes maintain at high frequency >170-200 days | (27) |
| S167-180 | Spike | YVSQPFLM | HLA-DPB1*04 | CD4 | Conservative | Not mentioned | PD-1+CXCR5 + Tfh and CD45RO +CCR7- cTfh | TRAV35,with CDR3α motif CA[G/A/V] XNYGGSQGNLIF | vaccination | | (26) |
| M198–206 | Membrane | RYRIGNYKL | HLA-A*24:02 | CD8 | Conservative | elicit T cell responses in 88.1% of COVID-19 convalescent individuals | CCR7-CD45RA- effector memory in moderate patients | ①TRBV6-4/TRBJ1-2, with public CDR3α motif CAVXYNQGGKLIF ②TRAV1-2/TRAJ23, with CDR3β motif CASSDSGXDGYTF | Infection | / | (38) |
| ORF1ab 1637-1646 | ORF1ab | TTDPSFLGRY | HLA-A*01:01 | CD8 | Conservative | reaching up to 7%-25% of the total CD8+ T cells in COVID-19 patients | Not mentioned | Highly diverse; Bias use of the TRBV27 gene fragment | Infection | / | (20, 29, 33) |
| ORF1ab 3886-3894 | ORF1ab | KLWAQCVQL | HLA-A*02:01 | CD8 | Not defined | elicit T cell responses in 88.9% of COVID-19 patient | Not mentioned | TRAV38-2/DV8 | Infection | / | (36) |
| ORF3a 139-147 | ORF3a | LLYDANYFL | HLA-A*02:01 | CD8 | Conservative | elicit T cell responses in | $T_{cm}$ and $T_{em1}$ | TRAV8-1 | Infection | / | (16, 36) |

*(Continued)*

TABLE 1 Continued

| Epitope Abbreviation | Peptide Source | Sequence | Known HLA restriction | Classification | Conservation (to Omicron) | Detailed information of epitope-specific T cells | | | | | Reference |
|---|---|---|---|---|---|---|---|---|---|---|---|
| | | | | | | Frequency or Magni-tude | phenotype in convalescents/ vaccinees | TCR reportoiese | Infection or Vaccination | Kinetics following vaccination | |
| | | | | | | 88.9% of COVID-19 patient | | | | | |

Epitope conservation was achieved by sequence alignment between the original SARS-CoV-2 strain and Omicron conducted by National Center for Biotechnology Information (NCBI, https://www.ncbi.nlm.nih.gov/) and China National Center For Bioinformation (CNCB, https://ngdc.cncb.ac.cn/ncov/).

ORF9b, ORF9c and ORF10. The functions of these accessory proteins are not fully understood and may indirectly regulate many viral biological processes (51).

The epitope is a critical region for host immune cells to recognize a specific pathogen, also known as antigenic determinant (56). The epitopes recognized by TCR are called T cell epitopes, which are mainly peptides derived from protein degradation. T cells recognize only peptide epitopes that bind to specific class I or class II major histocompatibility complex MHC molecules, also known as MHC restriction (57). MHC class I restricted epitopes are usually 8 to 10 amino acid residues and are presented to the surface of CD8+ T cells for recognition, while class II restricted epitopes are generally 13 to 17 residues and recognized by CD4+ T cells (58).

SARS-CoV-2 genome is composed of a large 30-kb mRNA fragment and encodes various structural and non-structural proteins, thus no doubt that it has numerous T cell epitopes. Over 2000 SARS-CoV-2-derived T cell epitopes have been identified in a considerable number of previous studies, covering almost all viral proteomic structures (59, 60). However, not every SARS-CoV-2 protein epitope has the same immunodominance hierarchy. The immunodominance of a specific SARS-CoV-2

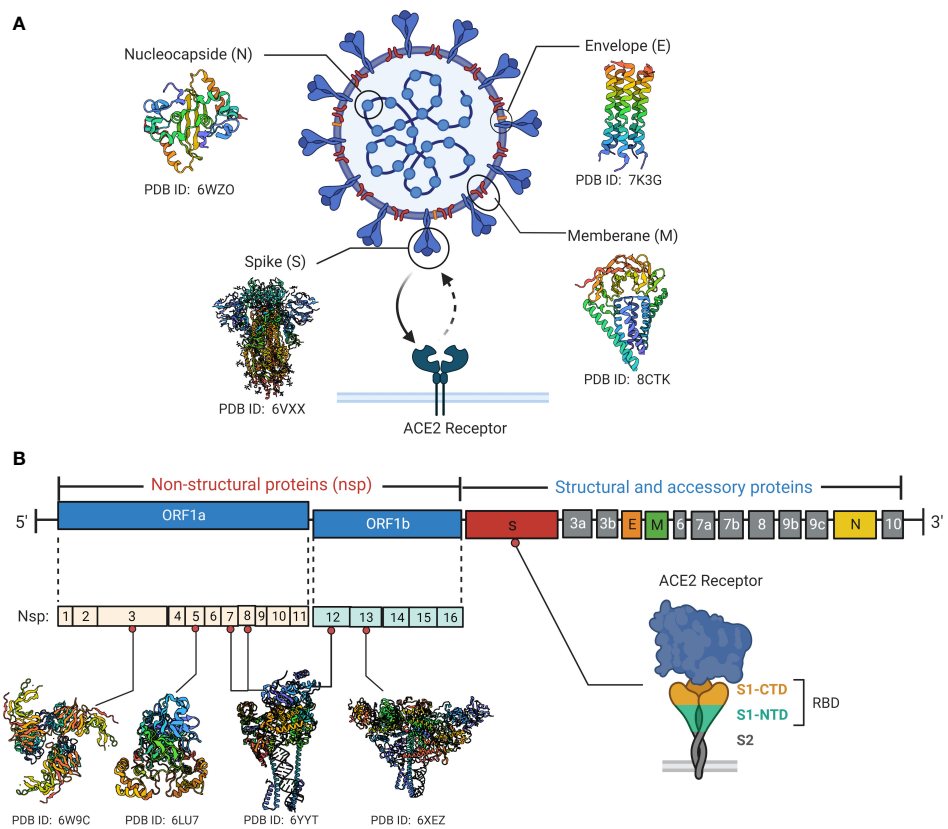


FIGURE 1
SARS-CoV-2 viral protein structure and genomic organization. **(A)** Schematic diagrams of the structural characteristics of SARS-CoV-2 as well as the crystal structures of key structural proteins obtained from RCSB protein data bank (PDB). The spike protein binds to the cell surface ACE2 receptor through the RBD. **(B)** Diagrammatic representation of SARS-CoV-2 genome contains 12 open reading frames (ORF) and encodes 16 non-structural proteins (nsp1-16), 9 accessory proteins (ORF3a-10) and 4 structural proteins. Crystal structures of Some key non-structural proteins are presented as well. Created by BioRender.com.

epitope usually refers to the recognition frequency and magnitude by immune cells in a given HLA-type individual or population (27, 28, 59). The epitope immunodominance is determined by multiple factors, including HLA binding affinity, TCR recognition of epitope peptide-HLA complex, and naïve T cell precursor frequency (61, 62). To date, numerous immunodominant and immunodominant epitopes have been identified not only in SARS-CoV-2 structural protein region, but also in the non-structural and accessory protein regions that are not covered by current vaccination strategies.

# 3 Detection methods of SARS-CoV-2 specific T cell

With the advancement of immunology-related basic research, the detection technologies for antigen-specific T lymphocytes are also rapidly developing and improving. ELISpot and ICS are classical techniques widely used to detect and enumerate activated antigen-specific T cells secreting cytokines such as IFN-γ or TNF-α (63, 64). Both assays combined with SARS-CoV-2 overlapping peptide pools or single epitope stimulation of peripheral blood mononuclear cells (PBMCs) or tissue samples are widely used in the detecting and identifying SARS-CoV-2 specific T cells, with the advantage of high sensitivity (17, 22, 28, 65, 66). However, these assays can only measure functional T cells with cytokine secretion, which may underestimate the number of antigen-specific T cells, and cannot isolate live cells for detailed molecular analysis (67, 68). Based on some activation-related clusters of differentiation (CD) on the T cells surface which is significantly upregulated after *in vitro* stimulation, the detection technology AIM assay (57) was developed. This assays play an important role in determining the T cell responses targeting SARS-CoV-2 that allows to detect more types of virus-specific T cell lineages and isolate live cells for multi-parameter multi-information analysis (67). In studies using AIM assay to detect SARS-CoV-2-specific T cells, there is wide variation in the activation markers chosen, with commonly used markers including CD154 (CD40L)+CD137+ OX40+ for CD4+ T cells and CD69+CD137+ for CD8+ T cells (11, 13, 27, 69). However, cell activation-based functional assays fail to detect non-functional viral specific T cells, and the cellular phenotype is prone to change under *in vitro* stimulation (31).

After nearly 25 years of development, the peptide-loaded major histocompatibility complex (pMHC) tetramer technology has become a key tool for the analysis of antigen-specific T cells, allowing direct *in vitro* detection of SARS-CoV-2 epitope-specific T cells and thus detailed exploration of the T cell response feature induced by nature infection or COVID-19 vaccine (20, 22, 27, 70, 71). Tetramer technology utilizes the biotin-streptavidin system to multimerize pMHC complexes, greatly improving the avidity and stability between pMHC and TCRs for more easily detecting or sorting for single epitope-specific T cell by flow cytometry (67). Furthermore, tetramer-associated magnetic enrichment (TAME) could be furtherly used to detect some rare SARS-CoV-2 epitope-specific T cell populations (16, 18, 32). Notably, the development of MHC class II tetramers is more difficult than the easier production of MHC class I tetramers. So, the analysis of epitope-specific CD4+ T cells is relatively limited compared to a large amount of data on epitope-specific CD8+ T cells (67, 72). Recently, Mallajosyula and his colleagues developed an improved multimeric T cell staining reagent, spheromer, that each can display 12 pMHC complexes, and reported that the staining and capture efficiency of SARS-CoV-2 epitope-specific T cells are higher than tetramer (23).

The advent of next-generation in-depth sequencing has facilitated for more detailed downstream functional and molecular characterization of single immune cell. Generally, bulk RNA sequencing for TCR repertoires can only tell the usage frequency of TCR alpha and beta chain, but could not correspond to the paring and the individual functionality. single-cell RNA sequencing (scRNA-seq) can be used to uncover the functional diversity and dissect the heterogeneity of different epitope-specific T cells based on tetramer or pentamer single cell sorted technique (73), while single-cell T cell receptor sequencing (scTCR-seq) can effectively obtain the paired TCRαβ sequences and the diversity information of clonal population, including clonotype, clonal expansion and clone functionality (25). In general, it is foreseeable that more detection, isolation and analysis techniques for antigen- and epitope-specific T cells will continue to emerge in the future, thereby clearing technical hurdles and facilitating the comprehensive and in-depth research on cellular immunity toward multiple pathogens, including SARS-CoV-2.

# 4 SARS-CoV-2 epitope-specific T cell after natural infection

## 4.1 Nucleocapsid-derived epitope-specific T cell

The nucleocapsid (N) protein is the most common CD4+ and CD8+ T cell target after SARS-CoV-2 infection (65, 74) which dominate the response magnitude, breadth and frequency (66), and polyfunctional N-specific CD8+ T cell response significantly associates with milder COVID-19 disease severity (28). Since N is conserved between different SARS-CoV-2 variants, N specific CD4+ T cells may provide broad protections thus important for universal vaccine against SARS-CoV-2 and even SARS-CoV. Tarke et al. and Heide et al. showed N contained the CD4+ epitopes DQB1*06:02 restricted N261-275, DRB1*07:01 restricted N306-320 and DRB1*03:01 restricted N336-350 et al., giving a possibility about N epitope-specific CD4+ T cells can become immunodominant in certain HLA subtypes, however, whether these epitopes of N protein can clonally expand and function in protection need to be further investigated (13, 65). And it is more interesting to study whether N specific T helper can only help anti-N antibody production, or they can help anti-S and neutralizing antibodies generation. The HLA-B*07:02 restricted N105-113 (SPRWYFYYL) epitope appears to be the most immunodominant SARS-CoV-2 CD8+ T cell epitope to date, and no mutations of this epitope have been observed in the variants of concern. The immunodominant B7/N105+ cytotoxic T cell responses exhibited highly functional avidity and antiviral

efficacy to SARS-CoV-2 ancestral strain and multiple variants, which is strongly associated with mild COVID-19 disease, and maintained the long-lasting functional capacity up to 6 months after infection (15, 16, 25). This suggests that N105 may be a preferable target for future vaccine design or adoptive immunotherapy (39, 40), especially against novel variants or subvariants that are prone to S protein mutations and neutralizing antibody escape. Two different views are presented for the origin of the immunodominant B7/N105-specific CD8+ T cell responses. Some studies suggest that they are pre-existing immune cells induced by the previous cross-infection with human coronaviruses (HCoVs). This is supported by evidence that SARS-CoV-2-derived N105 has close amino acid homology to multiple HCoVs (25), and N105-specific CD8+ T cells could medicate cross-reactivity between beta-coronaviruses such as OC43 and HKU-1 which is driven by private TCR repertoire with TRBV27 biased use and longer CDR3β loops (19). Another more prevalent view suggested that the high immunodominance of the N105 epitope stems from the high precursor T cell frequency in unexposed individuals rather than from cross-reaction with HCoVs. Nguyen et al. used the ICS assay combined with the pMHC-I tetramer to determine the mean frequency of B7/N105+ CD8+ T cells in the peripheral blood of COVID-19 patients was $6.88\times10^{-4}$, while a high precursor frequency of $3.00\times10^{-5}$ was also observed in unexposed individuals (25). Furthermore, analysis of B7/N105+CD8+ T cell phenotypic profiles in different populations revealed that pre-pandemic unexposed individuals exhibited a predominantly naive T ($T_{naive}$, CCR7+CD27+CD45RA+) cells phenotype, in contrast to the central memory T ($T_{cm}$, CCR7+CD27+CD45RA-) cells dominant phenotype in infected patients. These observations highly suggest that the high frequency of B7/N105+ CD8+ T cells is composed of a naive precursor pool, rather than the cross-reactive memory population formed by previous HCoVs exposure. Single-cell TCR sequencing analysis revealed that CD8+ T cells targeting the N105 epitope exhibit a diverse TCRαβ repertoire as well as promiscuous TCRα-TCRβ gene pairing, with no common clonotype among individuals. This supports that T cells with different clonotypes can respond to the N105 epitope, laying the foundation for the high immunodominance hierarchy (19, 25).

The HLA-B*44:03 and HLA-B*40:01 restricted N322-330 (MEVTPSGTWL)-specific T cell response feature and TCR repertoire signature have also been identified and characterized in several recent studies (16, 20). Robust expansion of B44/N322-specific CD8+ T cells elicited by SARS-CoV-2 infection occurred as early as day 7 after symptom onset, in contrast to anti-nucleocapsid-specific IgG which was not detected until 29 days after symptom onset (16). B44/N322-specific memory CD8+ T cells in COVID-19 convalescent individuals exhibit a high median frequency of approximately $3.6\times10^{-5}$, and remain functional capacity of cytokine production (IFN-γ and TNF) and degranulation (CD107a) with a frequency of about $1\times10^{-5}$ after 104 days post COVID-19 symptom onset, while the anti-S protein IgG titer fell below the detection limit after 79 days post symptom onset (16). These observations suggest that CD8+ T cell responses targeting N protein-derived epitopes at least partly have a faster immune response and long-term persistence after SARS-CoV-2 infection. Similar to B7/N105+ CD8+ T cells, T cells targeting B40/N322 bias use the TRBV27 gene fragment, with a difference that B40/N322-specific T cell TCR repertoire exhibit a common TCRβ chain CDR3 motif TRBV27/TRBJ1-4 (20), indicating the selective recruitment of epitope-specific T cells elicited by infection. The immunodominant conserved epitopes B7/N105- and B44/N322-specific CD8+ T cells have been generated from COVID-19 convalescents and utilized to develop adoptive immunotherapy, exhibited robust functional capacity and cytotoxic potential against different virus variants, which may have important clinical value for immunocompromised patients with lethal infectious complications (39). Other studies have also identified an immunodominant epitope N361-369 (KTFPPTEPK) that can induce specific CD8+ T cell responses in 75% of COVID-19 convalescent individuals in multiple global prevalent HLA allele variants including HLA-A11:01, HLA-B44:01, and HLA-A03:01 (20, 21, 35, 41). This epitope is reported to be highly immunogenic and can induce robust anti-SARS-CoV-2 CD8+ T cell responses in a broad HLA population. Consistent with previous studies, an immunodominant epitope could bind to multiple HLA molecules thereby amplifying the potential immunogenicity of the specific epitope region (13). In addition, Rowntree et al. used TAME technology and found that the magnitude of T cell responses against SARS-CoV-2 internal epitopes (A3/N361, B7/N105, B40/N322, A1/ORF1a1637) is significantly higher than viral surface S proteins (A2/S269, A24/S1208) in seroconverted children and adult, which may reflect the differences in immunodominant pattern and immunodominance hierarchy of different SARS-CoV-2 proteome epitopes (20). Through TCR sequencing analysis, Hu et al. identified two common TCR clonotypes presenting N361 antigen specificity, with TCRβ chain CDR3 sequences ASSRAGTGYNEQF and ASSPSVYFEVSGANVLT, respectively. These 2 TCRs have complementary recognition capacity and exhibit high functional avidity against SARS-CoV-2 ancestral strain and multiple variants, which has important clinical significance for current vaccine design against future variants and subvariants (21).

## 4.2 Spike-derived epitope-specific T cell

The SARS-CoV-2 surface dominant antigen Spike is a key component involving viral invasion. Spike-specific CD4+ T cell responses mediate critical anti-SARS-CoV-2 immune effects and associate with anti-RBD antibody titers suggesting that they are also capable of supporting antibody responses (13). However, it is noteworthy that the frequency and magnitude of Spike specific CD8+ T cell responses after natural infection are seem to generally lower than those of nucleocapsid (20), which may be related to the immunogenicity difference of viral antigens. Recently, a wide range of studies have focused on the immunodominant HLA-A*02:01 restricted S269-277 (YLQPRTFLL) epitope-specific CD8+ T cell response feature and TCR repertoire characteristics (16, 17, 20, 25, 42). Detected by direct *in vitro* TAME, the mean frequency of A2/S269-specific CD8+ T cells is approximately $1.65\times10^{-6}$ in healthy pre-pandemic individuals (25), and $1.44\times10^{-5}$ and $1.28\times10^{-5}$ in the COVID-19 acute and convalescent patients, respectively (17),

suggesting that A2/S269-specific CD8+ T cells exhibit a certain level of activation and expansion following natural infection, but significantly lower than N protein-derived N105+CD8+ T cell responses (25). The A2/S269+CD8+ T cells expressed multiple cytotoxic granzymes/perforin, indicating their killing capacity and activation status, but the similar level was also found on the total CD8+ T cells (17). Transient activation of A2/S269-specific CD8+ T cells in COVID-19 patients and $T_{naive}$ and stem cell-like memory T ($T_{scm}$, CCR7-CD27+CD45RA+) cells dominant naïve memory phenotypes in convalescents may further reflect the lower immunodominance hierarchy (17). The suboptimal characteristics of A2/S269+ CD8+ T cells may be derived from the low degree of TCRαβ repertoire diversity, manifested as biased use of TRAV12 gene fragments (37, 42), public TRAV/TRAJ pairing and CDR3α loop motif including TRAV12-1/TRAJ43 CVVNXXDMRF motif (X represents any amino acid) and TRAV12-2/TRAJ30 CAVNXDDKIIF motif (25), which also suggests the essential role of TCRα chain in recognizing this epitope. Although the TRBV gene usage is less common, there remains a bias of TRBV7-9 (20, 37), which is quite distinct from the highly diverse TCR repertoires of immunodominant B7/N105. Overall, the suboptimality of S269 is reflected in multiple aspects, including the specific T cell responses frequency, magnitude, biological function, phenotypic characteristics and TCR repertoires feature.

In contrast, HLA-A24:02-restricted S protein-derived epitopes S1208–1216 (QYIKWPWYI) and S448–456 (NYNYLYRLF) appear to have higher immunodominance over A2/S269. Previous studies using TAME readout showed that the detected frequencies of A24/S448+ and A24/S1208+ CD8+ T cells in COVID-19 individuals are about $6.30\sim7.71\times10^{-5}$, which was significantly higher than that of unexposed controls of $8.44\sim9.50\times10^{-6}$, suggesting that naive A24/SARS-CoV-2 epitope-specific CD8+ T cells can strongly clone expand about 7.5 folds following COVID-19 (18, 25). Notably, the biological functions and association with COVID-19 disease severity of A24/S1208- A24/S448-specific CD8+ T cells have not been fully investigated, and therefore future research could focus on. HLA stabilization assays and HLA-peptide complex dissociation assays revealed that the high antigen sensitivity of two A24/epitopes originated from different mechanisms (22). The high recognition of A24/S1208-specific CD8+ T cells results from the high binding stability of the epitope peptide S1208-1216 to HLA-A24:02, while the high TCR affinity of A24/S448-specific CD8 + T cells determines their high recognition with epitope S448-456 (22). Previous studies suggest that intrinsic properties of viral epitopes such as MHC binding affinity and TCR recognition capacity have critical impacts on shaping the immunodominance hierarchy (59, 62). Furthermore, there also seems to be a close relationship between epitope-reactive T cells TCRαβ repertoire characteristics and epitope immunodominance and immunoprevalence. Rowntree and colleagues revealed that A24/S448- and A24/S1208-specific CD8+ T cells have completely different TCR repertoire profiles (18). For A24/S448+CD8+ T cells, prominent gene segment usage (TRBV2/TRBJ2-7) and common TCRβ chain CDR3 motif XXXGYEQYF resulted in a lack of TCRαβ plasticity similar to the subdominant A2/S269 epitope TCR repertoire. In contrast, the A24/S1208+CD8+ T cells display a high degree of TCRαβ diversity among COVID-19 patients similar to B7/N105+ T cells, possibly reflecting their higher immunodominance hierarchy. The highly diverse TCRαβ repertoire can provide a wider range for the selection of high affinity clonotypes for pMHC complexes. Thus, CD8+ T cells with high TCR repertoire diversity can potentially produce a broader antiviral immune response to SARS-CoV-2 ancestral strain and variants (25).

A recent study using overlapping peptide pools stimulation and ICS assay showed that CD4+ T cells targeting multiple SARS-CoV-2 proteins produce a stronger immune response than CD8+ T cells and may mediate greater antiviral immune protection (17). These potent antiviral CD4+ T cell responses may be induced by several immunodominant CD4+ T cell epitopes. Wragg et al. recently identified an S protein-derived HLA-DRB1*15:01 restricted immunodominant CD4+ T cell epitope S751-767 (NLLLQYGSFCTQLNRAL) (27). The DR15/S751-specific CD4+ T cells frequency was detected by tetramer technique up to $1.36\times10^{-4}$ in early convalescent patients from mild to moderate COVID-19, which was 34-fold higher compared to uninfected individuals. Although DR15/S751-specific CD4+ T cells gradually declined over time, they remain stable with a half-life of >377 days and maintain a frequency of $3.8\times10^{-5}$ in the late convalescent phase of 365-450 days after symptom onset. This is significantly longer than the half-life of approximately 200 days of total SARS-CoV-2-specific CD4+ T cells reported in previous studies (74), suggesting that some immunodominant epitopes can potentially induce robust and durable CD4+ T cell responses. TCR sequencing analysis showed that the expression of the TRBV gene in DR15/S751+ T cells displayed a skewed bias toward TRVB24-1, TRVB20-1 and TRBV6-1, with a highly public CDR3β motif CSARRGTEAFF, but the usage of TRAV gene was more diverse. Therefore, its TCR specificity seems to be driven by the TCRβ chain rather than the TCRα chain (27). However, due to the limited availability of MHC class II tetramers, there are relatively few studies on SARS-CoV-2 epitope-specific CD4+ T cell responses, so future efforts should focus on elucidating its critical role in antiviral immunity.

## 4.3 Other peptide epitope-specific T cell

The M protein is a prominent antigen among SARS-CoV-2 structural proteins, but studies have noted that the epitopes from the M protein lack the strong binding capacity to HLA molecules. Thus, it is generally agreed that the high immunogenicity of the M protein comes from the highly expressed genome rather than containing high-quality epitopes (13). The HLA-A*24:02 restricted M198-206 is currently reported the most immunodominant membrane-derived SARS-CoV-2 epitope, and A24/M198-specific CD8+ T cell responses can effectively suppress propagation of variants of concern including omicron strain and associate with COVID-19 clinical severity (38), and thus it appears to be a potential favorable target for next-generation vaccines or adoptive immunotherapy. Notably, despite the low abundance of T cell responses toward SARS-CoV-2 accessory and non-structural proteins (13, 75), some of the early expressed viral proteins can still

induce robust T cell immune responses (76). Using single epitope peptide stimulation and IFN-γ production assays, Schulien et al. detected reactive CD8+ T cells toward a wide scope of SARS-CoV-2 proteins in 88.5% of COVID-19 individuals, mainly targeting ORF1ab region which may relate to the longer protein fragment length and containing more prominent epitopes (16). Among them, HLA-A*01:01 restricted immunodominant epitope ORF1ab1637-1646 (TTDPSFLGRY)-specific CD8+ T cells magnitude is remarkably high that reaching up to 7%-25% of the total CD8+ T cells after SARS-CoV-2 acute infection, which is significantly higher than T cell responses induced by other protein-derived epitopes such as S269, S1208, and comparable to immunodominant N105, supporting the previous study that internal epitopes induce stronger CD8+ T cell responses (20, 29, 33). Furthermore, A01/ORF1ab1637 + memory CD8+ T cells remain at a considerably high level with functional IFN-γ and TNF production within 5 months after recovery from critical and severe COVID-19 disease (29, 33). The TCR sequencing revealed that A01/ORF1ab 1637-specific CD8+ T cells exhibit high TCR repertoires diversity and bias use of the TRBV27 gene fragment same as the TCRβ chain characteristics of N105-specific T cells (19, 20). However, the specific role of the TRBV27 gene fragment in T cells-mediated immune response toward SARS-CoV-2 remains unknown. Remarkably, the population with a given HLA typing seem to be more inclined to present a certain SARS-CoV-2 antigenic epitope, such as the HLA-A*01:01 molecule presenting ORF1ab1637 and the HLA-B*07:02 allele variant presenting the N105, thus inducing robust CD8+ T cell responses that contribute to viral clearance and control of disease severity. A limited number of studies have also investigated other ORF1ab- and some ORF3a-derived epitope-specific T cell responses (16, 36). Ferretti et al. used an unbiased screening strategy combined with the ELISpot assay and tetramer technique and identified HLA-A*02:01 restricted immunodominant epitopes A02/ORF1ab3886-3894 (KLWAQCVQL) and A02/ORF3a139-147 (LLYDANYFL) from COVID-19 patients PBMC, and observed that patients with severe disease exhibited fewer tetramer+ T cells than those with mild disease (36). TCR sequencing revealed that both epitopes-specific T cells clonotypes enriched for TRAV gene segments between most COVID-19 individuals, while TRBV gene usage is less common, such as TRAV38-2/DV8 for A02/ORF1ab3886-specific TCR clonotypes and TRAV8-1 for A02/ORF3a139-147-reactive TCR clonotypes. This suggests that a specific TCR Vα composition forms a structural feature that can bind with high-affinity peptide-MHC, thereby supporting the recognition of antigenic epitope (36). In addition to incorporating the above epitopes into COVID-19 vaccine development, some epitope-specific T cells have the potential to be used in TCR-engineered T cell immunotherapy. For example, immunodominant SARS-CoV-2 CD8+ HLA-A*03:01 restricted ORF1 808-816 and HLA-A*01:01 restricted ORF3a 207-217 epitopes were recently found contain highly functional and cytotoxic TCRs and mediating direct killing virus-infected cells (34). Therefore, the information on the epitope-specific T cell TCR repertoire summarized in this review may be of significant value for future novel interventions toward SARS-CoV-2.

## 5 SARS-CoV-2 epitope-specific T cell following vaccination

Over the past three years, several COVID-19 vaccines have been approved for emergency usage by the WHO and were broadly vaccinated worldwide, proven to significantly reduce the hospitalization risk and mortality, dramatically changed vaccination strategies in response to COVID-19 pandemics (43, 44, 77). These vaccines can effectively induce the production of anti-S protein antibodies and poly-specific T cell responses (78). However, studies noted that different vaccine platforms induce different immune response types and intensity, with the adenovirus-based vaccines can elicit a higher magnitude of S protein-specific T cell responses, while mRNA vaccines produce higher antibody titers (79). Optimized vaccine forms that include multiple identified immunodominant T cell epitopes may benefit populations with poor T cell responses induced by vaccination and those with impaired antibody immunity.

Compared to previous studies on T cell responses toward SARS-CoV-2 overlapping peptide pools, focusing on a single epitope provides a more accurate picture of the breadth, magnitude, kinetics feature and functional capacity of vaccine-induced T cell immunity (14). M. Wragg et al. investigated vaccinees with multiple platforms and found that DR15/S751-specific CD4+ T cells expanded approximately 30-fold after the first vaccination in unexposed individuals and further increased following second and booster dose, and repeated vaccination can selectively expand high-avidity T cell clones (27). Longitudinal analysis of the kinetics following BNT162b2 vaccination revealed that rapid expansion of immunodominant epitope DP04/S167-180 (YVSQPFLM)-specific and DR15/S751-specific CD4+ T cells occur as early as day 7 after primary vaccination and peak at days 7-14 after the second dose, maintaining predominantly effector memory phenotype for at least 200 days (26, 27). mRNA vaccine BNT162b2 can also elicit functionally competent and long-lasting viral epitope-specific CD8+ T cell responses targeting A01/S865, A02/S269, A03/S378, A24/S448 and A24/S1208 with the peak frequency of ~$3.6\times10^{-4}$ and maintaining full function for at least 80-120 days (14, 22). These observations suggest that COVID-19 vaccines, at least partially such as BNT162b2, can effectively induce rapid, robust and long-lasting immunodominant S protein epitope-specific CD4+ and CD8+ T cell responses that play a critical anti-COVID-19 role. However, only the low frequency and magnitude of subdominant DR15/S236-specific CD4+ T cell responses were driven by the COVID-19 mRNA vaccine, suggesting that the current vaccination strategy will result in the generation of heterogeneous T cell responses against different viral epitopes (14, 27).

Follicular helper T (Tfh) cells located in the germinal centers of secondary lymphoid tissues are a specific subset of the CD4+ T cell population that specializes in helping B cells and mediating protective antibody production (80). A recent longitudinal follow-up analysis demonstrated that the COVID-19 mRNA vaccine can induce strong, persistent and high TCR clonal abundance of PD-1 +CXCR5+ DR15/S167-specific Tfh cell responses in lymph nodes, which maintain at high frequency >170-200 days, and were

consistent with long-term survival germinal center B cell responses (26). Furthermore, there is a subpopulation of CD4+ T cells with similar phenotype and functional capacity to Tfh cells in peripheral blood named circulating follicular helper T (cTfh) cells (41), which are also strongly driven following COVID-19 vaccination. Activated DR15/S751-specific cTfh cells are rapidly generated at day 5 after BNT162b2 of convalescent individuals, and subsequently remain in circulation at a resting state for long period (27). The frequency of tetramer+ cTfh memory cells prior to vaccination was positively correlated with neutralizing antibody titers after vaccination, emphasizing the value of previously established Sike epitopes-specific cTfh cells in supporting antibody response recall after re-antigen exposure (27).

Some studies demonstrated that there are many differences in SARS-CoV-2 specific T cell immunity induced by different antigen exposure patterns and orders such as COVID-19 vaccination, natural infection, hybrid immunization or breakthrough infection (14, 73). SARS-CoV-2-specific T cells in COVID-19 convalescent individuals predominantly target non-spike protein epitopes, whereas mRNA vaccinees exhibit a broad spike epitopes-specific T cell response (81). The mRNA vaccination for those who recovered from SARS-CoV-2 infection also led to the main expansion of S-protein-specific T cells, whereas breakthrough infections induce robust non-S-protein-specific T cell responses, suggesting that current vaccine strategies tend to recruit Spike-specific T cell population, whereas breakthrough infections increase the diversity of T cell repertoire (73). However, in the context of the constant mutation in the SARS-CoV-2 genome, especially the emergence of the Omicron variant with a wide scope of mutations in S protein epitopes. This should arouse public vigilance that future vaccine regimens may need to incorporate more SARS-CoV-2 proteomic epitopes, especially for immunodominant epitopes that are highly conserved among mutant strains.

## 6 Heterogenous phenotypic characteristics of SARS-CoV-2 specific T cells

Although quite a lot of studies showed that T cells play important role in COVID-19 recovery, the phenotype and the functionality of SARS-CoV-2 specific T cells are not clear, so far, some studies focus on the phenotype defined by CD137 and CD69 (AIM) for virus specific CD8+ T cells, and CD154 and CD137 for CD4+ (11, 27), some studies sticked to the phenotype defined based on IFN-γ+ and TNF-α (ICS) (15). However, Whether SARS-CoV-2 specific CD8+ T cells defined AIM is containing or overlapped with those defined by ICS is unknown, and which one play more important role is not clearly addressed. although both were proved to combating against COVID-19 infection and can be induced in vaccinees. To some extent, as known for its heterogenicity, whether both can differentiate into similar memory T cells subpopulation is also obscure. Here, we summarize the heterogenicity of virus specific T cell in COVID-19.

Among the memory T subpopulations, $T_{cm}$ preserved long-term specific immune memory to SARS-CoV-2 for rapid future responses (9, 82). $T_{scm}$ is capable for self-renewing and multilineage differentiating to broad spectrum of anti-SARS-CoV-2 memory and effector T cell population (83). Effector memory CD45RA T ($T_{emra}$, CCR7-CD27-CD45RA+) cells are virus-experienced cells that re-express the naïve cell marker CD45RA, which were increased in COVID-19 and correlate with milder disease (84). Many previous studies have performed phenotypic characterization and subsets division at the level of total SARS-CoV-2 specific memory T cells (8, 85), demonstrating that SARS-CoV-2-specific CD4+ memory T cells were predominantly $T_{cm}$ cells, whereas SARS-CoV-2-specific CD8+ memory T cells were mainly $T_{emra}$ cells. However, epitopes-specific memory T cells of the different immunodominance hierarchy toward SARS-CoV-2 also appeared to display convergent phenotypic feature, which are prevalent in both CD4+ and CD8+ T cells and exhibit differences from the total SARS-CoV-2-specific T cells. For example, immunodominant epitope DR15/S751+CD4+ and B7/N105+CD8+ memory T cells have similar phenotype profiles exhibiting a stable $T_{cm}$ phenotype (25, 27, 28), while epitopes with slightly lower immunodominance, such as A24/S448, A24/S1208 and A2/S269+CD8, their specific T cells have similar phenotype patterns, displaying highly diverse memory T cell phenotypes including $T_{cm}$, $T_{scm}$, $T_{emra}$ and $T_{naive}$ (18, 25, 31). In contrast, the subdominant DR15/S236+CD4+ memory T cells population exhibits a more $T_{naive}$ memory phenotype profile in COVID-19 convalescent patients (27). These memory phenotype differences observed in recent studies may associate to the longevity and biological function of epitope-specific T cells, thus affecting their immunodominance hierarchy. Notably, the relationship and potential mechanism still needs to be further validated by large sample sizes cohorts and consistent time point comparison in future, which may be of great value for multidimensional decoding of virus epitopes.

Previous studies have reported a significant correlation between different HLA allelic variants and COVID-19 disease severity and clinical outcome (86, 87), while HLA type also seems to associate with the phenotypic characteristics of restricted epitope-specific T cells (16). Schulien et al. found that HLA-A restricted epitopes-(A01/ORF3a207-215, A01/ORF1ab4163-4172, A02/ORF3a139-147) compared to HLA-B restricted epitopes- (B44/N322-330, B44/ORF1ab3946-3954, B07/N105) specific CD8+ T cell more bias to early differentiation of $T_{cm}$ and effector memory 1 T ($T_{em1}$, CCR7-CD27+CD45RA-) cells subsets, and are highly expressed with antigen recognition-related markers and low expression of cell differentiation-related markers (16). This may partially explain the effect of HLA allelic variants on the COVID-19 outcome by affecting the phenotypic and functional characteristics of various restricted epitopes-specific T cells, thereby changing the T cell immune responses of specific populations after SARS-CoV-2 infection.

Furthermore, the phenotypic characteristics of SARS-CoV-2 epitope-specific T cells distinctly differed among patients with different disease severity from mild or moderate, to severe and critical disease. W. Nelson et al. using the combinatorial TAME strategy analyzed two S-protein-derived epitopes- (S166-177 and

S310-320) and two N-protein-derived epitopes- (N305-316 and N329-340) specific CD4+ T cell responses in COVID-19 patients with HLA-DRB1*07:01 allele, and found that the tetramer+ T cell phenotypes differed between disease severity, with more CXCR3 +CCR4- Th1 cells in mildly infected individuals and impaired differentiation and formation of Th1-type CD4+ T cells in severe COVID-19 patients (32). This observation is consistent with previous reports that Th1 cells profile plays a key role in effective viral infection resolution and symptoms control, whereas Th2 and Th17 cells are usually associated with more severely ill, possibly due to the close association of lung immunopathology and ARDS, respectively (8, 88, 89). For acute COVID-19 patients with the critical disease, tetramer+CD8+ T cells lack polyfunctional cytokine production, and exhibit high expression of inhibitory receptors and gene expression profiles that limit T cell re-activation and migration (29). Notably, the expression of inhibitory receptors such as PD-1 is associated with T cell activation and function (31), whereas the co-expression of multiple inhibitory receptors (NKG2A, LAG-3, CD-95, and TIGIT) is the phenotypic marker of T cell dysfunction and exhaustion and correlates with the more severe COVID-19 course (30, 90). However, the distribution and contribution of SARS-CoV-2 specific cTfh cells in mild and severe infections are currently controversial (32, 90).

Multiple studies have observed that the phenotypic characteristics of SARS-CoV-2-specific T cells also exist differences in different age groups (20, 25, 91). Analysis of the ex vivo phenotype profiles of epitopes-specific T cells in seroconvert children and adults infected with SARS-CoV-2 revealed that tetramer+ CD8+ T cells of children mainly display naive phenotypes such as $T_{scm}$ or $T_{naive}$ cells, while adults had a higher frequency of effector memory populations (20). This difference may arise from varying degrees of previous exposure to HCoVs and the resulting antigen-experienced T cell differentiation (91). Moreover, a recent study showed that in response to a specific SARS-CoV-2 epitope such as B7/N105, reactive CD8+ T cells in the elderly often exhibit a highly heterogeneous $T_{naive}$, $T_{cm}$, or $T_{emra}$ phenotype, in contrast to the homogeneous phenotypic profile exhibited by adults, which may associate with T cells in the elderly experienced age-related dysregulated homeostatic proliferation or with previous coronavirus infection (25).

## 7 Cross-reactivity of SARS-CoV-2, variants of concern and HCoVs

Broad cross-reactive T cell responses targeting multiple SARS-CoV-2 structural and non-structural proteins have been reported in more than 50% of unexposed healthy individuals (11, 24, 92–95). These immune responses may be derived from preexisting memory T cells generated by previous HCoVs exposure and can cross-recognize SARS-CoV-2. The six existing HCoVs include α coronaviruses (HCoV-NL63, HCoV-229E) and β coronaviruses (HCoV-OC43, HCoV-HKU1, SARS-CoV, SARS-CoV-2, and MERS-CoV). The highly conserved cross-reactive epitopes in HCoVs and SARS-CoV-2 are shared in T cell immunity due to the presence of amino acid sequence homology (96, 97), and thus induce long-term maintenance of cross-reactive cellular immunity (93). Currently, the function and impact of preexisting cross-reactive T cell responses in COVID-19 remain controversial, and some researchers have pointed out that it may be a double-edged sword (9, 98). The highly conserved immunodominant region S811-831 (KPSKRSFIEDLLFNKVTLADA) in SARS-CoV-2 and multiple HCoVs contains multiple MHC class II-restricted CD4+ T cell epitopes (92, 99, 100). In this peptide region, S816-830 cross-reactive CD4+ T cell responses are efficiently recruited to most SARS-CoV-2-infected individuals and almost all mRNA vaccinees, and positively correlate with S protein-neutralizing antibodies, suggesting that coordinated cross-reactive immune responses may play an important anti-SARS-CoV-2 role (92). Moreover, some viral proteins are essential for the viral replication cycle, such as RNA polymerase and helicase, are often highly conserved among multiple coronaviruses and induce strong cross-reactive T cell responses, which may become potential candidate targets for future vaccine design. Swadling et al. and Le Bert et al. detected specific CD8+ T cell responses targeting nsp7, nsp12 and nsp13 in SARS-COV-2 unexposed individuals and exposed healthcare workers and found that these cross-reactive T cells were rapidly reactivated after virus exposure, producing anti-infective effect and having the potential to induce abortive infection (94, 101). Nesterenko et al. identified the SARS-CoV-2-derived nsp12 epitopes RQLLFVVEV and TMADLVYAL with extensive cross-reaction to HCoVs. Their specific TCRs can target and eliminate cells expressing viral RNA polymerase and associate with reduced disease severity (24). These observations support the previous findings that recent HCoVs infection or higher levels of cross-reactive epitope-specific T memory cells appear to be associated with a better COVID-19 clinical outcome (23, 92, 95). However, several other studies have pointed out that HCoV-specific T cells commonly have only low affinity against SARS-CoV-2 antigens (102, 103). These low-affinity and low-functional cross-reactive T cells prevent the formation of high-affinity T cell responses after primary SARS-CoV-2 infection, thus negatively affecting efficient antiviral immunity (98). In general, recall of preexisting cross-reactive memory T cells can produce a rapid early antiviral immune response, which, although not sufficient to prevent SARS-CoV-2 infection, may modulate COVID-19 disease severity or modulate vaccination responsiveness resulting in a faster or stronger vaccine response.

In the context of continually accruing mutations in the SARS-CoV-2 genome, many emerging viral variants such as Omicron and subvariants, which has been globally prevalent in the last two years, are able to generate immune escapes against the ancestral strain, thus greatly increasing the number of breakthrough infection cases. However, T cell immune responses elicited by prior infection or COVID-19 vaccines are greatly preserved and can cross-recognize variants of concern (VOCs) from Alpha to Omicron (104–107). These T cell immune responses are associated with efficient viral clearance and milder disease severity, which is clearly distinct from the severely impaired SARS-CoV-2-specific B cell responses and neutralizing antibody function (108). Based on HLA polymorphisms, each individual recognizes a group of unique T

cell epitopes estimated to be at least 30-40 SARS-CoV-2 antigen epitopes, including approximately 19 CD4+ T cell epitopes and 17 CD8+ T cell epitopes (13). At the population level, roughly 80% of the memory T cells elicited by natural infection or vaccination can cross-react with different SARA-CoV-2 variants, and <30% of the T cell responses are lost when identifying common VOCs (105, 106). Therefore, future new variants or subvariants are unlikely to escape this extensive T cell immunity from the individual and population levels. Previously established memory T cells also have extensive immune coverage and cross-recognition capacity against the Omicron variant, mainly targeting conserved immunodominant epitopes including B7/N105, B40/N322, A3/N361, A24/S1208, DPB4/S167, A24/M198, A1/ORF1a1637, thus playing a critical role in limiting the transmission and pathogenesis of Omicron. However, it is worth noting that some epitopes mutations in the RBD region of the Omicron proteome such as N440K mutation (S751-765) will reduce the binding affinity to HLA molecules (109, 110), and some mutations in the accessory protein regions such as A1708D mutation (ORF1ab1707-1716) and I2230T mutation (ORF1ab2230-2238) will impair the activation of CD8+ T cells (111). Under the influence of multiple mutations in critical epitopes, approximately 21% of individuals showed reduced T cell responses against Omicron (112), suggesting that some individuals target non-conserved epitopes resulting in limited T cell immunity. Thus, the constant evolution of SARS-CoV-2 forced vaccine design to focus on S protein sequences that were unaffected by epitope mutations, or to select more conserved immunodominant epitopes. Predicting future circulating variants is a major challenge for vaccine strategies that would otherwise lead to reduced efficacy of vaccination.

## 8 Prospectives

Albeit we accumulate various related studies into this review, in COVID-19 T cell immune filed, there are still a few questions remain to be answered in future. How the SARS-CoV-2 epitope-specific T cell responses were initiated, especially under different circumstance such as vaccinations, infections, vaccination-infection and infection-vaccination patterns, and how these cells rapidly response after several encountering antigen. And after multiple antigen training, whether those epitope-specific T cell multiple-functionality can be improved, whether the starting of epitope-specific T cell induction are different in mild and severe COVID-19 patients, especially under severe situation, and how antigen cross-dressing play in stimulating T cell response.

After epitope-specific T cell responses generated, it is still not known how those T cells differentiate into memory phase, do they correspondingly differentiated between immunodominant and subdominant epitopes, and did they have similar TCR clonal expansion and have similar functionality characteristics? And what host factors drive the clonal expansion, even divided the T cell response between activation and exhaustion. Notably, what role of these epitope-specific T cell responses in the cytokines storm generation, inhibition in early phase or loosen T activation induced overaction. More importantly, how epitope-specific T cells interact with B cell biology, is especially need to study in future. It will be related to the question whether epitope-specific T cells can be further divided into epitope specific Treg, and as mentioned in previous text, whether N, M or ORF specific CD4+ T cells can help anti-S or neutralizing antibodies generation. Additionally, more studies should be carried on the longevity and location of epitope-specific memory T cells, whether COVID-19 can generated T residential memory in lung tissue, how they keep regeneration, whether they could rapidly response secondary COVID-19 infection should be addressed in the future. Notably, while SARS-CoV-2-specific CD8+ T cell epitopes restricted by multiple predominant HLA-I have been well investigated, CD4+ T cell epitopes specific T cell responses have been understudied which is partly due to the limitations in reagents for class-II multimers. However, considering the critical role of CD4+ T cells in anti-SARS-CoV-2, future studies should pay more attention to this issue and balance this research gap.

Finally, what need for greater vigilance is the immune escape caused by SARS-CoV-2 genome mutation poses a great threat to the current vaccine effectiveness. Most of the immunodominant epitopes covered in this review have been confirmed to be highly conserved, and specific T cell response toward these epitopes can cross-recognize the multiple SARS-CoV-2 variants especially for Omicron (Table 1). Therefore, future vaccine regimens could incorporate those critical epitopes to improve the efficacy and longevity. When considering the inclusion of these epitopes in vaccine development, the issue of HLA restriction is indeed a concern, one way to overcome HLA limitations, we can constitute a peptide pools, to cover more different global frequent HLA-restricted SARS-CoV-2 immunodominant epitopes in vaccine design, and then combined with novel nanoparticles-based vaccine delivery, thus inducing a broad immune response that covering wider HLA alleles. Second way to constitute conserved SARS-CoV-2 proteins into viral vector or combining with special adjuvants, which can stimulate strong T cells targeting to SARS-CoV-2 proteins when viral vector-based vaccine replicated *in vivo*. Ideally, it will be great to design a live attenuated SARS-CoV-2 vaccine therefore contains all viral proteins, which contains all T cell epitopes and no matter HLA subtypes.

## Author contributions

ZW and JW contributed to the conception and design of this review article. GY wrote the manuscript. PS, JQ, and DC searched and collected the latest literature. NZ, ZW, YZ, and XY critically reviewed the manuscript. All authors contributed to the article and approved the submitted version.

## Funding

This work was supported by the National Key Research and Development Program of China [2019YFC0810900], Ministry of

Science and Technology of the People Republic of China [2021YFC0864400], NSFC [81971485, 82271801], Guangdong Basic and Applied Basic Research Foundation [2019B1515120068, 2020B1111330001, 2022B1111070002], Emergency Key Program of Guangzhou Laboratory [No.EKPG21-30-1], China Postdoctoral Science Foundation [2021M690792] and Zhongnanshan Medical Foundation of Guangdong Province [ZNSA-2020013].

## Acknowledgments

We thank Bio Render for providing materials to help us better beautify the figures.

## Conflict of interest

The authors declare that the research was conducted in the absence of any commercial or financial relationships that could be construed as a potential conflict of interest.

## Publisher's note



## References

1. COVID-19 Cumulative Infection Collaborators. Estimating global, regional, and national daily and cumulative infections with SARS-CoV-2 through Nov 14, 2021: a statistical analysis. *Lancet* (2022) 399:2351–80. doi: 10.1016/S0140-6736(22)00484-6

2. COVID-19 Excess Mortality Collaborators. Estimating excess mortality due to the COVID-19 pandemic: a systematic analysis of COVID-19-related mortality, 2020-21. *Lancet* (2022) 399:1513–36. doi: 10.1016/S0140-6736(21)02796-3

3. Nyberg T, Ferguson NM, Nash SG, Webster HH, Flaxman S, Andrews N, et al. Comparative analysis of the risks of hospitalisation and death associated with SARS-CoV-2 omicron (B.1.1.529) and delta (B.1.617.2) variants in England: a cohort study. *Lancet* (2022) 399:1303–12. doi: 10.1016/S0140-6736(22)00462-7

4. Guan W-J, Ni Z-Y, Hu Y, Liang W-H, Ou C-Q, He J-X, et al. Clinical characteristics of coronavirus disease 2019 in China. *N Engl J Med* (2020) 382:1708–20. doi: 10.1056/NEJMoa2002032

5. Menni C, Valdes AM, Polidori L, Antonelli M, Penamakuri S, Nogal A, et al. Symptom prevalence, duration, and risk of hospital admission in individuals infected with SARS-CoV-2 during periods of omicron and delta variant dominance: a prospective observational study from the ZOE COVID study. *Lancet* (2022) 399:1618–24. doi: 10.1016/S0140-6736(22)00327-0

6. Le Bert N, Clapham HE, Tan AT, Chia WN, Tham CYL, Lim JM, et al. Highly functional virus-specific cellular immune response in asymptomatic SARS-CoV-2 infection. *J Exp Med* (2021) 218:e20202617. doi: 10.1084/jem.20202617

7. Sekine T, Perez-Potti A, Rivera-Ballesteros O, Strålin K, Gorin J-B, Olsson A, et al. Robust T cell immunity in convalescent individuals with asymptomatic or mild COVID-19. *Cell* (2020) 183:158–168.e14. doi: 10.1016/j.cell.2020.08.017

8. Neidleman J, Luo X, Frouard J, Xie G, Gill G, Stein ES, et al. SARS-CoV-2-Specific T cells exhibit phenotypic features of helper function, lack of terminal differentiation, and high proliferation potential. *Cell Rep Med* (2020) 1:100081. doi: 10.1016/j.xcrm.2020.100081

9. Moss P. The T cell immune response against SARS-CoV-2. *Nat Immunol* (2022) 23:186–93. doi: 10.1038/s41590-021-01122-w

10. Lu X, Yamasaki S. Current understanding of T cell immunity against SARS-CoV-2. *Inflammation Regener* (2022) 42:51. doi: 10.1186/s41232-022-00242-6

11. Grifoni A, Weiskopf D, Ramirez SI, Mateus J, Dan JM, Moderbacher CR, et al. Targets of T cell responses to SARS-CoV-2 coronavirus in humans with COVID-19 disease and unexposed individuals. *Cell* (2020) 181:1489–1501.e15. doi: 10.1016/j.cell.2020.05.015

12. Kared H, Redd AD, Bloch EM, Bonny TS, Sumatoh H, Kairi F, et al. SARS-CoV-2–specific CD8+ T cell responses in convalescent COVID-19 individuals. *J Clin Invest* (2021) 131:e145476. doi: 10.1172/JCI145476

13. Tarke A, Sidney J, Kidd CK, Dan JM, Ramirez SI, Yu ED, et al. Comprehensive analysis of T cell immunodominance and immunoprevalence of SARS-CoV-2 epitopes in COVID-19 cases. *Cell Rep Med* (2021) 2:100204. doi: 10.1016/j.xcrm.2021.100204

14. Oberhardt V, Luxenburger H, Kemming J, Schulien I, Ciminski K, Giese S, et al. Rapid and stable mobilization of CD8+ T cells by SARS-CoV-2 mRNA vaccine. *Nature* (2021) 597:268–73. doi: 10.1038/s41586-021-03841-4

15. Peng Y, Felce SL, Dong D, Penkava F, Mentzer AJ, Yao X, et al. An immunodominant NP105-113-B*07:02 cytotoxic T cell response controls viral replication and is associated with less severe COVID-19 disease. *Nat Immunol* (2022) 23:50–61. doi: 10.1038/s41590-021-01084-z

16. Schulien I, Kemming J, Oberhardt V, Wild K, Seidel LM, Killmer S, et al. Characterization of pre-existing and induced SARS-CoV-2-specific CD8+ T cells. *Nat Med* (2021) 27:78–85. doi: 10.1038/s41591-020-01143-2

17. Habel JR, Nguyen THO, van de Sandt CE, Juno JA, Chaurasia P, Wragg K, et al. Suboptimal SARS-CoV-2-specific CD8+ T cell response associated with the prominent HLA-A*02:01 phenotype. *Proc Natl Acad Sci U.S.A.* (2020) 117:24384–91. doi: 10.1073/pnas.2015486117

18. Rowntree LC, Petersen J, Juno JA, Chaurasia P, Wragg K, Koutsakos M, et al. SARS-CoV-2-specific CD8+ T-cell responses and TCR signatures in the context of a prominent HLA-A*24:02 allomorph. *Immunol Cell Biol* (2021) 99:990–1000. doi: 10.1111/imcb.12482

19. Lineburg KE, Grant EJ, Swaminathan S, Chatzileontiadou DSM, Szeto C, Sloane H, et al. CD8+ T cells specific for an immunodominant SARS-CoV-2 nucleocapsid epitope cross-react with selective seasonal coronaviruses. *Immunity* (2021) 54:1055–1065.e5. doi: 10.1016/j.immuni.2021.04.006

20. Rowntree LC, Nguyen THO, Kedzierski L, Neeland MR, Petersen J, Crawford JC, et al. SARS-CoV-2-specific T cell memory with common TCRαβ motifs is established in unvaccinated children who seroconvert after infection. *Immunity* (2022) 55:1299–1315.e4. doi: 10.1016/j.immuni.2022.06.003

21. Hu C, Shen M, Han X, Chen Q, Li L, Chen S, et al. Identification of cross-reactive CD8+ T cell receptors with high functional avidity to a SARS-CoV-2 immunodominant epitope and its natural mutant variants. *Genes Dis* (2022) 9:216–29. doi: 10.1016/j.gendis.2021.05.006

22. Kuse N, Zhang Y, Chikata T, Nguyen HT, Oka S, Gatanaga H, et al. Long-term memory CD8+ T cells specific for SARS-CoV-2 in individuals who received the BNT162b2 mRNA vaccine. *Nat Commun* (2022) 13:5251. doi: 10.1038/s41467-022-32989-4

23. Mallajosyula V, Ganjavi C, Chakraborty S, McSween AM, Pavlovitch-Bedzyk AJ, Wilhelmy J, et al. CD8+ T cells specific for conserved coronavirus epitopes correlate with milder disease in COVID-19 patients. *Sci Immunol* (2021) 6:eabg5669. doi: 10.1126/sciimmunol.abg5669

24. Nesterenko PA, McLaughlin J, Tsai BL, Burton Sojo G, Cheng D, Zhao D, et al. HLA-A∗02:01 restricted T cell receptors against the highly conserved SARS-CoV-2 polymerase cross-react with human coronaviruses. *Cell Rep* (2021) 37:110167. doi: 10.1016/j.celrep.2021.110167

25. Nguyen THO, Rowntree LC, Petersen J, Chua BY, Hensen L, Kedzierski L, et al. CD8+ T cells specific for an immunodominant SARS-CoV-2 nucleocapsid epitope display high naive precursor frequency and TCR promiscuity. *Immunity* (2021) 54:1066–1082.e5. doi: 10.1016/j.immuni.2021.04.009

26. Mudd PA, Minervina AA, Pogorelyy MV, Turner JS, Kim W, Kalaidina E, et al. SARS-CoV-2 mRNA vaccination elicits a robust and persistent T follicular helper cell response in humans. *Cell* (2022) 185:603–613.e15. doi: 10.1016/j.cell.2021.12.026

27. Wragg KM, Lee WS, Koutsakos M, Tan H-X, Amarasena T, Reynaldi A, et al. Establishment and recall of SARS-CoV-2 spike epitope-specific CD4+ T cell memory. *Nat Immunol* (2022) 23:768–80. doi: 10.1038/s41590-022-01175-5

28. Peng Y, Mentzer AJ, Liu G, Yao X, Yin Z, Dong D, et al. Broad and strong memory CD4+ and CD8+ T cells induced by SARS-CoV-2 in UK convalescent individuals following COVID-19. *Nat Immunol* (2020) 21:1336–45. doi: 10.1038/s41590-020-0782-6

29. Gangaev A, Ketelaars SLC, Isaeva OI, Patiwael S, Dopler A, Hoefakker K, et al. Identification and characterization of a SARS-CoV-2 specific CD8+ T cell response with immunodominant features. *Nat Commun* (2021) 12:2593. doi: 10.1038/s41467-021-22811-y

30. Cords L, Knapp M, Woost R, Schulte S, Kummer S, Ackermann C, et al. High and sustained ex vivo frequency but altered phenotype of SARS-CoV-2-Specific CD4+

T-cells in an anti-CD20-Treated patient with prolonged COVID-19. *Viruses* (2022) 14:1265. doi: 10.3390/v14061265

31. Rha M-S, Jeong HW, Ko J-H, Choi SJ, Seo I-H, Lee JS, et al. PD-1-Expressing SARS-CoV-2-Specific CD8+ T cells are not exhausted, but functional in patients with COVID-19. *Immunity* (2021) 54:44–52.e3. doi: 10.1016/j.immuni.2020.12.002

32. Nelson RW, Chen Y, Venezia OL, Majerus RM, Shin DSMGH COVID-19 Collection & Processing Team, et al. SARS-CoV-2 epitope-specific CD4+ memory T cell responses across COVID-19 disease severity and antibody durability. *Sci Immunol* (2022) 7:eabl9464. doi: 10.1126/sciimmunol.abl9464

33. Saini SK, Hersby DS, Tamhane T, Povlsen HR, Hernandez SPA, Nielsen M, et al. SARS-CoV-2 genome-wide T cell epitope mapping reveals immunodominance and substantial CD8 $^{+}$ T cell activation in COVID-19 patients. *Sci Immunol* (2021) 6: eabf7550. doi: 10.1126/sciimmunol.abf7550

34. Wagner KI, Mateyka LM, Jarosch S, Grass V, Weber S, Schober K, et al. Recruitment of highly cytotoxic CD8+ T cell receptors in mild SARS-CoV-2 infection. *Cell Rep* (2022) 38:110214. doi: 10.1016/j.celrep.2021.110214

35. Zhang J, Lu D, Li M, Liu M, Yao S, Zhan J, et al. A COVID-19 T-cell response detection method based on a newly identified human CD8+ T cell epitope from SARS-CoV-2 - hubei province, China, 2021. *China CDC Wkly* (2022) 4:83–7. doi: 10.46234/ccdcw2021.258

36. Ferretti AP, Kula T, Wang Y, Nguyen DMV, Weinheimer A, Dunlap GS, et al. Unbiased screens show CD8+ T cells of COVID-19 patients recognize shared epitopes in SARS-CoV-2 that largely reside outside the spike protein. *Immunity* (2020) 53:1095–1107.e3. doi: 10.1016/j.immuni.2020.10.006

37. Shomuradova AS, Vagida MS, Sheetikov SA, Zornikova KV, Kiryukhin D, Titov A, et al. SARS-CoV-2 epitopes are recognized by a public and diverse repertoire of human T cell receptors. *Immunity* (2020) 53:1245–1257.e5. doi: 10.1016/j.immuni.2020.11.004

38. Ogura H, Gohda J, Lu X, Yamamoto M, Takesue Y, Son A, et al. Dysfunctional sars-CoV-2-M protein-specific cytotoxic T lymphocytes in patients recovering from severe COVID-19. *Nat Commun* (2022) 13:7063. doi: 10.1038/s41467-022-34655-1

39. Panikkar A, Lineburg KE, Raju J, Chew KY, Ambalathingal GR, Rehan S, et al. SARS-CoV-2-specific T cells generated for adoptive immunotherapy are capable of recognizing multiple SARS-CoV-2 variants. *PloS Pathog* (2022) 18:e1010339. doi: 10.1371/journal.ppat.1010339

40. Somogyi E, Csiszovszki Z, Molnár L, Lőrincz O, Tóth J, Pattijn S, et al. A peptide vaccine candidate tailored to individuals' genetics mimics the multi-targeted T cell immunity of COVID-19 convalescent subjects. *Front Genet* (2021) 12:684152. doi: 10.3389/fgene.2021.684152

41. Juno JA, Tan H-X, Lee WS, Reynaldi A, Kelly HG, Wragg K, et al. Humoral and circulating follicular helper T cell responses in recovered patients with COVID-19. *Nat Med* (2020) 26:1428–34. doi: 10.1038/s41591-020-0995-0

42. Chaurasia P, Nguyen THO, Rowntree LC, Juno JA, Wheatley AK, Kent SJ, et al. Structural basis of biased T cell receptor recognition of an immunodominant HLA-A2 epitope of the SARS-CoV-2 spike protein. *J Biol Chem* (2021) 297:101065. doi: 10.1016/j.jbc.2021.101065

43. Liu X, Shaw RH, Stuart ASV, Greenland M, Aley PK, Andrews NJ, et al. Safety and immunogenicity of heterologous versus homologous prime-boost schedules with an adenoviral vectored and mRNA COVID-19 vaccine (Com-COV): a single-blind, randomised, non-inferiority trial. *Lancet* (2021) 398:856–69. doi: 10.1016/S0140-6736(21)01694-9

44. Stuart ASV, Shaw RH, Liu X, Greenland M, Aley PK, Andrews NJ, et al. Immunogenicity, safety, and reactogenicity of heterologous COVID-19 primary vaccination incorporating mRNA, viral-vector, and protein-adjuvant vaccines in the UK (Com-COV2): a single-blind, randomised, phase 2, non-inferiority trial. *Lancet* (2022) 399:36–49. doi: 10.1016/S0140-6736(21)02718-5

45. Kuhlmann C, Mayer CK, Claassen M, Maponga T, Burgers WA, Keeton R, et al. Breakthrough infections with SARS-CoV-2 omicron despite mRNA vaccine booster dose. *Lancet* (2022) 399:625–6. doi: 10.1016/S0140-6736(22)00090-3

46. Hachmann NP, Miller J, Collier A-RY, Ventura JD, Yu J, Rowe M, et al. Neutralization escape by SARS-CoV-2 omicron subvariants BA.2.12.1, BA.4, and BA.5. *N Engl J Med* (2022) 387:86–8. doi: 10.1056/NEJMc2206576

47. Pardieck IN, van der Sluis TC, van der Gracht ETI, Veerkamp DMB, Behr FM, van Duikeren S, et al. A third vaccination with a single T cell epitope confers protection in a murine model of SARS-CoV-2 infection. *Nat Commun* (2022) 13:3966. doi: 10.1038/s41467-022-31721-6

48. Palatnik-de-Sousa I, Wallace ZS, Cavalcante SC, Ribeiro MPF, Silva JABM, Cavalcante RC, et al. A novel vaccine based on SARS-CoV-2 CD4+ and CD8+ T cell conserved epitopes from variants alpha to omicron. *Sci Rep* (2022) 12:16731. doi: 10.1038/s41598-022-21207-2

49. Wu F, Zhao S, Yu B, Chen Y-M, Wang W, Song Z-G, et al. A new coronavirus associated with human respiratory disease in China. *Nature* (2020) 579:265–9. doi: 10.1038/s41586-020-2008-3

50. Saville JW, Berezuk AM, Srivastava SS, Subramaniam S. Three-dimensional visualization of viral structure, entry, and replication underlying the spread of SARS-CoV-2. *Chem Rev* (2022) 122:14066–84. doi: 10.1021/acs.chemrev.1c01062

51. Abulsoud AI, El-Husseiny HM, El-Husseiny AA, El-Mahdy HA, Ismail A, Elkhawaga SY, et al. Mutations in SARS-CoV-2: Insights on structure, variants, vaccines, and biomedical interventions. *Biomed. Pharmacother.* (2023) 157:113977. doi: 10.1016/j.biopha.2022.113977

52. Arya R, Kumari S, Pandey B, Mistry H, Bihani SC, Das A, et al. Structural insights into SARS-CoV-2 proteins. *J Mol Biol* (2021) 433:166725. doi: 10.1016/j.jmb.2020.11.024

53. Mandala VS, McKay MJ, Shcherbakov AA, Dregni AJ, Kolocouris A, Hong M. Structure and drug binding of the SARS-CoV-2 envelope protein transmembrane domain in lipid bilayers. *Nat Struct Mol Biol* (2020) 27:1202–8. doi: 10.1038/s41594-020-00536-8

54. Lu S, Ye Q, Singh D, Cao Y, Diedrich JK, Yates JR, et al. The SARS-CoV-2 nucleocapsid phosphoprotein forms mutually exclusive condensates with RNA and the membrane-associated m protein. *Nat Commun* (2021) 12:502. doi: 10.1038/s41467-020-20768-y

55. Ghosh A, Kar PK, Gautam A, Gupta R, Singh R, Chakravarti R, et al. An insight into SARS-CoV-2 structure, pathogenesis, target hunting for drug development and vaccine initiatives. *RSC Med Chem* (2022) 13:647–75. doi: 10.1039/D2MD00009A

56. Peters B, Nielsen M, Sette A. T Cell epitope predictions. *Annu Rev Immunol* (2020) 38:123–45. doi: 10.1146/annurev-immunol-082119-124838

57. La Gruta NL, Gras S, Daley SR, Thomas PG, Rossjohn J. Understanding the drivers of MHC restriction of T cell receptors. *Nat Rev Immunol* (2018) 18:467–78. doi: 10.1038/s41577-018-0007-5

58. Sidney J, Peters B, Sette A. Epitope prediction and identification- adaptive T cell responses in humans. *Semin Immunol* (2020) 50:101418. doi: 10.1016/j.smim.2020.101418

59. Grifoni A, Sidney J, Vita R, Peters B, Crotty S, Weiskopf D, et al. SARS-CoV-2 human T cell epitopes: Adaptive immune response against COVID-19. *Cell Host Microbe* (2021) 29:1076–92. doi: 10.1016/j.chom.2021.05.010

60. Jin X, Liu X, Shen C. A systemic review of T-cell epitopes defined from the proteome of SARS-CoV-2. *Virus Res* (2023) 324:199024. doi: 10.1016/j.virusres.2022.199024

61. Yewdell JW, Bennink JR. Immunodominance in major histocompatibility complex class I-restricted T lymphocyte responses. *Annu Rev Immunol* (1999) 17:51–88. doi: 10.1146/annurev.immunol.17.1.51

62. Kotturi MF, Scott I, Wolfe T, Peters B, Sidney J, Cheroutre H, et al. Naive precursor frequencies and MHC binding rather than the degree of epitope diversity shape CD8+ T cell immunodominance. *J Immunol* (2008) 181:2124–33. doi: 10.4049/jimmunol.181.3.2124

63. Begue S, Waerlop G, Salaun B, Janssens M, Bellamy D, Cox RJ, et al. Harmonization and qualification of intracellular cytokine staining to measure influenza-specific CD4$^{+}$ T cell immunity within the FLUCOP consortium. *Front Immunol* (2022) 13:982887. doi: 10.3389/fimmu.2022.982887

64. Waerlop G, Leroux-Roels G, Lambe T, Bellamy D, Medaglini D, Pettini E, et al. Harmonization and qualification of an IFN-γ enzyme-linked ImmunoSpot assay (ELISPOT) to measure influenza-specific cell-mediated immunity within the FLUCOP consortium. *Front Immunol* (2022) 13:984642. doi: 10.3389/fimmu.2022.984642

65. Heide J, Schulte S, Kohsar M, Brehm TT, Herrmann M, Karsten H, et al. Broadly directed SARS-CoV-2-specific CD4+ T cell response includes frequently detected peptide specificities within the membrane and nucleoprotein in patients with acute and resolved COVID-19. *PloS Pathog* (2021) 17:e1009842. doi: 10.1371/journal.ppat.1009842

66. Taus E, Hofmann C, Ibarrondo FJ, Hausner MA, Fulcher JA, Krogstad P, et al. Dominant CD8+ T cell nucleocapsid targeting in SARS-CoV-2 infection and broad spike targeting from vaccination. *Front Immunol* (2022) 13:835830. doi: 10.3389/fimmu.2022.835830

67. Phetsouphanh C, Zaunders J, Kelleher A. Detecting antigen-specific T cell responses: From bulk populations to single cells. *IJMS* (2015) 16:18878–93. doi: 10.3390/ijms160818878

68. Ji N, Forsthuber TG. ELISPOT techniques. *Methods Mol Biol* (2016) 1304:63–71. doi: 10.1007/7651_2014_111

69. Dan JM, Mateus J, Kato Y, Hastie KM, Yu ED, Faliti CE, et al. Immunological memory to SARS-CoV-2 assessed for up to 8 months after infection. *Science* (2021) 371:eabf4063. doi: 10.1126/science.abf4063

70. Poluektov Y, George M, Daftarian P, Delcommenne MC. Assessment of SARS-CoV-2 specific CD4(+) and CD8 (+) T cell responses using MHC class I and II tetramers. *Vaccine* (2021) 39:2110–6. doi: 10.1016/j.vaccine.2021.03.008

71. Altman JD, Moss PA, Goulder PJ, Barouch DH, McHeyzer-Williams MG, Bell JI, et al. Phenotypic analysis of antigen-specific T lymphocytes. *Science* (1996) 274:94–6. doi: 10.1126/science.274.5284.94

72. Sims S, Willberg C, Klenerman P. MHC-peptide tetramers for the analysis of antigen-specific T cells. *Expert Rev Vaccines* (2010) 9:765–74. doi: 10.1586/erv.10.66

73. Minervina AA, Pogorelyy MV, Kirk AM, Crawford JC, Allen EK, Chou C-H, et al. SARS-CoV-2 antigen exposure history shapes phenotypes and specificity of memory CD8+ T cells. *Nat Immunol* (2022) 23:781–90. doi: 10.1038/s41590-022-01184-4

74. Cohen KW, Linderman SL, Moodie Z, Czartoski J, Lai L, Mantus G, et al. Longitudinal analysis shows durable and broad immune memory after SARS-CoV-2

infection with persisting antibody responses and memory b and T cells. *Cell Rep Med* (2021) 2:100354. doi: 10.1016/j.xcrm.2021.100354

75. Swaminathan S, Lineburg KE, Ambalathingal GR, Crooks P, Grant EJ, Mohan SV, et al. Limited recognition of highly conserved regions of SARS-CoV-2. *Microbiol Spectr* (2022) 10:e02780–21. doi: 10.1128/spectrum.02780-21

76. Weingarten-Gabbay S, Klaeger S, Sarkizova S, Pearlman LR, Chen D-Y, Gallagher KME, et al. Profiling SARS-CoV-2 HLA-I peptidome reveals T cell epitopes from out-of-frame ORFs. *Cell* (2021) 184:3962–3980.e17. doi: 10.1016/j.cell.2021.05.046

77. Amit S, Regev-Yochay G, Afek A, Kreiss Y, Leshem E. Early rate reductions of SARS-CoV-2 infection and COVID-19 in BNT162b2 vaccine recipients. *Lancet* (2021) 397:875–7. doi: 10.1016/S0140-6736(21)00448-7

78. Sahin U, Muik A, Vogler I, Derhovanessian E, Kranz LM, Vormehr M, et al. BNT162b2 vaccine induces neutralizing antibodies and poly-specific T cells in humans. *Nature* (2021) 595:572–7. doi: 10.1038/s41586-021-03653-6

79. Parry H, Bruton R, Stephens C, Brown K, Amirthalingam G, Otter A, et al. Differential immunogenicity of BNT162b2 or ChAdOx1 vaccines after extended-interval homologous dual vaccination in older people. *Immun Ageing* (2021) 18:34. doi: 10.1186/s12979-021-00246-9

80. Crotty S. Follicular helper CD4 T cells (TFH). *Annu Rev Immunol* (2011) 29:621–63. doi: 10.1146/annurev-immunol-031210-101400

81. Lang-Meli J, Luxenburger H, Wild K, Karl V, Oberhardt V, Salimi Alizei E, et al. SARS-CoV-2-specific T-cell epitope repertoire in convalescent and mRNA-vaccinated individuals. *Nat Microbiol* (2022) 7:675–9. doi: 10.1038/s41564-022-01106-y

82. Jarjour NN, Masopust D, Jameson SC. T Cell memory: Understanding COVID-19. *Immunity* (2021) 54:14–8. doi: 10.1016/j.immuni.2020.12.009

83. Jung MK, Shin E-C. Phenotypes and functions of SARS-CoV-2-Reactive T cells. *Mol Cells* (2021) 44:401–7. doi: 10.14348/molcells.2021.0079

84. Hanna SJ, Codd AS, Gea-Mallorqui E, Scourfield DO, Richter FC, Ladell K, et al. T Cell phenotypes in COVID-19 - a living review. *Oxf Open Immunol* (2021) 2:iqaa007. doi: 10.1093/oxfimm/iqaa007

85. Weiskopf D, Schmitz KS, Raadsen MP, Grifoni A, Okba NMA, Endeman H, et al. Phenotype and kinetics of SARS-CoV-2-specific T cells in COVID-19 patients with acute respiratory distress syndrome. *Sci Immunol* (2020) 5:eabd2071. doi: 10.1126/sciimmunol.abd2071

86. Pisanti S, Deelen J, Gallina AM, Caputo M, Citro M, Abate M, et al. Correlation of the two most frequent HLA haplotypes in the Italian population to the differential regional incidence of covid-19. *J Transl Med* (2020) 18:352. doi: 10.1186/s12967-020-02515-5

87. Shkurnikov M, Nersisyan S, Jankevic T, Galatenko A, Gordeev I, Vechorko V, et al. Association of HLA class I genotypes with severity of coronavirus disease-19. *Front Immunol* (2021) 12:641900. doi: 10.3389/fimmu.2021.641900

88. Notarbartolo S, Ranzani V, Bandera A, Gruarin P, Bevilacqua V, Putignano AR, et al. Integrated longitudinal immunophenotypic, transcriptional, and repertoire analyses delineate immune responses in patients with COVID-19. *Sci Immunol* (2021) 6:eabg5021. doi: 10.1126/sciimmunol.abg5021

89. Lucas C, Wong P, Klein J, Castro TBR, Silva J, Sundaram M, et al. Longitudinal analyses reveal immunological misfiring in severe COVID-19. *Nature* (2020) 584:463–9. doi: 10.1038/s41586-020-2588-y

90. Neidleman J, Luo X, George AF, McGregor M, Yang J, Yun C, et al. Distinctive features of SARS-CoV-2-specific T cells predict recovery from severe COVID-19. *Cell Rep* (2021) 36:109414. doi: 10.1016/j.celrep.2021.109414

91. Cohen CA, Li APY, Hachim A, Hui DSC, Kwan MYW, Tsang OTY, et al. SARS-CoV-2 specific T cell responses are lower in children and increase with age and time after infection. *Nat Commun* (2021) 12:4678. doi: 10.1038/s41467-021-24938-4

92. Loyal L, Braun J, Henze L, Kruse B, Dingeldey M, Reimer U, et al. Cross-reactive CD4+ T cells enhance SARS-CoV-2 immune responses upon infection and vaccination. *Science* (2021) 374:eabh1823. doi: 10.1126/science.abh1823

93. Braun J, Loyal L, Frentsch M, Wendisch D, Georg P, Kurth F, et al. SARS-CoV-2-reactive T cells in healthy donors and patients with COVID-19. *Nature* (2020) 587:270–4. doi: 10.1038/s41586-020-2598-9

94. Le Bert N, Tan AT, Kunasegaran K, Tham CYL, Hafezi M, Chia A, et al. SARS-CoV-2-specific T cell immunity in cases of COVID-19 and SARS, and uninfected controls. *Nature* (2020) 584:457–62. doi: 10.1038/s41586-020-2550-z

95. Nelde A, Bilich T, Heitmann JS, Maringer Y, Salih HR, Roerden M, et al. SARS-CoV-2-derived peptides define heterologous and COVID-19-induced T cell recognition. *Nat Immunol* (2021) 22:74–85. doi: 10.1038/s41590-020-00808-x

96. Johansson AM, Malhotra U, Kim YG, Gomez R, Krist MP, Wald A, et al. Cross-reactive and mono-reactive SARS-CoV-2 CD4+ T cells in prepandemic and COVID-19 convalescent individuals. *PloS Pathog* (2021) 17:e1010203. doi: 10.1371/journal.ppat.1010203

97. Low JS, Vaqueirinho D, Mele F, Foglierini M, Jerak J, Perotti M, et al. Clonal analysis of immunodominance and cross-reactivity of the CD4 T cell response to SARS-CoV-2. *SCIENCE* (2021) 372(6548):1336-1341. doi: 10.1101/2021.03.23.436642

98. Niessl J, Sekine T, Buggert M. T Cell immunity to SARS-CoV-2. *Semin Immunol* (2021) 55:101505. doi: 10.1016/j.smim.2021.101505

99. Becerra-Artiles A, Calvo-Calle JM, Co MD, Nanaware PP, Cruz J, Weaver GC, et al. Broadly recognized, cross-reactive SARS-CoV-2 CD4 T cell epitopes are highly conserved across human coronaviruses and presented by common HLA alleles. *Cell Rep* (2022) 39:110952. doi: 10.1016/j.celrep.2022.110952

100. Woldemeskel BA, Dykema AG, Garliss CC, Cherfils S, Smith KN, Blankson JN. CD4+ T cells from COVID-19 mRNA vaccine recipients recognize a conserved epitope present in diverse coronaviruses. *J Clin Invest* (2022) 132:e156083. doi: 10.1172/JCI156083

101. Swadling L, Diniz MO, Schmidt NM, Amin OE, Chandran A, Shaw E, et al. Pre-existing polymerase-specific T cells expand in abortive seronegative SARS-CoV-2. *Nature* (2022) 601:110–7. doi: 10.1038/s41586-021-04186-8

102. Bacher P, Rosati E, Esser D, Martini GR, Saggau C, Schiminsky E, et al. Low-avidity CD4+ T cell responses to SARS-CoV-2 in unexposed individuals and humans with severe COVID-19. *Immunity* (2020) 53:1258–1271.e5. doi: 10.1016/j.immuni.2020.11.016

103. Dykema AG, Zhang B, Woldemeskel BA, Garliss CC, Cheung LS, Choudhury D, et al. Functional characterization of CD4+ T cell receptors crossreactive for SARS-CoV-2 and endemic coronaviruses. *J Clin Invest* (2021) 131:e146922. doi: 10.1172/JCI146922

104. Redd AD, Nardin A, Kared H, Bloch EM, Abel B, Pekosz A, et al. Minimal crossover between mutations associated with omicron variant of SARS-CoV-2 and CD8+ T-cell epitopes identified in COVID-19 convalescent individuals. *mBio* (2022) 13:4. doi: 10.1128/mbio.03617-21

105. Tarke A, Coelho CH, Zhang Z, Dan JM, Yu ED, Methot N, et al. SARS-CoV-2 vaccination induces immunological T cell memory able to cross-recognize variants from alpha to omicron. *Cell* (2022) 185:847–859.e11. doi: 10.1016/j.cell.2022.01.015

106. Tarke A, Sidney J, Methot N, Yu ED, Zhang Y, Dan JM, et al. Impact of SARS-CoV-2 variants on the total CD4+ and CD8+ T cell reactivity in infected or vaccinated individuals. *Cell Rep Med* (2021) 2:100355. doi: 10.1016/j.xcrm.2021.100355

107. Riou C, Keeton R, Moyo-Gwete T, Hermanus T, Kgagudi P, Baguma R, et al. Escape from recognition of SARS-CoV-2 variant spike epitopes but overall preservation of T cell immunity. *Sci Transl Med* (2022) 14:eabj6824. doi: 10.1126/scitranslmed.abj6824

108. Zhou D, Dejnirattisai W, Supasa P, Liu C, Mentzer AJ, Ginn HM, et al. Evidence of escape of SARS-CoV-2 variant B.1.351 from natural and vaccine-induced sera. *Cell* (2021) 184:2348–2361.e6. doi: 10.1016/j.cell.2021.02.037

109. Li Y, Wang X, Jin J, Ma Z, Liu Y, Zhang X, et al. T-Cell responses to SARS-CoV-2 omicron spike epitopes with mutations after the third booster dose of an inactivated vaccine. *J Med Virol* (2022) 94:3998–4004. doi: 10.1002/jmv.27814

110. Dolton G, Rius C, Hasan MS, Wall A, Szomolay B, Behiry E, et al. Emergence of immune escape at dominant SARS-CoV-2 killer T cell epitope. *Cell* (2022) 185:2936–2951.e19. doi: 10.1016/j.cell.2022.07.002

111. Xiao C, Mao L, Wang Z, Gao L, Zhu G, Su J, et al. SARS-CoV-2 variant B.1.1.7 caused HLA-A2+ CD8+ T cell epitope mutations for impaired cellular immune response. *iScience* (2022) 25:103934. doi: 10.1016/j.isci.2022.103934

112. Naranbhai V, Nathan A, Kaseke C, Berrios C, Khatri A, Choi S, et al. T Cell reactivity to the SARS-CoV-2 omicron variant is preserved in most but not all individuals. *Cell* (2022) 185:1041–1051.e6. doi: 10.1016/j.cell.2022.01.029

frontiers | Frontiers in Immunology

TYPE Original Research
PUBLISHED 16 March 2023
DOI 10.3389/fimmu.2023.1152522



OPEN ACCESS

EDITED BY
Jingxin Li,
Jiangsu Provincial Center for Disease Control and Prevention, China

REVIEWED BY
Gagandeep Singh,
Icahn School of Medicine at Mount Sinai, United States
Matthew Zirui Tay,
A*STAR Infectious Disease Labs, Singapore

*CORRESPONDENCE
Jennifer Serwanga
Jennifer.Serwanga@mrcuganda.org

SPECIALTY SECTION
This article was submitted to Viral Immunology, a section of the journal Frontiers in Immunology

RECEIVED 27 January 2023
ACCEPTED 28 February 2023
PUBLISHED 16 March 2023

CITATION
Serwanga J, Ankunda V, Sembera J, Kato L, Oluka GK, Baine C, Odoch G, Kayiwa J, Auma BO, Jjuuko M, Nsereko C, Cotten M, Onyachi N, Muwanga M, Lutalo T, Fox J, Musenero M, Kaleebu P and The COVID-19 Immunoprofiling Team (2023) Rapid, early, and potent Spike-directed IgG, IgM, and IgA distinguish asymptomatic from mildly symptomatic COVID-19 in Uganda, with IgG persisting for 28 months.
*Front. Immunol.* 14:1152522.
doi: 10.3389/fimmu.2023.1152522



# Rapid, early, and potent Spike-directed IgG, IgM, and IgA distinguish asymptomatic from mildly symptomatic COVID-19 in Uganda, with IgG persisting for 28 months

Jennifer Serwanga[1,2]*, Violet Ankunda[2], Jackson Sembera[2], Laban Kato[1], Gerald Kevin Oluka[1,2], Claire Baine[2], Geoffrey Odoch[1], John Kayiwa[3], Betty Oliver Auma[1], Mark Jjuuko[4], Christopher Nsereko[5], Matthew Cotten[1,6], Nathan Onyachi[4], Moses Muwanga[5], Tom Lutalo[7], Julie Fox[8], Monica Musenero[9], Pontiano Kaleebu[1,2] and The COVID-19 Immunoprofiling Team[1,2]

[1]Pathogen Genomics, Phenotype, and Immunity Program, Medical Research Council, Uganda Virus Research Institute and London School of Hygiene and Tropical Medicine, Uganda Research Unit, Entebbe, Uganda, [2]Department of Immunology, Uganda Virus Research Institute, Entebbe, Uganda, [3]Department of Virology, Uganda Virus Research Institute, Entebbe, Uganda, [4]Department of Internal Medicine, Masaka Regional Referral Hospital, Masaka, Uganda, [5]Department of Internal Medicine, Entebbe Regional Referral Hospital, Entebbe, Uganda, [6]Medical Research Council, University of Glasgow Centre for Virus Research, Glasgow, United Kingdom, [7]Department of Epidemiology and Data Management, Uganda Virus Research Institute, Entebbe, Uganda, [8]Guy's and St Thomas' National Health Services Foundation Trust, King's College London, London, United Kingdom, [9]Science, Technology, and Innovation Secretariat, Office of the President, Government of Uganda, Kampala, Uganda

**Introduction:** Understanding how spike (S)-, nucleoprotein (N)-, and RBD-directed antibody responses evolved in mild and asymptomatic COVID-19 in Africa and their interactions with SARS-CoV-2 might inform development of targeted treatments and vaccines.

**Methods:** Here, we used a validated indirect in-house ELISA to characterise development and persistence of S- and N-directed IgG, IgM, and IgA antibody responses for 2430 SARS-CoV-2 rt-PCR-diagnosed Ugandan specimens from 320 mild and asymptomatic COVID-19 cases, 50 uninfected contacts, and 54 uninfected non-contacts collected weekly for one month, then monthly for 28 months.

**Results:** During acute infection, asymptomatic patients mounted a faster and more robust spike-directed IgG, IgM, and IgA response than those with mild symptoms (Wilcoxon rank test, p-values 0.046, 0.053, and 0.057); this was more pronounced in males than females. Spike IgG antibodies peaked between 25 and 37 days (86.46; IQR 29.47-242.56 BAU/ml), were significantly higher and more durable than N- and RBD IgG antibodies and lasted for 28 months. Anti-spike

seroconversion rates consistently exceeded RBD and nucleoprotein rates. Spike- and RBD-directed IgG antibodies were positively correlated until 14 months (Spearman's rank correlation test, p-values 0.0001 to 0.05), although RBD diminished faster. Significant anti-spike immunity persisted without RBD. 64% and 59% of PCR-negative, non-infected non-contacts and suspects, exhibited baseline SARS-CoV-2 N-IgM serological cross-reactivity, suggesting undetected exposure or abortive infection. N-IgG levels waned after 787 days, while N-IgM levels remained undetectable throughout.

**Discussion:** Lower N-IgG seroconversion rates and the absence of N-IgM indicate that these markers substantially underestimate the prior exposure rates. Our findings provide insights into the development of S-directed antibody responses in mild and asymptomatic infections, with varying degrees of symptoms eliciting distinct immune responses, suggesting distinct pathogenic pathways. These longer-lasting data inform vaccine design, boosting strategies, and surveillance efforts in this and comparable settings.

KEYWORDS

**SARS-CoV-2 antibody persistence, Spike and RBD, nucleoprotein, mild and asymptomatic COVID-19, IgG, IgM, IgA, Uganda**

## Introduction

In 2019, a new human coronavirus illness (COVID-19) caused by the severe acute respiratory syndrome coronavirus 2 (SARS-CoV-2) appeared, sparking a serious public health crisis. By September 2022, there were 613,410,796 COVID-19 cases, including 6,518,749 deaths, and 12,659,951,094 vaccine doses administered (https://covid19.who.int, accessed September 29, 2022). Of these, 9,327,413 cases and 174,509 deaths occurred in sub-Saharan Africa (SSA), revealing a considerably lower impact in SSA (1). Several hypotheses were proposed to explain this lesser disease burden, including a younger demographic structure in SSA (2), less testing, undercounting of deaths, genetic predispositions, and cross-reactive immunity against previous coronaviruses. Pre-existing cross-reactive immune responses have been reported in many geographical locations (3–6) and in some cases were significantly higher in SSA than in other continents (4), probably due to the high sequence homology between SARS-CoV-2 and the common coronaviruses in SSA. Such cross-reactive immune responses to other coronaviruses were linked to a decreased likelihood of COVID-19 disease severity in the United States (7), but not in other regions, such as SSA (8–10).

The Spike (S) protein of SARS-CoV-2 is composed of the S1 and S2 subunits. A receptor-binding domain (RBD) within the S1 subunit interacts with human host cells expressing ACE2 receptors to promote viral entry (11). Antibodies against RBD block virus interaction with the host cell receptors, thus providing protection (12). Accordingly, antibodies directed against the S protein, particularly the RBD, are critical targets for developing vaccines and therapeutics (13–15) due to their positive associations with viral neutralisation titres (16–19). On the other hand, the Nucleoprotein serves as the primary target in many serosurveillance test systems, and serological responses to N infer prior SARS-CoV-2 exposure (20–22).

It is essential to examine the dynamics of humoral immune responses to SARS-CoV-2 to infer protective immunity and determine vaccination-induced immunity. However, the dynamics of the anti-SARS-CoV-2 antibody response and persistence after infection are still debatable and have primarily been studied in the context of more severe disease, which is uncommon in African patients. While antibody persistence was associated with severe disease, comparable seropositivity was reported between symptomatic and asymptomatic individuals in some contexts (23, 24) but not in others (25). Mild COVID-19 disease has been linked to a weaker humoral response, raising fears of faster waning of immunity. Severe disease has been associated with longer persistence of humoral immunity for 12 months post-infection (26, 27). Some populations have shown delayed onset of S-IgG and IgM, making early serological screening less significant (28). Median anti-Spike titres in symptomatic and hospital-admitted cases are significantly higher than in asymptomatic participants, persisting for at least one year. There is a need to establish the dynamics of antibody development in SSA settings where the disease impact has been distinctively different.

It is vital to monitor changes in S-, RBD-, and N-directed IgM, IgG, and IgA levels in sub-Saharan Africa to guide diagnostic strategies, public health policy, and immunological correlates pertinent to vaccine formulation. Multiple viral proteins (29, 30) elicit prompt and long-lasting immunity that persists for several months (31–33). SARS-CoV-2-directed S- and N-IgG, -IgM, and -IgA antibody profiles have guided inference of the serological response to COVID-19 and provided insight into the relevance of targeting the Spike-protein for vaccine

design (34, 35). Using data from European cohorts, mathematical modellers predicted the persistence of functional Spike and RBD-directed antibodies 465 days post-infection and faster decay of N-directed antibodies, providing data that inform vaccination and serosurveillance strategies (36). Nevertheless, there is limited knowledge on the development, kinetics, and profile of immune responses to the milder and asymptomatic COVID-19 epidemic that primarily occurred in the African setting. Geographically relevant data is needed to inform vaccination, diagnostic and surveillance strategies in this setting.

On March 21, 2020, Uganda confirmed her first COVID-19 case in a returning traveller, prompting a countrywide lockdown to prevent further spread, except for cargo truck drivers and vital front-line professionals required to safeguard the economy and combat the epidemic, respectively. All inbound cargo truck drivers were mandated to undergo cross-border PCR testing for COVID-19, and all detected cases were quarantined in designated referral hospitals until viral clearance was confirmed by PCR. This approach allowed for possibility of assembling a cohort of newly infected PCR-confirmed COVID-19 cases to profile the local immune response to the epidemic. Consequently, we examined the profile, timing, durability, specificity, seroconversion rates, and targets of humoral immunity to SARS-COV-2 over 28 months in PCR-confirmed COVID-19 convalescent participants with or without re-exposure, as well as the influence of gender and symptom status on induced antibody responses.

# Materials and methods

## Study design and population

A prospective cohort of rt-PCR-confirmed SARS-CoV-2 positive, slightly symptomatic, and asymptomatic participants and rt-PCR-confirmed negative, exposed, and unexposed persons was established. The cohort was established in response to the mandatory requirement for the purposive sampling of all incoming travellers for COVID-19 PCR positivity, while the rest of the country as under lock down. All PCR-positive cases were subjected to mandatory isolation at Masaka and Entebbe Referral Hospitals until they were deemed PCR-negative. Participants were recruited through regional referral hospitals in Entebbe and Masaka, which served as COVID-19 isolation and treatment centres at the start of the Ugandan outbreak. Available hospital records from the participant's admission were used to obtain participant-related health information. Access to participant-related health information was only possible through available hospital admission records. When possible, an acute blood sample was obtained to assist the COVID-19 care team in obtaining a complete blood count (CBC) report. In some cases, records of conditions such as hypertension, diabetes, and asthma were also collected to better understand the participants' health status. Participants were chosen because they were under mandatory isolation for COVID-19 after a positive rt-PCR result was detected during a national sampling for SARS-CoV-2. During sample collection, the most prevalent circulating variants were A23.1 and Delta. Dates of infection (Day 0) were calculated using the initial rt-PCR-confirmed COVID-19 diagnosis and, if available, the date of the first hospitalization. Participants were contacted weekly for the first month, then monthly for the next 28 months. Volunteers reflected typical hospital admissions at the time, consisting of a spectrum of mild and largely asymptomatic illnesses with a one-day median gap between PCR and admission dates (IQR, 1-3). During the follow-up, we gathered participant demographics, clinical complaints, and complete blood counts.

Negative controls included specimens collected between 2012 and 2017, prior to the outbreak. PCR-negative suspects (SUS) and non-cases (NC) recruited simultaneously at the outbreak's onset were utilized to establish baseline cross-reactivity. The suspects were PCR-negative individuals isolated due to past close interaction with a PCR-verified COVID-19 case. Participants who had no known prior contact with a COVID case were categorized as "non-cases." Suspects were followed on days 0, 4, 7, 14, 20, 21, and 28 between June 10, 2020, and November 5, 2020, while non-contacts were tracked for 35 days on days 0, 7, 14, 21, 28, and 35 days after the initial PCR, between June 17, 2020, and September 21, 2020. All study procedures were approved by the Research and Ethics Committee of the Uganda Virus Research Institute (GC/127/833) and the Uganda National Council for Science and Technology (HS637ES). Participants gave their written informed consent to take part in the study. Between May 11, 2020, and May 24, 2022, 320 participants aged 14–87 years (median 31, IQR [25–37]) were recruited and followed for up to 837 days (median 155, IQR [58–277]). Two individuals lacked age information: 245 were males and 75 were females. 47 were symptomatic, 192 were asymptomatic, and 81 did not have admission information. A maximum of three symptoms were recorded per individual; 15, 19, and 13 participants, respectively, exhibited one, two, and three symptoms. The most common symptoms were cough, fever, and headache, as shown in Table 1.

## Study specimens

The median duration between diagnosis and the collection of the first plasma sample from 320 patients was one day (IQR 1 to 3). A total of 2,430 plasma samples were analysed. Overall, 225/320 (70%) participants had at least four longitudinal samples, allowing studies of the development and persistence of antibody responses against SARS-CoV-2, regardless of re-infection. In addition, we assessed fifty non-contacts (NC) and fifty-four suspects (SUS).

## Conventional in-House ELISA for detection of anti-SARS-CoV-2 binding antibodies

Spike-, RBD-, and N-directed IgG, IgM, and IgA antibodies were quantified using an in-house ELISA adapted from Pickering et al. (37), optimized and validated for use in this largely asymptomatic or mildly symptomatic COVID-19infected population (38). Briefly, 96-well flat-bottomed medium-binding plates (Greiner Bio-One, #655001) coated with 50 µl of N-, RBD-,

TABLE 1 Summary of recorded admission symptoms.

| Symptom | n |
|---|---|
| Cough | 17 |
| Fever | 16 |
| Headache | 16 |
| Runny Nose | 11 |
| Sore Throat | 8 |
| Chest Pain | 5 |
| Shortness of Breath | 3 |
| General Weakness | 2 |
| Flu | 2 |
| Loss of Smell | 2 |
| Severe Abdominal Pain | 2 |
| Sneezing | 1 |
| Mild Headache | 1 |
| Blocked Nostrils | 1 |
| Loss of Taste | 1 |
| Chills | 1 |
| Feels hotter | 1 |
| Sharp Pain Around Arm | 1 |
| Slight Cough | 1 |
| Total | 47 |

The table shows the frequency of symptomatic participants per registered symptom at the time of initial admission among the 47 symptomatic participants.

or S-Protein antigens based on the wildtype prototype strain (R&D Systems #10474-CV-01M, #10549-CV-01M) at three µg/ml (0.15µg per well) in PBS were incubated overnight at 4°C. The plates were then washed 5x with 0.01M PBS containing 0.05% Tween 20 (PBS-T) with a BioTek 405 TS microplate washer and blocked with PBS-T containing 1% BSA (Sigma, #A3803) for 1 hour at RT. Heat-inactivated (56˚C for 30 mins) plasma/serum samples diluted at 1:100 in PBS-T with 1% BSA were added in duplicate and incubated for 2 hours at RT. Following five washes with PBS-T, horseradish peroxidase-conjugated, goat anti-human IgG (γ-chain specific, Sigma, #A0170, 1:10,000 dilution), IgM (µ-chain specific, Sigma, #A6907, 1:1,000 for S and 1:5000 for N), or IgA (α-chain specific, Sigma, #A0295, 1:1,000 dilution) detection antibodies in PBS-T containing 1% BSA was added for 1 hour at room temperature (RT). Pre-determined negative and positive plasma samples, monoclonal antibodies, CR3009 (2µg/ml) for N or CR3022 (0.1µg/ml) for S and included two sets of duplicate blank wells as controls. Finally, the wells were washed and dried by tapping on absorbent paper towels. 50 µl of 3,3′,5,5′-Tetra-methyl benzidine (TMB) substrate (Sera Care, #5120-0075) was then added for 3 minutes, followed by 50 µl of 1M Hydrochloric acid (Sera Care #5150-0021) to stop the reaction. We read the plates at 450nm with a BioTek ELx808 microplate reader using the BioTek GEN5 software. Blank well OD values were subtracted from those in specimen wells to obtain the net response. Receiver operator characteristic (ROC) analysis derived cut-offs for S-, RBD-, and N-directed IgG, IgM, and IgA optical densities were 0.432, 0.356, 0.201(S protein), 0.214, 0.350, 0.303 (RBD), and 0.395, 0.229, 0.188 (N protein), respectively, as described elsewhere (38).

## Estimating binding IgG, IgM, and IgA antibody concentrations

We diluted 10 mg/ml of purified human IgG (Sigma, #12511) and 5 mg/ml of purified IgA (Sigma, #12636) commercial standards to 4.52 and 2 mg/ml, respectively, subjected them to seven 10-fold serial dilutions ranging from 1000 to 0.001 ng/ml and incubated them together with the test samples. Purified human IgM (Sigma, # 18260) was reconstituted from 10 to 1 mg/ml and subjected to seven 5-fold serial dilutions ranging from 1000 to 0.06 ng/ml. Standards were incubated in wells pre-coated with 50µl of anti-human kappa and lambda capture antibodies (Southern Biotech, #2060-01, #2070-01, 1:1 ratio, diluted 1:500). The OD450 values of the standards were used to create a non-linear, 4-parameter logistic (4-PL) modelled standard curve using the BioTek GEN5 software. The best linear range fit of the different standard curves was used to extrapolate antibody concentrations, which were then corrected for the associated dilution factor. Concentrations less than the detection limit were assigned a value of 0 ng/ml.

## Serological inference for reinfection after primary SARS-CoV-2 infection

Reinfections are typically identified through viral genomic sequencing of nasopharyngeal swab samples (39). Here, self-reports were used to detect possible reinfections, since all the cases we recruited as incident cases. Others have used varied methods to differentiate reinfection from initial infection (40, 41). One macaque study showed a 7.6-fold rise in N-IgG antibody as indicative of reinfection (21), while a human West Africa study suggested a 7-fold rise (20); similar titre rises were also observed in studies from high-income settings (42, 43). Our serological data from two SARS-CoV-2 reinfected patients with rt-PCR confirmation showed an 11-fold rise in N-IgG antibody concentration after reinfection. Then, to strongly suggest the absence of reinfection, we applied a stricter threshold of no more than a 2-fold increase in N-IgG antibody concentration. Consequently, 24 individuals were assumed to have never been infected again, and 127 individuals were presumed to have been re-infected during the follow-up period.

## Serological inference for vaccination after primary infection

Exactly one year after reporting the first COVID-19 case, Uganda launched its first COVID-19 mass vaccination program on March 10, 2021, using the AstraZeneca (AZN) vaccine and

initially targeting front-line staff. Consequently, specimens taken before March 10, 2021, or around 10 months of this cohort follow-up, are deemed vaccine naïve. Immunization was subsequently validated using vaccination certificates and, if missing, serological data. Using available full-dose AZN serological data from nine participants, we calculated a fold-rise in S-IgG ranging from 3.7 to 255.8 ng/ml (median 21.1; IQR: 9.3-31.1; mean 45.3; 95% CI; 15-98) from baseline before the first vaccination to 14 days post-boost. We then used a stricter threshold of a 2-fold rise or less in S-IgG to denote the lack of vaccination uptake. Accordingly, 12 participants with less than a 2-fold rise in S-IgG across the follow-up period were classified as never having been vaccinated.

## Missing data management

Antibody concentrations over the assay's upper detection limit were serially titrated to achieve optimum titres, and those below detection were given a value of 0 ng/ml. Samples lacking categorical variables were excluded from analyses of those categories, and "n" was stated in the corresponding figure and table.

## Statistical analysis

Concentrations, and optical densities of S-, N-, and RBD-directed IgG, IgM, and IgA antibodies were measured over time. From categorical data, proportions were derived using descriptive analyses, while summary statistics were derived from continuous variables. Using box plots and Wilcoxon rank sum tests, ODs and concentrations by gender and symptoms were compared. Using Spearman's rank correlation test, correlations between continuous variables were estimated. Individual profile plots were calculated to visualize the progression of antibodies for each subject. Due to the imbalanced nature of the specimen time points, locally weighted scatterplot smoothing (LOWESS) analysis was used to visualize the average antibody evolutions across time. Statistical and graphical displays were generated using R Version 4.1, STATA Version 15, and GraphPad Prism Version 9.40; p-values 0.05 were deemed statistically significant.

# Results

## Baseline clinical chemistry and comorbidities

Baseline comorbidity data was captured for 62 subjects. Diabetes (1), HIV+ (1), hypertension (1), and peptic ulcer disease (1) were identified as comorbidities in four participants. There was no statistically significant difference between antibody levels in participants with comorbidities and those without. Baseline CBC parameters were assessed in 71 participants and there was no significant difference between SARS-CoV-2 PCR-positive and negative individuals. However, given the small sample size and lack of baseline data for more participants, no definitive conclusions can be drawn as to whether or not comorbidities had an effect on antibody levels in this study. This analysis lacked the power to detect any significant differences between those with and without comorbidities.

## Males and asymptomatic cases had higher early Spike-directed antibodies

Since the initial data were collected on a weekly basis, we first evaluated the antibody formation profiles during the acute period, then examined the first two months to determine the cohort peak of the primary IgG response, and then reported the overall durability. Using 434 specimens collected from 202 people with a median age of 31 between 10 June 2020 and 27 September 2021, the first month of S- and N-directed IgG, IgM, and IgA antibody profiles were established. (IQR 25–37 years). The age of one of the 202 participants with first-month specimens was unavailable; 148 (73.27%) were males, 31 (15.35%) reported minor symptoms, and 138 (68.32%) were asymptomatic. In this group, 33 individuals who lacked admission symptom reports were eliminated from the analysis by symptoms.

A Wilcoxon rank sum test to stratify early antibodies by gender revealed that the median S-IgM and N-IgG concentrations tended to be greater in men than in females, with p-values of 0.032 and 0.022, respectively, as seen in Figure 1A. Males' concomitant high anti-Spike IgM and anti-N antibody concentrations indicate an early antigenic load-driven antibody response. S-IgG concentration was considerably greater in asymptomatic individuals than in symptomatic participants, with a p-value of 0.046 (3820; IQR 1300–12875 vs. 2120; IQR 977–7322 ng/ml [71.63; IQR 24.35-241.16 BAU/ml vs. 39.71; 18.30-137.13 BAU/ml]). Spike-directed IgM ODs, which are suggestive of the early antibody response, were shown to be greater in asymptomatic than in mildly symptomatic participants (0.373 vs. 0.146; p-value 0.053; Figure 1B). These findings suggest that rapid, early, and potent Spike-directed IgG, IgM, and IgA antibody responses are characteristic correlates that distinguish asymptomatic COVID-19 from COVID-19 with moderate symptoms. This emphasises the need for prompt induction of Spike-directed antibodies to control the progression of COVID-19 disease.

## Baseline Spike cross-reactivity in PCR-negative contacts and non-contacts was low

Among 89 patients evaluated at baseline (days 0-6), Spike-directed IgG, IgM, and IgA seroconversion rates increased from 57.3%, 66.3%, and 42.7% to 88%, 66%, and 34%, by week 5 post-infection, respectively (Figure 2A). During the first month of the epidemic, S-IgG, -IgM, and -IgA antibody concentrations in cases were 20, 21, 10, 7, 2, and 3-fold higher than in NC and SUS, respectively. Some NC and SUS participants had detectable cross-reactive anti-Spike IgG and IgM antibodies at baseline (day 0). Three (6.38%) and seven (14.89%) of the 47 NC with baseline specimens revealed baseline cross-reactive S-IgG and -IgM antibodies. In contrast, only one (9.09%) and two (18.18%) of the eleven SUS cross-reacted, with no significant difference between

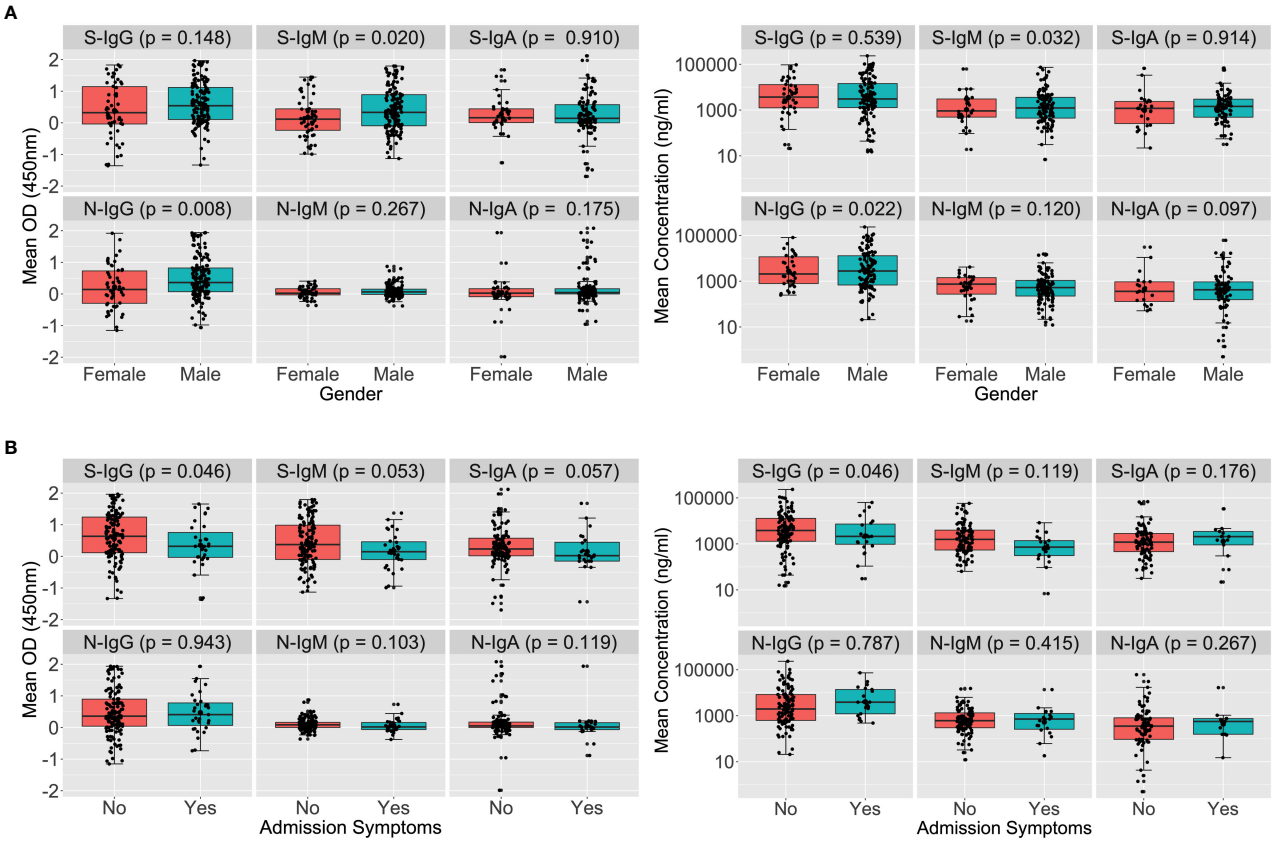


FIGURE 1
Early Spike and Nucleoprotein-directed antibodies by gender and symptoms. Figure 1 illustrates SARS-CoV-2-specific antibody responses throughout the first month of infection using the Wilcoxon rank sum test. The optical densities and concentrations (ng/ml) of Spike- and Nucleoprotein-directed IgG, IgM, and IgA antibodies are compared, stratified by gender **(A)** and symptoms **(B)**. P-values less than or equal to 0.05 were regarded as statistically significant.

NCs and SUS. There were no cross-reactive anti-Spike IgA responses at baseline, Figure 2B.

## Baseline N-IgM cross-reactivity in PCR-negative participants was high

Nucleoprotein-directed IgG, IgM, and IgA seroconversion rates were 55.1%, 30.3%, and 25.8% among 89 infected patients assessed at baseline (days 0-6), respectively; and these rates increased to 74%, 32%, and 28% five weeks later. As anticipated, N-IgG and N-IgA antibodies at baseline were significantly higher in patients than in controls. Anti-N IgM levels were suboptimal and comparable across infected and uninfected individuals (Figure 3A). Among 47 NCs with day 0 specimens, cross-reactive Nucleoprotein-directed IgG (n = 13; 27.66%), IgM (30; 63.84%), and IgA (1; 2.13%) antibodies were present at baseline. Five (22.7%), thirteen (59.1%), and three (13.6%) of the eleven SUS participants had IgG, IgM, and IgA cross-reactivity at baseline, respectively. As demonstrated in Figure 3B, baseline -IgG and -IgM cross-reactivity with the Nucleoprotein was more prevalent among NCs than the Spike, Fisher exact test (p-values 0.006 and 0.00001, respectively). The unusual SARS-CoV-2 Nucleoprotein-specific cross-reactivity among certain SARS-CoV-2 PCR-negative individuals implies probable undiagnosed exposure at the outbreak's onset.

## Robust anti-Spike IgG was rapidly elicited, while IgM and IgA waned early

LOWESS analysis was used to describe the chronologies of the first month of S- and N-directed IgG, IgM, and IgA antibodies in 434 samples collected from 202 individuals with a median age of 31 (IQR: 25-37 years) between June 10, 2020, and September 27, 2021. One individual had missing age information, 148 (73.27%) were males, and 54 (26.73%) were females. In terms of clinical presentation, 31 (15.35%) patients had moderate symptoms at the time of admission, 138 (68.32%) had no symptoms, and 33 (16.33%) had no symptoms reported at the time of admission. IgM and IgA were temporary and peaked early in the infection, alongside steadily rising IgG, which quickly surpassed IgM and IgA on the seventh day. Spike-directed IgM peaked at 8-12 days with a median concentration of 1229 (IQR 535-3752 ng/ml) equivalent to 45.27 (IQR; 19.82-138.44BAU/ml), while IgA peaked at 7-10 days

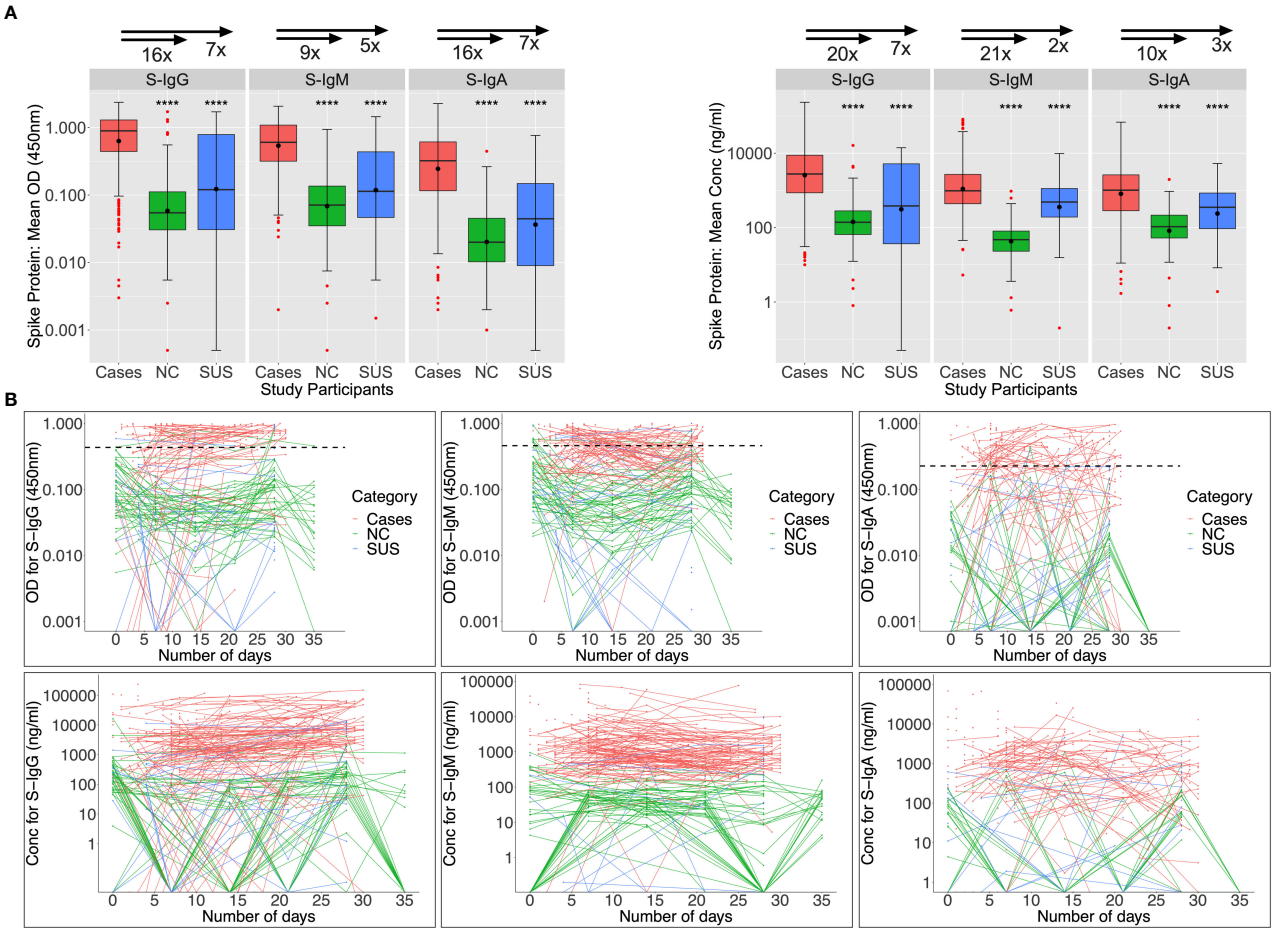


FIGURE 2
Anti-Spike antibody responses during the first month of infection. Individual subject patterns of Spike-directed IgG, IgM, and IgA antibody responses throughout the first 35 days of primary infection are shown in Figure 2. SARS-CoV-2 cases with PCR diagnosis of infection are compared with PCR-negative uninfected contacts (SUS) and non-contacts (NCs). **(A)** compares medians and interquartile ranges for antibody optical densities at 450 nm and concentrations (ng/ml) among cases, NC, and SUS individuals using box plots and the Kruskal-Wallis test. Profiles of spike-directed IgG, IgM, and IgA optical densities and concentrations are shown in **(B)** as spaghetti plots, with the graphs stratified by exposure and PCR-confirmed infection status. P-values less than or equal to 0.05 are regarded as statistically significant; ****p ≤ 0.0001. Optical Density (OD) threshold values for S-IgG, S-IgM, and S-IgA were 0.432, 0.459, and 0.226, respectively.

with a median concentration of 1162 (IQR 289-2572 ng/ml) equivalent to 221.77 (IQR; 55.24-490.87 BAU/ml) and decreased at 19 days. For the Nucleoprotein, IgG surged above the cut-off after three days and subsequently increased for the duration of the month. For the duration of the first month, both IgM and IgA levels remained below the threshold (Supplementary Figure 1).

Considering the Spike-directed antibodies in the first two months of infection, IgM started higher than IgG, gradually dropped, and waned at 59 days. S-IgG overtook IgM by 4.5 days, reached its peak between 25 and 37 days (4612; 1569-12947 ng/ml [86.38; 29.47-242.57 BAU/ml]), then began to decline while continuing to be over the cut-off. Regarding the Nucleoprotein, IgG levels were consistent until day 36 (1801.9; 543.5-7926.9 ng/ml), after which they declined for the remainder of the research period. In contrast, N-IgM remained below the cut-off throughout the duration of the research (Supplementary Figure 2).

## Spike antibodies dominated and persisted longer than Nucleoprotein antibodies

The overall chronology of induced S- and N-directed antibodies across 837 days (IQR 60–287) of follow-up was then evaluated. During the period from 11 May 2020 to 20 October 2022, 2,498 specimens obtained from 320 patients were analysed. Participants' ages ranged from 14 to 87 (median: 31; interquartile range: 25–37), with 245 men, 75 females, 47 symptomatic, 192 asymptomatic, and 81 having no symptom reports. Based on a twofold increase in N- and S-IgG to infer reinfection and vaccination, respectively, 24 people were presumptively not reinfected, and 12 participants were neither reinfected nor vaccinated over the course of this investigation. Using an 11-fold increase in N-IgG concentration, 127 participants were presumed to have been reinfected.

Regardless of reinfection or immunization status, Spike-directed IgG peaked between 25 and 37 days and was greater and more durable

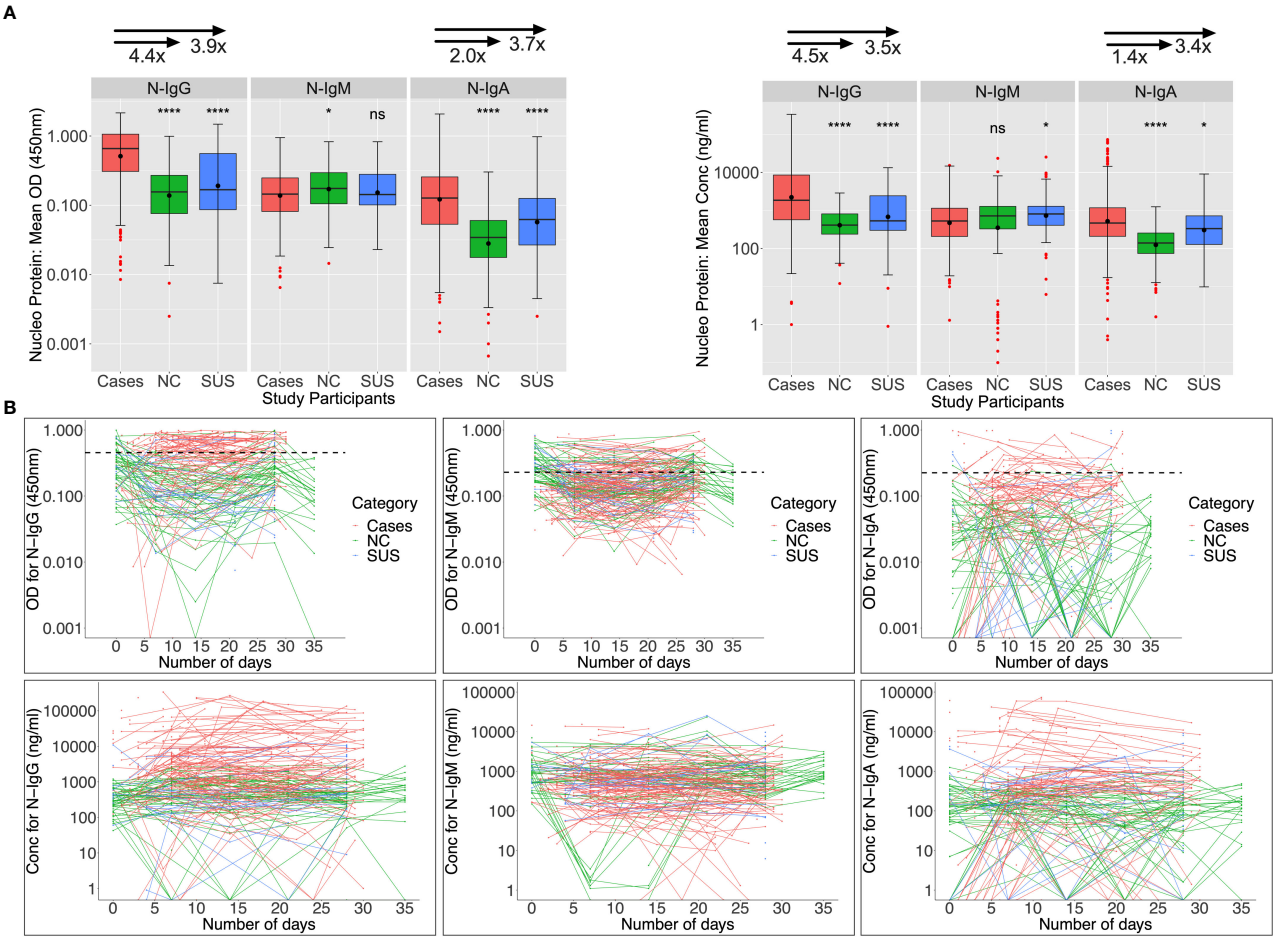


FIGURE 3
Anti-Nucleoprotein antibody responses during the first month of infection. The Nucleoprotein-directed antibodies throughout the first month of infection are summarised in Figure 3. Comparisons are made between PCR-negative, uninfected suspected contacts (SUS), uninfected non-contacts, and SARS-CoV-2 infected patients (NCs). IgG, IgM, and IgA antibody optical densities at 450 nm and concentrations (ng/ml) are compared using box plots and the Kruskal-Wallis test for cases, NC, and SUS participants **(A)**. Individual anti-spike IgG, IgM, and IgA antibody profiles are shown as spaghetti plots in **(B)**, stratified by exposure to infection and PCR-confirmed infection status from the first date of PCR or admission. Significant P-values are those that are less than or equal to 0.05; otherwise, they are not significant (ns); ns $p > 0.05$, $*p \leq 0.05$, $****p \leq 0.0001$. The respective IgG, IgM, and IgA cut-off values for the nucleoprotein were 0.454, 0.229, and 0.225.

than N-IgM. From 500 days on, there was an apparent increase in IgG (11524; 2453-32438 ng/ml [215.91; 46.032-607.61 BAU/ml]), presumably owing to downstream reinfections and vaccines, as well as the large confidence interval due to the few final data sets. Concurrently, IgM levels gradually decreased and faded after 59 days (Figure 4A). Initial IgG levels were stable among the 127 reinfected participants, with OD values more than the threshold. Throughout the study, IgG gradually increased at 500 days, but S-IgM decreased at 56 days (Figure 4B). There was a quick increase in IgG levels among the 24 people who were never reinfected; IgG levels surpassed IgM after just three days, peaked between 125 and 138 days (5236; IQR 3218-10185 ng/ml [98.15; 60.35-190.84 BAU/ml]), and subsequently steadily decreased. At 122 days, S-IgM levels declined and faded (Figure 4C). For the 12 individuals who were never vaccinated or reinfected, IgG exceeded IgM by five days, peaked between 64 and 69 days (4665; interquartile range [IQR]: 4665–4665 ng/ml [87.37; 87.37-87.37 BAU/ml]), and subsequently fell progressively during the remainder of the follow-up period. Contrarily, S-IgM decreased 358 days after the first infection (Figure 4D).

Considering the Nucleoprotein, IgG levels were initially high, then declined and finally disappeared by day 698, whereas N-IgM levels remained undetectable throughout (Supplementary Figure 3A). The mean N-IgG level among the 127 reinfected participants was 1012 (interquartile range [IQR] 305.5–2880 ng/ml [11.87; 3.64-33.55 BAU/ml]) after 245 days, and subsequently it remained stable at that level for the remainder of the research. For the duration of the study, N-IgM never exceeded the threshold (Supplementary Figure 3B). Among the 24 people who were never reinfected, N-IgG levels were highest between days 75 and 95 (5816.5; 2309.8-10046.6 ng/ml [67.84; 27.0-117.13 BAU/ml]), and then gradually declined over the next 295 days (Supplementary Figure 3C). N-IgG levels in 12 people who were never re-infected or vaccinated dropped after 276 days but N-IgM levels remained below the cut-off level the whole time (Supplementary Figure 3D).

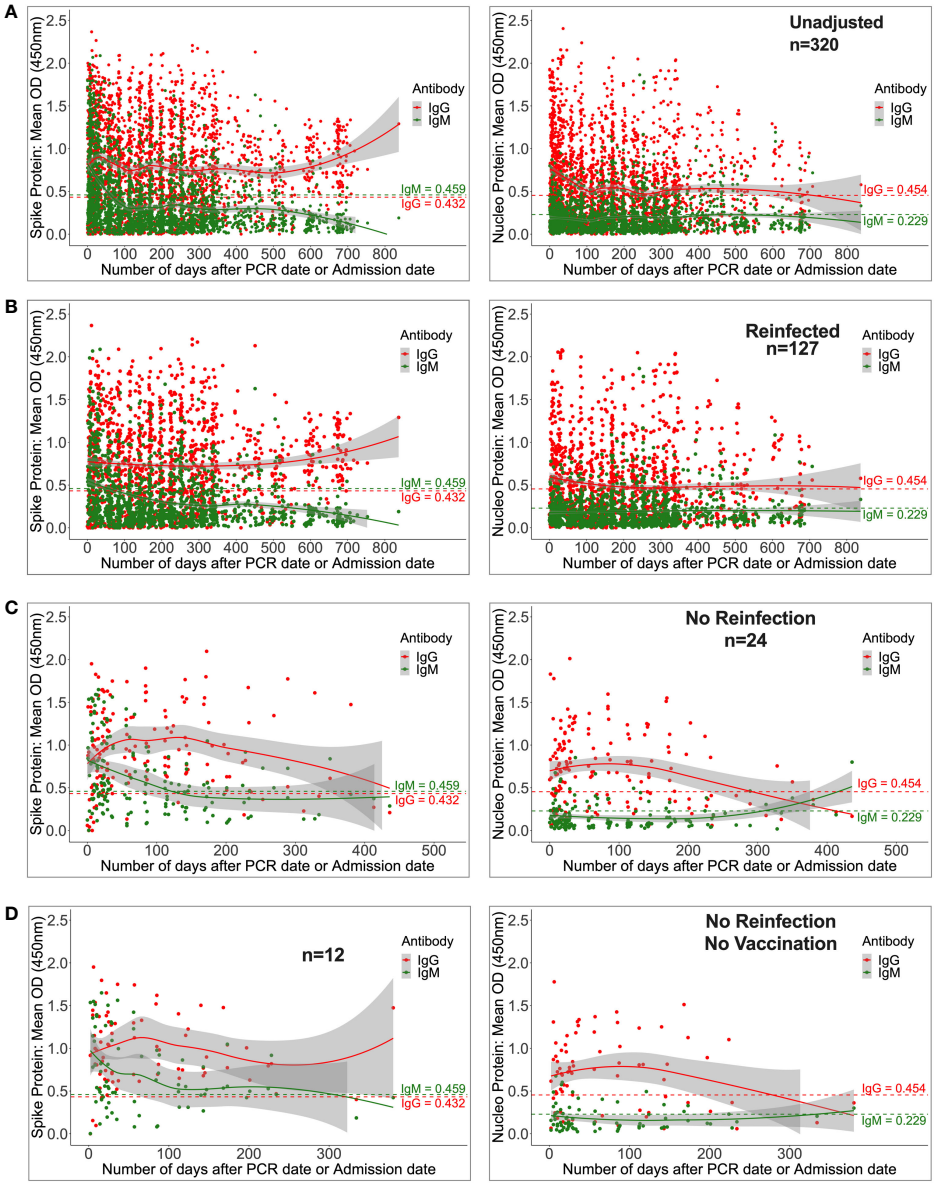


FIGURE 4
Durability of anti-Spike antibodies with or without reinfection and vaccination. Figure 4 shows LOWESS analysis curves that summarise the longitudinal persistence of Spike-directed IgG and IgM antibodies over the duration of the study investigation. Antibody optical densities at 450 nm and concentrations (ng/ml) for 320 individuals **(A)** with moderate or asymptomatic original COVID-19 illness with **(B)** or without downstream reinfection **(C)** and vaccination **(D)** are shown. The broken horizontal lines represent seropositivity cut-offs for IgG (red) and IgM (green) antibodies. The data is more reliable where the confidence intervals are smaller.

Anti-Nucleoprotein antibodies are a primary target of current surveillance tests, and 48 (24%) of the 202 SARS-CoV-2 PCR-confirmed cases evaluated during the first month of infection lacked detectable Nucleoprotein antibodies. There was no difference in the prevalence of this finding between mild and asymptomatic cases. Nucleoprotein seropositivity rates steadily reduced after initial infection, dropping below 50% after five months and 21% after 24 months (Supplementary Table 1). Collectively, our results demonstrate that in individuals with a history of moderate and asymptomatic COVID-19, Spike-directed antibodies predominate and persist longer than the Nucleoprotein-directed antibodies, and this holds true regardless of subsequent reinfection and immunization. In addition, the results suggest that the use of N-IgG for monitoring of mild and asymptomatic convalescent populations may grossly underestimate the true frequencies of past exposure.

## Spike IgG antibodies were higher than and positively correlated with anti-RBD IgG

We then analysed for correlations between Spike- and RBD-directed targeting, a known hallmark of antibody functionality (17). For the 128 first-week specimens evaluated, Spike IgG, IgM, and IgA antibody concentrations were higher (2638.7, 1532.5, and 825.5

ng/ml) than RBD concentrations (931.5, 1435.25, and 487.5 ng/ml), Figure 5A. Correspondingly, first-week anti-Spike OD values for IgG and IgA antibodies were also higher (0.518; IQR 0.161–0991 nm and 0.170; IQR 0.041-0.540 nm) than RDB (RBD-IgG: 0.170; IQR 0.041-0.540 nm vs. RBD-IgA: 0.084; IQR 0.033–0.234 nm), paired Wilcoxon signed-rank test, with all p-values 0.0001, Supplementary Figure 4). However, IgM antibody OD values were comparable across Spike and RBD (S-IgM: 0.451; IQR 0.218-0.857 nm) and 0.419; IQR 0.230-0.753 nm), respectively, and consistent with the low IgM levels observed throughout this cohort (Supplementary Figure 4).

A similar pattern was observed using the 124 peak specimens, with Spike IgG OD values and concentrations occurring at significantly higher levels (S-IgG: 0.672 nm and 5433.7 ng/ml) than the corresponding RBD (RBD-IgG: 0.434 nm and 2264.35 ng/ml), respectively, with p-values of 0.0001 in Figure 5B and Supplementary Figure 4. Spike and RBD antibodies positively correlated during the first week and cohort peak, Spearman's rank correlation test, all p-values 0.0001, Figures 5C, D.

## Frequency and longevity of Spike IgG superseded RBD IgG levels

Finally, we evaluated all data for the overall chronology of Spike- and RBD-directed IgG antibodies throughout the course of 28 months of cohort follow-up, irrespective of vaccination and reinfection status. The persistence of antibodies varied according to reinfection and vaccination status. For the 127 patients that were reinfected, RBD-IgG concentrations first decreased to 830.3 (355.9–1946.1 ng/ml [15.63; 6.75-36.53 BAU/ml]) at 205 days, then gradually increased. RBD-IgG peaked between 138 and 142 days (5206.2; IQR 2807.8-34145.1 ng/ml) in 24 subjects without reinfection but with some vaccinated and waned by 402 days. In 12 naturally infected unvaccinated volunteers with no reinfection, RBD-IgG peaked at 36-40 days (11317; 8535-14100 ng/ml [293.05]; 221.03-365.10 BAU/ml) then levelled out slightly above the threshold (Figure 6).

Anti-Spike IgG antibodies were substantially greater (0.892; IQR 0.442, 1.294 450nm) than RBD IgG antibodies in the first month (0.301; 0.123, 0.611 450nm). By one month, 85.6% and 73.3% of 202 and 165 participants seroconverted to the Spike and RBD IgG, compared to 75.81% and 78.22% of 124 at the cohort peak, respectively. The median S-IgG seropositivity rates were consistently over 50% throughout. Within seven months, almost three months after the IgG primary peak (days 115–127), the percentage of seropositive individuals for RBD-IgG had declined below 50%. Spike seropositivity was greater than RBD up to 14 months; Supplementary Table 2. While Spike IgG OD readings stayed above the cut-off throughout, RBD OD values dropped below the cut-off after six months (Figure 7). With p-values of 0.05, there were greater probabilities of losing RBD than Spike IgG seropositivity for up to 16 months (Supplementary Table 2). The results reveal that Spike- and RBD-directed IgG antibodies can linger for up to two years following a moderate, asymptomatic case of COVID-19 illness, even if no subsequent symptomatic reinfections occur during this time. The much faster fading of RBD-directed antibodies may be indicative of diminishing functionality over time.

# Discussion

To evaluate exposure and relationships with protection, longitudinal studies of Spike- and Nucleoprotein-directed antibody levels in moderate and asymptomatic COVID-19 illness, that primarily occurred in sub-Saharan Africa, are required. This is, to our knowledge, the first and longest study to comprehensively examine the longitudinal profiles of adaptive response to mild and asymptomatic COVID-19 illness in a sub-Saharan African setting. The strength of this study lies in its early and standardised sampling of a participant group representative of the country's initial infection with known dates of infection, which was chosen with minimal bias. This approach allowed for statistically significant comparisons and conclusions between virus-positive and virus-negative individuals. In addition, the design permitted a comprehensive assessment of the intensity and duration of immunity across waves and its decline over time. This study provides a comprehensive overview of the pandemic in a sub-Saharan African context, distinct from other geographies and for which no data exist on the evolution of immunity, yet it is required for evidence-based policy in this region. Using a validated in-house binding antibody ELISA, we describe the chronology of SARS-CoV-2 Spike-, RBD-, and Nucleoprotein-specific IgG, IgM, and IgA antibodies, including their evolution, duration, seroconversion rates, and protection associations, as the pandemic spread throughout Uganda starting in March 2020. Participants were confirmed rt-PCR SARS-CoV-2 infected Ugandans and uninfected Ugandans with extremely mild and asymptomatic COVID-19. In the first week of infection, 51 (57.3%), 59 (66.3%), and 38 (42.7%) of 89 confirmed cases seroconverted for Spike-directed IgG, IgM, and IgA seroconversion antibodies, respectively. Within a week of infection, robust Spike-directed antibodies were elicited (S-IgG: 49.50 (13.51, 134.37 BAU/ml; S-IgM: 56.61, IQR 23.20, 154.91ng/ml; and S-IgA: 157.63 (40.83, 676.58 BAU/ml), with levels peaking between 25 and 37 days (S-IgG: 4612; 1569-12947 ng/ml and S-IgM 2264.35 (1033.15, 5346.98 ng/ml). Antibodies specific to the virus were found to be much more robust in asymptomatic than in symptomatic infection, with strong Spike-directed IgG, IgM, and IgA antibodies dominating early in the course of the infection.

The clinical significance of antibody responses in COVID-19 disease is still debated. Despite effective disease control, asymptomatic patients had far less SARS-CoV-2-specific antibodies than symptomatic patients in some settings, which might be linked to the higher antigenic load in symptomatic disease (44). Mild and asymptomatic infections in China were linked to a faster decline in virus-specific antibodies (45), suggesting a less durable immunity. Antibodies were found in only a few asymptomatic participants in Europe (25). This study in a sub-Saharan African setting shows that asymptomatic infection induces faster and higher levels of anti-Spike antibodies,

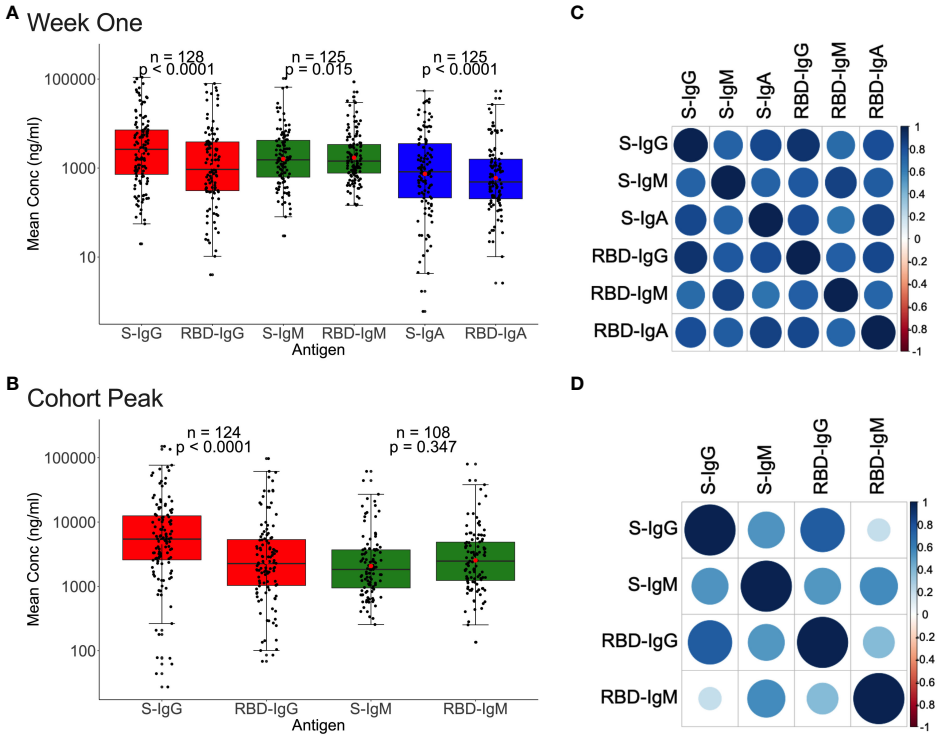


FIGURE 5
Relationships between Spike and RBD antibody concentrations. Figure 5 demonstrates the association between whole Spike- and RBD-directed antibody concentrations during the first week **(A)** and the cohort peak **(B)** of the primary antibody response. Box plots compare Spike and RBD antibody concentration medians using a paired Wilcoxon test. Correlation plots show the pairwise Spearman's rank correlations between entire Spike and RBD ODs during the first week of the primary antibody response **(C)** and the cohort peak **(D)**. Positive correlations are symbolized by blue, while negative correlations are indicated by red. Darker and larger circles represent stronger correlations, lighter and smaller circles represent weaker correlations, and blank squares represent insignificant correlations; p-values lee than or equal to 0.05 were deemed significant. See also Supplementary Figure 4.

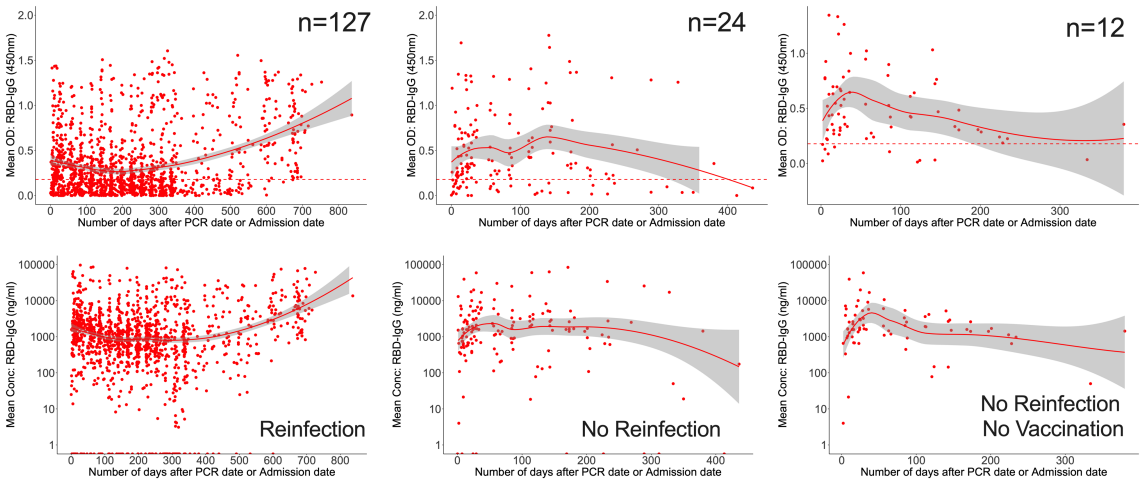


FIGURE 6
Longevity of anti-RBD antibodies. Figure 6 illustrates LOWESS curves summarizing the dynamics of RBD-directed antibodies over time. Medians of ODs and concentrations are shown since initial infection. Dashed lines indicate cut-off points for RBD seropositivity.

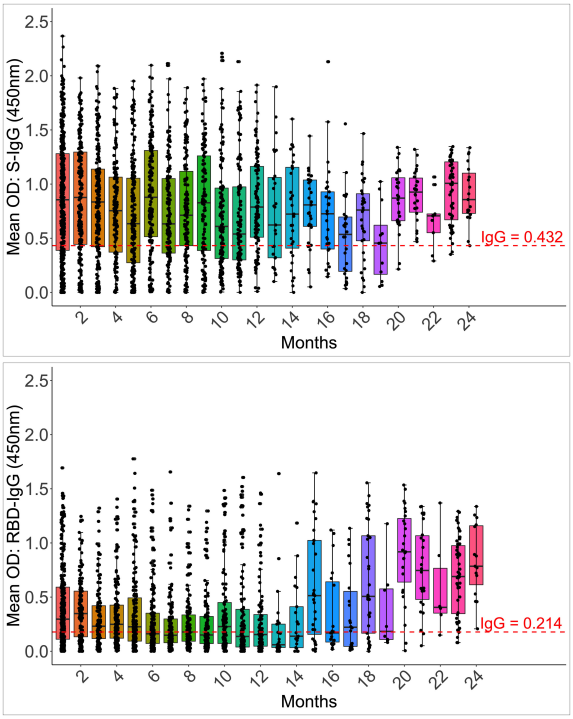


FIGURE 7
Longevity of S-IgG and RBD-IgG antibodies. Figure 7 illustrates the frequency and longevity of S-IgG and RBD-IgG antibodies since initial infection to 24 months, post-infection. Box plots illustrate the median ODs and interquartile ranges over time. Dashed lines indicate cut-off ODs for S-IgG and RBD-IgG seropositivity.

demonstrating the importance of early Spike targeting and reducing disease severity. Our findings are consistent with the time-dependent correlations described by others (46). We show distinctive immune protective correlates distinguishing asymptomatic from symptomatic COVID-19.

Because the dates of initial positive PCR-test testing were known, Spike and Nucleoprotein IgG, IgM, and IgA antibody trajectories could be established. The early peaking of Spike-directed IgM and IgA antibodies at 9 and 10 days and their declining at 87 and 21 days, respectively, guide the interpretation of serosurveillance findings in this setting and are consistent with previous cohorts that demonstrated the simultaneous and early appearance of both antibody subsets (45). Overlapping of S-IgM with PCR negativity suggests a reasonable proxy for virus clearance in resource-limited, largely asymptomatic settings, which starkly contrasts with symptomatic, hospitalized patients in whom IgM remained detectable long after recovery (47). The early dominance of S-IgG and rapid waning of S-IgM observed here, with S-IgG surpassing S-IgM within five days, reveal early affinity maturation and isotype class switching of IgM to IgG, a known good prognostic marker in COVID-19 (48).

Antibodies to the SARS-CoV-2 Nucleoprotein can predict past infection (49), making it a primary target in many serosurveillance studies. The loss of N-IgG seropositivity in over half of the population after seven months, regardless of vaccination or reinfection status, and the absence of measurable N-IgM levels across the board suggests that the use of these markers to predict past infection may dramatically underestimate exposure rates. Anti-Spike antibodies were shown to be higher and more persistent than anti-Nucleocapsid antibodies, just as they are in non-Sub-Saharan African settings (50, 51). Anti-Spike IgG antibodies continued to rise for the duration of the study period possibly due to vaccination and transient, clinically undetectable reinfections. S-IgG levels maintained and even rose from 234 days, but S-IgM levels stayed for just 59 days. In contrast to other geographical locations where Nucleocapsid detection rates were lower in asymptomatic patients (22, 52), we found no difference in N-directed IgG between mild and asymptomatic infection, implying that N-IgG might not be a criterion for differentiating disease severity in this SSA setting. Baseline antibody cross-reactivity was present in both SARS-CoV-2 rt-PCR-confirmed negative contacts and non-contacts at the onset of the pandemic, indicating that some degree of undetected exposure occurred in both groups. The unusually high baseline N-IgM cross-reactivity in non-cases (64%) and suspects (59%) was indicative of abortive infection, as has been suggested in other settings (53).

Antibodies that target RBDs are hallmarks of protection (54, 55). Here, in a population with spontaneous infection, reinfection, and vaccination, monthly Spike antibodies were positively correlated with the respective RBD antibodies up to 14 months, indicating that protection is likely to be durable. Under natural infection, RBD-IgG peaks around 36–40 days after the initial infection and then declines to just above the threshold at roughly 9.5 months, providing useful information for efforts to boost immunization. The higher frequency and longer duration of

Spike-than-RBD-directed IgG antibodies suggests that binding to other areas beyond the RBD contributes considerably to the maintenance of Spike-directed immunity in this population. While severe illness cohorts correlated antibody persistence with older age, male gender, and severe disease (23), we found no age relationships, which could be attributed to the younger cohort (31; IQR 25-37 years) studied here. We found significantly higher S-IgG levels in men early in the infection, but this coincided with high anti-N antibodies, indicating an antigenic load-driven early response. Beyond the initial response, no gender differences were discernible. We showed that even when the disease is mild and symptomatic, humoral responses to SARS-CoV-2 can persist for a very long time.

Our study has some limitations. To begin with, the impact of age, gender, disease severity, and underling conditions conditions such as HIV, hypertension, and diabetes on the evolution of SARS-CoV-2 antibody responses has been reported before (56–58). In this study, the small sample size and the lack of baseline clinical data for most participants meant that no definitive conclusions could be drawn about whether or not comorbidities affected antibody levels. More studies are needed with larger sample sizes and more detailed baseline clinical information to draw more meaningful conclusions about comorbidity effects on antibody levels. Second, these data were collected during the initial outbreak, with follow-ups during subsequent waves. The virus has evolved, and new variants have emerged, with Omicron currently dominating (59–62); this threatens the effectiveness and recognition of previous antibodies (63–65). Efforts are underway to evaluate the antibody recognition of circulating strains and the effectiveness of prior vaccination or natural infection antibodies in neutralising circulating viruses. Third, the known correlation between RBD antibodies and viral neutralisation established elsewhere (66) suggests that these antibodies provide early and long-term immune protection. To confirm their functionality, it is necessary to evaluate their ability to neutralise circulating virus strains. Additional studies are planned to establish the precise nature of the immunological memory associated with the SARS-CoV-2 spike protein, including its functionality and durability over time and across virus variants. Another limitation is that exposure to viral antigens, whether through natural infection, vaccination, or both, is an important driver of antibody persistence. We cannot rule out the possibility of undetected re-infections occurring during the follow-up period. Using estimates of nucleoprotein antibody concentrations from other contexts (42, 67) we observed substantial increases in N-IgG antibody concentrations, suggesting the possibility of reinfection.

Additional factors, such as the introduction of vaccines and boosters, nosocomial exposures, which are important in maintaining antibody levels (68, 69), may have also contributed to the long antibody persistence. There is a need for additional research into the re-infection rate and the effect of vaccines and boosters on antibody levels. The study was also limited by the uneven gender distribution due to the predominance of males in the commercial truck driver profession. More research will be required to adequately assess gender-related determinants in this setting. Finally, while the median age of these individuals is 31 years, antibody evolution may occur at a different rate in older populations. Overall, the data is representative of Sub-Saharan Africa's broader demography, whose median age is 19.7 years, but it highlights the need for additional research into the immune response among older populations, as this is an area of particular concern for public health due to their higher risk of severe COVID-19 outcomes.

In conclusion, we have shown that a Spike-directed humoral response to SARS-CoV-2 was formed and maintained in recovered mild and asymptomatic Ugandans, strongly suggesting the formation of lasting immunological memory that may contribute to herd immunity. A faster and more robust antibody response in asymptomatic infection suggests that those who do not experience symptoms may still have strong immunity, protecting them from progression to severe disease. Vaccines could be developed to take advantage of the strong immunological response in asymptomatic infection, reducing disease severity. Anti-SARS-CoV-2 antibody analysis can be complicated by vaccine uptake, reinfection, and diminishing antibody levels over time. Defining IgG, IgM, and IgA antibody longevity against Spike and Nucleoprotein antigens in this context with or without reinfection and vaccination provides data to guide vaccination, boosting strategies, and interpretation of serosurveillance in this and other comparable settings.

## The COVID-19 Immunoprofiling Team

Patricia Namubiru, Hermilia Christine Akoli, Susan Mugaba, Amina Nalumansi, Geoffrey Odoch, Kibengo Freddie, Deus Mwesigwa, Joseph Ssebwana Katende.

## Data availability statement

The raw data supporting the conclusions of this article will be made available by the authors, without undue reservation.

## Ethics statement

All study procedures were approved by the Research and Ethics Committee of the Uganda Virus Research Institute (GC/127/833) and the Uganda National Council for Science and Technology (HS637ES). The patients/participants provided their written informed consent to participate in this study.

## Author contributions

Conceptualization and methodology: JSer. Laboratory investigation: JSem, LK, GKO, CB, GO, JK and The COVID-19 Immunoprofiling team. Data curation, software, and formal statistical analysis: VA, TL and JSer. Resources: CN, MJ, NO and MMuw. Clinical Management of study cohort: CN, MJ, NO and MMuw. Writing- original draft; JSer, GKO and VA. Writing- reviewing and editing; PK, JF, and MC. Funding acquisition; MMus, JSer, JF, MC.

Project administration: JSer and BA. Supervision; PK. All authors contributed to the article and approved the submitted version.

## Funding

The work was funded by the Government of Uganda under the Science, Technology, and Innovation Secretariat-Office of the President (STI-OP), grant number: MOSTI-PRESIDE-COVID-19-2020/15. This publication is based on research funded in part by the Bill & Melinda Gates Foundation through the GIISER Uganda Grant Agreement Investment ID; INV-036306. The findings and conclusions contained within are those of the authors and do not necessarily reflect positions or policies of the Bill & Melinda Gates Foundation. This project is part of the EDCTP2 program supported by the European Union (grant number RIA2020EF- 3008-COVAB). The work was conducted at the MRC/UVRI and LSHTM Uganda Research Unit which is jointly funded by the UK Medical Research Council (MRC), part of the UK Research and Innovation (UKRI) and the UK Foreign, Commonwealth, and Development office (FDCO) under the MRC/FDCO Concordat agreement, and is also part of the EDCTP2 programme supported by the European Union. Initial specimen collections were supported by the University of Glasgow GCRF COVID-19 Rapid Response Fund (Uganda COVID-19 Serological Responses UGANCOSER).

## Acknowledgments

The authors are grateful to the study-cohort participants who donated the specimens used in this study. The following reagent was produced under HHSN272201400008C and obtained through BEI Resources, NIAID, NIH: Monoclonal Anti-SARS Coronavirus Recombinant Human Antibody, Clone CR3022 (produced in HEK293 Cells), NR-52481. The following reagent was obtained through BEI Resources, NIAID, NIH: Monoclonal Anti-SARS Coronavirus Recombinant Human IgG1, Clone CR3022 (produced in *Nicotiana benthamiana*), NR-52392. The Nucleoprotein mAb CR3009 (NIBSC Repository, Product No. 101011) used as a positive control was obtained from the Centre for AIDS Reagents, NIBSC, UK. The first WHO international standard for SARS-CoV-2, RN 20/136, Immunoglobulin, human, S321534 was obtained from the Centre for AIDS Reagents, NIBSC, UK. The first WHO international standard for SARS-CoV-2, Immunoglobulin, human, 20/B770 was obtained from the Centre for AIDS Reagents, NIBSC, UK. A mammalian expression plasmid for the RBD of SARS-CoV-2 was kindly provided by the Katie Doores laboratory at King's College London.

## Conflict of interest

The authors declare that the research was conducted in the absence of any commercial or financial relationships that could be construed as a potential conflict of interest.

## Publisher's note



## Supplementary material

The Supplementary Material for this article can be found online at: https://www.frontiersin.org/articles/10.3389/fimmu.2023.1152522/full#supplementary-material

SUPPLEMENTARY FIGURE 1
Chronology of IgG, IgM, and IgA antibody trends during the first month of infection. Supplementary Figure 1 shows Locally Weighted Scatter Plot Smoothing (LOWESS) curves summarising the profiles of the development of Spike-directed IgG and IgM antibodies. IgG, IgM, and IgA antibody optical densities **(A)** and concentrations **(B)** are indicated for 202 cases during their first 30 days of infection. Broken horizontal lines indicate IgG (red) and IgM (green) seropositivity cut-offs.

SUPPLEMENTARY FIGURE 2
Chronology of IgG, IgM, and IgA antibody trends during the first two months of infection. Supplementary Figure 2 shows Locally Weighted Scatter Plot Smoothing (LOWESS) curves summarising the profiles of the development of Nucleoprotein-directed IgG and IgM antibodies. IgG, IgM, and IgA antibody optical densities **(A)** and concentrations **(B)** are indicated for 269 cases during their first two months of infection. Broken horizontal lines indicate IgG (red) and IgM (green) seropositivity cut-offs.

SUPPLEMENTARY FIGURE 3
Durability of Nucleoprotein IgG and IgM antibodies over time. Supplementary Figure 3 shows LOWESS analysis curves that summarise the longitudinal persistence of Nucleoprotein-directed IgG and IgM antibodies over the duration of the study investigation. Antibody optical densities at 450 nm and concentrations (ng/ml) for 320 individuals **(A)** with moderate or asymptomatic primary COVID-19 illness with **(B)** or without downstream reinfection **(C)** and vaccination **(D)** are shown. The broken horizontal lines represent seropositivity cut-offs for IgG (red) and IgM (green) antibodies.

SUPPLEMENTARY FIGURE 4
Spike and RBD ODs during the first week and cohort peak time-points. Supplementary Figure 4 demonstrates the association between whole spike- and RBD-directed antibody optical densities (nm) during the first week (Figure 4A) and the cohort peak (Figure 4B) of the primary antibody response. Box plots compare spike and RBD antibody concentration medians using a paired Wilcoxon test. Correlation plots show the pairwise Spearman's rank correlations between entire spikes and RBD ODs during the first week of the primary antibody response (Figure 4C) and the cohort peak (Figure 4D). Positive correlations are symbolized by blue, while negative correlations are indicated by red. Darker and larger circles represent stronger correlations, lighter and smaller circles represent weaker correlations, and blank squares represent insignificant correlations; p-values of 0.05 were deemed significant.

SUPPLEMENTARY TABLE 1
Proportions of nucleoprotein IgG seropositivity over time.

SUPPLEMENTARY TABLE 2
Proportions of Spike and RBD seropositive individuals. OR (Odds ratio), IQR (Interquartile range).

# References


1. Collaborators C-CI. Estimating global, regional, and national daily and cumulative infections with SARS-CoV-2 through Nov 14, 2021: a statistical analysis. *Lancet* (2022), 399(10344):2351–80. doi: 10.1016/S0140-6736(22)00484-6

2. *Population of subsaharan Africa 2020* (2022). Available at: https://www.populationpyramid.net/sub-saharan-africa/2020/.

3. Shrock E, Fujimura E, Kula T, Timms RT, Lee IH, Leng Y, et al. Viral epitope profiling of COVID-19 patients reveals cross-reactivity and correlates of severity. *Science* (2020) 370(6520):eabd4250. doi: 10.1126/science.abd4250

4. Tso FY, Lidenge SJ, Pena PB, Clegg AA, Ngowi JR, Mwaiselage J, et al. High prevalence of pre-existing serological cross-reactivity against severe acute respiratory syndrome coronavirus-2 (SARS-CoV-2) in sub-Saharan Africa. *Int J Infect Dis* (2021) 102:577–83. doi: 10.1016/j.ijid.2020.10.104

5. Mateus J, Grifoni A, Tarke A, Sidney J, Ramirez SI, Dan JM, et al. Selective and cross-reactive SARS-CoV-2 T cell epitopes in unexposed humans. *Science* (2020) 370 (6512):89–94. doi: 10.1126/science.abd3871

6. Gumanova NG, Gorshkov AU, Bogdanova NL, Korolev AI, Drapkina OM. Detection of anti-SARS-CoV-2-S1 RBD-specific antibodies prior to and during the pandemic in 2011-2021 and COVID-19 observational study in 2019-2021. *Vaccines (Basel)* (2022) 10(4):581. doi: 10.3390/vaccines10040581

7. Sagar M, Reifler K, Rossi M, Miller NS, Sinha P, White LF, et al. Recent endemic coronavirus infection is associated with less-severe COVID-19. *J Clin Invest* (2021) 131 (1):e143380. doi: 10.1172/JCI143380

8. Poston D, Weisblum Y, Wise H, Templeton K, Jenks S, Hatziioannou T, et al. Absence of severe acute respiratory syndrome coronavirus 2 neutralizing activity in prepandemic sera from individuals with recent seasonal coronavirus infection. *Clin Infect Dis* (2021) 73(5):e1208–e11. doi: 10.1093/cid/ciaa1803

9. Stoddard CI, Sung K, Ojee E, Adhiambo J, Begnel ER, Slyker J, et al. Distinct antibody responses to endemic coronaviruses pre- and post-SARS-CoV-2 infection in Kenyan infants and mothers. *bioRxiv* (2022) 14(7):1517. doi: 10.1101/2022.06.02.493651

10. de Vries RD. SARS-CoV-2-specific T-cells in unexposed humans: presence of cross-reactive memory cells does not equal protective immunity. *Signal Transduct Target Ther* (2020) 5(1):224. doi: 10.1038/s41392-020-00338-w

11. Jiang S, Hillyer C, Du L. Neutralizing antibodies against SARS-CoV-2 and other human coronaviruses. *Trends Immunol* (2020) 41(5):355–9. doi: 10.1016/j.it.2020.03.007

12. Cao X. COVID-19: immunopathology and its implications for therapy. *Nat Rev Immunol* (2020) 20(5):269–70. doi: 10.1038/s41577-020-0308-3

13. Chi X, Yan R, Zhang J, Zhang G, Zhang Y, Hao M, et al. A neutralizing human antibody binds to the n-terminal domain of the spike protein of SARS-CoV-2. *Science* (2020) 369(6504):650–5. doi: 10.1126/science.abc6952

14. Cerutti G, Guo Y, Zhou T, Gorman J, Lee M, Rapp M, et al. Potent SARS-CoV-2 neutralizing antibodies directed against spike n-terminal domain target a single supersite. *Cell Host Microbe* (2021) 29(5):819–33.e7. doi: 10.1016/j.chom.2021.03.005

15. Seydoux E, Homad LJ, MacCamy AJ, Parks KR, Hurlburt NK, Jennewein MF, et al. Characterization of neutralizing antibodies from a SARS-CoV-2 infected individual. *Immunity* (2020) 53(1):98–105.e5. doi: 10.1016/j.immuni.2020.06.001

16. Premkumar L, Segovia-Chumbez B, Jadi R, Martinez DR, Raut R, Markmann A, et al. The receptor binding domain of the viral spike protein is an immunodominant and highly specific target of antibodies in SARS-CoV-2 patients. *Sci Immunol* (2020) 5 (48):eabc8413. doi: 10.1126/sciimmunol.abc8413

17. Amanat F, Strohmeier S, Lee W-H, Bangaru S, Ward AB, Coughlan L, et al. Murine monoclonal antibodies against RBD of SARS-CoV-2 neutralize authentic wild type SARS-CoV-2 as well as B.1.1.7 and B.1.351 viruses and protect *in vivo* in a mouse model in a neutralization dependent manner. *mBio* (2021) 12(4):e0100221. doi: 10.1101/2021.04.05.438547

18. Kemp SA, Collier DA, Datir RP, Ferreira I, Gayed S, Jahun A, et al. SARS-CoV-2 evolution during treatment of chronic infection. *Nature* (2021) 592(7853):277–82. doi: 10.1038/s41586-021-03291-y

19. Solastie A, Virta C, Haveri A, Ekstrom N, Kantele A, Miettinen S, et al. A highly sensitive and specific SARS-CoV-2 spike- and nucleoprotein-based fluorescent multiplex immunoassay (FMIA) to measure IgG, IgA, and IgM class antibodies. *Microbiol Spectr* (2021) 9(3):e0113121. doi: 10.1128/Spectrum.01131-21

20. Abdullahi A, Oladele D, Owusu M, Kemp SA, Ayorinde J, Salako A, et al. SARS-COV-2 antibody responses to AZD1222 vaccination in West Africa. *Nat Commun* (2022) 13(1):6131. doi: 10.1038/s41467-022-33792-x

21. Siddiqui SM, Bowman KA, Zhu AL, Fischinger S, Beger S, Maron JS, et al. Serological markers of SARS-CoV-2 reinfection. *mBio* (2022) 13(1):e0214121. doi: 10.1128/mbio.02141-21

22. Yang L, Xu Q, Yang B, Li J, Dong R, Da J, et al. IgG antibody titers against SARS-CoV-2 nucleocapsid protein correlate with the severity of COVID-19 patients. *BMC Microbiol* (2021) 21(1):351. doi: 10.1186/s12866-021-02401-0

23. Alshami A, Al Attas R, Anan H, Al Maghrabi A, Ghandorah S, Mohammed A, et al. Durability of antibody responses to SARS-CoV-2 infection and its relationship to disease severity assessed using a commercially available assay. *Front Microbiol* (2021) 12:770727. doi: 10.3389/fmicb.2021.770727

24. Goh YS, Chavatte JM, Lim Jieling A, Lee B, Hor PX, Amrun SN, et al. Sensitive detection of total anti-spike antibodies and isotype switching in asymptomatic and symptomatic individuals with COVID-19. *Cell Rep Med* (2021) 2(2):100193. doi: 10.1016/j.xcrm.2021.100193

25. Marchi S, Viviani S, Remarque EJ, Ruello A, Bombardieri E, Bollati V, et al. Characterization of antibody response in asymptomatic and symptomatic SARS-CoV-2 infection. *PloS One* (2021) 16(7):e0253977. doi: 10.1371/journal.pone.0253977

26. Balachandran H, Phetsouphanh C, Agapiou D, Adhikari A, Rodrigo C, Hammoud M, et al. Maintenance of broad neutralizing antibodies and memory b cells 1 year post-infection is predicted by SARS-CoV-2-specific CD4+ T cell responses. *Cell Rep* (2022) 38(6):110345. doi: 10.1016/j.celrep.2022.110345

27. Abraha I, Eusebi P, Germani A, Pasquarelli E, Pascolini S, Antonietti R, et al. Temporal trends and differences of SARS-CoV-2-specific antibody responses in symptomatic and asymptomatic subjects: a longitudinal study from umbria in Italy. *BMJ Open* (2022) 12(7):e056370. doi: 10.1136/bmjopen-2021-056370

28. Bao Y, Ling Y, Chen YY, Tian D, Zhao GP, Zhang XH, et al. Dynamic anti-spike protein antibody profiles in COVID-19 patients. *Int J Infect Dis* (2021) 103:540–8. doi: 10.1016/j.ijid.2020.12.014

29. Sette A, Crotty S. Adaptive immunity to SARS-CoV-2 and COVID-19. *Cell* (2021) 184(4):861–80. doi: 10.1016/j.cell.2021.01.007

30. Grifoni A, Sidney J, Vita R, Peters B, Crotty S, Weiskopf D, et al. SARS-CoV-2 human T cell epitopes: Adaptive immune response against COVID-19. *Cell Host Microbe* (2021) 29(7):1076–92. doi: 10.1016/j.chom.2021.05.010

31. Primorac D, Vrdoljak K, Brlek P, Pavelic E, Molnar V, Matisic V, et al. Adaptive immune responses and immunity to SARS-CoV-2. *Front Immunol* (2022) 13:848582. doi: 10.3389/fimmu.2022.848582

32. Keeton R, Tincho MB, Ngomti A, Baguma R, Benede N, Suzuki A, et al. Author correction: T cell responses to SARS-CoV-2 spike cross-recognize omicron. *Nature* (2022) 604(7907):E25. doi: 10.1038/s41586-022-04708-y

33. Riou C, Keeton R, Moyo-Gwete T, Hermanus T, Kgagudi P, Baguma R, et al. Escape from recognition of SARS-CoV-2 variant spike epitopes but overall preservation of T cell immunity. *Sci Transl Med* (2022) 14(631):eabj6824. doi: 10.1126/scitranslmed.abj6824

34. Ijaz S, Dicks S, Jegatheesan K, Parker E, Katsanovskaja K, Vink E, et al. Mapping of SARS-CoV-2 IgM and IgG in gingival crevicular fluid: antibody dynamics and linkage to severity of COVID-19 in hospital inpatients. *J Infect* (2022) 85(2):152–60. doi: 10.1016/j.jinf.2022.05.033

35. Levring MB, Holm DK, Nilsson AC, Bauer JM, Jensen IS, Davidsen JR, et al. SARS-CoV-2 antibody kinetics in blood donors with a previously positive SARS-CoV-2 antibody test within a seroprevalence survey. *J Med Virol* (2022) 94(4):1711–6. doi: 10.1002/jmv.27486

36. Grandjean L, Saso A, Torres Ortiz A, Lam T, Hatcher J, Thistlethwayte R, et al. Long-term persistence of spike protein antibody and predictive modeling of antibody dynamics after infection with severe acute respiratory syndrome coronavirus 2. *Clin Infect Dis* (2022) 74(7):1220–9. doi: 10.1093/cid/ciab607

37. Pickering S, Betancor G, Galao RP, Merrick B, Signell AW, Wilson HD, et al. Comparative assessment of multiple COVID-19 serological technologies supports continued evaluation of point-of-care lateral flow assays in hospital and community healthcare settings. *PLoS Pathog* (2020) 16(9):e1008817. doi: 10.1371/journal.ppat.1008817

38. Oluka GK, Namubiru P, Kato L, Ankunda V, Gombe B, Cotten M, et al. Optimisation and validation of a conventional ELISA and cut-offs for detecting and quantifying anti-SARS-CoV-2 spike, RBD, and nucleoprotein IgG, IgM, and IgA antibodies in Uganda. *Front Immunol (B cell Biology)* (2023) 14:1113194. doi: 10.3389/fimmu.2023.1113194

39. Matthew C. *SARS-CoV-2 diversity in Uganda, December, 2020*. (2020).

40. Deeks JJ, Dinnes J, Takwoingi Y, Davenport C, Spijker R, Taylor-Phillips S, et al. Antibody tests for identification of current and past infection with SARS-CoV-2. *Cochrane Database Syst Rev* (2020) 6(6):CD013652. doi: 10.1002/14651858.CD013652

41. Fox T, Geppert J, Dinnes J, Scandrett K, Bigio J, Sulis G, et al. Antibody tests for identification of current and past infection with SARS-CoV-2. *Cochrane Database Syst Rev* (2022) 11(11):CD013652. doi: 10.1002/14651858.CD013652.pub2

42. Manisty C, Otter AD, Treibel TA, McKnight A, Altmann DM, Brooks T, et al. Antibody response to first BNT162b2 dose in previously SARS-CoV-2-infected individuals. *Lancet* (2021) 397(10279):1057–8. doi: 10.1016/S0140-6736(21)00501-8

43. Epsi NJ, Richard SA, Lindholm DA, Mende K, Ganesan A, Huprikar N, et al. Understanding 'hybrid immunity': comparison and predictors of humoral immune responses to SARS-CoV-2 infection and COVID-19 vaccines. *Clin Infect Dis* (2022) 76 (3):e439–49. doi: 10.1093/cid/ciac392

44. Wellinghausen N, Plonne D, Voss M, Ivanova R, Frodl R, Deininger S. SARS-CoV-2-IgG response is different in COVID-19 outpatients and asymptomatic contact persons. *J Clin Virol* (2020) 130:104542. doi: 10.1016/j.jcv.2020.104542

45. Long QX, Tang XJ, Shi QL, Li Q, Deng HJ, Yuan J, et al. Clinical and immunological assessment of asymptomatic SARS-CoV-2 infections. *Nat Med* (2020) 26(8):1200–4. doi: 10.1038/s41591-020-0965-6

46. Lucas C, Klein J, Sundaram ME, Liu F, Wong P, Silva J, et al. Delayed production of neutralizing antibodies correlates with fatal COVID-19. *Nat Med* (2021) 27(7):1178–86. doi: 10.1038/s41591-021-01355-0

47. Wenzheng G, Siyuan Y, Guangbo L, Qiankun X, Simin Y, Donghua W, et al. The analysis of characteristics of anti-SARS-CoV-2 antibodies in clinically COVID-19 patients. *J Clin Res Ophthalmol* (2020) 7(2):081–6. doi: 10.17352/2455-1414.000077

48. Sun B, Feng Y, Mo X, Zheng P, Wang Q, Li P, et al. Kinetics of SARS-CoV-2 specific IgM and IgG responses in COVID-19 patients. *Emerg Microbes Infect* (2020) 9 (1):940–8. doi: 10.1080/22221751.2020.1762515

49. van den Hoogen LL, Verheul MK, Vos ERA, van Hagen CCE, van Boven M, Wong D, et al. SARS-CoV-2 spike S1-specific IgG kinetic profiles following mRNA or vector-based vaccination in the general Dutch population show distinct kinetics. *Sci Rep* (2022) 12(1):5935. doi: 10.1038/s41598-022-10020-6

50. Terpos E, Stellas D, Rosati M, Sergentanis TN, Hu X, Politou M, et al. SARS-CoV-2 antibody kinetics eight months from COVID-19 onset: Persistence of spike antibodies but loss of neutralizing antibodies in 24% of convalescent plasma donors. *Eur J Intern Med* (2021) 89:87–96. doi: 10.1016/j.ejim.2021.05.010

51. Choe PG, Hong J, Park J, Chang E, Kang CK, Kim NJ, et al. Persistent antibody responses up to 18 months after mild SARS-CoV-2 infection. *J Infect Dis* (2022) 226 (7):1224–30. doi: 10.1093/infdis/jiac099

52. Tutukina M, Kaznadzey A, Kireeva M, Mazo I. IgG antibodies develop to spike but not to the nucleocapsid viral protein in many asymptomatic and light COVID-19 cases. *Viruses* (2021) 13(10):1945. doi: 10.3390/v13101945

53. Swadling L, Diniz MO, Schmidt NM, Amin OE, Chandran A, Shaw E, et al. Pre-existing polymerase-specific T cells expand in abortive seronegative SARS-CoV-2. *Nature* (2022) 601(7891):110–7. doi: 10.1038/s41586-021-04186-8

54. Jia L, Liu YP, Tian LF, Xiong C, Xu X, Qu H, et al. Potent neutralizing RBD-specific antibody cocktail against SARS-CoV-2 and its mutant. *MedComm (2020)* (2021) 2(3):442–52. doi: 10.1002/mco2.79

55. Rogers TF, Zhao F, Huang D, Beutler N, Burns A, He WT, et al. Isolation of potent SARS-CoV-2 neutralizing antibodies and protection from disease in a small animal model. *Science* (2020) 369(6506):956–63. doi: 10.1126/science.abc7520

56. Li K, Huang B, Wu M, Zhong A, Li L, Cai Y, et al. Dynamic changes in anti-SARS-CoV-2 antibodies during SARS-CoV-2 infection and recovery from COVID-19. *Nat Commun* (2020) 11(1):6044. doi: 10.1038/s41467-020-19943-y

57. Kashiwagi K, Maeda T, Yoshizawa S, Sato T, Aoki K, Ishii Y, et al. IgG antibodies, SARS-CoV-2 load, and prognostic indicators in patients with severe and mild COVID-19 in Japan. *J Nippon Med Sch* (2021) 88(4):380–3. doi: 10.1272/jnms.JNMS.2021_88-417

58. Kotsiou OS, Karakousis N, Papagiannis D, Matsiatsiou E, Avgeri D, Fradelos EC, et al. The comparative superiority of SARS-CoV-2 antibody response in different immunization scenarios. *J Pers Med* (2022) 12(11):1756. doi: 10.3390/jpm12111756

59. Bugembe DL, V.T.Phan M, Ssewanyana I, Semanda P, Nansumba H, Dhaala B, et al. A SARS-CoV-2 lineage a variant (A.23.1) with altered spike has emerged and is dominating the current Uganda epidemic. *Nat Microbiol* (2021) 6:1094–101. doi: 10.1101/2021.02.08.21251393

60. Bbosa N, Ssemwanga D, Namagembe H, Kiiza R, Kiconco J, Kayiwa J, et al. Rapid replacement of SARS-CoV-2 variants by delta and subsequent arrival of omicron, Uganda, 2021. *Emerg Infect Dis* (2022) 28(5):1021–5. doi: 10.3201/eid2805.220121

61. Mugisha J, Mpairwe B, Newton R, Cotten M, Phan MVT. SARS-CoV-2 omicron BA.5 infections in vaccinated persons, rural Uganda. *Emerg Infect Dis* (2023) 29 (1):224–6. doi: 10.3201/eid2901.220981

62. Harris JR, Owusu D, O'Laughlin K, Cohen AL, Ben Hamida A, Patel JC, et al. SARS-CoV-2 breakthrough infections among US embassy staff members, Uganda, may-June 2021. *Emerg Infect Dis* (2022) 28(6):1279–80. doi: 10.3201/eid2806.220427

63. Fernandes Q, Inchakalody VP, Merhi M, Mestiri S, Taib N, Moustafa Abo El-Ella D, et al. Emerging COVID-19 variants and their impact on SARS-CoV-2 diagnosis, therapeutics and vaccines. *Ann Med* (2022) 54(1):524–40. doi: 10.1080/07853890.2022.2031274

64. Aleem A, Akbar Samad AB, Slenker AK. *Emerging variants of SARS-CoV-2 and novel therapeutics against coronavirus (COVID-19)*. Treasure Island (FL: StatPearls (2022).

65. Chatterjee S, Bhattacharya M, Nag S, Dhama K. Chakraborty c. a detailed overview of SARS-CoV-2 omicron: Its Sub-variants, mutations and pathophysiology, clinical characteristics, immunological landscape, immune escape, and therapies. *Viruses* (2023) 15(1):167. doi: 10.3390/v15010167

66. Rosadas C, Khan M, Parker E, Marchesin F, Katsanovskaja K, Sureda-Vives M, et al. Detection and quantification of antibody to SARS CoV 2 receptor binding domain provides enhanced sensitivity, specificity and utility. *J Virol Methods* (2022) 302:114475. doi: 10.1016/j.jviromet.2022.114475

67. Briggs J, Takahashi S, Nayebare P, Cuu G, Rek J, Zedi M, et al. Seroprevalence of antibodies to SARS-CoV-2 in rural households in Eastern Uganda, 2020-2022. *JAMA Netw Open* (2023) 6(2):e2255978. doi: 10.1001/jamanetworkopen.2022.55978

68. Łysek-Gładysińska M, Starz M, Borowiec-Sęk A, Sufin I, Wieczorek A, Chrapek M, et al. The levels of anti-SARS-CoV-2 spike protein IgG antibodies before and after the third dose of vaccination against COVID-19. *J Inflammation Res* (2023) 16:145–60. doi: 10.2147/JIR.S394760

69. Ssuuna C, Galiwango RM, Kankaka EN, Kagaayi J, Ndyanabo A, Kigozi G, et al. Severe acute respiratory syndrome coronavirus-2 seroprevalence in south-central Uganda, during 2019-2021. *BMC Infect Dis* (2022) 22(1):174. doi: 10.1186/s12879-022-07161-4

frontiers | Frontiers in Immunology

TYPE Review
PUBLISHED 21 March 2023
DOI 10.3389/fimmu.2023.1132250



OPEN ACCESS

EDITED BY
Wei Wang,
Jiangsu Institute of Parasitic Diseases (JIPD), China

REVIEWED BY
Celestine Wanjalla,
Vanderbilt University Medical Center, United States
Luminița-Smaranda Iancu,
Grigore T. Popa University of Medicine and Pharmacy, Romania

*CORRESPONDENCE
Xiao Liu
liux587@mail.sysu.edu.cn
Peng Yu
yu8220182@163.com

†These authors have contributed equally to this work

SPECIALTY SECTION
This article was submitted to Viral Immunology, a section of the journal Frontiers in Immunology

RECEIVED 27 December 2022
ACCEPTED 02 March 2023
PUBLISHED 21 March 2023

CITATION
Niu L, Liang D, Ling Q, Zhang J, Li Z, Zhang D, Xia P, Zhu Z, Lin J, Shi A, Ma J, Yu P and Liu X (2023) Insights into monkeypox pathophysiology, global prevalence, clinical manifestation and treatments. *Front. Immunol.* 14:1132250. doi: 10.3389/fimmu.2023.1132250



# Insights into monkeypox pathophysiology, global prevalence, clinical manifestation and treatments

Liyan Niu[1,2†], Dingfa Liang[1,3†], Qin Ling[1,4†], Jing Zhang[3], Ziwen Li[4], Deju Zhang[5], Panpan Xia[5], Zicheng Zhu[5], Jitao Lin[5], Ao Shi[6,7], Jianyong Ma[6], Peng Yu[5*] and Xiao Liu[8*]

[1]Department of Endocrinology and Metabolism, The Second Affiliated Hospital of Nanchang University, Nanchang, Jiangxi, China, [2]Huan Kui College of Nanchang University, Nanchang, China, [3]Queen Mary College of Nanchang University, Nanchang, China, [4]Department of Anesthesiology, The Second Affiliated Hospital of Nanchang University, Nanchang, Jiangxi, China, [5]Third Department of Internal Medicine, Dexing Hospital of Traditional Chinese Medicine, Dexing, Jiangxi, China, [6]Department of Pharmacology and Systems Physiology, University of Cincinnati College of Medicine, Cincinnati, OH, United States, [7]School of Medicine, St. George University of London, London, United Kingdom, [8]Department of Cardiology, Sun Yat-Sen Memorial Hospital of Sun Yat-Sen University, Guangzhou, Guangdong, China

On 23rd July 2022, the World Health Organization (WHO) recognized the ongoing monkeypox outbreak as a public medical crisis. Monkeypox virus (MPV), the etiological agent of monkeypox, is a zoonotic, linear, double-stranded DNA virus. In 1970, the Democratic Republic of the Congo reported the first case of MPV infection. Human-to-human transmission can happen through sexual contact, inhaled droplets, or skin-to-skin contact. Once inoculated, the viruses multiply rapidly and spread into the bloodstream to cause viremia, which then affect multiple organs, including the skin, gastrointestinal tract, genitals, lungs, and liver. By September 9, 2022, more than 57,000 cases had been reported in 103 locations, especially in Europe and the United States. Infected patients are characterized by physical symptoms such as red rash, fatigue, backache, muscle aches, headache, and fever. A variety of medical strategies are available for orthopoxviruses, including monkeypox. Monkeypox prevention following the smallpox vaccine has shown up to 85% efficacy, and several antiviral drugs, such as Cidofovir and Brincidofovir, may slow the viral spread. In this article, we review the origin, pathophysiology, global epidemiology, clinical manifestation, and possible treatments of MPV to prevent the propagation of the virus and provide cues to generate specific drugs.

KEYWORDS

**monkeypox virus (MPV), origin, pathophysiology, global prevalence, clinical manifestation, treatment**

**Abbreviations:** MPV, Monkeypox virus; CDC, Centers for Disease Control; WHO, World Health Organization; COVID-19, coronavirus disease 2019; OPV, orthopoxvirus; RT-PCR, real-time polymerase chain reaction; MSM, males who have sex with other men; VACV, vaccinia virus; EEV, extracellular-enveloped virus; IMV, intracellular mature virus; MV, mature virion; EV, enveloped virion; DRC, Democratic Republic of Congo; VIGIV, Vaccinia Immune Globulin Intravenous; CMV, cytomegalovirus.

# 1 Introduction

Threats from the pandemic coronavirus disease 2019 (COVID-19) have not been eliminated, and worries about the possibility of another viral pandemic reached a crescendo (1). The monkeypox virus (MPV), a zoonotic DNA orthopoxvirus (OPV) causes the zoonotic disease monkeypox marked by fever and a red rash which is related to smallpox virus and vaccinia virus (VACV) (2, 3). In 1970, the Democratic Republic of Congo (DRC) reported the first human case of infection, accounting for the majority of early cases (4). Recently, more than 57,000 total cases have been found at more than 100 total locations since May 2022 (5). According to the Centers for Disease Control (CDC), there are no specific medications available, and smallpox vaccines, vaccinia immune globulin, and antivirals were used to regulate small-scale outbreaks (6, 7). Such unexpected, unprecedented, and unusually high-frequency transmission outbreaks worldwide have spurred scientific, political, and media attention. Investigation of pathophysiological features, routes of transmission, clinical features and preliminary diagnosis is urgently needed and has the potential to help improve prevention and early intervention and promote the development of specific drugs.

# 2 Origins and transmission routes

In 1958, MPV was first identified and isolated from cynomolgus (*Macaca cynomolgus*) monkeys as laboratory animals, which were kept by a research facility after shipment from Singapore to Denmark (8). MPV is a member of the OPV of the Chordopoxvirinae subfamily, Poxviridae family, the same genus as other viruses such as smallpox and cowpox (9). There are some similarities between monkeypox and smallpox, such as structures, clinical manifestations, and responses to some antiviral drugs (10, 11). The MPV of human cases originated in the tropical rainforests of western and central Africa, and there are two clades in the phylogenetic analysis: the West African clade and the Congo clade, with an average mortality rate of up to 11% (12). The first isolates from cynomolgus (*Macaca cynomolgus*) monkeys belonged to the West African clade while the Congo clade contributed to the first human case in 1970 (13). In addition, monkeypox is a zoonotic disease similar to smallpox, but it is still unclear which is the reservoir host of MPV (14). Rodents from Africa are thought to be the largest animal reservoirs involved in the spread of the virus, and it can be transmitted from some rodents (prairie dogs) to various monkeys and apes, such as anthropoid apes. By coming into contact with the infected animals' respiratory droplets, skin sores, or body fluids, MPV can transmit from one animal to another. The virus enters a healthy person *via* the respiratory system, mucous membranes (such as the nose, mouth, or eyes), or skin wounds (15). Simultaneously, it can be transmitted from animals, such as rodents or monkeys, to humans through bushmeat, bites, scratches, and direct or indirect exposure to body substances or fluids from the lesion (16) (Figure 1). In 1970, the first reported case of MPV was a 9-month-old child (A. I.) infected with a smallpox-like disease in the village of Bokenda, Basankusu Province, the Democratic Republic of the Congo (4). Transmission from humans to animals has not been documented. While transmission from person to person is a major problem, it mostly occurs through the respiratory tract by sneezing, coughing, large respiratory droplets, and other similar actions. Direct contact with infected lesions and bodily fluids or indirect contact with contaminated items like patient-used garments or linens (17). In addition to the placenta (congenital monkeypox), intimate contact during labor and after delivery can also result in mother-to-child transmission (18). Currently, with an increasing number of transmissions of Health-Care Associated Infections

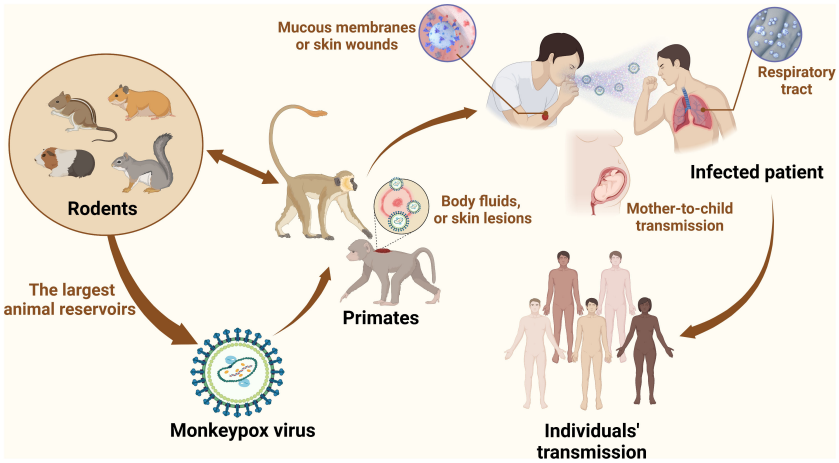


FIGURE 1
MPV transmission. Zoonotic dissemination of MPV. Animal hosts mainly include rodents (African rope squirrels, prairie dogs, hamsters, and rats) and primates (cynomolgus, rhesus, and gorillas). MPV is an enveloped dsDNA virus belonging to the Poxviridae family, and smallpox is also one of the most prevalent viruses in this family. Wildlife trafficking, habitat degradation, and climate change contribute to the transmission of MPV from new species to other species and increase the bond between people and animals. In the case of wildlife trafficking and illegal hunting, animals are caught, trapped, transported, and sold as food, medicine, and pets. Wildlife trade markets promote disease dissemination, making it possible for viruses from many neighboring species to jump the species barrier. Animal-to-human transmission is mediated by bites, scratches, and slaughtering. Human-to-human transmission occurs through close contact with infected people, such as through respiratory droplets and skin contact, especially MSM. The virus can remain on fomites, such as bedding, linen, and clothes.

(HCAI) reported, infection of healthcare workers has recently garnered attention. Prolonged exposure to patients increases the risk of infection among hospital staff and family members (2). According to the European Centre for Disease Prevention and Control, the 2021 incident in the UK was the first chain of transmission to be reported in Europe without epidemiological links with western and central Africa. It was also the first instance documented among males who had sex with men (MSM) (19). Infection preferentially occurs in gays, bisexuals, the MSM community, and other populations more susceptible to other sexually transmitted diseases, such as human immunodeficiency virus/acquired immunodeficiency syndrome (18, 20).

## 3 Pathophysiology

MPV can infect the human body through intradermal, mucosal, oropharyngeal, and nasopharyngeal routes after contact with susceptible people. After replication in the inoculated site for an appropriate 6-13 days, they spread to regional lymph nodes and then entered the circulation system (also called viremia) (21). The viruses in the blood infect host cells to spread to multiple sites and exhibit immunomodulation ability to escape immunosurveillance caused by horizontal gene transfer (22, 23). Although viral tropism in human tissue has not been well established, numerous animal models provide important clues regarding this scientific question. Osorio et al. detected MPV antigens in the lung, liver, heart, brain, kidney, ovarian, and pancreatic tissues of severely immunodeficient mice through immunohistochemical and histopathological tests (24). Moreover, the histopathological results of infected cynomolgus monkeys (*Macca fasicularis*) exhibited viral accumulation in the salivary epithelium, sebaceous and follicular tissue of the lip, especially in lymphoid tissues (25). Numerous animal reservoirs (e.g., dormice, prairie dogs, giant pouched rats) and various infected tissues reveal that MPV has a wide spectrum tropism, making it difficult to identify specific tissues as a site of infection (26).

MPV has structural and functional similarities to other OPVs. An exterior lipoprotein membrane with a geometric pattern of corrugations surrounds the virus's ovoid or brick-like particle (8). The outer membrane wraps around and protects a tight core and membrane bonds that contain linear double-stranded DNA (197 kb), transcription factors, and enzymes from external stress (27). The genes essential to housekeeping activities are situated in the middle area and are highly conserved, while the genes necessary for virus-host interactions (required for virulence) are found in the terminal area and are less conserved among OPVs (28–31). Although MPV is a DNA virus, its replication, assembly, and maturation are all completed in the cytoplasm of host cells (Figure 2). Furthermore, most of the characteristics of the life cycle of VACV are likely to be common to MPV even though the life cycle of MPV is not well understood (30). In VACV (and

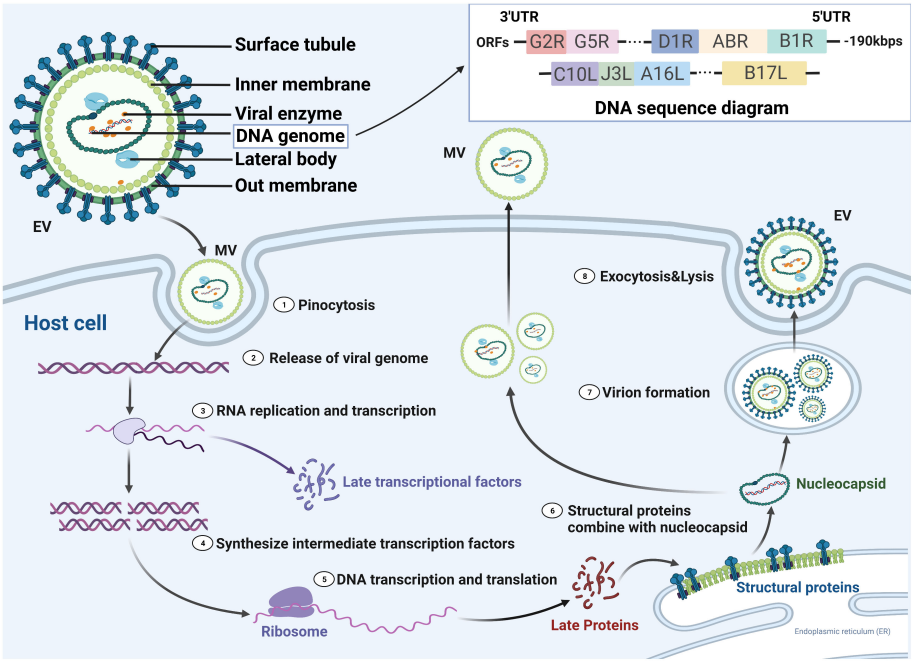


FIGURE 2
MPV life cycle in susceptible host cells. There are two forms of the virus, enveloped virion (EV) and mature virion (MV), which enter the host cell by fusion and micropinocytosis, respectively. MPV genomic structure and compositions are linear double-stranded DNA with nearly 190 kilobase pairs and contained more than 190 open reading frames (ORFs). 5′- and 3′- ends of the genome were inverted terminal repetitions, which formed hairpin-like structures. Double-stranded DNA is released and partially translated into early proteins that are processed into polymerases and immune modulators, while the others undergo replication in the cytoplasm. The resultant DNA partially transcripts into RNA, and the other part translates into intermediate proteins that are transformed into late transcription factors. Viral proteins translated from cytoplasmic RNA together with replicated DNA are assembled into nucleocapsid proteins and then processed into MVs and EVs, which are transported to the cell membrane for exocytosis. UTR, untranslated region.

probably most MPV), there are two types of infectious virions: intracellular mature virus (IMV) and extracellular-enveloped virus (EEV) generated from infected host cells (32, 33). IMVs enter the host cell through activation of macropinocytosis, while EEVs through membranous fusion (34). When compared to EEVs, which are hypothesized to facilitate viral dissemination within an infected host, IMVs are the more common infective type and mediate host-to-host transmission. For the EEVs, they continuously released from infected cells and are believed to spread locally from tissue to tissue through bodily fluids (35). Although the fact that the aforementioned characteristics are for VACV, they likely apply to all OPVs. Conversely, different agents exist among OPV species. Most OPVs like the cowpox virus evade immune function through downregulation of MHC expression of antigen-presenting cells such as monocytes. While MPV demonstrated the ability to inhibit T-cell responses against other viruses through anti-CD3 stimulation (36).

## 4 Global prevalence, from the past to present

Monkeypox is not a novel event and has been known as a zoonotic virus for more than 50 years. As mentioned earlier, in 1958, MPV was first found in an incidence of pox-like symptoms in monkeys at a shipment, which gives the name "monkeypox" (8). But now, it is inappropriate since MPV can infect various species and the majority of animal reservoirs are rodents, including giant pouched rats and squirrels. After the introduction of the virus by an imported animal trading company, there were at least 14 different kinds of rodents infected (37). Correspondingly, in 1970 a 9-month-old boy in the Bukenda village of the Zaire Equatorial region (now DRC) was documented to have the first human case (4). Since then, sporadic, intermittent cases of monkeypox limited in the African continent have been transmitted from local wild animals to humans. The accumulated cases are shown in Figure 3. From 1970 to 1979, 48 confirmed cases were detected in 6 African nations, including DRC (n=38), Cameroon (n = 1), Cote ˆ d'Ivoire (n = 1), Liberia (n = 4), Nigeria (n = 3), and Sierra Leone (n = 1) (18). In the 1980s, over 400 patients were documented, with an appropriate 10% fatality and a nine-fold increase in confirmed and probable cases recorded, and 14 infected patients were found in four additional African nations (38, 39). During the 1990s, 511 infected patients were found in DRC alone, and small outbreaks emerged across equatorial West and Central Africa (39). In 2003, 47 probable and confirmed patients of MPV infection were documented in six states of the USA who might have been exposed to prairie dogs kept as pets. The infected prairie dogs were kept in the same enclosure as Ghanaian small mammals. This was the first time that MPV occurred outside of Africa (40). From 2010 to 2019, increasing reports were documented in seven African nations (CAR, DRC, Cameroon, Nigeria, Liberia, Sierra Leone, and Republic of the Congo), the United Kingdom, Israel, and Singapore compared to past decades (39). On July 15, 2021, a patient with MPV traveling from Nigeria to the United States was found and controlled by the Texas Department of State Health Services and the CDC. More than 200 people contacted the patient and had the potential to be infected by this disease. Fortunately, there was no additional case in early September, and the contacted people were proven to be without MPV (18). However, in May 2022, a new monkeypox outbreak expanded in several countries on almost every continent. As of 14 July 2022, 1,856 laboratory-confirmed patients were documented in the UK. Among them, 12 were from Northern Ireland, 20 were from Wales, 46 were from Scotland, and 1,778 were from England (41). Given that the number of cases in the past few decades has already surpassed the whole number of infections in the first 40 years following the detection of monkeypox, it is apparent that the transmission rate of the disease is rapidly rising. The transmission between humans is increasing exponentially due to adoption by gene loss, instead of progressive mutation such as COVID-19 (42) (Table 1). This phenomenon is a reminder of the outbreak, indicating that prevention of monkeypox transmission and urgent treatment are essential.

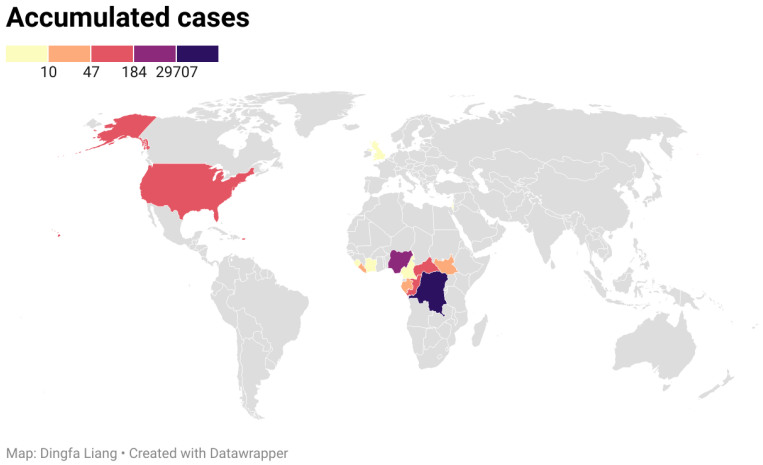


FIGURE 3
Accumulated cases of MPV from 1970 to 2020. The disease spread within 15 countries, with the Democratic Republic of the Congo being the worst hit area by the epidemic, followed by Nigeria.

TABLE 1 The differences between COVID-SARS CoV2 and Monkeypox.

| | Monkeypox | COVID-19 |
|---|---|---|
| Type of virus | Monkeypox virus (2) | SARS-CoV-2 (43) |
| Major transmission routes | Respiratory droplets and sexual contact (18) | Liquid droplets and contaminated contact (44) |
| Cell tropism | Lymphocytes, surface epithelia (45) | Respiratory epithelia and alveolar macrophages (46) |
| Genetic revolution | Gene loss (42) | Progressive mutation (47) |
| Incubation time | 6 to 13 days (21) | 2 to 14 days (48) |
| Major manifestations | Skin rash, fever, adenopathy and chills (38) | Fever, headache, nausea, cough, muscle pain, taste or smell loss, fatigue, proteinuria, hematuria, depression (43, 49) |
| Confirmed cases/ deaths | 85,536/91 (41) | 753,258,129/6,811,531 (50) |
| Treatments | Antiviral treatment: Tecovirimat, Cidofovir, Brincidofovir (51–53)<br>Vaccination: ACAM2000, VIGIV (54) | Antiviral treatment: Nirmatrelvir with Ritonavir, Remdesivir, Molnupiravir (55) |

SARS-CoV-2: severe acute respiratory syndrome coronavirus 2;
The number of total confirmed cases and deaths was up to February 1 in 2023.

MPV infection in humans is currently a growing public health concern as more than 85,000 clinical infections of MPV infection have been published in more than 100 different countries around the world, compared to only 48 cases in the 1970s (18). And the continuing monkeypox outbreak was regarded as a general populace crisis of international concern by the WHO on July 23, 2022 (56). As opposed to other outbreaks connected to travel from endemic nations or contact with animals transported in from the affected area, the infection source has not been identified as of yet (23). It was reported that patients with monkeypox in the current outbreak generally had close, prolonged physical contact with other monkeypox patients. During investigation, many reports documented that approximately 98% of these patients are gays, bisexuals, or other MSM (57–59). According to CDC data published on February 1, 2023, 84,243 cases were located in 103 distinct places that had never before recorded monkeypox, such as Spain (7,528 cases) and Germany (3,692 cases) (60) (Figure 4). A total of 1,293 human patients were documented in 7 places where monkeypox was historically reported, such as Nigeria (775 cases) and the DRC (348 cases). The total number of MPV cases reached 85,536 on February 1 in 2023, with the most of cases accumulating in Europe, the USA, and South America (41) (Table 2).

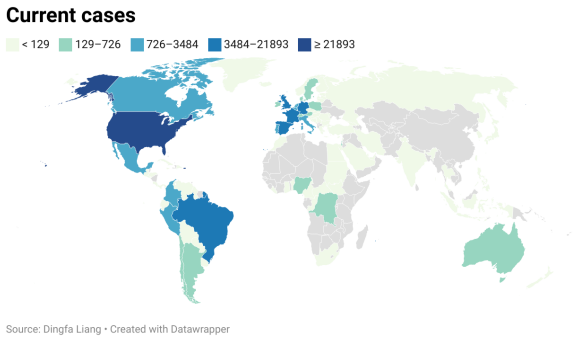


FIGURE 4
Current cases of MPVX from 1 Jan. to 9 Sep. 2022. More than 57,000 human cases spread globally in more than 100 locations. The United States of America was the worst-hit area, with 2,1893 cases.

# 5 Clinical manifestations

From infection to the beginning of clinical manifestations, the incubation period of MPV was estimated to be 12 days and may extend to 21 days in some cases (40). The first signs or symptoms of patients include rash, fever, cough, headache, nausea and/or vomiting, confusion, wheezing, chills, sweats, runny nose, red eyes, stiff neck, lymphadenopathy, shortness of breath, sore throat, joint pain, back pain, chest pain, abdominal pain, myalgia, and conjunctivitis (38) (Table 3). It was reported that patients initially presented with signs or symptoms, such as rash (97%), fever (85%), adenopathy (71%), and chills (71%), which constituted the initial syndrome of MPV infection. The fever lasted for an average of 8 days (range: 2-13 days), and the rash continued for an average of 12 days (range: 7-24 days). The median time interval between the start of the fever and the appearance of the rash was 2 days (range: 0-12 days). Other signs and symptoms were evident between 0 and 14 days after the onset of fever or rash (62) (Figure 5).

## 5.1 End organ diseases

### 5.1.1 Skin mucous membranes

The rashes with various sizes appear within 1 to 5 days following the commencement of the fever, initially on the face and then spreading to include the hands, feet, and legs (69). The rash progresses through several stages, from spots and papules to blisters (fluid-filled blisters) and pustules, before gradually going away as crusts and scabs wear off over time (38). Sixty-eight percent of patients had monomorphic lesions, and 48% of patients had centrifugally distributed lesions. Ulcerative or necrotic lesions are

10.3389/fimmu.2023.1132250

TABLE 2 The current cases of MPV until 1 Feb. 2023 (41).

| Country | Total confirmed cases |
|---|---|
| Central African Republic | 20 |
| Ghana | 121 |
| Cameroon | 18 |
| Democratic Republic of the Congo | 348 |
| Republic of the Congo | 5 |
| Liberia | 6 |
| Nigeria | 775 |
| Aruba | 3 |
| Andorra | 4 |
| United Arab Emirates | 16 |
| Argentina | 1,075 |
| Australia | 144 |
| Austria | 327 |
| Belgium | 793 |
| Benin | 3 |
| Bulgaria | 6 |
| Bahrain | 1 |
| Bahamas | 2 |
| Bosnia and Herzegovina | 9 |
| Bermuda | 1 |
| Bolivia | 264 |
| Brazil | 10,745 |
| Barbados | 1 |
| Canada | 1,460 |
| Switzerland | 551 |
| Chile | 1,416 |
| China | 1 |
| Colombia | 4,072 |
| Costa Rica | 140 |
| Cuba | 8 |
| Curaçao | 3 |
| Cyprus | 5 |
| Czechia | 71 |
| Germany | 3,692 |
| Denmark | 196 |
| Dominican Republic | 52 |
| Ecuador | 483 |
| Egypt | 3 |
| Spain | 7,528 |
| Estonia | 11 |
| Finland | 42 |
| France | 4,128 |
| United Kingdom | 3,735 |
| Georgia | 2 |
| Gibraltar | 6 |
| Guadeloupe | 1 |
| Greece | 86 |
| Greenland | 2 |
| Guatemala | 348 |
| Guyana | 2 |
| Hong Kong | 1 |
| Honduras | 13 |
| Croatia | 33 |
| Hungary | 80 |
| Indonesia | 1 |
| India | 22 |
| Ireland | 228 |
| Iran | 1 |
| Iceland | 16 |
| Israel | 262 |
| Italy | 954 |
| Jamaica | 18 |
| Jordan | 1 |
| Japan | 15 |
| South Korea | 4 |
| Lebanon | 26 |
| Sri Lanka | 2 |
| Lithuania | 5 |
| Luxembourg | 57 |
| Latvia | 6 |
| Saint Martin | 1 |
| Morocco | 3 |
| Monaco | 3 |
| Moldova | 2 |
| Mexico | 3,768 |
| Malta | 33 |
| Montenegro | 2 |
| Mozambique | 1 |

(Continued)

(Continued)

10.3389/fimmu.2023.1132250

TABLE 2 Continued

| Country | Total confirmed cases |
|---|---|
| Martinique | 7 |
| New Caledonia | 1 |
| Netherlands | 1,260 |
| Norway | 95 |
| New Zealand | 41 |
| Panama | 118 |
| Peru | 3,727 |
| Philippines | 4 |
| Poland | 215 |
| Portugal | 951 |
| Paraguay | 82 |
| Qatar | 5 |
| Romania | 47 |
| Russia | 2 |
| Saudi Arabia | 8 |
| Sudan | 18 |
| Singapore | 21 |
| El Salvador | 88 |
| San Marino | 1 |
| Serbia | 40 |
| Slovakia | 14 |
| Slovenia | 47 |
| Sweden | 260 |
| Thailand | 13 |
| Turkey | 12 |
| China | 4 |
| Ukraine | 5 |
| Uruguay | 19 |
| United States | 30,123 |
| Venezuela | 12 |
| Vietnam | 2 |
| South Africa | 5 |

reported in 25% of patients, with a very small number presenting as hemorrhagic pustules (62). Different stages of the rash may appear simultaneously, and areas of skin erythema or hyperpigmentation are usually found as discrete lesions (70). Once the prodromal symptoms or rash appear, patients are considered infectious until the lesion crusts and the crusts fall off (71).

### 5.1.2 Blood

Recent studies have shown that in addition to lymphocytopenia and thrombocytopenia observed in over one-third of evaluable patients, leukocytosis, low blood urea nitrogen levels, high transaminase levels, and hypoalbuminemia are common symptoms during the disease (72, 73). Only 2 MPV individuals had hemorrhagic pustular lesions, according to a review of 34 verified patients in the USA. Disseminated intravascular coagulation has not been reported by any individuals, and the thrombocytopenia was typically minor (40).

### 5.1.3 Lymph

Despite the symptoms and lesions of monkeypox being difficult to distinguish from those of smallpox, the sign and symptoms of MPV infection are less severe. Up to 90% of MPV patients suffered from lymphadenopathy, which is thought to be a clinical characteristic that separates human monkeypox from smallpox (74). The appearance of swollen lymph nodes, especially in the inguinal, submental, submandibular, and cervical nodes, distinguishes monkeypox from smallpox and chickenpox (75). Meanwhile, the lymphatogenous spread of MPV caused by viremia affects the skin, spleen, thymus, oral mucosa, reproductive system, and gastrointestinal tract in monkeys that have been experimentally infected with aerosolized MPV (26).

### 5.1.4 Gastrointestinal tract

According to case studies, MPV-infected individuals also suffer from gastrointestinal disorders, including vomiting, diarrhea, and dehydration (40). Infected individuals with mucosal and gastrointestinal clinical manifestations may require volume replenishment due to gastrointestinal losses caused by poor nutritional balance or negative protein. Gastrointestinal fluid losses and hypoalbuminemia are associated with the fluid transfer from intravascular to extravascular compartments that takes place in systemic illness (76).

### 5.1.5 Genitals

A rash normally begins on the face but can extend to other tissues, including the genitalia (19). According to the European Centre for Disease Prevention and Control, many cases in the ongoing outbreak are associated with sexual contact, particularly with men who were identified as gay, bisexual, or males who have sex with other men (58). Furthermore, the transmission of viruses can be achieved *via* sharing clothing and bedding as well as being directly exposed to infectious ulcers, scar tissue, or bodily fluids (19). Although less severe, the symptoms of monkeypox are similar to those of smallpox and consist of a characteristic rash that is preceded by mild prodromal manifestations (including lymphadenopathy, fever, and flu-like symptoms) (7). The cases in the present outbreak are characterized by a distinct rash that begins in the vaginal and perianal regions and extends to other parts of the human body with or without it (40).

TABLE 3 Laboratory/clinical manifestations in MPV patients.

| Organ system involved | Laboratory/clinical manifestation |
|---|---|
| Blood | • lymphocytosis, leukocytosis, and thrombocytopenia (40)<br>• hypoalbuminemia, low blood urea nitrogen level, and high transaminase levels (40)<br>• hemorrhagic pustular lesions (61)<br>• significant loss of intravascular volume (61) |
| Lymph | • swollen lymph nodes (62)<br>• affects the oral mucosa, skin, thymus, spleen, reproductive system, and gastrointestinal tract by spread from viremia (63) |
| Gastrointestinal | • vomiting, diarrhea, and dehydration (54)<br>• hypoalbuminemia and gastrointestinal fluid losses (40) |
| Skin mucous membranes | • rash, spots, papules, blisters and pustules (9)<br>• areas of erythema or hyperpigmentation of the skin<br>• ulcerative or necrotic lesions (64) |
| Genitals | • rash (7)<br>• infectious sores (7)<br>• spread by sexual contact (65) |
| Brain/Neurological | • encephalitis<br>• headache (66) |
| Lung/Respiratory Pulmonary | • massive retropharyngeal abscess (67)<br>• compromised tracheal airway (61) |
| Eyes | • keratitis and corneal ulceration (68) |

### 5.1.6 Other clinical complications

A series of complications reported that 5 cases were identified as severely ill, and 9 cases were hospitalized as inpatients in the United States. Among those cases hospitalized as inpatients, a 6 years old child with encephalitis required intubation and mechanical breathing, while a 10-year-old girl with severe cervical lymphadenopathy and a retropharyngeal abscess had a constructed tracheal airway (77, 78). The intensive care units were allowed for these two patients. In addition, there was a patient with comorbidity (hepatitis C) who had a serious illness and was kept in the hospital as an inpatient. The individual is fully rehabilitated without experiencing any negative consequences. One adult with infection-related issues was found to

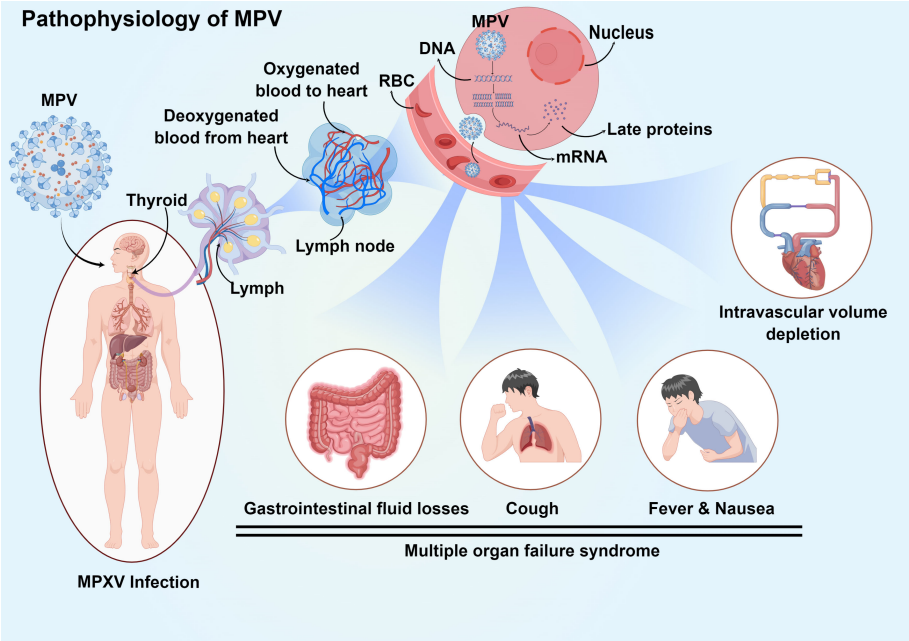


FIGURE 5
Pathophysiology and clinical manifestation of systemic MPV infection. Infection initiates in the upper respiratory tract and progresses to lymph, and then the virus enters the bloodstream through lymphocytes. The MPV in the blood spreads through the circulatory system to all parts of the body, enters the cell through endocytosis, releases DNA, and uses the substances in the cell to transcribe proteins, finally affecting the normal physiological function of the cell. MPV causes lymphocytosis and leukocytosis, thrombocytopenia, elevated aminotransferase levels, and decreased blood urea nitrogen levels. At the same time, symptoms such as multiorgan inflammation and cough and fever also occur.

have bacterial superinfection (unknown microorganism) (79), while another had keratitis and corneal erosion, which eventually necessitated a corneal transplant (40). There was no underlying medical condition in any of these patients. These cases show that monkeypox can cause a range of complications in addition to direct disease. This further illustrates the dangers of monkeypox and the need for prevention and control and provides another way of thinking about reducing the dangers of monkeypox, namely, the prevention of complications.

### 5.2 Diagnosis

Tests for diagnosing diseases are of vital importance for the confirmation of MPV infection. Medical history, clinical symptoms, and laboratory tests all contribute to the diagnosis of MPV infection. The enlargement of the lymph nodes is the most typical symptom that separates monkeypox from diseases such as smallpox and chickenpox, which also present with rash symptoms, while confirmation of monkeypox also requires laboratory test assistance (80). Swabs are used to collect crusts or exudates from the infective site to isolate viral nucleic acids for diagnostic purposes. This is followed by an MPV genome-specific real-time polymerase chain reaction (RT-PCR) assay to detect viral DNA (71). Moreover, western blot (WB) analysis using MPV proteins can also be used to confirm MPV infection. WB has lower requirements for detection equipment or laboratories and the detection results are more accurate, but there are some limitations compared with RT-PCR. Such as infection cannot be detected until 7 days after the infection; Blood collection is required and the operation is relatively difficult; not suitable for application to the large-scale collection, etc. (81, 82). So according to the WHO, the preferred test for identifying MPV during acute infection is the RT-PCR test (83). If the mother is infected by MPV, the fetus requires ultrasound surveillance to determine if he/she is infected with MPV by examining the existence of ultrasound anomalies such as fetal hepatomegaly or hydrops (84).

## 6 Treatments

Most people recover from the disease without treatment and the symptoms of monkeypox are typically mild (54). Despite the lack of specific therapies for monkeypox, studies have shown that the smallpox vaccine has an 85% success rate in preventing monkeypox. Furthermore, several antiviral drugs may also be effective in treating monkeypox infections (63) (Table 4).

### 6.1 Smallpox vaccine (ACAM2000)

The US CDC has approved the use of ACAM2000 in emergencies, and it can offer 85% cross-protective resistance against monkeypox (54). Patients must be informed of the abnormal risk of fetal vaccinia by ACAM2000 if high-risk monkeypox exposure occurs during pregnancy. Fetal vaccinia can cause stillbirth, neonatal death, premature delivery, and possibly unfavorable maternal reactions (94). The third-generation MVA-BN (Modified Vaccinia Ankara-Bavarian Nordic) smallpox vaccine, which has received universal approval within the EU, Canada, and the USA, may be gentler because it comprises the virus that cannot replicate and has not been proven to cause problems during pregnancy (95).

### 6.2 Tecovirimat (TPOXX/ST-246)

Tecovirimat (TPOXX/ST-246), an FDA-approved antiviral medicine, is used to alleviate both pediatric and adult patients with human smallpox illnesses. It acts as a suppressor of the OPV VP37 envelope protein and can be administered as a pill or injection (51). The capsule can be opened and the drug mixed with semisolid food for kids under the weight of 12.9 kilograms (96). Although studies on numerous animal species have shown that tecovirimat is beneficial in treating diseases brought on by OPVs, it is still unclear if tecovirimat is effective in treating human monkeypox infections. One case study was an adult patient who received tecovirimat and made a full recovery after spending a month in the hospital (97), while in another case study, a patient underwent oral tecovirimat (200 mg twice a day for two weeks) treatment without experiencing any negative side effects (67). The CDC has an enhanced access protocol, also known as a "compassionate use" approach, that allows the application of tecovirimat for the mitigation of monkeypox when an outbreak occurs (98, 99).

### 6.3 Vaccinia immune globulin intravenous

The FDA has authorized the use of VIGIV, a hyperimmune globulin, to treat the side effects of vaccinia-related conditions such as progressive vaccinia, severe generalized vaccinia, *dermatitis vaccinatum*, vaccinia infections in persons with skin issues, and abnormal infections brought on by VACV (except in cases of isolated keratitis). The application of VIGIV for the therapy of OPVs outbreak such as monkeypox is permitted by the CDC's expanded access protocol (100). Although it is a potential strategy, there is little data on how VIGIV acts against smallpox and monkeypox, and the utilization of VIGIV for smallpox or monkeypox has not been tested in humans. However, in extreme circumstances, medical professionals might consider their use incurring monkeypox. Notably, individuals with severely compromised T-cell functionality should not be vaccinated against the MPV. Instead, VIGIV may be administered to them if they have a history of exposure (101).

### 6.4 Cidofovir (Vistide)

The antiviral medicine Cidofovir (Vistide), which blocks viral DNA polymerase from functioning, has been proven to be effective against poxviruses *in vitro* and in preclinical studies (52). It is an antiviral medication that the FDA has approved for use in treating cytomegalovirus (CMV) retinitis in AIDS patients. The

TABLE 4 A list of treatments for monkeypox management.

| Treatments | Route | Dosing | Biologic and/or clinical efficacy | Adverse events | Contraindications | Use in specific populations |
|---|---|---|---|---|---|---|
| Vaccinia Immune Globulin Intravenous | IV | Adults:6000 U/kg (9000 U/kg might be taken into consideration if the patient doesn't respond to the first dose); Pediatrics: Children should not use this medication because it has not been proven safe and effective in people under the age of 18 (7). | Passive immunity is provided by antibodies derived from the combined human plasma of people who have received the smallpox vaccination (85) | Dizziness, rigors, nausea, headache (86) | An IgA deficit with antibodies against IgA, a history of IgA hypersensitivity, a history of severe systemic or anaphylactic reactions to human globulins, and isolated vaccinia keratitis (7). | Use caution in pregnant women and patients with renal insufficiency (52, 86). |
| Tecovirimat | PO, IV | For adults, take 600 mg twice daily for 14 days. For children (13 kg to less than 25 kg), take 200 mg BID for 14 days. For those between 25 and 40 kg, take 400 mg BID for 14 days. For those over 40 kg, take 800 mg BID for 14 days. 14 days at 600 mg twice a day (87). | Restrain orthopoxvirus VP37 envelope wrapping protein (88). | Headache, nausea, abdominal pain, vomiting (89). | Have not reported. | PO: Hepatic/ renal adjustment not needed. IV: should not be administered to patients with severe renal impairment (87). |
| Cidofovir | IV | 5 mg/kg once weekly for two weeks, followed by 5 mg/kg IV once every other week (90). | Selectively inhibits orthopoxvirus DNA polymerase-mediated viral DNA synthesis by cellular phosphorylation (53). | Diarrhea, nausea, vomiting, and abdominal pain (86). | Serum creatinine > 1.5 mg/dL; urine protein ≥ 100 mg/dL (≥ 2+ proteinuria); history of clinically severe hypersensitivity to probenecid or other sulfa-containing drugs; CrCl ≤ 55 mL/minute (87). | It is required to change the dosage based on renal function (91). |
| Brincidofovir | PO | Adults over 48 kg should take 200 mg once per week in two doses. Adults and pediatric patients between 10 kg and 48 kg should take 4 mg/kg of oral suspension once per week in two doses. Pediatric patients under 10 kg should take 6 mg/kg of oral suspension once per week in two doses (92). | Cidofovir diphosphate selectively inhibits orthopoxvirus DNA polymerase-mediated viral DNA synthesis (93). | Fever, infection, proteinuria, iritis, hypotony of the eye, decreased serum bicarbonate, uveitis, neutropenia, nephrotoxicity (87) | Have not reported. | Not recommended in pregnant and breast-feeding women. |

BID twice a day, IV intravenous, PO per os (orally), CrCl creatinine clearance, and DNA deoxyribonucleic acid.

effectiveness of Cidofovir in treating monkeypox in people is not well understood. However, investigations on animals and *in vitro* have shown that it is effective against OPVs (102). To mitigate OPV (including monkeypox) in an outbreak, the CDC has an enhanced access protocol that permits the utilization of stocked cidofovir. Cidofovir treatment may be implemented in cases with severe monkeypox infection, although it is unknown whether such a patient will benefit from it. Cidofovir may be less safe than Brincidofovir since Cidofovir can cause serious renal damage or other side effects (90). Currently, the CDC is working on an Expanded Access Investigational New Drugs to enable the drugs to be used for the treatment of monkeypox. They could pick the CMX-001 medication, a modified version of cidofovir, which has demonstrated antiviral activity against OPV species but lacks the level of nephrotoxicity typically associated with cidofovir (103).

## 6.5 Brincidofovir (Tembexa)

On June 4, 2021, FDA licensed Brincidofovir (Tembexa) as an antiviral drug to alleviate human smallpox in newborns, children, and adults. Although the small numbers involved make it difficult to extrapolate the effectiveness of Brincidofovir in the therapy of monkeypox infection, their efficacy against OPV has been illustrated *in vitro* and animal models (53, 104). However, a review of patients enrolled since the launch of the HCID (airborne) network between August 15, 2018, and September 10, 2021, revealed that all 3 adult patients receiving oral Brincidofovir (200 mg once a week) had high hepatic enzymes, which led to the termination of therapy (67). The CDC is now working on an EA-IND (Expanded Access Investigational New Drug) to make it easier to utilize Brincidofovir as a monkeypox treatment.

## 7 Conclusion and future perspectives

Monkeypox is no longer "a viral zoonotic disease that occurs mainly in remote portions of Central and West Africa, near tropical rainforests", as the expansion of the disease over the past several years and the ongoing outbreak (105). Although most MPV infections cause self-limited and mild diseases, with supportive treatment being relatively sufficient, there is no specific therapy available for it to date, and it can be transmitted in a variety of ways, such as droplets, contact, and sexual contact. Its possibility for additional regional and worldwide spread is therefore still a serious concern. The majority of information on the illness is gathered from individual cases or outbreak reports, as well as from passive sporadic monitoring, none of which provides a complete overview. To effectively lead data collection, prevention, preparedness, response and surveillance efforts for monkeypox and other emerging or re-emerging diseases with pandemic possibility, there is still an urgent need to improve surveillance and public health skills.

Numerous antiviral drugs that may be beneficial in the mitigation of monkeypox were authorized for the treatment of smallpox based on model studies, such as Tecovirimat, VIGIV, Cidofovir, and Brincidofovir, but the efficacy of these agents has not been completely characterized; thus, more research on these therapies in humans is needed. In addition, there are several variables can affect the prognosis of monkeypox, such as prior vaccination records, baseline health state, and co-occurring illnesses or comorbidities. Therefore, the most sensible course of action is to design treatments specifically for each patient in accordance with their likelihood of contracting a severe illness.

## Author contributions

Conceptualization and design: XL and PY; data acquisition and writing-original draft preparation, LN and DL; data analysis and interpretation: JZ and ZL; revision for intellectual content: all authors. All authors agree to be accountable for all aspects of the work. All authors contributed to the article and approved the submitted version.

## Acknowledgments

This work was supported by the Natural Science Foundation of Jiangxi Province [grant numbers 20192ACBL21037, 202004BCJL23049 and 202002BAB216022], the National Natural Science Foundation of China [grant number 82160371, 82100869, 21866019, and 82100347], the China Postdoctoral Science Foundation [grant number 2021M703724], the Natural Science Foundation of Guangdong Province [grant number 2022A1515010582], and the Science and Technology Projects in Guangzhou [grant number 202102010007]. The graphical abstracts were created with BioRender, Figdraw and Datawrapper software (biorender.com, Figdraw.com and datawrapper.de).

## Conflict of interest

The authors declare that the research was conducted in the absence of any commercial or financial relationships that could be construed as a potential conflict of interest.

## Publisher's note



## References

1. Lai CC, Hsu CK, Yen MY, Lee PI, Ko WC, Hsueh PR. Monkeypox: An emerging global threat during the COVID-19 pandemic. *J Microbiol Immunol Infect* (2022) 55 (5):787–94. doi: 10.1016/j.jmii.2022.07.004

2. Nolen LD, Osadebe L, Katomba J, Likofata J, Mukadi D, Monroe B, et al. Extended human-to-Human transmission during a monkeypox outbreak in the democratic republic of the Congo. *Emerg Infect Dis* (2016) 22(6):1014–21. doi: 10.3201/eid2206.150579

3. Falendysz EA, Lopera JG, Lorenzsonn F, Salzer JS, Hutson CL, Doty J, et al. Further assessment of monkeypox virus infection in Gambian pouched rats (Cricetomys gambianus) using *In vivo* bioluminescent imaging. *PloS Negl Trop Dis* (2015) 9(10):e0004130. doi: 10.1371/journal.pntd.0004130

4. Marennikova SS, Seluhina EM, Mal'ceva NN, Cimiskjan KL, Macevic GR. Isolation and properties of the causal agent of a new variola-like disease (monkeypox) in man. *Bull World Health Organ* (1972) 46(5):599–611.

5. 2022 monkeypox outbreak global map. Available at: https://www.cdc.gov/poxvirus/monkeypox/response/2022/world-map.html2022.

6. Huang YA, Howard-Jones AR, Durrani S, Wang Z, Williams PC. Monkeypox: A clinical update for paediatricians. *J Paediatr Child Health* (2022) 58(9):1532–8. doi: 10.1111/jpc.16171

7. Rizk JG, Lippi G, Henry BM, Forthal DN, Rizk Y. Prevention and treatment of monkeypox. *Drugs* (2022) 82(9):957–63. doi: 10.1007/s40265-022-01742-y

8. Cho CT, Wenner HA. Monkeypox virus. *Bacteriol Rev* (1973) 37(1):1–18. doi: 10.1128/br.37.1.1-18.1973

9. Luo Q, Han J. Preparedness for a monkeypox outbreak. *Infect Med* (2022) 1 (2):124–34. doi: 10.1016/j.imj.2022.07.001

10. Marennikova SS, Shelukhina EM. Whitepox virus isolated from hamsters inoculated with monkeypox virus. *Nature* (1978) 276(5685):291–2. doi: 10.1038/276291a0

11. Marennikova SS, Shelukhina EM, Maltseva NN, Matsevich GR. Monkeypox virus as a source of whitepox viruses. *Intervirology* (1979) 11(6):333–40. doi: 10.1159/000149055

12. Nakazawa Y, Mauldin MR, Emerson GL, Reynolds MG, Lash RR, Gao J, et al. A phylogeographic investigation of African monkeypox. *Viruses* (2015) 7(4):2168–84. doi: 10.3390/v7042168

13. Parker S, Buller RM. A review of experimental and natural infections of animals with monkeypox virus between 1958 and 2012. *Future Virol* (2013) 8(2):129–57. doi: 10.2217/fvl.12.130

14. Thakur S, Kelkar D, Garg S, Raina SK, Lateef F, Gilada I, et al. Why should RNA viruses have all the fun - monkeypox, a close relative of smallpox and a DNA virus. *J Glob Infect Dis* (2022) 14(2):47–9. doi: 10.4103/jgid.jgid_104_22

15. Angelo KM, Petersen BW, Hamer DH, Schwartz E, Brunette G. Monkeypox transmission among international travellers-serious monkey business? *J Travel Med* (2019) 26(5):taz002. doi: 10.1093/jtm/taz002

16. Grant R, Nguyen LL, Breban R. Modelling human-to-human transmission of monkeypox. *Bull World Health Organ* (2020) 98(9):638–40. doi: 10.2471/BLT.19.242347

17. Lansiaux E, Jain N, Laivacuma S, Reinis A. The virology of human monkeypox virus (hMPXV): A brief overview. *Virus Res* (2022) 322:198932. doi: 10.1016/j.virusres.2022.198932

18. Kumar N, Acharya A, Gendelman HE, Byrareddy SN. The 2022 outbreak and the pathobiology of the monkeypox virus. *J Autoimmun* (2022) 102855. doi: 10.1016/j.jaut.2022.102855

19. Mahase E. Monkeypox: What do we know about the outbreaks in Europe and north America? *BMJ* (2022) 377:o1274. doi: 10.1136/bmj.o1274

20. Inigo Martinez J, Gil Montalban E, Jimenez Bueno S, Martin Martinez F, Nieto Julia A, Sanchez Diaz J, et al. Monkeypox outbreak predominantly affecting men who have sex with men, Madrid, Spain, 26 April to 16 June 2022. *Euro Surveill* (2022) 27 (27):2200471. doi: 10.2807/1560-7917.ES.2022.27.27.2200471

21. Zhu F, Li L, Che D. Monkeypox virus under COVID-19: Caution for sexual transmission - correspondence. *Int J Surg* (2022) 104:106768. doi: 10.1016/j.ijsu.2022.106768

22. McFadden JWBaG. Origin and evolution of poxviruses. *Origin and Evolution of Viruses* (*Second* Edition) Chapter 19. (2008) 431–46. doi: 10.1016/B978-0-12-374153-0.00019-9

23. Velavan TP, Meyer CG. Monkeypox 2022 outbreak: An update. *Trop Med Int Health* (2022) 27(7):604–5. doi: 10.1111/tmi.13785

24. Thomassen HA, Fuller T, Asefi-Najafabady S, Shiplacoff JA, Mulembakani PM, Blumberg S, et al. Pathogen-host associations and predicted range shifts of human monkeypox in response to climate change in central Africa. *PloS One* (2013) 8(7): e66071. doi: 10.1371/journal.pone.0066071

25. Osorio JE, Iams KP, Meteyer CU, Rocke TE. Comparison of monkeypox viruses pathogenesis in mice by *in vivo* imaging. *PloS One* (2009) 4(8):e6592. doi: 10.1371/journal.pone.0006592

26. Zaucha GM, Jahrling PB, Geisbert TW, Swearengen JR, Hensley L. The pathology of experimental aerosolized monkeypox virus infection in cynomolgus monkeys (Macaca fascicularis). *Lab Invest* (2001) 81(12):1581–600. doi: 10.1038/labinvest.3780373

27. Kugelman JR, Johnston SC, Mulembakani PM, Kisalu N, Lee MS, Koroleva G, et al. Genomic variability of monkeypox virus among humans, democratic republic of the Congo. *Emerg Infect Dis* (2014) 20(2):232–9. doi: 10.3201/eid2002.130118

28. Esposito JJ, Knight JC. Orthopoxvirus DNA: a comparison of restriction profiles and maps. *Virology* (1985) 143(1):230–51. doi: 10.1016/0042-6822(85)90111-4

29. Takemura M. Poxviruses and the origin of the eukaryotic nucleus. *J Mol Evol* (2001) 52(5):419–25. doi: 10.1007/s002390010171

30. Remichkova M. Poxviruses: Smallpox vaccine, its complications and chemotherapy. *Virus Adaptat. Treat* (2010) 2:41–6. doi: 10.2147/VAAT.S8563

31. Moss B. The molecular biology of poxviruses. *Mol Bas. Viral Replicat* (1987) 136:499–516. doi: 10.1007/978-1-4684-5350-8_21

32. Alakunle E, Moens U, Nchinda G, Okeke MI. Monkeypox virus in Nigeria: Infection biology, epidemiology, and evolution. *Viruses* (2020) 12(11):1257–87. doi: 10.3390/v12111257

33. Schmidt FI, Bleck CK, Mercer J. Poxvirus host cell entry. *Curr Opin Virol* (2012) 2(1):20–7. doi: 10.1016/j.coviro.2011.11.007

34. Schmelz M, Sodeik B, Ericsson M, Wolffe EJ, Shida H, Hiller G, et al. Assembly of vaccinia virus: The second wrapping cisterna is derived from the trans golgi network. *J Virol* (1994) 68(1):130–47. doi: 10.1128/jvi.68.1.130-147.1994

35. Smith GL, Murphy BJ, Law M. Vaccinia virus motility. *Annu Rev Microbiol* (2003) 57:323–42. doi: 10.1146/annurev.micro.57.030502.091037

36. Hammarlund E, Dasgupta A, Pinilla C, Norori P, Fruh K, Slifka MK. Monkeypox virus evades antiviral CD4+ and CD8+ T cell responses by suppressing cognate T cell activation. *Proc Natl Acad Sci U S A* (2008) 105(38):14567–72. doi: 10.1073/pnas.0800589105

37. Hutson CL, Davidson W, Regnery RL, Reynolds MG, Li YU, Damon IK, et al. Monkeypox zoonotic associations: Insights from laboratory evaluation of animals associated with the multi-state us outbreak. *Am J Trop Med Hygiene* (2007) 76(4):757–68. doi: 10.4269/ajtmh.2007.76.757

38. Meyer H, Perrichot M, Stemmler M, Emmerich P, Schmitz H, Varaine F, et al. Outbreaks of disease suspected of being due to human monkeypox virus infection in the democratic republic of Congo in 2001. *J Clin Microbiol* (2002) 40(8):2919–21. doi: 10.1128/JCM.40.8.2919-2921.2002

39. Bunge EM, Hoet B, Chen L, Lienert F, Weidenthaler H, Baer LR, et al. The changing epidemiology of human monkeypox-a potential threat? A systematic review. *PloS Negl Trop Dis* (2022) 16(2):e0010141. doi: 10.1371/journal.pntd.0010141

40. Huhn GD, Bauer AM, Yorita K, Graham MB, Sejvar J, Likos A, et al. Clinical characteristics of human monkeypox, and risk factors for severe disease. *Clin Infect Dis* (2005) 41(12):1742–51. doi: 10.1086/498115

41. 2022 monkeypox outbreak global map. Available at: https://www.cdc.gov/poxvirus/monkeypox/response/2022/world-map.html2022.

42. Hendrickson RC, Wang C, Hatcher EL, Lefkowitz EJ. Orthopoxvirus genome evolution: the role of gene loss. *Viruses* (2010) 2(9):1933–67. doi: 10.3390/v2091933

43. Machhi J, Herskovitz J, Senan AM, Dutta D, Nath B, Oleynikov MD, et al. The natural history, pathobiology, and clinical manifestations of SARS-CoV-2 infections. *J Neuroimmune Pharmacol* (2020) 15(3):359–86. doi: 10.1007/s11481-020-09944-5

44. Anfinrud P, Stadnytskyi V, Bax CE, Bax A. Visualizing speech-generated oral fluid droplets with laser light scattering. *N Engl J Med* (2020) 382(21):2061–3. doi: 10.1056/NEJMc2007800

45. Guarner J, Johnson BJ, Paddock CD, Shieh WJ, Goldsmith CS, Reynolds MG, et al. Monkeypox transmission and pathogenesis in prairie dogs. *Emerg Infect Dis* (2004) 10(3):426–31. doi: 10.3201/eid1003.030878

46. Yuki K, Fujiogi M, Koutsogiannaki S. COVID-19 pathophysiology: A review. *Clin Immunol* (2020) 215:108427. doi: 10.1016/j.clim.2020.108427

47. Amoutzias GD, Nikolaidis M, Tryfonopoulou E, Chlichlia K, Markoulatos P, Oliver SG. The remarkable evolutionary plasticity of coronaviruses by mutation and recombination: Insights for the COVID-19 pandemic and the future evolutionary paths of SARS-CoV-2. *Viruses* (2022) 14(1):78–102. doi: 10.3390/v14010078

48. Backer JA, Klinkenberg D, Wallinga J. Incubation period of 2019 novel coronavirus (2019-nCoV) infections among travellers from wuhan, China, 20-28 January 2020. *Euro Surveill* (2020) 25(5):2000062. doi: 10.2807/1560-7917.ES.2020.25.5.2000062

49. Martinez-Rojas MA, Vega-Vega O, Bobadilla NA. Is the kidney a target of SARS-CoV-2? *Am J Physiol Renal Physiol* (2020) 318(6):F1454–F62. doi: 10.1152/ajprenal.00160.2020

50. WHO. *Weekly epidemiological update on COVID-19 - 1 February 2023* (2023). Available at: https://www.who.int/publications/m/item/weekly-epidemiological-update-on-covid-19—1-february-2023.

51. Russo AT, Grosenbach DW, Chinsangaram J, Honeychurch KM, Long PG, Lovejoy C, et al. An overview of tecovirimat for smallpox treatment and expanded anti-orthopoxvirus applications. *Expert Rev Anti Infect Ther* (2021) 19(3):331–44. doi: 10.1080/14787210.2020.1819791

52. Lanier R, Trost L, Tippin T, Lampert B, Robertson A, Foster S, et al. Development of CMX001 for the treatment of poxvirus infections. *Viruses* (2010) 2 (12):2740–62. doi: 10.3390/v2122740

53. Smee DF. Progress in the discovery of compounds inhibiting orthopoxviruses in animal models. *Antivir Chem Chemother* (2008) 19(3):115–24. doi: 10.1177/095632020801900302

54. Reynolds MG, McCollum AM, Nguete B, Shongo Lushima R, Petersen BW. Improving the care and treatment of monkeypox patients in low-resource settings: Applying evidence from contemporary biomedical and smallpox biodefense research. *Viruses* (2017) 9(12):380–94. doi: 10.3390/v9120380

55. Atmar RL, Finch N. New perspectives on antimicrobial agents: Molnupiravir and Nirmatrelvir/Ritonavir for treatment of COVID-19. *Antimicrob Agents Chemother* (2022) 66(8):e0240421. doi: 10.1128/aac.02404-21

56. See KC. Vaccination for monkeypox virus infection in humans: A review of key considerations. *Vaccines (Basel)* (2022) 10(8):1342–54. doi: 10.3390/vaccines10081342

57. Control ECfDPa. epidemiological update: Monkeypox outbreak. Available at: https://www.ecdc.europa.eu/en/news-events/epidemiological-update-monkeypox-outbreak2022.

58. Thornhill JP, Barkati S, Walmsley S, Rockstroh J, Antinori A, Harrison LB, et al. Monkeypox virus infection in humans across 16 countries - April-June 2022. *N Engl J Med* (2022) 387(8):679–91. doi: 10.1056/NEJMoa2207323

59. Philpott D, Hughes CM, Alroy KA, Kerins JL, Pavlick J, Asbel L, et al. Epidemiologic and clinical characteristics of monkeypox cases - united states, may 17-July 22, 2022. *MMWR Morb Mortal Wkly Rep* (2022) 71(32):1018–22. doi: 10.15585/mmwr.mm7132e3

60. CDC. 2022 monkeypox outbreak global map. Available at: https://www.cdc.gov/poxvirus/monkeypox/response/2022/world-map.html2022.

61. Adnan N, Haq ZU, Malik A, Mehmood A, Ishaq U, Faraz M, et al. Human monkeypox virus: An updated review. *Med (Baltimore)* (2022) 101(35):e30406. doi: 10.1097/MD.0000000000030406

62. Jezek Z, Szczeniowski M, Paluku KM, Mutombo M. Human monkeypox: clinical features of 282 patients. *J Infect Dis* (1987) 156(2):293–8. doi: 10.1093/infdis/156.2.293

63. Kmiec D, Kirchhoff F. Monkeypox: A new threat? *Int J Mol Sci* (2022) 23 (14):7866. doi: 10.3390/ijms23147866

64. de Sousa D, Patrocínio J, Frade J, Brazão C, Mancha D, Correia C, et al. Monkeypox diagnosis by cutaneous and mucosal findings. *Infect Dis Rep* (2022) 14 (5):759–64. doi: 10.3390/idr14050077

65. Lapa D, Carletti F, Mazzotta V, Matusali G, Pinnetti C, Meschi S, et al. Monkeypox virus isolation from a semen sample collected in the early phase of infection in a patient with prolonged seminal viral shedding. *Lancet Infect Dis* (2022) 22 (9):1267–9. doi: 10.1016/S1473-3099(22)00513-8

66. Shafaati M, Zandi M. Monkeypox virus neurological manifestations in comparison to other orthopoxviruses. *Travel Med Infect Dis* (2022) 49:102414. doi: 10.1016/j.tmaid.2022.102414

67. Adler H, Gould S, Hine P, Snell LB, Wong W, Houlihan CF, et al. Clinical features and management of human monkeypox: A retrospective observational study in the UK. *Lancet Infect Dis* (2022) 22(8):1153–62. doi: 10.1016/S1473-3099(22)00228-6

68. Abdelaal A, Serhan HA, Mahmoud MA, Rodriguez-Morales AJ, Sah R. Ophthalmic manifestations of monkeypox virus. *Eye (Lond)* (2022) 37(3):383–5. doi: 10.1038/s41433-022-02195-z

69. Petersen E, Kantele A, Koopmans M, Asogun D, Yinka-Ogunleye A, Ihekweazu C, et al. Human monkeypox: Epidemiologic and clinical characteristics, diagnosis, and prevention. *Infect Dis Clin North Am* (2019) 33(4):1027–43. doi: 10.1016/j.idc.2019.03.001

70. Singhal T, Kabra SK, Lodha R. Monkeypox: A review. *Indian J Pediatr* (2022) 89 (10):955–60. doi: 10.1007/s12098-022-04348-0

71. Pastula DM, Tyler KL. An overview of monkeypox virus and its neuroinvasive potential. *Ann Neurol* (2022) 92(4):527–31. doi: 10.1002/ana.26473

72. Haviland JW. Purpura variolosa; its manifestations in skin and blood. *Yale J Biol Med* (1952) 24(6):518–24.

73. McKenzie PJ, Githens JH, Harwood ME, Roberts JF, Rao AR, Kempe CH. Haemorrhagic smallpox. 2. specific bleeding and coagulation studies. *Bull World Health Organ* (1965) 33(6):773–82.

74. Gordon SN, Cecchinato V, Andresen V, Heraud JM, Hryniewicz A, Parks RW, et al. Smallpox vaccine safety is dependent on T cells and not b cells. *J Infect Dis* (2011) 203(8):1043–53. doi: 10.1093/infdis/jiq162

75. Osadebe L, Hughes CM, Shongo Lushima R, Kabamba J, Nguete B, Malekani J, et al. Enhancing case definitions for surveillance of human monkeypox in the democratic republic of Congo. *PloS Negl Trop Dis* (2017) 11(9):e0005857. doi: 10.1371/journal.pntd.0005857

76. Bone RC. The pathogenesis of sepsis. *Ann Intern Med* (1991) 115(6):457–69. doi: 10.7326/0003-4819-115-6-457

77. Sejvar JJ, Chowdary Y, Schomogyi M, Stevens J, Patel J, Karem K, et al. Human monkeypox infection: A family cluster in the midwestern united states. *J Infect Dis* (2004) 190(10):1833–40. doi: 10.1086/425039

78. Anderson MG, Frenkel LD, Homann S, Guffey J. A case of severe monkeypox virus disease in an American child: Emerging infections and changing professional values. *Pediatr Infect Dis J* (2003) 22(12):1093–6. discussion 6-8. doi: 10.1097/01.inf.0000101821.61387.a5

79. Mailhe M, Beaumont AL, Thy M, Le Pluart D, Perrineau S, Houhou-Fidouh N, et al. Clinical characteristics of ambulatory and hospitalised patients with monkeypox virus infection: An observational cohort study. *Clin Microbiol Infect* (2022) 29(2):233–9. doi: 10.1016/j.cmi.2022.08.012

80. Macneil A, Reynolds MG, Braden Z, Carroll DS, Bostik V, Karem K, et al. Transmission of atypical varicella-zoster virus infections involving palm and sole manifestations in an area with monkeypox endemicity. *Clin Infect Dis* (2009) 48(1):e6–8. doi: 10.1086/595552

81. Adalja A, Inglesby T. A novel international monkeypox outbreak. *Ann Internal Med* (2022) 175(8):1175–6. doi: 10.7326/M22-1581

82. Huggett JF, French D, O'Sullivan DM, Moran-Gilad J, Zumla A. Monkeypox: Another test for PCR. *Euro Surveill* (2022) 27(32):2200497. doi: 10.2807/1560-7917.ES.2022.27.32.2200497

83. Pal M, Singh R, Gutama KP, Savalia CV, Thakur R. Human monkeypox: An emerging and re-emerging infectious viral disease. *Acta Sci Microbiol* (2022) 5:146–50. doi: 10.31080/ASMI.2022.05.1045

84. Dashraath P, Nielsen-Saines K, Mattar C, Musso D, Tambyah P, Baud D. Guidelines for pregnant individuals with monkeypox virus exposure. *Lancet* (2022) 400 (10345):21–2. doi: 10.1016/S0140-6736(22)01063-7

85. O'Shea J FT, Morris SB, Weiser J, Petersen B, Brooks JT. Interim guidance for prevention and treatment of monkeypox in persons with HIV infection - United States, August 2022. *MMWR Morb Mortal Wkly Rep* (2022) 71(32):1023–28. doi: 10.15585/mmwr.mm7132e4

86. Dashraath P, Nielsen-Saines K, Rimoin A, Mattar CNZ, Panchaud A, Baud D. Monkeypox in pregnancy: Virology, clinical presentation, and obstetric management. *Am J Obstet Gynecol* (2022) 227(6):849–61. doi: 10.1016/j.ajog.2022.08.017

87. Siegrist EA, Sassine J. Antivirals with activity against monkeypox: A clinically oriented review. *Clin Infect Dis* (2022) 76(1):155–64. doi: 10.1093/cid/ciac622

88. Akazawa D, Ohashi H, Hishiki T, Morita T, Iwanami S, Kim KS, et al. Potential anti-monkeypox virus activity of atovaquone, mefloquine, and molnupiravir, and their potential use as treatments. *bioRxiv* (2022). doi: 10.1101/2022.08.02.502485

89. Matias WR, Koshy JM, Nagami EH, Kovac V, Moeng LR, Shenoy ES, et al. Tecovirimat for the treatment of human monkeypox: An initial series from Massachusetts, united states. *Open Forum Infect Dis* (2022) 9(8):ofac377. doi: 10.1093/ofid/ofac377

90. Chittick G, Morrison M, Brundage T, Nichols WG. Short-term clinical safety profile of brincidofovir: A favorable benefit-risk proposition in the treatment of smallpox. *Antiviral Res* (2017) 143:269–77. doi: 10.1016/j.antiviral.2017.01.009

91. Andrei G, Snoeck R. Cidofovir activity against poxvirus infections. *Viruses* (2010) 2(12):2803–30. doi: 10.3390/v2122803

92. Islam MR, Hossain MJ, Roy A, Hasan A, Rahman MA, Shahriar M, et al. Repositioning potentials of smallpox vaccines and antiviral agents in monkeypox outbreak: A rapid review on comparative benefits and risks. *Health Sci Rep* (2022) 5(5): e798. doi: 10.1002/hsr2.798

93. Chan-Tack K, Harrington P, Bensman T, Choi SY, Donaldson E, O'Rear J, et al. Benefit-risk assessment for brincidofovir for the treatment of smallpox: U.S. food and drug administration's evaluation. *Antiviral Res* (2021) 195:105182. doi: 10.1016/j.antiviral.2021.105182

94. Mbala PK, Huggins JW, Riu-Rovira T, Ahuka SM, Mulembakani P, Rimoin AW, et al. Maternal and fetal outcomes among pregnant women with human monkeypox infection in the democratic republic of Congo. *J Infect Dis* (2017) 216(7):824–8. doi: 10.1093/infdis/jix260

95. Khalil A, Samara A, O'Brien P, Morris E, Draycott T, Lees C, et al. Monkeypox vaccines in pregnancy: Lessons must be learned from COVID-19. *Lancet Global Health* (2022) 10(9):e1230–e1. doi: 10.1016/S2214-109X(22)00284-4

96. Gountia IA, Mati P. Monkey pox: A ambient review of transmission, improving care and treatments. *Int Res J Modern. Eng Technol Sci* (2022) 04(Issue:07):July–2022.

97. Rao AK, Schulte J, Chen TH, Hughes CM, Davidson W, Neff JM, et al. Monkeypox in a traveler returning from Nigeria - Dallas, Texas, July 2021. *MMWR Morb Mortal Wkly Rep* (2022) 71(14):509–16. doi: 10.15585/mmwr.mm7114a1

98. Laudisoit A, Tepage F, Colebunders R. Oral tecovirimat for the treatment of smallpox. *N Engl J Med* (2018) 379(21):2084–5. doi: 10.1056/NEJMc1811044

99. Quenelle DC, Buller RM, Parker S, Keith KA, Hruby DE, Jordan R, et al. Efficacy of delayed treatment with ST-246 given orally against systemic orthopoxvirus infections in mice. *Antimicrob Agents Chemother* (2007) 51(2):689–95. doi: 10.1128/AAC.00879-06

100. Wittek R. Vaccinia immune globulin: Current policies, preparedness, and product safety and efficacy. *Int J Infect Dis* (2006) 10(3):193–201. doi: 10.1016/j.ijid.2005.12.001

101. Nalca A, Rimoin AW, Bavari S, Whitehouse CA. Reemergence of monkeypox: prevalence, diagnostics, and countermeasures. *Clin Infect Dis* (2005) 41(12):1765–71. doi: 10.1086/498155

102. Rice AD, Adams MM, Wallace G, Burrage AM, Lindsey SF, Smith AJ, et al. Efficacy of CMX001 as a post exposure antiviral in new Zealand white rabbits infected with rabbitpox virus, a model for orthopoxvirus infections of humans. *Viruses* (2011) 3 (1):47–62. doi: 10.3390/v3010047

103. Parker S, Handley L, Buller RM. Therapeutic and prophylactic drugs to treat orthopoxvirus infections. *Future Virol* (2008) 3(6):595–612. doi: 10.2217/17460794.3.6.595

104. Baker RO, Bray M, Huggins JW. Potential antiviral therapeutics for smallpox, monkeypox and other orthopoxvirus infections. *Antiviral Res* (2003) 57(1-2):13–23. doi: 10.1016/S0166-3542(02)00196-1

105. Sklenovska N, Van Ranst M. Emergence of monkeypox as the most important orthopoxvirus infection in humans. *Front Public Health* (2018) 6:241. doi: 10.3389/fpubh.2018.00241

frontiers | Frontiers in Immunology

TYPE Original Research
PUBLISHED 22 May 2023
DOI 10.3389/fimmu.2023.1196031



OPEN ACCESS

EDITED BY
Yuejin Liang,
University of Texas Medical Branch at Galveston, United States

REVIEWED BY
Tomohisa Tanaka,
University of Yamanashi, Japan
Huibin Yu,
Yale University, United States

*CORRESPONDENCE
Ning-yi Jin
ningyik@126.com
Hui-jun Lu
huijun_lu@126.com
Wen-chao Sun
sunwenchao131@163.com

†These authors have contributed equally to this work and share first authorship

RECEIVED 29 March 2023
ACCEPTED 09 May 2023
PUBLISHED 22 May 2023

CITATION
Huang H-x, Zhao C-c, Lei X-x, Zhang X-y, Li Y-y, Lan T, Zhao B-p, Lu J-y, Sun W-c, Lu H-j and Jin N-y (2023) Swine acute diarrhoea syndrome coronavirus (SADS-CoV) Nsp5 antagonizes type I interferon signaling by cleaving DCP1A. *Front. Immunol.* 14:1196031. doi: 10.3389/fimmu.2023.1196031



# Swine acute diarrhoea syndrome coronavirus (SADS-CoV) Nsp5 antagonizes type I interferon signaling by cleaving DCP1A

Hai-xin Huang[1,2†], Chen-chen Zhao[2†], Xiao-xiao Lei[2], Xin-yu Zhang[2], Yu-ying Li[2], Tian Lan[2], Bao-peng Zhao[2], Jing-yi Lu[2], Wen-chao Sun[2*], Hui-jun Lu[3*] and Ning-yi Jin[1,3*]

[1]College of Veterinary Medicine, Northwest A&F University, Xianyang, China, [2]Institute of Virology, Wenzhou University, Wenzhou, China, [3]Changchun Institute of Veterinary Medicine, Chinese Academy of Agricultural Sciences, Changchun, China

Swine acute diarrhoea syndrome coronavirus (SADS-CoV), which is a recently discovered enteric coronavirus, is the major aetiological agent that causes severe clinical diarrhoea and intestinal pathological damage in pigs, and it has caused significant economic losses to the swine industry. Nonstructural protein 5, also called 3C-like protease, cleaves viral polypeptides and host immune-related molecules to facilitate viral replication and immune evasion. Here, we demonstrated that SADS-CoV nsp5 significantly inhibits the Sendai virus (SEV)-induced production of IFN-β and inflammatory cytokines. SADS-CoV nsp5 targets and cleaves mRNA-decapping enzyme 1a (DCP1A) via its protease activity to inhibit the IRF3 and NF-κB signaling pathways in order to decrease IFN-β and inflammatory cytokine production. We found that the histidine 41 and cystine 144 residues of SADS-CoV nsp5 are critical for its cleavage activity. Additionally, a form of DCP1A with a mutation in the glutamine 343 residue is resistant to nsp5-mediated cleavage and has a stronger ability to inhibit SADS-CoV infection than wild-type DCP1A. In conclusion, our findings reveal that SADS-CoV nsp5 is an important interferon antagonist and enhance the understanding of immune evasion by alpha coronaviruses.

KEYWORDS

**swine acute diarrhoea syndrome coronavirus (SADS-CoV), interferon signaling, mRNA-decapping enzyme 1a (DCP1A), nonstructural protein 5 (nsp5), antiviral activity**

## Introduction

Swine acute diarrhoea syndrome coronavirus (SADS-CoV) is also known as swine enteric alphacoronavirus (SeACoV) or porcine enteric alpha coronavirus (PEAV), and it is a novel HKU2-related bat coronavirus that belongs to the alpha coronavirus family. SADS-CoV was first discovered during a catastrophic epidemic in pigs in Guangdong Province,

China, in 2017, which led to the death of nearly 24,500 newborn piglets and caused significant economic losses (1–3). In 2018, seven pig farms in Fujian Province reported the presence of a new SADS-CoV strain in pig stool and small intestine samples (4). In 2019, the re-emergence of SADS-CoV infection in pig herds in southern China resulted in an outbreak of diarrhoea that caused approximately 2000 piglet deaths (5). An outbreak of a fatal swine diarrhoea disease occurred on an intensive-scale pig farm in Guangxi, China, in May 2021, and it led to more than 3000 deaths in piglets. The clinical symptoms of infected animals include severe acute diarrhoea, vomiting, and weight loss, and the mortality rate can reach 100% (6). SADS-CoV has been reported to infect a wide variety of cell lines in culture, including cell lines derived from its natural hosts (bats, monkeys, cats, dogs, minks, hamsters), susceptible hosts (pigs), and potential hosts (humans and other animals) (7, 8). Chickens are susceptible to infection with SADS-CoV under laboratory conditions, suggesting that chickens may be asymptomatic carriers of SADS-CoV and that the virus has the potential to spread to susceptible flocks near pig farms (9).

The full-length genome of SADS-CoV is approximately 27 kb in length, and it is arranged in the order of 5'UTR-ORF1a/1b-S-NS3-E-M-N-NS7a-NS7b-3'UTR. ORF1a and ORF1b encode polyprotein 1a (pp1a) and polyprotein 1b (pp1b), respectively, and pp1a and pp1b are processed into 16 nonstructural proteins (Nsp1-16) that are responsible for viral RNA synthesis. Maturation of viral proteins requires cleavage by proteases. Nonstructural protein 5 (nsp5), which is a 3 chymotrypsin-like protease ($3CL^{pro}$, also called main protease), is an attractive drug target because it can recognize sequences containing Leu and Gln at positions P2 and P1 and play an important role in cleaving viral polyproteins to generate functional proteins (10, 11). To date, there are still no effective vaccination strategies or antiviral drugs to control SADS-CoV infection. The development of more effective control measures will be made easier with a better understanding of the mechanisms by which SADS-CoV evades the host immune system.

Interferons (IFNs) are a broad class of cytokines that are elicited upon challenge to host defences, and they are essential for mobilizing immune responses to pathogens and activating signal transduction cascades that lead to the induction of hundreds of interferon-stimulated genes (ISGs). As ISGs play important roles in antiviral responses, viruses develop strategies to counteract their functions (12). mRNA-decapping enzyme 1a (DCP1A), which is a regulatory factor that is involved in removing the 5'-methylguanosine cap from eukaryotic mRNAs, has recently been identified as an IFN-stimulated gene. The study suggested that DCP1A phosphorylation modulates the host chemokine response to respiratory syncytial virus (RSV) infection (13). The study reported that porcine reproductive and respiratory syndrome virus (PRRSV) infection significantly downregulates DCP1A expression at the protein level by cleaving DCP1A, and PRRSV nsp4 is responsible for DCP1A cleavage, specifically at glutamic acid 238 (E238) of DCP1A (14). Porcine delta coronavirus (PDCoV) nsp5 cleaves porcine DCP1A via its protease activity and cleaves DCP1A at glutamine 343 (Q343) (10). Severe acute respiratory syndrome coronavirus 2 (SARS-CoV-2) nsp5 inhibits HDAC-dependent ISG antiviral responses and abolishes the activity of the ISG effector DCP1A (15).

Currently, there are few reports about the pathogenesis of SADS-CoV, and there are no relevant reports about whether SADS-CoV nsp5 contributes to the escape of SADS-CoV from innate immune responses and whether it plays roles in SADS-CoV pathogenesis and transmission. And there is no effective vaccine or antiviral drug for SADS-CoV. The nsp5 of SADS-CoV provides an excellent target for antivirals, due to its essentialand conserved function in the viral replication cycle. In this study, we found that SADS-CoV nsp5 antagonized IFN-β production and targeted DCP1A, thus impairing the antiviral activity of DCP1A. Additionally, nsp5 from different CoVs cleaves DCP1A, suggesting a common mechanism underlying immune evasion. It may be possible to gain a better understanding of SADS-CoV disease pathogenesis and transmission by elucidating the mechanism underlying nsp5-mediated catalysis and IFN antagonism.

# Materials and methods

## Cell culture and virus

HEK-293T cells, LLC-PK1 cells, IPEC-J2 cells, Vero-E6 cells and ST cells were maintained in Dulbecco's modified Eagle medium (DMEM) (HyClone, Logan, UT, USA) supplemented with 10% foetal bovine serum (FBS, Gibco, Grand Island, NY, USA) and penicillin–streptomycin at 37°C in a 5% $CO_2$ atmosphere. The SADS-CoV strain was previously preserved in our laboratory. SADS-CoV was diluted in DMEM supplemented with 10 mg/mL trypsin and inoculated into Vero-E6 cells, which were replaced with fresh DMEM medium containing 2% FBS after 2 h. Vesicular stom atitis virus carrying the green fluorescent protein gene (VSV-GFP) and Sendai virus (SeV) were previously preserved in our laboratory.

## Plasmids, siRNA and transfection

Nsp5 from SADS-CoV was cloned into a pCAGGS-FLAG vector. Full-length cDNA sequences of *sus scrofa* (pig) DCP1A (GenBank accession number NM_001244358.1), *Homo sapiens* (human) DCP1A (GenBank accession number NM_001290204.2), and *Chlorocebus sabaeus* (green monkey) (GenBank accession number XM_007984575.2) were cloned into a pXJ40-HA vector. Full-length cDNA sequences of porcine IFIT1, IFIT3 and IFIT5 was also cloned into a pXJ40-HA vector. Vectors expressing P65, IKBKE, TRAF3, MDA-5, STAT1, STAT2, RIG-I, NEMO, IKKα, IKKβ, IκBα, IRF3 were purchased from HonorGene. *Homo sapiens* DCP1A small interfering RNAs (siRNAs) were designed and purchased from Tsingke Biotech (Beijing, China), together with the control siRNA. The constructs were transfected using Lipofectamine 3000 Reagent (Invitrogen) and siRNAs were transfected using Lipofectamine RNAi MAX (Invitrogen) according to procedures recommended by the manufacturer.

## Antibodies and reagents

A DYKDDDDK Tag(9A3) mouse mAb (#8146), HA-Tag (C29F4) rabbit mAb (#3724), phospho-NF-κB P65 (Ser536) rabbit mAb (#3033), phospho-IRF-3 (Ser386) rabbit mAb (#37829), Lamin A/C rabbit antibody (#2032), anti-mouse IgG(H+L), F(ab')$_2$ fragment (Alexa Fluor 488 Conjugate) (#4408), anti-rabbit IgG (H+L), and F (ab')$_2$ fragment (Alexa Fluor® 594 Conjugate) (#8889) were purchased from Cell Signaling Technology (CST, Boston, MA, USA). A phospho-TBK1 (Ser172) rabbit antibody (#AF8190), phospho-IκBα (Ser32/Ser36) rabbit antibody (#AF2002), phospho-STAT1 (Tyr701) rabbit antibody (#AF3300), TBK1 rabbit antibody (#DF7026), phospho-STAT2 (Tyr690) antibody (#AF3342) were purchased from Affinity Biosciences (Cincinnati, OH, USA). A DCP1A rabbit mAb was purchased from ABclonal (#A6824) (Wuhan, China). A RSAD2 rabbit polyclonal antibody (#28089-1-AP), HRP-conjugated AffiniPure donkey anti-rabbit IgG (H+L) (#SA00001-9), IRF3 rabbit polyclonal antibody (#11312-1-AP), STAT1 rabbit polyclonal antibody (#10144-2-AP), STAT2 rabbit polyclonal antibody (#16674-1-AP), IKBKG rabbit polyclonal antibody (#18474-1-AP), NF-κB P65 rabbit polyclonal antibody (#10745-1-AP), His-Tag mouse monoclonal antibody (#66005-1-Ig), GAPDH monoclonal antibody (#60004-1-Ig), and HRP-conjugated AffiniPure goat anti-mouse IgG (H+L) were purchased from Proteintech Group (Rosemont, IL, USA). Z-VAD(OMe)-FMK (#T6013), PF-00835231 (#T9458), 3-MA (#T1879), and MG132 (#T2154) were purchased from Target Mol (Boston, USA). Poly(I:C) (#P1530) was purchased from Sigma–Aldrich (St. Louis, MO, USA), ProteinIso® Protein A/G Resin (#DP501), and the TransDetect® Double-Luciferase Reporter Assay Kit (#FR201) were purchased from TransGen Biotech (Beijing, China). The UNlQ-10 Column TRIzol Total RNA Isolation Kit was purchased from Sangon Biotech (#B511321) (Shanghai, China). PrimeScript™ RT Master Mix (Perfect Real Time) was purchased from TaKaRa (#RR037A) (Beijing, China). Taq Pro Universal SYBR qPCR Master Mix was purchased from Vazyme (#Q702) (Nanjing, China).

## Dual-luciferase reporter activity assays

When the cell confluence in 12-well plates reached approximately 80%, HEK-293T or ST cells were cotransfected with the reporter plasmid (IFN-β-Luc) at 0.2 μg/well and the plasmid pRL-TK (internal control for normalization of the transfection efficiency) at 0.01 μg/well with Lipofectamine 3000 reagent. After transfection for 24 h, the cells were lysed. Then, the levels of firefly luciferase and Renilla luciferase were measured using the Dual-Luciferase reporter assay system. The data are shown as the relative firefly luciferase activities normalized to the Renilla luciferase activities from three independent experiments.

## Confocal immunofluorescence assay

LLC-PK1 cells were transfected with porcine DCP1A, SADS-CoV nsp5 or nsp14 expression vectors. After 24 h, the cells were fixed with 4% paraformaldehyde for 20 min and then permeabilized with 0.1% Triton-X 100 in PBS. Then, the cells were incubated with 3% BSA in PBS for 2 h at room temperature. LLC-PK1 cells were then stained with the DYKDDDDK Tag(9A3) mouse mAb and DCP1A rabbit mAb diluted in 1% BSA in PBS at 4°C overnight. The cells were then incubated with fluorochrome-conjugated secondary Abs for 2 h at room temperature. After incubation with the secondary Abs, the specimens were covered with DAPI and incubated for 6 min to stain the nuclei. The images were collected by forwarding fluorescence microscopy and confocal microscopy.

## RNA isolation and quantitative PCR analysis

Total RNA was extracted from cultured cells using TRIzol reagent and reverse transcribed into cDNA using reverse transcriptase. Quantitative real-time PCR (RT–qPCR) experiments were performed in triplicate. Relative mRNA expression levels were normalized to the expression level of GAPDH. All the RT–qPCR experiments were performed using Taq Pro Universal SYBR qPCR Master Mix and an ABI QuantStudio 3 Real-time PCR system.

## Western blotting analysis

HEK-293T cells were transfected with the indicated plasmids as mentioned above, harvested after 30 h by the addition of lysis buffer, and incubated on ice for 15 min. The cell lysates were centrifuged at 12,000 × g for 15 min before the supernatants were either subjected to immunoprecipitation (IP) or directly denatured at 100°C for 10 min. The denatured cell lysates were separated by SDS–PAGE and transferred to PVDF membranes using a Trans-Blot® SD Semi-Dry Electrophoretic Transfer cell at 15 V for 50 min. For immunoblotting, the indicated primary antibodies were incubated with the membranes for 2 h at room temperature or overnight at 4°C; HRP-conjugated goat anti-mouse or goat anti-rabbit IgG were used as secondary antibodies. The bands were visualized with chemiluminescent reagent (NCM Biotech, Shanghai, China) and were imaged by an ECL imaging system (Bio-Rad, Hercules, CA, USA). GAPDH expression in each sample was used as a control to demonstrate equal loading of the protein samples across lanes.

## Coimmunoprecipitation assay

HEK-293T cells were seeded in 10 cm dishes, transfected with the indicated plasmids as mentioned above and lysed at 30 h posttransfection in 1 mL lysis buffer per dish. The lysates were centrifuged at 14,000 × g for 15 min, and the supernatants were subjected to IP, with 100 μL reserved for use as a whole cell lysate (WCL) control. Briefly, ProteinIso® Protein A/G Resin was added to 400 μL of cell lysate and incubated on a shaker at 4°C for 1 h. The mixture was centrifuged at 1,000 × g for 5 min, and the supernatant was extracted. Then, 2 μL of antibody was added to 400 μL of cell lysate and incubated on a shaker at 4°C overnight. Then,

ProteinIso® Protein A/G Resin (#DP501, TransGen Biotech, Beijing, China), which had been washed with lysis buffer three times, was added. The mixture was centrifuged at 1,000 × g for 5 min, and the sample was collected and washed in lysis buffer three times at 1,000 × g for 5 min. Next, the beads were mixed with 1× loading buffer, and the mixture was denatured at 100°C for 10 min before analysis along with the WCL by Western blotting.

## Statistical analysis

The data were analysed with GraphPad Prism 9 software, and Student's t-test were performed to determine significance. The data are expressed as the mean ± standard deviation (SD) of three independent experiments. *P* values < 0.05 were considered statistically significant.

# Results

## SADS-CoV antagonizes type I IFN and inflammatory cytokine production

Several coronaviruses have been reported to inhibit type I IFN production in order to evade host innate immunity (16–19). To investigate the effects of SADS-CoV infection on the expression of IFN-β and inflammatory cytokines in swine testicular (ST) cells, the mRNA expression levels of various factors were measured after viral infection. As shown in Figure 1A, compared with those in the control group, the SeV-induced mRNA expression levels of IFN-β, TNF-α, CXCL10, RIG-I, ISG15, RSAD2, ISG56, and IFIT3 were significantly inhibited by SADS-CoV. Next, we infected Vero-E6, IPEC-J2, and LLC-PK1 cells with SADS-CoV and analysed the proliferation of the virus and the copy number of the N gene by RT−qPCR (Figure 1B). We also measured the expression of the SADS-CoV N protein (Figure 1C). The results showed that the replication of viral genes and the expression of the N protein significantly increased with the time of infection.

## SADS-CoV nsp5 suppresses the type I IFN and NF-κB signaling pathways

SeV infection strongly induced IFN-β promoter activity. However, transfection with nsp5 strongly inhibited the SeV-induced IFN-β promoter activity in HEK-293T, ST, and LLC-PK1 cells in a dose-dependent manner (Figures 2A–C). To assess the role of SADS-CoV nsp5 in regulating type I IFN signaling, we evaluated the mRNA levels of IFN-β, RIG-I, ISG15, RSAD2, ISG56, and IFIT3 after transfection of HEK-293T, ST, and LLC-PK1 cells with SADS-CoV nsp5. As shown in Figure 2D, compared with the control group, the transcription of ISGs induced by SeV was significantly inhibited by SADS-CoV nsp5. The role of nsp5 in regulating inflammatory cytokine signaling pathways was also evaluated. We

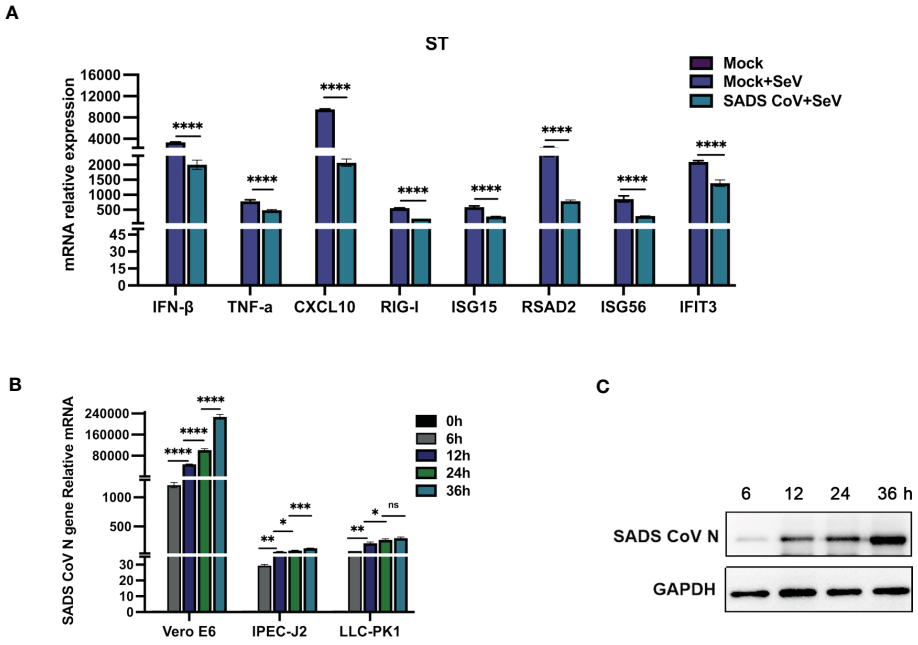


FIGURE 1
SADS-CoV antagonizes type I IFN and inflammatory cytokine production. **(A)** ST cells were cultured in 6-well plates infected with SADS-CoV. After 24 h, the cells were infected with 0.1 MOI SeV for an additional 12 h IFN-β, TNF-α, CXCL10, RIG-I, ISG15, RSAD2, ISG56, and IFIT3 mRNA levels were analysed by RT–qPCR. **(B)** Vero-E6, IPEC-J2, LLC-PK1 cells were infected with the SADS-CoV strain (MOI=0.1) and then harvested at 0 h, 6 h, 12 h, 24 h and 36 h to measure SADS-CoV N mRNA levels by RT–qPCR. **(C)** Vero-E6 cells (MOI=0.1) were infected with the SADS-CoV strain at 6 h, 12 h, 24 h and 36 h Cell lysates were analysed by Western blotting with anti-SADS-CoV N protein antibodies. All data are reported as mean±SD. For all experiments, *p < 0.05, **p < 0.01, and ***p < 0.001, ****p < 0.0001 were considered to be statistically significant. ns, nonsignificant differences in data.

10.3389/fimmu.2023.1196031

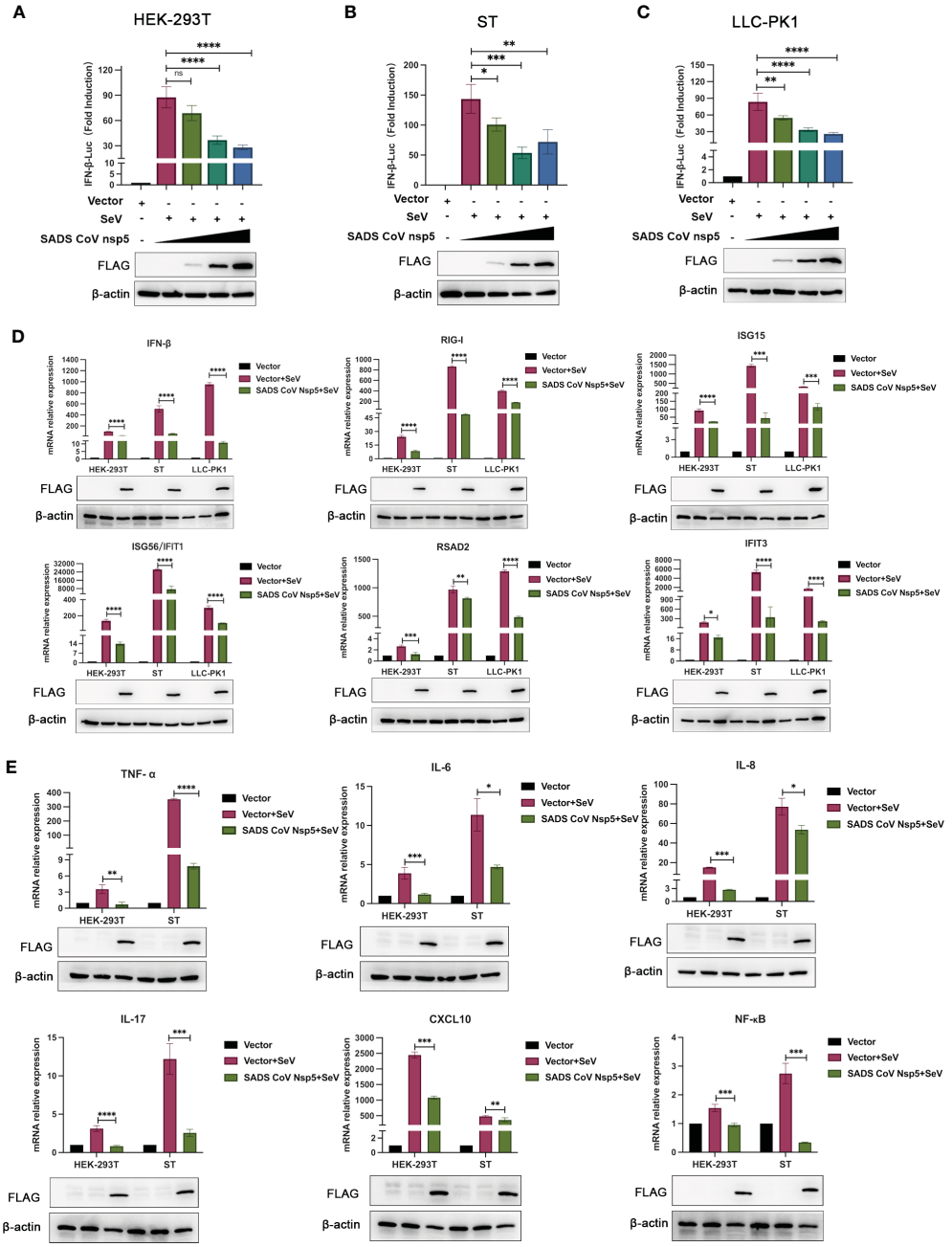


FIGURE 2
SADS-CoV nsp5 inhibits SeV-induced IFN-β and inflammatory cytokine production. **(A)** HEK-293T cells, **(B)** ST cells, or **(C)** LLC-PK1 cells were cotransfected with IFN-β Luc and pRL-TK plasmids, along with 1μg, 1.5 μg and 2.5μg of the SADS-CoV nsp5 plasmid for 24 h. Then, the cells were infected with or without SeV for 12 h. The cells were lysed and subjected to a dual-luciferase assay. And the expressions of SADS-CoV nsp5 protein and β-actin were detected by Western blot. **(D)** HEK-293T cells, ST cells and LLC-PK1 cells were transfected with 1.5 μg of the SADS-CoV nsp5 plasmid or an empty vector. After 24 h of initial transfection, the cells were further infected or mock infected with SEV. The cells and supernatants were collected at 12 h post infection, and the IFN-β, RIG-I, ISG15, RSAD2, ISG56, IFIT1, and IFIT3 mRNA levels were analysed by RT–qPCR. **(E)** HEK-293T cells and ST cells were transfected with 1.5 μg of the SADS-CoV nsp5 plasmid or an empty vector. After 24 h of initial transfection, the cells were further infected or mock infected with SEV. The cells and supernatants were collected at 12 h post infection, and the TNF-α, IL-6, IL-8, IL-17, CXCL10, and NF-κB mRNA levels were analysed by RT–qPCR. And the expressions of SADS-CoV nsp5 protein and β-actin were detected by Western blot. All data are reported as mean±SD. For all experiments, *p < 0.05, **p < 0.01, and ***p < 0.001, ****p < 0.0001 were considered to be statistically significant. ns, nonsignificant differences in data.

evaluated the mRNA levels of TNF-α, IL-6, IL-8, IL-17, CXCL10, and NF-κB after transfection of HEK-293T and ST cells with nsp5 (Figure 2E). The results showed that nsp5 significantly suppressed the SeV-induced expression of inflammatory cytokines. To analyse the effect of SADS-CoV on the type I IFN and NF-κB signaling pathways, His-TBK1 and SADS-CoV nsp5 were cotransfected into HEK-293T cells, and the expression level of TBK1 was slightly decreased after SADS-CoV nsp5 expression. Transfection of nsp5

after poly(I:C) treatment reduced the level of phosphorylated IRF3 and inhibited NF-κB activation (Supplementary Figure 1A). In addition, the poly(I:C)-induced nuclear translocation of IRF3 was also limited. The protein levels of IRF3 in the cytoplasm of HEK-293T cells were increased by the expression of the nsp5 protein after poly(I:C) treatment. However, after poly(I:C) treatment, the IRF3 levels in the nucleus were decreased (Supplementary Figure 1B). As shown in Supplementary Figures 1C, D, transfection of nsp5 inhibited STAT1 expression and phosphorylation after poly(I:C) or IFN-β treatment as well as the phosphorylation of STAT2 and IκBα after poly(I:C) treatment.

## SADS-CoV nsp5 targets DCP1A for cleavage

We hypothesized that SADS-CoV nsp5 inhibits IFN-β and NF-κB production by inhibiting their upstream stimulatory molecules. Therefore, we cotransfected SADS-CoV nsp5 and pXJ40-HA-IFIT1, DCP1A, IFIT3, IFIT5, P65, IKBKE, TRAF3, MDA-5, STAT1, STAT2, RIG-I, NEMO, IKKα, IKKβ, IκBα or IRF3 into HEK-293T cells. The results showed that the expression levels of DCP1A, STAT1, STAT2, RIG-I, NEMO, IKKα, IKKβ, IκBα and IRF3 were decreased when SADS-CoV nsp5 was expressed, and the effect on DCP1A was the most significant (Figure 3A). Additionally, we also verified the effect of SADS-CoV on the expression of DCP1A, and we found that SADS-CoV infection significantly reduced the expression of DCP1A in a dose-dependent manner (Figure 3B). In addition, we examined the cleavage effect of SADS-CoV on DCP1A at different time points of infection in ST cells (Figure 3C). Further studies on the regulatory effect of SADS-CoV nsp5 on DCP1A expression showed that nsp5 could cleave DCP1A and produce obvious cleavage products; the levels of these cleavage products depended on the dose of SADS-CoV nsp5 (Figure 3D). Next, we verified the interaction between nsp5 and DCP1A by a coimmunoprecipitation assay. Flag-nsp5 and HA-DCP1A were cotransfected into HEK-293T cells, and immunoprecipitation (IP) experiments using anti-HA or anti-Flag antibodies showed that SADS-CoV nsp5 did indeed interact with DCP1A (Figure 3E). The interaction between SADS-CoV nsp5 and endogenous DCP1A was further verified by IFA colocalization experiments. In LLC-PK1 cells, the fluorescence signal of Flag-nsp5 overlapped with that of DCP1A. However, the fluorescence signal of Flag-nsp14 did not overlap with that of DCP1A (Figure 3F).

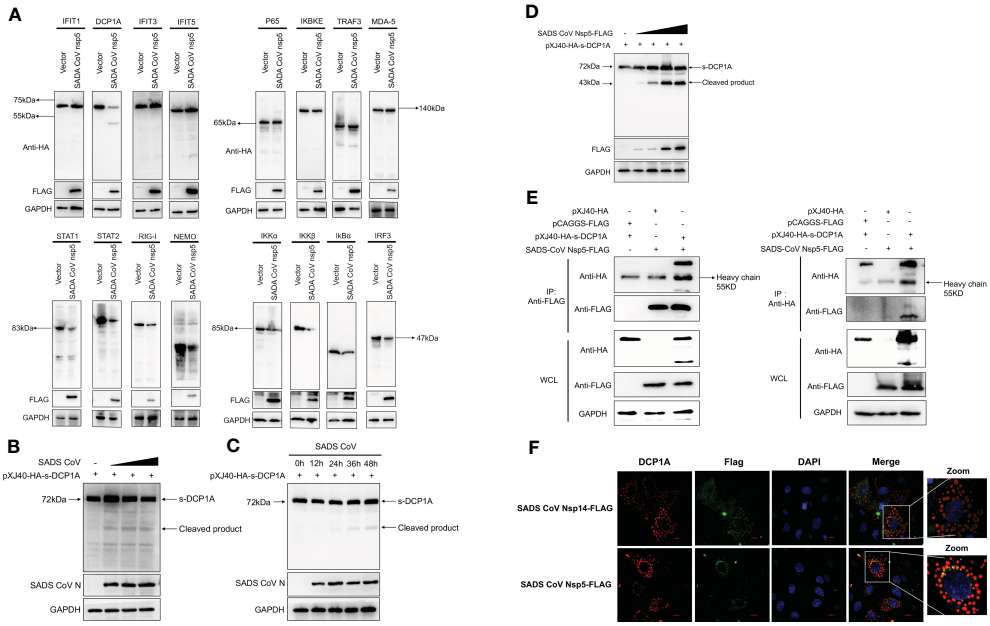


FIGURE 3
SADS-CoV nsp5 targets DCP1A for cleavage. **(A)** HEK-293T cells were cultured in 6-well plates and cotransfected with SADS-CoV nsp5 expression plasmid or empty vector along with 1.5 μg of HA-tagged IFIT1, DCP1A, IFIT3, IFIT5, P65, IKBKE, TRAF3, MDA-5, STAT1, STAT2, RIG-I, NEMO, IKKα, IKKβ, IκBα or IRF3 expression plasmid. After 28 h, the cells were lysed and analysed by Western blotting with an anti-HA antibody. **(B)** ST cells were transfected with 2 μg/well pXJ40-HA-sDCP1A expression plasmid. After 24 h of transfection, the ST cells were infected with SADS-CoV at different MOIs. **(C)** ST cells were infected with SADS-CoV strain (MOI=0.1) and then harvested at 0h, 12h, 24h, 36h, 48h, the cells were lysed for Western blotting. **(D)** HEK-293T cells were cotransfected with pXJ40-HA-sDCP1A and various amounts of the SADS-CoV nsp5 expression plasmid. After 30 h, the cells were lysed for Western blotting. **(E)** HEK-293T cells were transfected with expression constructs encoding SADS-CoV nsp5 and pXJ40-HA-sDCP1A. The cells were lysed 30 h after transfection and subjected to immunoprecipitation with an anti-FLAG antibody or anti-HA antibody. The whole-cell lysates (WCL) and immunoprecipitation (IP) complexes were analysed by immunoblotting (IB) using anti-FLAG, anti-HA, or anti-GAPDH antibodies. **(F)** LLC-PK1 cells were transfected with SADS-CoV nsp5 and nsp14. At 24 h, cells were fixed and then stained with an anti-rabbit monoclonal antibody against DCP1A and anti-mouse flag Tag antibody, followed by incubation with an Alexa Fluor 488-conjugated goat anti-mouse IgG antibody (green) or 594-conjugated goat anti-rabbit IgG antibody (red). The nuclei were stained with DAPI (blue).

## DCP1A activates the type I IFN signaling pathway

It has been reported that overexpression of DCP1A causes decreases in the RSV-induced expression of IL-8, indicating its ability to regulate cellular chemokine expression (13). Therefore, we hypothesized that DCP1A may be the upstream molecule that regulates IFN-β and NF-κB. We then transfected HEK-293T, ST, and Vero-E6 cells with pXJ40-HA-DCP1A and infected them with VSV-GFP. As shown in Figure 4A, the replication of VSV-GFP was significantly inhibited in DCP1A-expressing cells, suggesting that overexpression of DCP1A inhibited viral infection. We then overexpressed DCP1A to various degrees in HEK-293T cells and measured the expression of IRF3, STAT, and NF-κB. The results showed that the phosphorylation of STAT1, STAT2, IRF3, and P65 was markedly increased with increasing DCP1A expression (Figure 4B). Next, we used siRNA to knock down the expression of DCP1A and overexpress DCP1A with pXJ40-HA-DCP1A. The results showed that reducing the expression of DCP1A inhibited the activation of STAT1, STAT2, IRF3, and P65, and conversely increasing the expression of DCP1A promoted their expression (Figure 4C, D). These results indicate that DCP1A is a key regulator of the IFN signaling pathway.

## SADS-CoV nsp5-mediated of DCP1A depends on its protease activity

Nsp5 proteins from several coronavirus-related viruses have also been shown to cleave host proteins and disrupt molecular pathways that are involved in innate immunity (20–22). To further determine whether SADS-CoV nsp5 cleaves DCP1A proteins from different species, we constructed pXJ40-HA-mDCP1A (monkey) derived from Vero-E6 cells, pXJ40-HA-sDCP1A (swine) derived

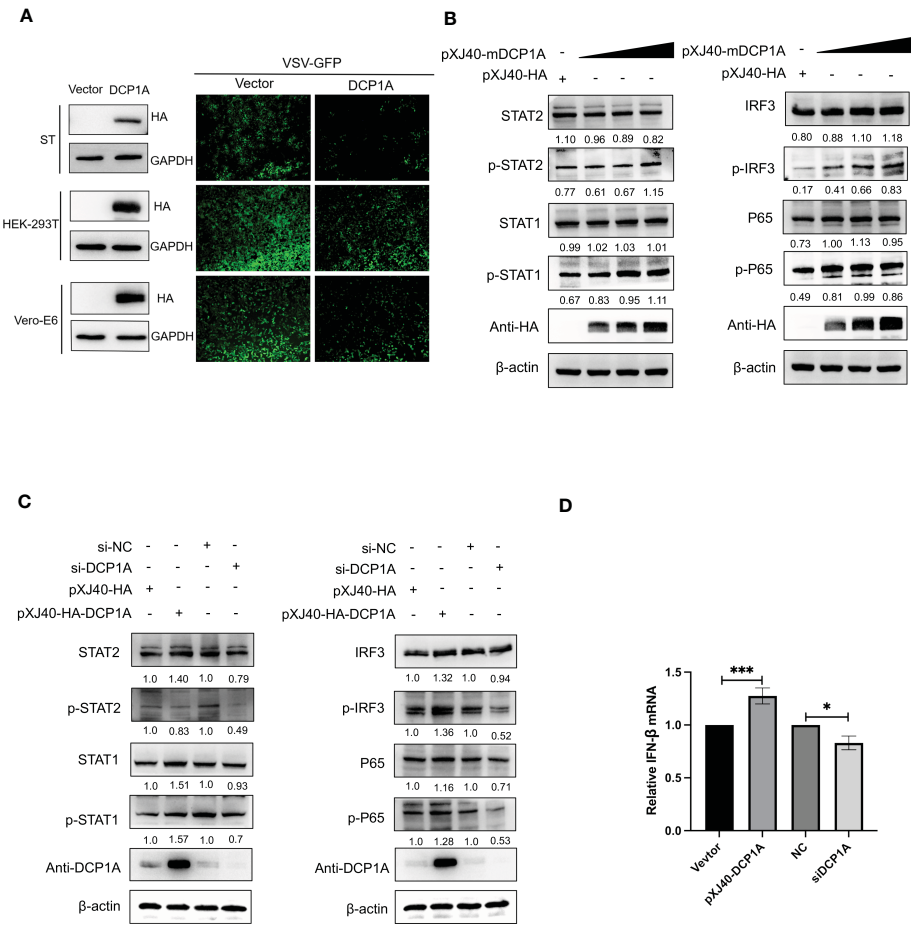


FIGURE 4
DCP1A activates the type I IFN signaling pathway. **(A)** ST, HEK-293T, and Vero-E6 cells were transfected with 2 μg/well empty vector or pXJ40-HA-sDCP1A, pXJ40-HA-hDCP1A, and pXJ40-HA-mDCP1A expression plasmids. After 24 h of transfection, the cells were infected with VSV-GFP for 12 h, and the expression of DCP1A was examined by Western blotting with an anti-HA antibody. Then, the replication of VSV-GFP was analysed via fluorescence microscopy. **(B)** HEK-293T cells were transfected with pXJ40-HA vector and various amounts of the pXJ40-HA-mDCP1A expression plasmid. **(C)** pXJ40-HA vector, pXJ40-HA-h-DCP1A expression plasmid, DCP1A siRNA and negative control siRNA were transfected into HEK-293T cells. After 30 h, cells were collected for Western blot analysis. Cells were analyzed by Western blotting with anti-STAT2, anti-phospho STAT2, anti-STAT1, anti-phospho STAT1, anti-IRF3, anti-phospho IRF3, anti-P65, anti-phospho P65, anti-HA, and β-actin antibodies. **(D)** pXJ40-HA vector, pXJ40-HA-h-DCP1A expression plasmid, DCP1A siRNA and negative control siRNA were transfected into HEK-293T cells. After 30 h, IFN-β mRNA levels were analysed by RT–qPCR. All data are reported as mean±SD. For all experiments, *p < 0.05 and ***p < 0.001 were considered to be statistically significant.

10.3389/fimmu.2023.1196031

from LLC-PK1 cells and pXJ40-HA-hDCP1A (human) derived from HEK-293T cells. Then, we cotransfected HEK-293T cells with DCP1A from different species and SADS-CoV nsp5. The results showed that the cleavage products of DCP1A increased with increasing SADS-CoV nsp5 expression (Figure 5A), and treatment with the coronavirus nsp5 inhibitor PF-00835231 significantly reduced the cleavage of sDCP1A and mDCP1A by SADS-CoV nsp5 (Figure 5B). To further investigate whether SADS-CoV nsp5-mediated cleavage of DCP1A depends on its protease activity, we constructed two mutants of nsp5 (H41A and C144A) with mutations that targeted its protease active sites (10), and we cotransfected these mutants with pXJ40-HA-mDCP1A and pXJ40-

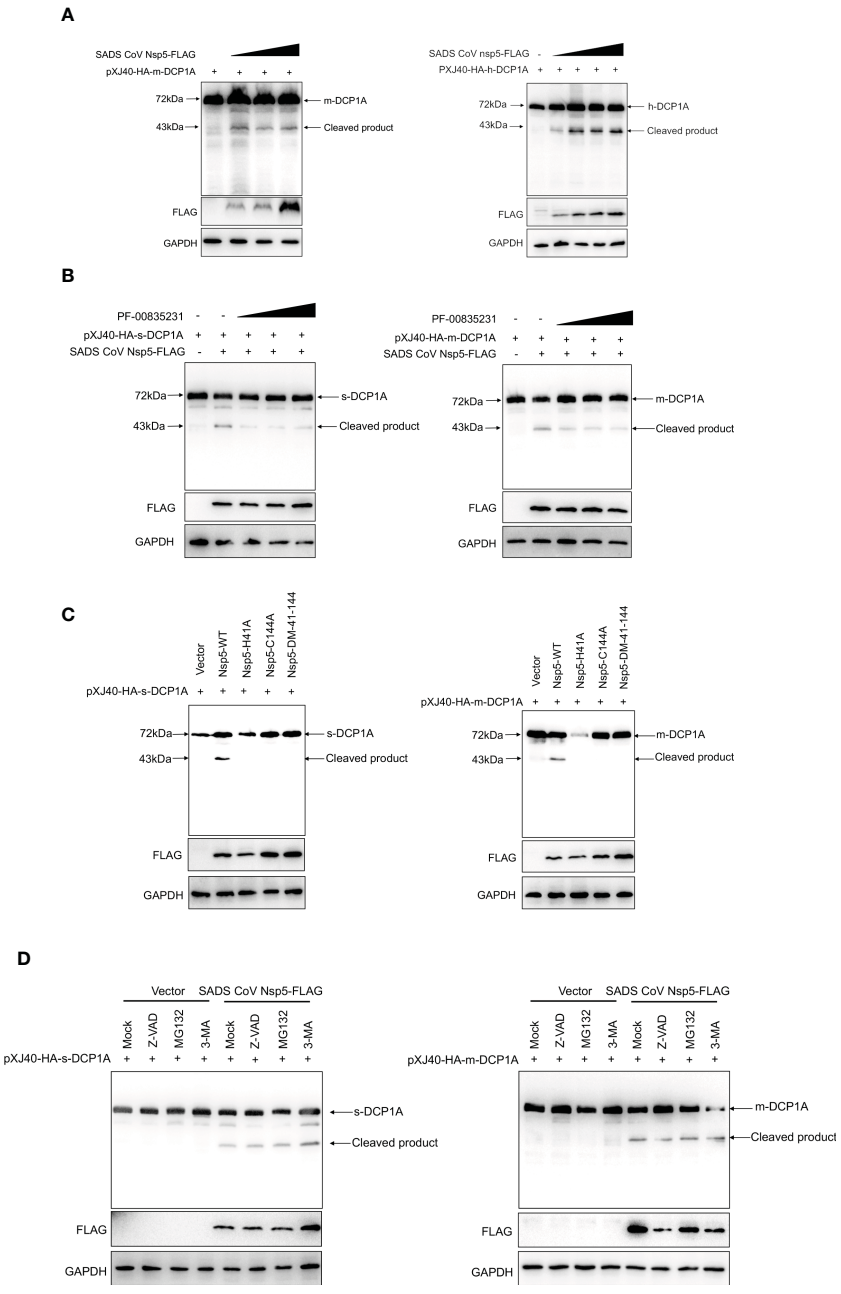


FIGURE 5
SADS-CoV nsp5 cleaves DCP1A via its protease activity. **(A)** HEK-293T cells were cotransfected with pXJ40-HA-mDCP1A, pXJ40-HA-hDCP1A and various amounts of the SADS-CoV nsp5 expression plasmid. After 30 h, the cells were lysed for Western blotting. **(B)** HEK-293T cells were cotransfected with plasmids encoding sDCP1A or mDCP1A and nsp5 from SADS-CoV. At 24 h after transfection, the cells were mock treated or treated with PF-00835231. After 12 h, the cells were lysed for Western blotting. **(C)** HEK-293T cells were cotransfected with plasmids expressing the wild-type SADS-CoV nsp5 or its protease-defective mutants (C144A and H41A) and the pXJ40-HA-sDCP1A or pXJ40-HA-mDCP1A expression plasmid. **(D)** HEK-293T cells were cotransfected with plasmids expressing the wild-type SADS-CoV nsp5 and pXJ40-HA-sDCP1A or pXJ40-HA-mDCP1A expression plasmids. After 24 h, the cells were treated with MG132, Z-VAD-FMK (final concentration of 20 μM) or 3-MA for 8 h Cell lysates were prepared and analysed by Western blotting.

HA-sDCP1A, respectively. As shown in Figure 5C, the two nsp5 mutants H41A and C144A were unable to cleave mDCP1A and sDCP1A. Then, HEK-293T cells were cotransfected with SADS-CoV nsp5 and DCP1A and then treated with the proteasome inhibitor MG132, the caspase inhibitor Z-VAD-FMK, or the autophagy inhibitor 3-MA. The results showed that none of the three inhibitors could block the cleavage of DCP1A by SADS-CoV nsp5, indicating that the cleavage of DCP1A by nsp5 was dependent on the protease activity of nsp5 (Figure 5D).

## SADS-CoV nsp5 recognizes and cleaves DCP1A at residue Q343

To further identify the site of DCP1A that is recognized by SADS-CoV nsp5, we generated three DCP1A truncation mutants, namely, $DCP1A_{1-251}$, $DCP1A_{1-285}$ and $DCP1A_{1-330}$, from different species, and we cotransfected them with nsp5. Since the size of the product that is recognized by anti-HA antibodies after the nsp5-mediated cleavage of sDCP1A and mDCP1A were approximately 43 kDa in size, the cleavage site should be near the 330 amino acid position in the N-terminus (Figure 6A). As shown in Figure 6B, CoV nsp5 showed a preference for substrate cleavage at a Q residue in the P1 position, which is common among other CoV subfamilies. Since the protease activity site of nsp5 usually recognizes Q-Gln motifs (23), we constructed several DCP1A constructs with mutations between amino acids 285 and 360 in the N-terminus, where Q residues (Q330, Q343, and Q351) were mutated to alanine residues, and we cotransfected these constructs with SADS-CoV nsp5 into HEK-293T cells (Figure 6C). The results showed that the DCP1A-Q330A and DCP1A-Q351A mutants from different species could still be cleaved by SADS-CoV nsp5, while the DCP1A-Q343A mutants were resistant. These results indicate that amino acid Q343 of DCP1A is a recognition and cleavage site for nsp5 (Figures 6D, E).

## DCP1A is a common target of nsp5 from different coronaviruses

Coronavirus nsp5 has a catalytic site between cysteine (Cys) residues and histidine (His) residues, and any change in the catalytic site disrupts its protease activity (24–26). Comparison of the secondary structure of nsp5 showed that the His41 and Cys144 residues of the protease active site (numbering based on SADS-CoV nsp5) were highly conserved among α-, β-, γ-, and δ-CoV (Supplementary Figure 2A). Therefore, we investigated whether nsp5 from other mammalian coronaviruses can also cleave DCP1A in the host. The results showed that nsp5 from different coronaviruses could cleave DCP1A in infected cells (Supplementary Figures 2B, C). These results demonstrate that DCP1A cleavage is a conserved mechanism by which coronavirus escapes host immune responses.

# Discussion

Here, we found that DCP1A is a possible target of SADS-CoV during infection. We show that following host infection, SADS-CoV nsp5 uses its protease activity to cleave DCP1A at residue Q343, and nsp5 from many different coronavirus species can also cleave DCP1A. The results reveal a previously unknown mechanism of intracellular antagonism that is driven by virus–host interactions, and these results provide new evidence to explain why hosts often exhibit limited ISG responses during SADS-CoV infection.

SADS-CoV was infectious in pigs when inoculated orally into 3-day-old newborn piglets, leading to clinical signs of diarrhea and subclinicalinfection (3). SADS-CoV has been reported to have a broad cell tropism, Vero-E6, IPEC-J2, ST and LLC-PK1 have been showed signicant susceptibility to SADS-CoV infection (27). In the immune system, IFN/ISG plays a crucial role in preventing virus infection in cells. We demonstrated that SADS-CoV inhibits the secretion of type I IFN and multiple inflammatory cytokines in ST cells. In our study, we also confirmed that SADS-CoV infected in different host cells (Figure 1). NF-κB is the primary transcription factor that regulates numerous cellular responses, including early innate immune responses and viral infections (28). It has also been reported that SARS-CoV-2 nsp5 enhances cytokine production by activating the NF-κB signaling pathway (29). In this study, we found that SADS-CoV nsp5 antagonizes the host antiviral response by inhibiting the IRF3, STAT, and NF-κB signaling pathways, reducing the secretion of antiviral cytokines by cells and thereby allowing the virus to evade host innate immunity (Figure 2 and Supplementary Figure 1).

Coronavirus nsp5 is a cysteine protease that is required to process viral polyproteins, so it is essential for viral replication and can antagonize host immune proteins, promoting viral escape from host immune responses and replication. Nsp5 proteins from several coronaviruses have been reported to cleave host proteins, disrupting molecular pathways that are involved in innate immunity. For example, nsp5 proteins PEDV and PDCoV target NEMO and cleave it at a unique site (Q231), inhibiting the host innate immune response and promoting viral proliferation (30, 31). PEDV nsp5 inhibits pyroptosis by cleaving GSDMD, which is a key executioner of pyroptosis, at amino acids R238, T239, and F240 (22). SARS-CoV-2 nsp5 prevents the autophagic degradation of viral membrane proteins by cleaving the selective autophagy receptor SQSTM1/p62 (21). In addition, histone deacetylases (HDACs) have a significant effect in inhibiting viral infection. SARS-CoV-2 and PDCoV nsp5 can recognize and cleave HDACs to antagonize their antiviral effects and promote their own proliferation (15, 32). In this study, we demonstrated that the nsp5 protein from SADS-CoV directly interacts with DCP1A and cleaves DCP1A to disrupt the innate immune pathways of the host and escape from the host immune response (Figure 3). We also found that DCP1A is a key molecule in the regulation of the IRF3, STAT and NF-κB pathways, induces the secretion of downstream

10.3389/fimmu.2023.1196031

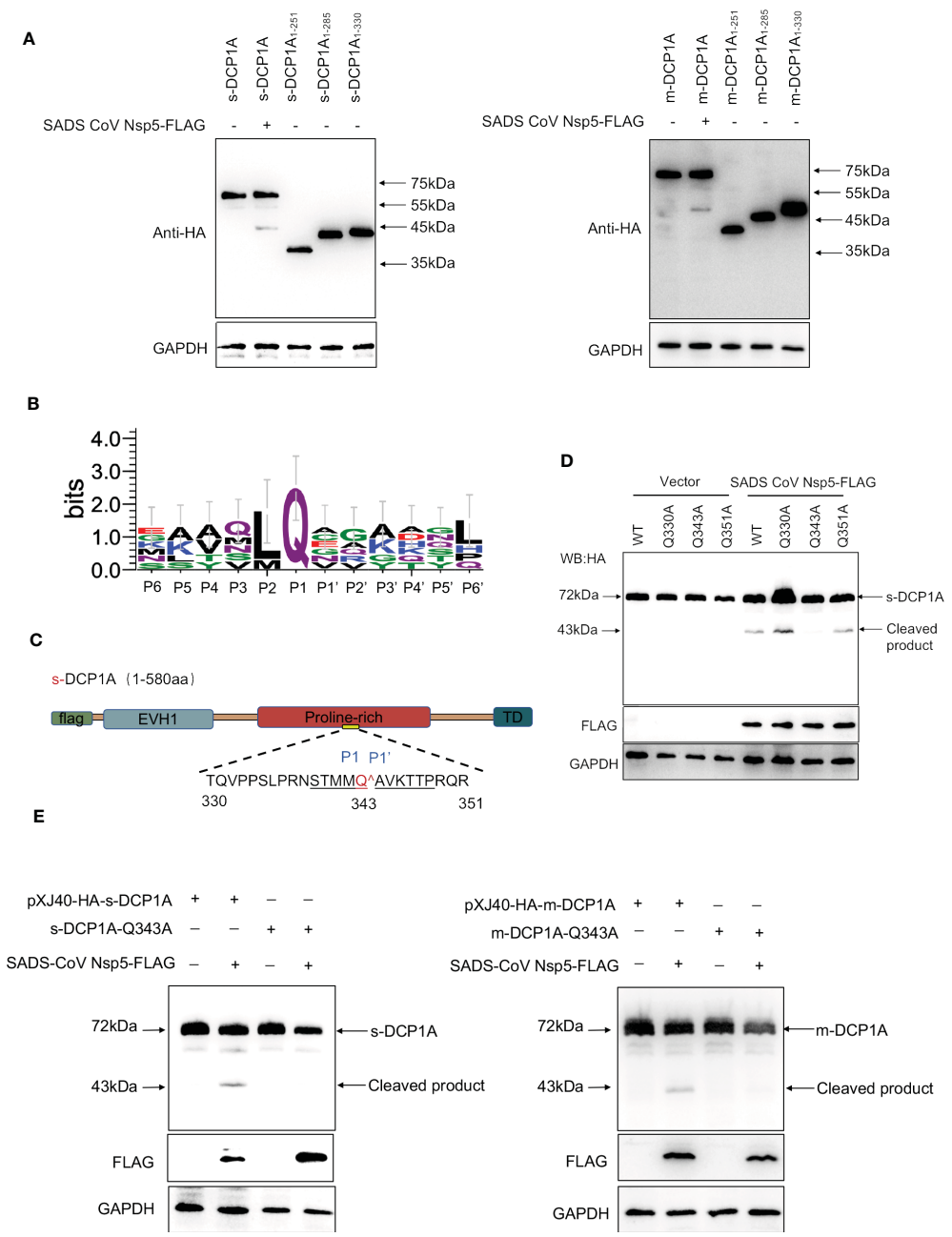


FIGURE 6
SADS-CoV nsp5 mediates DCP1A cleavage at residue Q343. **(A)** The estimated product of DCP1A cleavage by SADS-CoV nsp5. HEK-293T cells were transfected with expression constructs encoding mDCP1A$_{1-251}$ or sDCP1A$_{1-251}$, mDCP1A$_{1-285}$ or sDCP1A$_{1-285}$, mDCP1A$_{1-330}$ or sDCP1A$_{1-330}$ truncated mutants and collected after 30 h for Western blotting. **(B)** Sequence logo of the polyprotein junctions that are cleaved by SADS-CoV nsp5. An amino acid sequence logo of the substrate was generated by WebLogo, version 3 (http://weblogo.threeplusone.com/). **(C)** Schematic representation of mDCP1A and its mutant sites. **(D)** HEK-293T cells were cotransfected with the SADS-CoV nsp5 expression plasmid along with expression constructs encoding wild-type mDCP1A or mDCP1A mutants, including mDCP1A-Q330A, mDCP1A-Q343A, and mDCP1A-Q351A. The cells were then lysed after 30 h and evaluated by Western blotting. **(E)** HEK-293T cells were cotransfected with the SADS-CoV nsp5 expression plasmid along with wild-type sDCP1A/mDCP1A or sDCP1A-Q343A/mDCP1A-Q343A and collected after 30 h for Western blotting.

type I IFN and inflammatory cytokines, and is an important molecule for host antiviral innate immunity (Figure 4). Since cysteine (Cys) and histidine (His) are the major sites of coronavirus nsp5 protease activity, mutations in these catalytic sites disrupts nsp5 activity (33). Coronavirus nsp5 proteins target DCP1A at a unique site (Q343) to disrupt its antiviral activity, revealing a common recognition mechanism that is used to suppress the host innate immune response (10). In this study, we

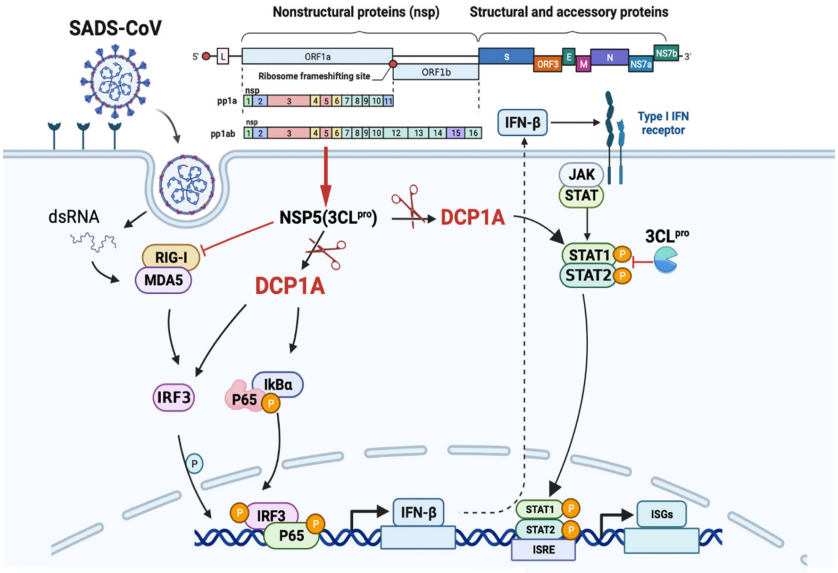


FIGURE 7
SADS-CoV nsp5 interferes with the innate immune response by directly cleaving DCP1A. SADS-CoV nsp5 antagonizes the type I interferon signaling pathway; the schematic was drawn using the Biorender website (https://www.biorender.com). SADS-CoV infects swine cells and releases its genome into the cytoplasm to produce nsp5 protein, which binds to DCP1A and cleaves it, inhibiting the activation of downstream molecules IRF3, NF-κB, STAT1, and STAT2, thereby reducing the production of type I IFN and inflammatory cytokines in the cells.

used mutant with mutations in the protease active site, namely, H41A and C144A, to confirm the protease active site of SADS-CoV nsp5. Additionally, a truncated form of DCP1A was used to confirm that the Q343 site is the site that is recognized and cleaved by SADS-CoV nsp5 (Figures 5, 6).

This specific and identifiable mode of cleavage via protease activity that targets a constant site is an effective way for coronaviruses to combat host innate immunity. It has been reported that DCP1A is a good antiviral target due its interaction with the nsp5 proteins from SARS-CoV-2 and PDCoV. We also verified that the nsp5 proteins from alpha-, beta- and delta-coronaviruses can target DCP1A for cleavage (Supplementary Figure 2). Therefore, further detailed analysis of the complete crystal structure of the viral nsp5 protein and elucidation of the molecular mechanism underlying its target gene recognition will provide more guidance for designing anti-coronavirus drugs that specifically targeting nsp5. According to the schematic diagram showing the molecular mechanism, these findings advance our understanding of the role of nsp5 during SADS-CoV infection (Figure 7).

In conclusion, these data contribute to a better understanding of the potential mechanisms by which SADS-CoV fights host innate immunity, increases its pathogenicity and infectivity in the host, and promotes its own replication and transmission. This study provides new insights for the prevention and control of SADS-CoV in clinical practice and provides guidance for the research and development of anti-SADS-CoV drugs and inhibitors in the future.

## Data availability statement

The original contributions presented in the study are included in the article/Supplementary Material. Further inquiries can be directed to the corresponding authors.

## Author contributions

N-YJ and W-CS designed the research. H-XH and C-CZ performed the majority of the experiments and were involved in preparation of the manuscript. H-XH, C-CZ, X-XL, X-YZ, and Y-YL analysed the data. H-XH prepared the manuscript. TL, B-PZ, J-YL, and H-JL revised the manuscript. All authors contributed to the article and approved the submitted version.

## Funding

This work was supported by the Wenzhou Basic Medical Health Science and Technology Project (Grant Numbers Y20220136).

## Acknowledgments

Thanks to Dr. Cong Feng and Dr. Zheng Min from Guangxi University for their great support of this experiment.

## Conflict of interest

The authors declare that they have no known competing financial interests or personal relationships that could have appeared to influence the work reported in this paper.

## Publisher's note

All claims expressed in this article are solely those of the authors and do not necessarily represent those of their affiliated organizations, or those of the publisher, the editors and the reviewers. Any product that may be evaluated in this article, or claim that may be made by its manufacturer, is not guaranteed or endorsed by the publisher.

## Supplementary material

The Supplementary Material for this article can be found online at: https://www.frontiersin.org/articles/10.3389/fimmu.2023.1196031/full#supplementary-material

## References


1. Gong L, Li J, Zhou Q, Xu Z, Chen L, Zhang Y, et al. A new bat-HKU2-like coronavirus in swine, China, 2017. *Emerg Infect Dis* (2017) 23:1607–9. doi: 10.3201/eid2309.170915

2. Zhou P, Fan H, Lan T, Yang XL, Shi WF, Zhang W, et al. Fatal swine acute diarrhoea syndrome caused by an HKU2-related coronavirus of bat origin. *Nature* (2018) 556:255–8. doi: 10.1038/s41586-018-0010-9

3. Pan Y, Tian X, Qin P, Wang B, Zhao P, Yang YL, et al. Discovery of a novel swine enteric alphacoronavirus (SeACoV) in southern China. *Vet Microbiol* (2017) 211:15–21. doi: 10.1016/j.vetmic.2017.09.020

4. Li K, Li H, Bi Z, Gu J, Gong W, Luo S, et al. Complete genome sequence of a novel swine acute diarrhea syndrome coronavirus, CH/FJWT/2018, isolated in Fujian, China, in 2018. *Microbiol Resour Announc* (2018) 7(22):e01259–18. doi: 10.1128/mra.01259-18

5. Zhou L, Li QN, Su JN, Chen GH, Wu ZX, Luo Y, et al. The re-emerging of SADS-CoV infection in pig herds in southern China. *Transboundary emerging Dis* (2019) 66:2180–3. doi: 10.1111/tbed.13270

6. Sun Y, Xing J, Xu ZY, Gao H, Xu SJ, Liu J, et al. Re-emergence of severe acute diarrhea syndrome coronavirus (SADS-CoV) in guangxi, China, 2021. *J Infect* (2022) 85:e130–3. doi: 10.1016/j.jinf.2022.08.020

7. Luo Y, Chen Y, Geng R, Li B, Chen J, Zhao K, et al. Broad cell tropism of SADS-CoV *In vitro* implies its potential cross-species infection risk. *Virol Sin* (2021) 36:559–63. doi: 10.1007/s12250-020-00321-3

8. Edwards CE, Yount BL, Graham RL, Leist SR, Hou YJ, Dinnon KH3rd, et al. Swine acute diarrhea syndrome coronavirus replication in primary human cells reveals potential susceptibility to infection. *Proc Natl Acad Sci USA* (2020) 117:26915–25. doi: 10.1073/pnas.2001046117

9. Mei XQ, Qin P, Yang YL, Liao M, Liang QZ, Zhao Z, et al. First evidence that an emerging mammalian alphacoronavirus is able to infect an avian species. *Transboundary emerging Dis* (2022) 69:e2006–19. doi: 10.1111/tbed.14535

10. Zhu X, Chen J, Tian L, Zhou Y, Xu S, Long S, et al. Porcine deltacoronavirus nsp5 cleaves DCP1A to decrease its antiviral activity. *J Virol* (2020) 94(15):e02162–19. doi: 10.1128/jvi.02162-19

11. Anderson-Daniels J, Gribble J, Denison M. Proteolytic processing of the coronavirus replicase nonstructural protein 14 exonuclease is not required for virus replication but alters RNA synthesis and viral fitness. *J Virol* (2022) 96:e0084122. doi: 10.1128/jvi.00841-22

12. Schneider WM, Chevillotte MD, Rice CM. Interferon-stimulated genes: a complex web of host defenses. *Annu Rev Immunol* (2014) 32:513–45. doi: 10.1146/annurev-immunol-032713-120231

13. Dickey LL, Duncan JK, Hanley TM, Fearns R. Decapping protein 1 phosphorylation modulates IL-8 expression during respiratory syncytial virus infection. *Virology* (2015) 481:199–209. doi: 10.1016/j.virol.2015.02.043

14. Tao R, Fang L, Bai D, Ke W, Zhou Y, Wang D, et al. Porcine reproductive and respiratory syndrome virus nonstructural protein 4 cleaves porcine DCP1a to attenuate its antiviral activity. *J Immunol (Baltimore Md.: 1950)* (2018) 201:2345–53. doi: 10.4049/jimmunol.1701773

15. Song L, Wang D, Abbas G, Li M, Cui M, Wang J, et al. The main protease of SARS-CoV-2 cleaves histone deacetylases and DCP1A, attenuating the immune defense of the interferon-stimulated genes. *J Biol Chem* (2023) 299(3):102990. doi: 10.1016/j.jbc.2023.102990

16. Sui C, Xiao T, Zhang S, Zeng H, Zheng Y, Liu B, et al. SARS-CoV-2 NSP13 inhibits type I IFN production by degradation of TBK1 via p62-dependent selective autophagy. *J Immunol (Baltimore Md.: 1950)* (2022) 208:753–61. doi: 10.4049/jimmunol.2100684

17. Zhang Y, Gargan S, Roche FM, Frieman M, Stevenson NJ. Inhibition of the IFN-α JAK/STAT pathway by MERS-CoV and SARS-CoV-1 proteins in human epithelial cells. *Viruses* (2022) 14(4):667. doi: 10.3390/v14040667

18. Dong S, Kong N, Shen H, Li Y, Qin W, Zhai H, et al. KLF16 inhibits PEDV replication by activating the type I IFN signaling pathway. *Vet Microbiol* (2022) 274:109577. doi: 10.1016/j.vetmic.2022.109577

19. Ding L, Li J, Li W, Fang Z, Li N, Guo Q, et al. p53 mediated IFN-β signaling to affect viral replication upon TGEV infection. *Vet Microbiol* (2018) 227:61–8. doi: 10.1016/j.vetmic.2018.10.025

20. Moustaqil M, Ollivier E, Chiu HP, Van Tol S, Rudolffi-Soto P, Stevens C, et al. SARS-CoV-2 proteases PLpro and 3CLpro cleave IRF3 and critical modulators of inflammatory pathways (NLRP12 and TAB1): implications for disease presentation across species. *Emerg Microbes Infect* (2021) 10:178–95. doi: 10.1080/22221751.2020.1870414

21. Zhang Y, Liu S, Xu Q, Li H, Lu K. Cleavage of the selective autophagy receptor SQSTM1/p62 by the SARS-CoV-2 main protease NSP5 prevents the autophagic degradation of viral membrane proteins. *Mol BioMed* (2022) 3:17. doi: 10.1186/s43556-022-00083-2

22. Shi F, Lv Q, Wang T, Xu J, Xu W, Shi Y, et al. Coronaviruses Nsp5 antagonizes porcine gasdermin d-mediated pyroptosis by cleaving pore-forming p30 fragment. *mBio* (2022) 13:e0273921. doi: 10.1128/mbio.02739-21

23. Stobart CC, Sexton NR, Munjal H, Lu X, Molland KL, Tomar S, et al. Chimeric exchange of coronavirus nsp5 proteases (3CLpro) identifies common and divergent regulatory determinants of protease activity. *J Virol* (2013) 87:12611–8. doi: 10.1128/jvi.02050-13

24. Grum-Tokars V, Ratia K, Begaye A, Baker SC, Mesecar AD. Evaluating the 3C-like protease activity of SARS-coronavirus: recommendations for standardized assays for drug discovery. *Virus Res* (2008) 133:63–73. doi: 10.1016/j.virusres.2007.02.015

25. Hsu MF, Kuo CJ, Chang KT, Chang HC, Chou CC, Ko TP, et al. Mechanism of the maturation process of SARS-CoV 3CL protease. *J Biol Chem* (2005) 280:31257–66. doi: 10.1074/jbc.M502577200

26. Roe MK, Junod NA, Young AR, Beachboard DC, Stobart CC. Targeting novel structural and functional features of coronavirus protease nsp5 (3CL(pro), m(pro)) in the age of COVID-19. *J Gen Virol* (2021) 102(3):001558. doi: 10.1099/jgv.0.001558

27. Yang YL, Qin P, Wang B, Liu Y, Xu GH, Peng L, et al. Broad cross-species infection of cultured cells by bat HKU2-related swine acute diarrhea syndrome coronavirus and identification of its replication in murine dendritic cells *In vivo* highlight its potential for diverse interspecies transmission. *J Virol* (2019) 93(24):e01448–19. doi: 10.1128/jvi.01448-19

28. Brignall R, Moody AT, Mathew S, Gaudet S. Considering abundance, affinity, and binding site availability in the NF-κB target selection puzzle. *Front Immunol* (2019) 10:2019.00609. doi: 10.3389/fimmu.2019.00609

29. Li W, Qiao J, You Q, Zong S, Peng Q, Liu Y, et al. SARS-CoV-2 Nsp5 activates NF-κB pathway by upregulating SUMOylation of MAVS. *Front Immunol* (2021) 12:2021.750969. doi: 10.3389/fimmu.2021.750969

30. Zhu X, Fang L, Wang D, Yang Y, Chen J, Ye X, et al. Porcine deltacoronavirus nsp5 inhibits interferon-β production through the cleavage of NEMO. *Virology* (2017) 502:33–8. doi: 10.1016/j.virol.2016.12.005

31. Wang D, Fang L, Shi Y, Zhang H, Gao L, Peng G, et al. Porcine epidemic diarrhea virus 3C-like protease regulates its interferon antagonism by cleaving NEMO. *J Virol* (2016) 90:2090–101. doi: 10.1128/jvi.02514-15

32. Li Z, Fang P, Duan P, Chen J, Fang L, Xiao S. Porcine deltacoronavirus infection cleaves HDAC2 to attenuate its antiviral activity. *J Virol* (2022) 96:e0102722. doi: 10.1128/jvi.01027-22

33. Anand K, Ziebuhr J, Wadhwani P, Mesters JR, Hilgenfeld R. Coronavirus main proteinase (3CLpro) structure: basis for design of anti-SARS drugs. *Science* (2003) 300:1763–7. doi: 10.1126/science.1085658

frontiers | Frontiers in Immunology

TYPE Original Research
PUBLISHED 13 July 2023
DOI 10.3389/fimmu.2023.1166765



OPEN ACCESS

EDITED BY
Jingxin Li,
Jiangsu Provincial Center for Disease Control And Prevention, China

REVIEWED BY
Stephen Crooke,
Centers for Disease Control and Prevention (CDC), United States
Dubravka Drabek,
Erasmus Medical Center, Netherlands

*CORRESPONDENCE
Günther Schönrich
guenther.schoenrich@charite.de
Jakob Trimpert
jakob.trimpert@fu-berlin.de

†These authors have contributed equally to this work

RECEIVED 15 February 2023
ACCEPTED 19 June 2023
PUBLISHED 13 July 2023

CITATION
Abdelaziz MO, Raftery MJ, Weihs J, Bielawski O, Edel R, Köppke J, Vladimirova D, Adler JM, Firsching T, Voß A, Gruber AD, Hummel LV, Fernandez Munoz I, Müller-Marquardt F, Willimsky G, Elleboudy NS, Trimpert J and Schönrich G (2023) Early protective effect of a ("pan") coronavirus vaccine (PanCoVac) in Roborovski dwarf hamsters after single-low dose intranasal administration.
*Front. Immunol.* 14:1166765.
doi: 10.3389/fimmu.2023.1166765



# Early protective effect of a ("pan") coronavirus vaccine (PanCoVac) in Roborovski dwarf hamsters after single-low dose intranasal administration

Mohammed O. Abdelaziz[1,2], Martin J. Raftery[1,2,3], Julian Weihs[1,4], Olivia Bielawski[1], Richard Edel[1], Julia Köppke[1], Daria Vladimirova[5], Julia M. Adler[5], Theresa Firsching[6], Anne Voß[6], Achim D. Gruber[6], Luca V. Hummel[1], Ivan Fernandez Munoz[1], Francesca Müller-Marquardt[1], Gerald Willimsky[7,8,9], Nooran S. Elleboudy[1,10], Jakob Trimpert[5*†] and Günther Schönrich[1*†]

[1]Institute of Virology, Charité – Universitätsmedizin Berlin, Corporate Member of Freie Universität Berlin and Humboldt-Universität zu Berlin, Berlin, Germany, [2]Berlin Institute of Health, Charité – Universitätsmedizin Berlin, Berlin, Germany, [3]Department of Hematology, Oncology and Tumor Immunology, Charité – Universitätsmedizin Berlin, Corporate Member of Freie Universität Berlin and Humboldt-Universität zu Berlin, Berlin, Germany, [4]Department of Pediatrics, Division of Gastroenterology, Charité – Universitätsmedizin Berlin, Corporate Member of Freie Universität Berlin and Humboldt-Universität zu Berlin, Berlin, Germany, [5]Institute of Virology, Freie Universität Berlin, Berlin, Germany, [6]Institute of Veterinary Pathology, Freie Universität Berlin, Berlin, Germany, [7]Institute of Immunology, Charité-Universitätsmedizin Berlin, Corporate Member of Freie Universität Berlin and Humboldt-Universität zu Berlin, Berlin, Germany, [8]German Cancer Research Center, Heidelberg, Germany, [9]German Cancer Consortium, Partner Site Berlin, Berlin, Germany, [10]Department of Microbiology and Immunology, Faculty of Pharmacy, Ain Shams University, Cairo, Egypt

**Introduction:** The coronavirus disease 2019 (COVID-19) pandemic caused by severe acute respiratory syndrome coronavirus 2 (SARS-CoV-2) has highlighted the danger posed by human coronaviruses. Rapid emergence of immunoevasive variants and waning antiviral immunity decrease the effect of the currently available vaccines, which aim at induction of neutralizing antibodies. In contrast, T cells are marginally affected by antigen evolution although they represent the major mediators of virus control and vaccine protection against virus-induced disease.

**Materials and methods:** We generated a multi-epitope vaccine (PanCoVac) that encodes the conserved T cell epitopes from all structural proteins of coronaviruses. PanCoVac contains elements that facilitate efficient processing and presentation of PanCoVac-encoded T cell epitopes and can be uploaded to any available vaccine platform. For proof of principle, we cloned PanCoVac into a non-integrating lentivirus vector (NILV-PanCoVac). We chose Roborovski dwarf hamsters for a first step in evaluating PanCoVac *in vivo*. Unlike mice, they are naturally susceptible to SARS-CoV-2 infection. Moreover, Roborovski dwarf hamsters develop COVID-19-like disease after infection with SARS-CoV-2 enabling us to look at pathology and clinical symptoms.

**Results:** Using HLA-A*0201-restricted reporter T cells and U251 cells expressing a tagged version of PanCoVac, we confirmed *in vitro* that PanCoVac is processed and presented by HLA-A*0201. As mucosal immunity in the respiratory tract is crucial for protection against respiratory viruses such as SARS-CoV-2, we tested the protective effect of single-low dose of NILV-PanCoVac administered *via* the intranasal (i.n.) route in the Roborovski dwarf hamster model of COVID-19. After infection with ancestral SARS-CoV-2, animals immunized with a single-low dose of NILV-PanCoVac i.n. did not show symptoms and had significantly decreased viral loads in the lung tissue. This protective effect was observed in the early phase (2 days post infection) after challenge and was not dependent on neutralizing antibodies.

**Conclusion:** PanCoVac, a multi-epitope vaccine covering conserved T cell epitopes from all structural proteins of coronaviruses, might protect from severe disease caused by SARS-CoV-2 variants and future pathogenic coronaviruses. The use of (HLA-) humanized animal models will allow for further efficacy studies of PanCoVac-based vaccines *in vivo*.

KEYWORDS

**universal COVID-19 vaccine, coronaviruses, multi-epitope vaccine, T cell epitopes, pan-coronavirus vaccine, dwarf hamster COVID-19 model, T-cell-directed vaccine**

# 1 Introduction

The coronavirus disease 2019 (COVID-19) pandemic illustrates the great danger posed by coronaviruses. These enveloped viruses belong to the subfamily *Coronavirinae* from the family *Coronaviridae* (1). They can jump from bats *via* bridging hosts into humans thereby adapting to and spreading in human populations (2, 3). This happened three times in the past 20 years. Severe acute respiratory syndrome coronavirus (SARS-CoV)-1 emerged in 2002 (4) and Middle East respiratory syndrome coronavirus (MERS-CoV) was first detected in 2012 (5). They were responsible for separate viral epidemics with case fatality rates of up to 10% for SARS-CoV-1 (6) and 35% for MERS-CoV (7). The currently circulating pandemic SARS-CoV-2 emerged in 2019 and is causing huge detrimental socio-economic damage and millions of deaths (8) although it has a much lower case fatality rate in unvaccinated populations compared to SARS-CoV-1 and MERS-CoV (9). In South East Asia, numerous bat species are infected with coronaviruses belonging to the *Sarbecovirus* subgenus of the genus *Betacoronavirus* like SARS-CoV-1 and SARS-CoV-2 (10–13). In this region, significant levels of bat-to-human coronavirus spillover are observed suggesting that future outbreaks with sarbecoviruses are likely (14). Thus, universal coronavirus vaccines that provide a broad, robust, and durable protection are urgently needed (15–19).

The coronavirus genome consists of non-segmented, single-stranded, positive-sense RNA and is the largest known amongst RNA viruses (20). It encodes non-structural and structural proteins. The latter encompass the spike (S), envelope (E), membrane (M), and nucleocapsid (N) protein. A receptor-binding domain (RBD) located on the S protein interacts with host cell surface receptors thereby facilitating viral entry. Currently available SARS-CoV-2 vaccines are administered *via* intramuscular injection and aim at systemic induction of neutralizing antibodies, which mostly bind to the RBD thereby preventing virus infection (21). Although these first generation vaccines have mitigated the effects of the pandemic (22), major problems remain. Firstly, the levels of neutralizing antibodies quickly decrease after vaccination (23, 24). Secondly, intramuscular injection only weakly stimulates antiviral mucosal immunity in the respiratory tract, the site of viral entry (25). Thirdly, emerging viral variants of concern (VOC) such as B.1.1.7 (Alpha), B.1.351 (Beta), P.1 (Gamma), B.1.617.2 (Delta), and the recently identified B.1.1.529 (Omicron) with its numerous subvariants (notably BA.1, BA.2, BA.4 and BA.5) evade neutralizing antibodies due to mutations mainly within the RBD sequence (26–30). These disadvantages combined explain why the effectiveness of current vaccines is waning rapidly resulting in loss of protection from infection and possibly also from disease (31–33).

Besides neutralizing antibodies, T cells originating in the thymus fulfill essential antiviral functions (34). CD8+ T cells eliminate virus-infected cells thereby preventing viral cell-to-cell spread and CD4+ T cells optimize antibody production by B cells (35). In addition, CD4+ T cells provide signals that help to generate and program memory CD8+ T cells (36, 37). In non-severe SARS-CoV-2 infections of unvaccinated virus-naive individuals virus-specific T cell responses precede PCR detection and occur 1-2 weeks before virus-specific antibodies (38). T cells, either induced by infection, by vaccination or by their combination, protect from severe COVID-19 and are more important players than neutralizing antibodies in elimination of SARS-CoV-2 (15, 39–43). For example,

patients deficient in B cells but with intact T cell function can cope with SARS-CoV-2 infection (44–46). In macaques that had recovered from SARS-CoV-2 infection, depletion of CD8+ T cells decreases the protective effect of acquired immunity against re-challenge (47). In line with these observations, a SARS-CoV-2 N protein-based vaccine, which does not elicit neutralizing antibodies, established protective immunity in small animal models of COVID-19 (48).

The T cell responses against SARS-CoV-2 persist most likely for many years and are detectable even in the absence of memory B cell responses (49–57). In contrast to neutralizing antibodies that bind to the RBD, T cell responses are directed against a broad spectrum of epitopes and are not disrupted by the antigenic evolution of SARS-CoV-2 (58–70). This is explained by the polymorphic HLA molecules, which present a highly diverse repertoire of T cell epitopes derived from all viral proteins thereby preventing efficient viral immune escape (71).

Intriguingly, pre-existing T cell responses to SARS-CoV-2 epitopes are found frequently in unexposed individuals and pre-pandemic blood samples (51, 72–77). They are best explained by previous exposure to the four known endemic coronaviruses (HCoV-OC43, HCoV-229E, HCoV-HKU1, and HCoV-NL63) that cause about one-third of common colds in humans (78–80). There is accumulating evidence that these cross-reactive T cells are functional *in vivo* and have a positive effect on COVID-19 outcome and COVID-19 vaccination (41, 49, 55, 75, 81–88). It has been reported that pre-existing cross-reactive memory T cells predict efficient COVID-19 vaccine-induced immune responses (82–84). In addition, T cell epitopes have been identified that are highly conserved between human and animal coronaviruses (89) and bind to common human MHC molecules (90). Thus, induction of a broad and durable cross-reactive T cell response specific for highly conserved epitopes of pathogenic coronaviruses in the upper respiratory tract is an attractive strategy for urgently needed pan-coronavirus vaccines (91).

In this study, we generated a codon optimized DNA sequence (PanCoVac) that encodes in a compact form the conserved T cell epitopes from all structural proteins. For this purpose, we deconstructed coronavirus genomes and generated a multi-epitope vaccine with a special architecture facilitating processing and presentation of epitopes. We cloned PanCoVac into a non-integrating lentivirus vector (NILV-PanCoVac) and tested the protective effect of intranasal (i.n.) administration of a single low dose of NILV-PanCoVac in the Roborovski dwarf hamster model of COVID-19.

# 2 Materials and methods

## 2.1 *In silico* identification of epitopes

For PanCoVac design, NetMHCpan-4.1 in combination with data available in the Immune Epitope Database (IEDB, http://www.iedb.org/) were used to identify peptides potentially binding to human MHC-I (HLA-I) alleles (HLA-A, HLA-B, and HLA-C). NetMHCIIpan 4.0 was used for bioinformatic analysis of peptide binding to human MHC-II (HLA-II) alleles (92). Conserved regions of at least 8 amino acids from the structural proteins of SARS-CoV-1 (Tor 2), ancestral SARS-CoV-2 (Wuhan-Hu-1), SARS-CoV-2 variants (B.1.1.7, Alpha; B.1.351, Beta; P.1, Gamma), and common cold coronaviruses (HKU1, 229E, NL63 and OC43) were considered using the commonly applied half-maximal inhibitory concentration ($IC_{50}$) threshold of 500 nM for HLA-I and 1000 nM for HLA-II.

## 2.2 *In silico* testing of antigenicity, allergenicity, and toxicity

For predicting antigenicity of PanCoVac, we used VaxiJen, the web server for alignment independent prediction of protective antigens (http://www.ddgpharmfac.net/vaxijen/VaxiJen/VaxiJen.html). Prediction is based on auto- and cross-covariance (ACC) transformation method. The threshold was adjusted to 0.5, the recommended threshold for maximal accuracy (93). The web server AllerCatPro 2.0 (https://allercatpro.bii.a-star.edu.sg/) was used for predicting allergenic potential (94). We analyzed peptide toxicity using the web server ToxinPred (https://webs.iiitd.edu.in/raghava/toxinpred/pep_test.php). This tool was adjusted to screen all PanCoVac peptides at fragment length of 20 amino acids. We applied a hybrid approach that combines support vector machine (SVM) output, at a threshold of 1.0, with motif information for a biologically reliable prediction of toxic peptides (95).

## 2.3 Codon optimization

PanCoVac amino acid sequence was reverse translated and the DNA codon usage was optimized for human cell expression using the Codon Optimization tool from Integrated DNA Technologies (IDT) (www.idtdna.com). The final PanCoVac DNA sequence was synthesized by Thermo-Fisher Scientific and cloned into pLeGO-iG2 (96). LeGO-iG2 was a gift from Boris Fehse (Addgene plasmid # 27341; http://n2t.net/addgene:27341; RRID: Addgene_27341). The PanCoVac sequences were inserted at the BamHI and NotI multiple-cloning site, followed by an internal ribosome entry site (IRES), which drives expression of enhanced green fluorescence protein (EGFP).

## 2.4 Detection of PanCoVac protein

We generated a FLAG-tagged version of PanCoVacE6 (see 2.9) by fusing the FLAG peptide to the C-terminus of PanCoVacE6 (PanCoVacE6-FLAG). U251 cells were left untransfected or transfected with PanCoVacE6-FLAG mRNA using lipofectamineTM MessengerMaxTM (Thermo-Fisher Scientific) following the manufacturer´s instructions. After 24 h, the medium was removed and the cells were washed two times with PBS and subsequently lysed with M-PER™ Mammalian protein extraction reagent (Thermo-Fisher Scientific). Immunoblotting of PanCoVacE6-FLAG and glyceraldehyde-3-phosphate dehydrogenase (GAPDH) encoded by a

housekeeping gene was performed using anti-FLAG Antibody (FG4R) and anti-GAPDH antibody (1A10A10), respectively (both from Thermo-Fisher Scientific). The membrane was visualized using SuperSignal™ West Pico PLUS chemiluminescent substrate (Thermo-Fisher Scientific).

## 2.5 Cells and media

The glioblastoma cell line U251, which expresses HLA-A*0201, was a kind gift of L. Wiebusch (The Children's Hospital, Laboratory for Molecular Biology, Charité-Universitätsmedizin Berlin, Berlin, Germany). Human Embryonic Kidney (HEK)-293T cells were purchased from Sigma-Aldrich. HEK-293 T and U251 cells were cultured in Dulbecco's Modified Eagle Medium (DMEM) (Gibco™) supplemented with 1 mM sodium pyruvate (Gibco), 50 µg/ml gentamicin (Sigma-Aldrich), and 10% heat inactivated FBS (hiFBS) (HyClone™). Jurkat cells were cultured in RPMI 1640 medium (Gibco) supplemented with 2 mM L-glutamine (Gibco), 25 mM HEPES Buffer (Gibco), 50 µg/ml gentamicin, and 10% heat inactivated fetal bovine serum (hiFBS). Vero E6 cells (ATCC CRL-1586) were cultured in DMEM supplemented with 5% fetal bovine serum (PAN Biotech) as well as 100 IU/ml penicillin G and 100 µg/ml streptomycin (Corning).

## 2.6 Production and titration of lentivirus particles

Non-integrating lentiviral vector (NILV) particles were produced using HEK-293 T cells, as previously described (97, 98). Briefly, HEK-293T cells were transiently co-transfected with pLeGo-iG2-PanCoVac or empty vector, pMD2.G expressing the envelope glycoprotein of vesicular stomatitis virus Indiana (VSV-G), and encapsidation plasmid pD64V by using Lipofectamine™ 3000 (Thermo-Fisher Scientific). The plasmid pMD2.G (Addgene plasmid # 12259; http://n2t.net/addgene:12259; RRID: Addgene_12259) was a gift from Didier Trono (Laboratory for Virology and Genetics, School of Life Sciences, École Polytechnique Fédérale de Lausanne, Switzerland). For production of integrating lentiviral vector (LV) particles, pMDLg/pRRE (99) and pRSV-Rev (99) were used as packaging plasmids. Both, pMDLg/pRRE (Addgene plasmid # 12251; http://n2t.net/addgene:12251; RRID: Addgene_12251) and pRSV-Rev (Addgene plasmid # 12253; http://n2t.net/addgene:12253; RRID : Addgene_12253) were also gifts from Didier Trono.

At 24 h after transfection, the medium was changed. The supernatants were harvested at 48 h after transfection and cell debris was removed by 10 min centrifugation at 600 × g at 4°C. The virus particles were concentrated by ultracentrifugation at 30,000 rpm for 90 min at 4°C in thinwall polypropylene tubes (Beckmann Coulter) containing a 2 ml layer of 20% sucrose in PBS at the bottom. Lentivirus particles were resuspended in PBS, aliquoted and stored in -80°C until further use. Lentivirus vector copies were quantified by RT-qPCR as previously described (100) using SYBR Green and EGFP specific primers (EGFP_F: CACATGAAGCAGCACGACTT and EGFP_R: TGCTCAGGTAGTGGTTGTCG).

## 2.7 Transduction of U251 cells

Transduction of U251 cells with lentivirus particles was carried out as previously described (101). Briefly, the U251 cell suspensions ($1 \times 10^6$ cells in 1 ml of DMEM) were transduced with concentrated viral particles at a multiplicity of infection (MOI) of 2 in the presence of 8 µg/ml polybrene (Sigma-Aldrich). The cells were incubated at 37°C for 1 h, then spinoculated by centrifugation for 90 min at 600 × g at room temperature followed by seeding in 1.5 ml of fresh media in 6-well cell culture plates. Transduced cells were expanded and passaged in supplemented DMEM. The maximum number of passages before being included in assays was 2 for NILV- and 15 for LV-transduced cells.

## 2.8 *In vitro* mRNA transcription and mRNA transfection

First, we amplified the sequences of interest by PCR. The primer sequences for EGFP were: TAATACGACTCACTATAGATG GTGAGCAAGGGCGAGGAGC (forward primer) and TTA CTTGTACAGCTCGTCCATG (reverse primer). PanCoVac was amplified with GCTAATACGACTCACTATAGGGACAGGCC ACCATGGACTGGACCTGGATCCT as forward and TCATTT CTTTTTTTTGTCCTTTTTAGGCT as reverse primers, respectively. Then, *in vitro*-transcribed (IVT) mRNA of EGFP and PanCoVac were synthesized by using the HiScribe™ T7 ARCA mRNA Kit with tailing (New England Biolabs). Pseudo-UTP and 5-Methyl-CTP (Jena Bioscience) were used as modified nucleotides for mRNA synthesis. The synthesized mRNA was purified by the Monarch®RNA Cleanup Kit (New England Biolabs), aliquoted and stored at -80°C until further use. The mRNA purity and concentrations were analyzed using Nanodrop™ spectrophotometer (Thermo-Fisher Scientific). The mRNA transfection into U251 cells was carried out using lipofectamine™ MessengerMax™ (Thermo-Fisher Scientific) following the manufacturer´s instructions.

## 2.9 Reporter T cell assays

The reporter T cell assay was carried out as described previously (101). We used Jurkat cells expressing a HLA-A*0201-restricted TCR recognizing the epitope $E6_{29-38}$ (TIHDIILECV) derived from the E6 protein of human papillomavirus (HPV) type 16 (102). These cells also express an EGFP reporter driven by activation of nuclear factor kappa-light-chain-enhancer of activated B-cells (NF-κB) (103). In order to investigate processing and presentation, the HPV 16 $E6_{29-38}$ epitope was inserted in the middle of the S module of PanCoVac resulting in PanCoVacE6. To address the influence of the furin cleavage sites on processing and presentation of PanCovacE6, we generated a version of PanCoVacE6 lacking all

the furin cleavage sites (PanCoVacE6Δfurin). The reporter T cells were stimulated with HLA-A*0201 expressing U251 cells, which had been transduced with integrating lentiviral vector (LV) or NILV encoding PanCoVacE6 (LV-PanCoVacE6 and NILV-PanCoVacE6, respectively). Moreover, we transfected U251 cells with 100 ng of *in vitro*-transcribed PanCoVacE6 mRNA or PanCoVacE6Δfurin. As a negative control, the cells were transduced with lentiviral vector encoding untagged PanCoVac (LV-PanCoVac) or transfected with 100 ng of EGFP mRNA. U251 cells pulsed with 1 µg/ml of HPV $E6_{29-38}$ peptide were used as a positive control. The transduced or transfected U251 cells as well as positive and negative control cells were seeded in 96-well plates and incubated for 18 h. Afterwards, the reporter cells were added at a reporter cell to antigen-presenting cell (APC) ratio of 2:1. Co-culture was done for 24 h, then cells were removed and reporter cells were stained with Brilliant Violet 711™ anti-human CD3ϵ antibody (BioLegend) and the viability dye Zombie Violet™ (BioLegend). Stimulation of the reporter T cells with HPV E6-peptide bound to HLA-A*0201 was analyzed by detection of NF-κB driven EGFP fluorescence using FACS.

## 2.10 Roborovski dwarf hamster model and vaccination

The COVID-19 model based on Roborovski dwarf hamster (*P. roborovskii*) has been described previously (104). All animal procedures were performed according to the European Guidelines for Animal Studies after approval by the Institutional Animal Care Committee and the relevant state authority (Landesamt für Gesundheit und Soziales, Berlin, Permit number 0086/20). We obtained male and female Roborovski dwarf hamsters of 5 to 7 weeks of age from the German pet trade. Animals were housed in groups of 3–6 hamsters in GR-900 IVC cages (Tecniplast, Buguggiate) and provided with bountiful enrichment and nesting materials (Carfil, Oud-Turnhout). We randomly distributed animals into two groups; the test group (9 animals) was immunized with NILV-PanCoVac whereas the control group (9 animals) was immunized with empty vector (NILV) (Supplementary Table 1) shows number, sex distribution, and analysis date of experimental animals). All experimental animals were individually marked with a subcutaneously implanted IPTT-300 transponder (BMDS, Seaford) that facilitates remote identification and measurement of body temperature. The hamsters were inoculated i.n. with 30 µl PBS containing $1\times10^5$ NILV-PanCoVac particles or NILV. After 21 days, the hamsters were challenged with a sub-lethal dose ($1\times10^4$ pfu) of the ancestral SARS-CoV-2 (BetaCoV/Germany/BavPat1/2020) strain in 30 µl cell culture medium. SARS-CoV-2 infection was performed i.n. as previously described (104).

RNA was extracted from oropharyngeal swabs and 50 mg lung tissue using the innuPREP Virus DNA/RNA Kit (Analytic Jena) according to the manufacturer's instructions. Genomic virus RNA was quantified using a one-step RT–qPCR reaction with the NEB Luna Universal Probe One-Step RT–qPCR (New England Biolabs) and the 2019-nCoV RT–qPCR primers and probe (E_Sarbeco) on a qTOWER³ Real-Time PCR System (Analytik Jena), as previously described (104, 105). To obtain virus titers, duplicate ten-fold serial dilutions of lung tissue homogenates were plated on Vero E6 monolayers for 2 h at 37 °C. Afterwards, cells were washed with PBS and overlaid with semi-solid cell culture medium containing 1.5% microcrystalline cellulose (Vivapur MCG 611P, JRS Pharma) and incubated for 48 h at 37 °C. Plates were then fixed with 4% formalin and stained with 0.75% crystal violet for plaque counting

## 2.11 Lung histopathology

Samples from the lung tissue of hamsters were fixed with formalin, embedded in paraffin and analyzed as described previously (106). Briefly, paraffin sections of 2 µm thickness were prepared and stained with hematoxylin and eosin (HE). Microscopic changes were qualitatively described and scored according to standardized reporting criteria using a four-scale severity grading system (0: no lesions, 1: mild, 2: moderate, and 3: severe).

## 2.12 Serum neutralization tests

The capacity of sera obtained from dwarf hamsters after SARS-CoV-2 challenge to neutralize SARS-CoV-2 was assessed *in vitro* as previously described (107). After inactivation of complement for 30 min at 56 C°, sera were prepared in duplicates as two fold serial dilutions in Minimum Essential Medium (MEM) supplemented with 10% FBS and penicillin/streptomycin in 96-well cell culture plates (Sarstedt). To each serum dilution and the respective control wells, 40 pfu of SARS-CoV-2 was added and neutralization was allowed to proceed for 30 min at room temperature. Afterwards, approximately $1 \times 10^4$ Vero E6 cells were added to each well. Subsequently, the plates were incubated at 37 C° under a 5% $CO_2$ atmosphere for 3 days, fixed with 4% formaldehyde and stained with 0.75% crystal violet (aqueous solution) for quantification of cytopathic effects (CPE). Virus neutralization was considered successful in wells with no evidence of CPE and the last effective serum dilution was counted.

## 2.13 Statistical analysis

FACS results were evaluated with FlowJo V10.8.0 (Tree Star, Inc). Statistical analyses were performed using GraphPad Prism 9.5.0. The statistical details of all experiments are described in the respective figure legends. Significance of the data was assumed if $p \leq 0.05$.

# 3 Results

## 3.1 Design of the pan-coronavirus vaccine

Using bioinformatic tools, we deconstructed coronavirus genomes and designed a DNA sequence (PanCoVac) encoding

the conserved T-cell epitopes of all structural proteins (S, E, M, and N) from coronaviruses (Figure 1). The most essential step during processing and presentation of T cell epitopes is binding to MHC molecules, which are extremely polymorphic. CD8+ T cells recognize peptides bound to the polymorphic regions of MHC class I (MHC-I) molecules on the surface of virus-infected cells. These peptides are mostly derived from intracellular proteins undergoing proteasomal degradation in the cytosol. The resulting cytosolic peptides are transferred *via* transporter associated with antigen processing (TAP) molecules into the endoplasmic reticulum (ER) and subsequently loaded onto MHC-I molecules (108). In contrast, CD4+ T cells detect peptides bound to MHC class II (MHC-II) molecules on the surface of professional APCs. These peptides are obtained from extracellular proteins after cellular uptake and digestion (108).

Conserved regions of at least 8 amino acids from the structural proteins of SARS-CoV-1 (Tor2), ancestral SARS-CoV-2 (Wuhan-Hu-1), SARS-CoV-2 variants (B.1.1.7, Alpha; B.1.351, Beta; B.1.617.2, Delta; P.1, Gamma; BA.1, Omicron), and common cold coronaviruses (HKU1, 229E, NL63 and OC43) were considered. The alignment of these conserved amino acid sequences with PanCoVac is shown in Supplementary Figure 1. PanCoVac-encoded peptides are supposed to bind to all nine HLA-I supertypes, which are defined as groups of molecules that share largely overlapping peptide binding specificities (109), as well as other common HLA-I alleles (Supplementary Table 2). In addition, we determined PanCoVAc-encoded peptides that are supposed to bind to HLA-II molecules (Supplementary Table 3). Due to the high and comprehensive workload, we have not analyzed all HLA-II molecules but focused on frequent HLA-DR alleles (HLA-DRB1*01:01, HLA-DRB1*04:01, HLA-DRB1*07:01, HLA-DRB1*09:01, HLA-DRB1*1302, HLA-DRB1*15:01, HLA-DRB5*01:01). A very high percentage of experimentally validated HLA-I epitopes matches those that have been predicted by *in silico* analysis but experimental epitope screenings may be slightly biased due to the low frequency of some alleles analyzed (110). Thus, most of the SARS-CoV-2-derived peptides that have been shown to stimulate T cells from convalescent individuals are present in PanCoVac (42, 111). PanCoVac also encodes immunodominant CD8+ T cell epitopes (e.g. N105–113, SPRWYFYYL) and CD4+ T cell epitopes (e.g. M176–190, LSYYKLGASQRVAGD), which have broad HLA binding capacity as their main feature (42, 111).

The DNA sequences encoding the identified T cell epitopes were fused to generate a "string of beads" multi-epitope vaccine. It has been demonstrated that oligo-alanine spacing of epitopes can increase their processing and recognition by T cells (112, 113). For this reason, we joined epitopes belonging to the same structural protein by double alanine linkers (AA) thereby generating a single immunogenic compact module. The different immunogenic modules (S, E, M, and N) were separated by furin cleavage sites

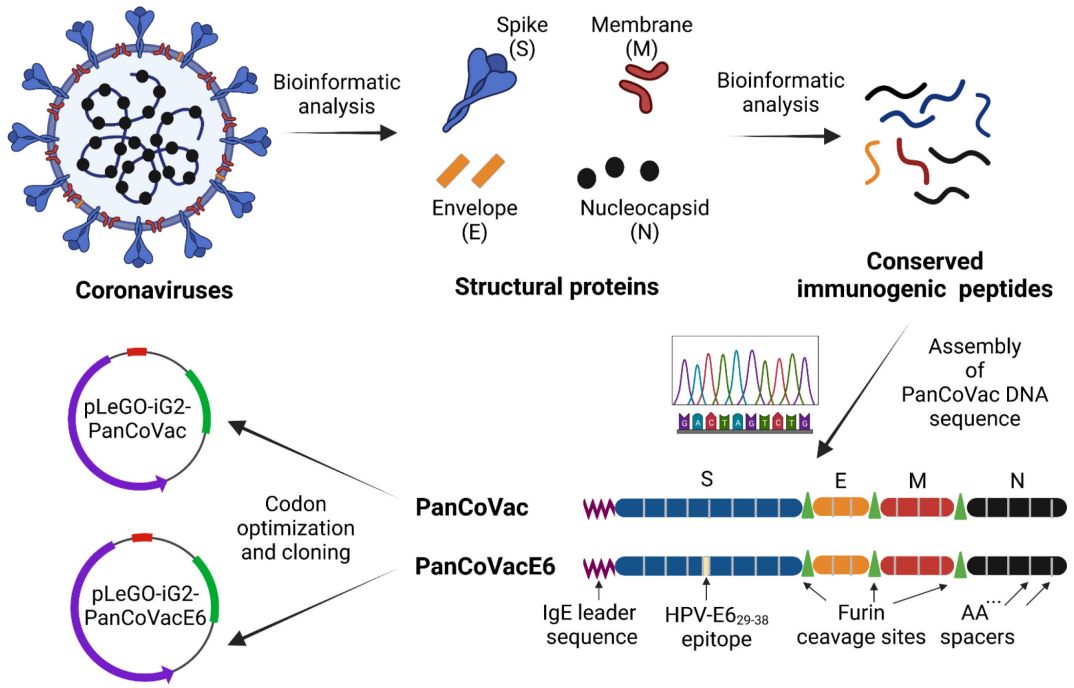


FIGURE 1
PanCoVac design. Structural proteins (S, E, M, N) from coronaviruses were analyzed. Conserved immunogenic peptides from all structural proteins were identified by bioinformatics analyses. The conserved immunogenic peptides from each protein were linked together with double alanine (AA) spacers resulting in four polypeptide blocks which were fused together by furin cleavage sites. An IgE leader sequence was attached to the N terminus. In order to investigate processing and presentation, the HPV 16 E6$_{29–38}$ (TIHDIILECV) epitope, which binds to HLA-A*0201, was inserted in the middle of the S module (PanCoVacE6). The amino acid sequences of PanCoVac and PanCovacE6 were codon optimized for human expression and cloned into pLeGo-iG2 plasmids (pLeGo-iG2-PanCoVac, pLeGo-iG2-PanCoVacE6).

(Figure 1). Furin is a cellular endoprotease that is principally located in the *trans*-Golgi network (TGN), which is responsible for sorting secretory pathway proteins to their final destinations, including the cell surface, endosomes, lysosomes and secretory granules (114). Importantly, furin processes T cell epitopes independently from TAP and the proteasome (115–117). In addition, an immunoglobin E (IgE) leader sequence consisting of 18 amino acids (118) was attached to the 5′end (N-Terminus) of PanCoVac to achieve strong expression (Figure 1). Moreover, the PanCoVac was codon optimized to further increase its expression. Finally, *in-silico* antigenicity prediction using VaxiJen, showed an antigen score of 0.5308 indicating the probable antigenic nature of PanCoVac. Neither the *in silico* testing of the allergenic potential of PanCoVac protein using AllerCatPro 2.0 nor the peptide toxicity testing using ToxinPred provided evidence that PanCoVac is allergenic or yields additional toxic peptides as compared to the original sequences of the viral proteins. Accordingly, bioinformatic tools predicted that PanCoVac is probably an antigenic protein but has no allergic or toxic side effects. PanCoVac can be loaded onto any available vaccine platform to create coronavirus vaccines that could provide broad, robust, and durable T cell responses.

## 3.2 Processing and presentation of PanCoVac-encoded epitopes *in vitro*

We confirmed that PanCoVac is expressed, processed and presented *in vitro* by using a T cell reporter assay. For this purpose, we tagged PanCoVac in the middle of the S module with a sequence encoding the HLA-A*0201-binding epitope $E6_{29-38}$ (TIHDIILECV) derived from the E6 protein of HPV type 16 resulting in PanCoVacE6 (Figure 1) (102). We transduced U251 cells (HLA-A*0201+) with LV or NILV expressing PanCoVacE6 or untagged PanCoVac as a negative control. U251 cells were also transfected with PanCoVacE6 mRNA or EGFP mRNA as a negative control. U251 cells transfected with PanCoVacE6 mRNA, but not U251 cells transfected with EGFP mRNA, stimulated HPV E6-specific reporter T cells (Figure 2A). Moreover, U251 cells transduced with LV or NILV expressing PanCoVacE6 both strongly activated HPV $E6_{29-38}$ specific reporter T cells whereas U251 cells transduced with untagged PanCoVac did not (Figure 2A). We also transfected U251 cells with PanCoVac mRNA containing a FLAG tag-encoding sequence and detected PanCoVac in western blot analysis using antibodies against the FLAG tag (Supplementary Figure 2).

Finally, we tested whether the furin cleavage sites of PanCoVac affects processing and presentation the HPV $E6_{29-38}$ –peptide. For this purpose, we compared PanCoVacE6 with a PanCoVacE6 construct that has no furin cleavage sites (PanCoVacE6Δfurin). We observed a very small but significant increase in HPV E6-specific reporter T cell activation when U251 cells transfected with PanCoVacE6 (containing furin cleavage sites) were used for stimulation as compared to cells transfected with PanCoVacE6Δfurin (Figure 2B). However, the binding affinity of the HPV $E6_{29-38}$ –peptide for HLA-A*0201 is very high (102) and our reporter T cell assay operates in the saturated range. Thus, the positive effect of furin cleavage on processing and presentation of PanCoVac-encoded epitopes with lower binding affinity for MHC-I molecules is most likely much more pronounced. Altogether, these results strongly suggest PanCoVac-encoded epitopes are processed and presented in cells expressing PanCoVac.

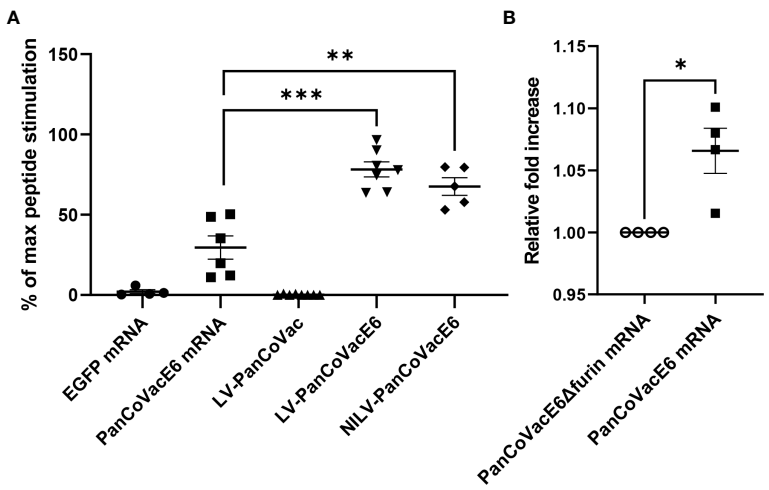


FIGURE 2
Stimulation of HPV E6-specific reporter T cells by PanCoVacE6 expressing cells. **(A)** U251 cells were transduced with PanCoVac or PanCoVacE6 using LV or NILV. In addition, U251 cells were transfected with either EGFP mRNA or PanCoVacE6 mRNA. After 18 h, the medium was removed and HPV E6 peptide-specific reporter cells were added at a ratio 2:1 for 24 h. Subsequently, the cells were collected, washed and stained with BV711 mouse anti-human CD3 antibody and live/dead Zombie Violet dye. Stimulation of reporter cells is given as percentage of maximal peptide stimulation, i.e. stimulation of reporter cells with U251 cells pulsed with HPV E6 peptide (TIHDIILECV). Results are derived from at least 5 independent experiments; error bars represent the mean ± SEM.; ***P < 0.001; **P < 0.01; ns not significant, unpaired t-test. **(B)** U251 cells were transfected with PanCoVacE6Δfurin mRNA (control) and PanCoVacE6 mRNA, respectively. HPV E6 peptide-specific reporter cells were added to transfected U251 cells as described in **(A)**. The results are shown as fold change relative to the control. Results are derived from 4 independent experiments; error bars represent the mean ± SEM.; *P < 0.05, unpaired t-test.

## 3.3 Mild course of SARS-CoV-2 infection in Roborovski dwarf hamsters after vaccination with NILV-PanCoVac

The protective effect of PanCoVac was tested in Roborovski dwarf hamsters, which represent an appropriate model for analyzing the pathology of COVID-19 (104, 119). To this end, hamsters were vaccinated i.n. either with a single-low dose ($1 \times 10^5$ pfu) of NILV-PanCoVac (9 animals) or empty NILV particles (9 animals) as a control. After 21 days, the animals were challenged i.n. with a sublethal dose ($1{\times}10^4$ pfu) of the ancestral SARS-CoV-2 (Wuhan) strain. We observed a drop in body temperature in the control group vaccinated with empty NILV particles (Figure 3A), which indicates a more severe course of SARS-CoV-2 infection in Roborovski dwarf hamsters (104). *Vis-a-vis*, NILV-PanCoVac vaccinated hamsters kept more steady body temperatures demonstrating a very mild infection course (Figure 3A). In addition, body weights of dwarf hamsters that had received empty NILV particles went down until 5 dpi then returned to pre-infection values whereas body weights of animals vaccinated with NILV-PanCoVac were stable (Figure 3B).

At 2 dpi, 5 dpi, and 7 dpi, three animals of each group were sacrificed and sera, oropharyngeal swabs and lung tissue were collected for further analysis. The histopathological analysis of lung tissue also demonstrates the protective effect of a single-low dose of i.n. NILV-PanCoVac. The representative histopathology in Figure 4 shows pathological changes at 2 dpi especially in lung tissue derived from NILV-vaccinated animals: bronchioli with mild bronchiolitis and moderate epithelial cell necrosis; respiratory parenchyma with moderate to severe inflammation, alveolar wall necrosis and alveolar edema; and blood vessels with endothelialitis. Cumulative histopathological scoring illustrates the finding that lung tissue from NILV-PanCoVac vaccinated animals was less affected by virus-induced damage and inflammation than the corresponding control tissue from animals vaccinated with empty NILV particles (Figure 5). The corresponding histopathological scoring at 2 dpi, 5 dpi and 7 dpi 2 is shown in Supplementary Figure 3. Altogether, these clinical and histopathological findings demonstrate a comparatively mild course of SARS-CoV-2 infection in Roborovski dwarf hamsters vaccinated i.n. with NILV-PanCoVac.

## 3.4 Independence of NILV-PanCoVac induced protection from SARS-CoV-2 neutralizing antibodies

Although PanCoVac is a T cell-based vaccine, we could not exclude *a priori* that NILV-PanCoVac induces virus-specific humoral immune responses. To clarify this issue, we performed

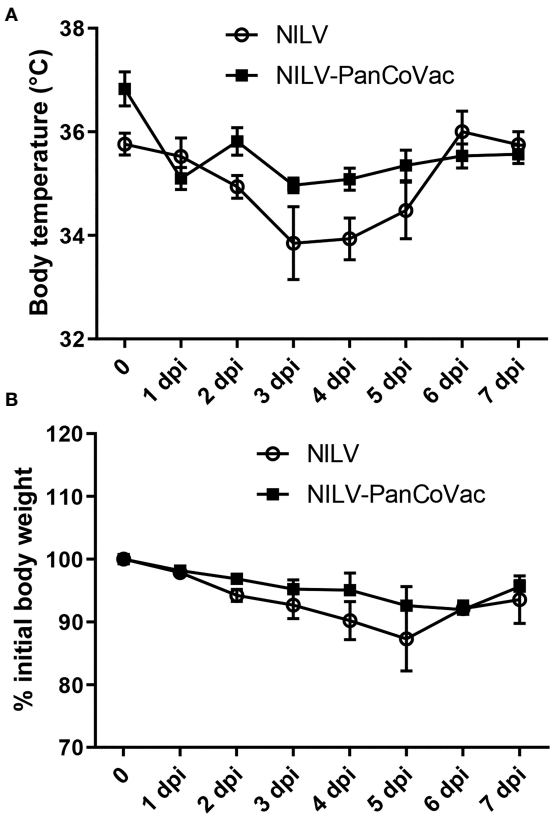


FIGURE 3
Body weight, body temperature and lung histopathology after challenge of vaccinated dwarf hamsters with SARS-CoV-2. Body temperature **(A)** and body weight **(B)** of dwarf hamsters vaccinated with NILV-PanCoVac or NILV were monitored on a daily basis until the experiment was terminated at 7 days post infection (dpi).

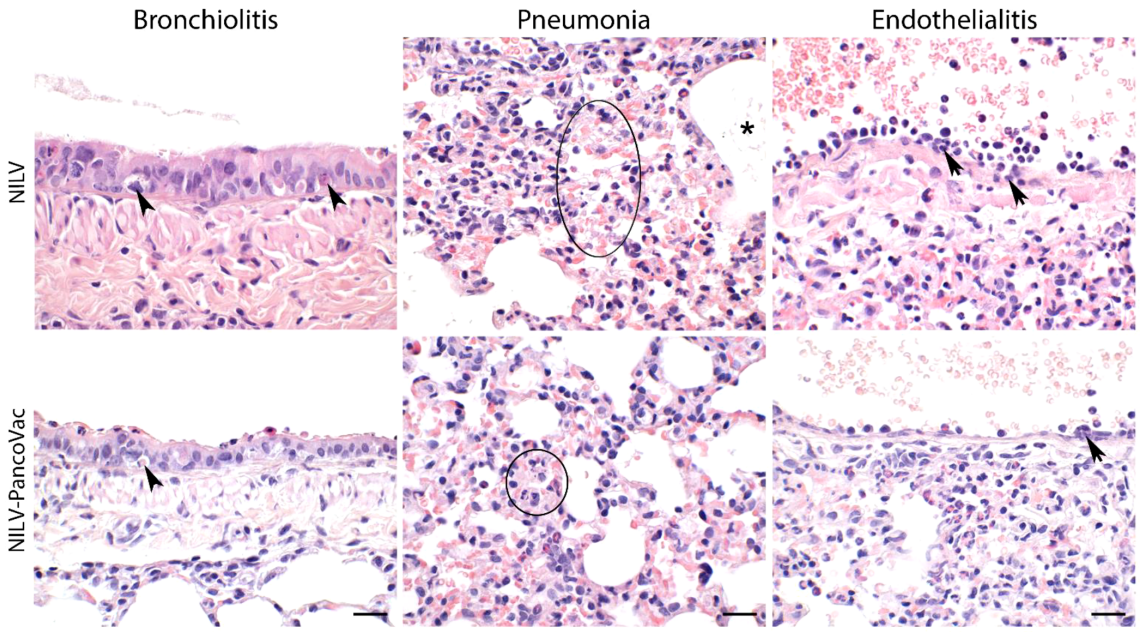


FIGURE 4
Representative histopathology of lung tissue derived from NILV or NILV-PanCoVac vaccinated Roborovski dwarf hamsters after challenge with SARS-CoV-2. At 2 dpi, bronchioli with mild bronchiolitis and moderate epithelial cell necrosis (arrow heads; left panel) were observed. The respiratory parenchyma presented with moderate to severe inflammation, alveolar wall necrosis (circle; central panel) and alveolar edema (asterisk; central panel). Histopathological analysis of blood vessels revealed endothelialitis (arrows; right panel). Haematoxylin and eosin stain; bars represent 20 µm.

neutralization assays with sera from Roborovski dwarf hamsters after i.n. vaccination with NILV-PanCoVac and empty NILV particles, respectively. The systemic humoral immunity induced by i.n. vaccination is usually comparable to or even stronger than that after intramuscular injection (25, 120, 121). This is also true for hamsters immunized against SARS-CoV-2 with a single-low dose of a vectored S protein-based vaccine administered i.n (120). In serum neutralization assays, we did not detect any difference in the timing or level of neutralizing antibody production between animals vaccinated i.n. with NILV-PanCoVac and those vaccinated i.n. with empty NILV particles (Figure 6A). Neutralizing antibody production was not detectable at 2 dpi and started at 5 dpi (Figure 6A). At 7 dpi, high neutralizing antibody titers were measured in both NILV-PanCoVac animals and animals immunized with empty NILV (Figure 6A). This result suggested that the protective effect of NILV-PanCoVac was not associated with sterilizing immunity, which requires induction of neutralizing antibodies at the site of infection (122). To analyze sterilizing immunity, we determined the viral load in the oropharyngeal mucosa using quantitative RT-qPCR. As shown in Figure 6B, we did not observe significant differences between NILV-PanCoVac vaccinated and control animals regarding the viral load in the oropharynx. This experiment confirms that NILV-PanCoVac did not stimulate production of neutralizing antibodies in the oropharyngeal mucosa. Thus, in Roborovski dwarf hamsters a single-low dose of NILV-PanCoVac did induce SARS-CoV-2 neutralizing antibodies neither systemically nor in the mucosa of the oropharynx.

### 3.5 Early protective effect of NILV-PanCoVac in Roborovski dwarf hamsters

Next, we determined the viral load in lung tissue. The cumulative SARS-CoV-2 genome copy numbers (Figure 7A, right graph) and virus titers (Figure 7B, right graph) were significantly lower in lung tissue from NILV-PanCoVac vaccinated animals as compared to control animals that had received empty NILV particles. Intriguingly, the protective effect of NILV-PanCoVac vaccination on the viral load in lung tissue was already very strong at 2 dpi (Figures 7A, B, left graphs). At this time point, SARS-CoV-2 neutralizing antibodies were detectable neither in animals vaccinated with NILV-PanCoVac nor in animals vaccinated with empty NILV particles (Figure 6A). Taken together these results provide evidence that the protective effect of i.n. administered NILV-PanCoVac in Roborovski dwarf hamsters challenged with SARS-CoV-2 was most likely due to airway memory T cells that can mount a strong early antiviral response.

## 4 Discussion

We designed a codon-optimized universal coronavirus vaccine (PanCoVac) encoding conserved T-cell epitopes derived from all structural proteins (S, E, M, and N) for use in human populations. Using a tagged version of PanCoVac, we demonstrated in T cell reporter assays that the PanCoVac-design allows expression, processing, and presentation by human cells. Finally, we

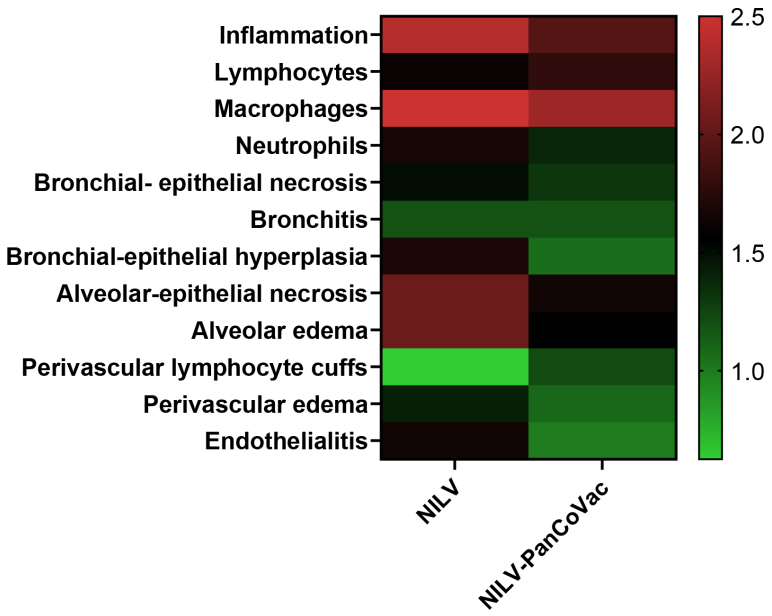


FIGURE 5
Histopathological scores of lung tissue derived from NILV or NILV-PanCoVac vaccinated Roborovski dwarf hamsters after challenge with SARS-CoV-2. At 2 days post infection (dpi), 5 dpi and 7 dpi, three animals of each group were sacrificed and histopathological changes in the lung were scored using a four-scale severity grading system (0: no lesions, 1: mild, 2: moderate, and 3: severe). The cumulative results are also shown.

evaluated the vaccine in the Roborovski dwarf hamster model of COVID-19. We observed a milder course of sublethal SARS-CoV-2 infection in Roborovski dwarf hamsters after vaccination with a single-low dose of NILV-PanCoVac as compared to animals receiving empty NILV particles. In vaccinated animals the viral load was reduced within 2 days after challenge. The NILV-PanCoVac induced immunity, however, was not sterilizing and independent of neutralizing antibodies.

Conserved T-cell epitopes of coronaviruses can elicit broadly cross-reactive T cells. For example, CD8+ T cells specific for a highly conserved N-encoded epitope of SARS-CoV-2 were found in unexposed donors and could be stimulated by homologous peptide sequences of seasonal coronaviruses (123). Mounting evidence suggests that during vaccination or infection, cross-reactive T cells are integrated into SARS-CoV-2 specific immunity and contribute to protection from COVID-19 (41, 124, 125). Epidemiological studies revealed that individuals infected recently with common cold coronaviruses had less severe COVID-19 outcomes (126, 127). Healthcare workers with cross-reactive T cells against the virus-encoded RNA polymerase, a protein that is highly conserved across coronaviruses, cleared subclinical SARS-CoV-2 infection before seroconversion (88). This is confirmed by studies of household contacts of COVID-19 patients demonstrating that induction of virus-specific T cell responses without seroconversion protect from SARS-CoV-2 infection (81, 128). Finally, in the absence of neutralizing antibodies, T cells provided effective protection against the Beta variant of SARS-CoV-2 in a transgenic mouse model of SARS-CoV-2 infection (129). Thus, clinical studies and animal experiments suggest that cross-reactive T cells can clear SARS-CoV-2 independently of humoral immunity.

Why did pre-existing cross-reactive T cell immunity not have a greater impact on the course of the pandemic although it was detected in a large proportion of healthy, SARS-CoV-2–naive individuals? There are at least two mutually not exclusive explanations. Firstly, cross-reactive T cells protect from severe disease but less efficiently from infection and virus transmission to other persons. Secondly, cross-reactive immunity is virtually absent in individuals that are at risk of severe SARS-CoV-2 infection. Indeed, functional pre-existing SARS-CoV-2-reactive memory T cells are induced by common cold coronavirus in early childhood, peak at age six, and subsequently decline with age (130, 131). This finding explains the age-dependent ability to control SARS-CoV-2 infection with older adult people, who often suffer from comorbidities, at risk of an unfavorable outcome (132). In accordance, CD8+ T cells specific for conserved coronavirus epitopes are much more abundant in patients with mild COVID-19 as compared to individuals with more severe illness (133). This indicates that especially individuals at high-risk of COVID-19 could benefit from vaccines that strengthen T cell responses against conserved coronavirus epitopes.

Current COVID-19 vaccines are approved for intramuscular application notwithstanding that SARS-CoV-2 is spreading *via* the mucosa of the respiratory tract. For this type of viral pathogens, the innate and adaptive immune responses in the lung and airways following infection and vaccination play a pivotal role (reviewed in (25, 134). In SARS-CoV-2 susceptible mice, even a single-dose i.n. immunization with a replication-deficient adenoviral vector expressing the RBD of SARS-CoV-2 S protein induced robust immunity both in the mucosa of the respiratory tract and systemically (135, 136). Along this line, a trivalent vaccine based

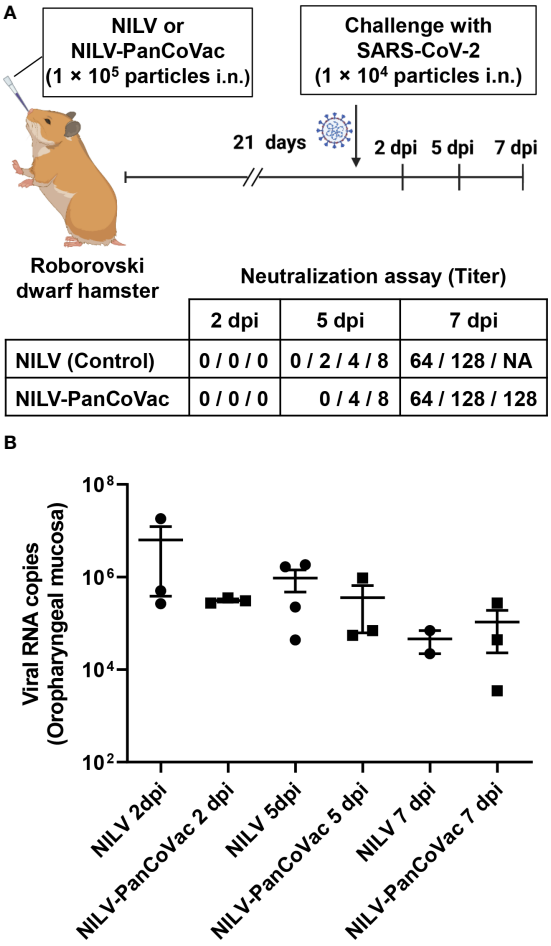


FIGURE 6
Titers of SARS-CoV-2 neutralizing antibodies in sera and SARS-CoV-2 quantification in oropharyngeal swabs derived from of infected dwarf hamsters. Roborovski dwarf hamsters (*P. roborovskii*) were immunized i.n. with $1x10^5$ particles either NILV-PanCoVac (9 animals) or NILV (9 animals). After 21 days, the hamsters were challenged with a sublethal dose ($1x10^4$ pfu) of the ancestral SARS-CoV-2 (Wuhan) strain. At 2 dpi, 5 dpi, and 7 dpi, three animals of each group were sacrificed and sera and oropharyngeal swabs were collected for further analysis. **(A)** Titers of SARS-CoV-2 neutralizing antibodies were determined. Shown is the maximal serum dilution that still completely neutralized SARS-CoV-2 in a cell culture assay. **(B)** SARS-CoV-2 genome copy numbers in oropharyngeal swabs derived from animals vaccinated either with NILV-PanCoVac or NILV (control) were determined. One animal in the NILV-vaccinated group scheduled for the analysis at 7 dpi (Hamster No. 8) died at 4 dpi. The corresponding serum and oropharyngeal swab, respectively was analyzed together with the probes scheduled for 5 dpi resulting in 4 measured values at this time point.

on adenoviral vectors expressing antigens derived from the S-protein, N protein, and RNA-dependent RNA polymerase induced local and systemic antibody responses and protected against both the ancestral SARS-CoV-2 strain and two VOCs (137).

After i.n. immunization with a single-low dose of NILV-PanCoVac, we observed a strong protective effect at 2 dpi. At this early time point, we did not detect neutralizing antibodies in the sera of vaccinated animals suggesting that T cells were responsible. In accordance, antiviral CD8+ T cells induced by a neutralizing antibody-independent i.n. vaccine curbed viral spread in the respiratory tract of macaques after SARS-CoV-2 challenge (138). PanCoVac also encodes a highly conserved region of the N protein, which not only cross-protected mice from human and bat coronaviruses after i.n. vaccination but also is presented by human MHC-II molecules (139). The protective effect was observed within 1-2 days after challenge and mediated by memory CD4+ T cells that secreted interferon-γ and supported strong innate as well as virus-specific CD8+ T cell responses (139). Moreover, systemic immunization of mice with dendritic cells (DCs) presenting a single SARS-CoV-1 epitope followed by i.n. boosting with recombinant vaccinia virus encoding the same epitope resulted in accumulation of virus-specific memory CD8+ T cells in lungs and protected from lethal infection (140). Similarly, repeated booster vaccinations with a single T cell epitope induced CD8+ T cells that protected against lethal SARS-CoV-2 infection in a mouse model of COVID-19 (141). Others investigators have also demonstrated that in the absence of neutralizing antibodies, lung-resident memory CD4+ and CD8+ T cells provide effective protection against SARS-CoV-2 (142). It is conceivable that PanCoVac could induce similar memory T cells in Roborovski dwarf hamsters. Although virus neutralization is a key function of antiviral antibodies, they can also contribute to protection by other means, e.g. *via* binding to and triggering Fc receptors (143). Thus, we cannot categorically exclude the possibility that PanCoVac-

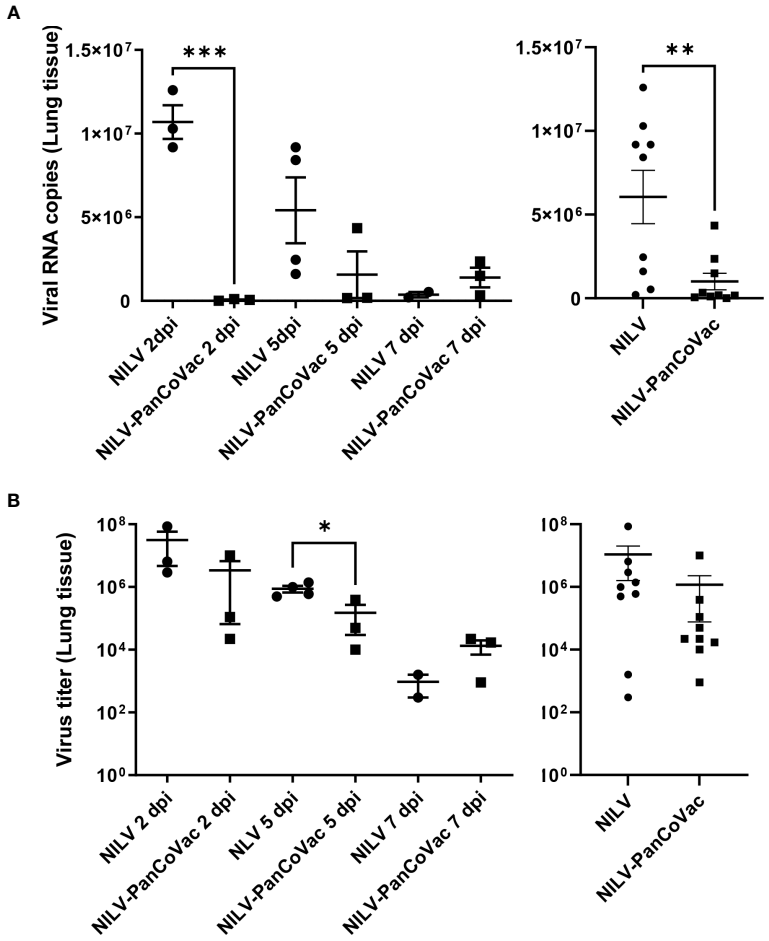


FIGURE 7
SARS-CoV-2 quantification in lung tissue from Roborovski dwarf hamsters after challenge with SARS-CoV-2. Roborovski dwarf hamsters (*P. roborovskii*) were immunized i.n. ($1x10^5$ particles) with NILV-PanCoVac (9 animals) or NILV (9 animals). After 21 days, the hamsters were challenged with a sublethal dose ($1x10^4$ pfu) of the ancestral SARS-CoV-2 (Wuhan) strain. At 2 dpi, 5 dpi and 7 dpi, three animals of each group were sacrificed and lung tissue was analyzed. **(A)** SARS-CoV-2 genome copy numbers per 2.5 mg lung tissue derived from animals vaccinated either with NILV-PanCoVac or NILV (control) were determined at the indicated time points (left graph). The cumulative results are also shown (right graph). **(B)** Virus titers in 50 mg lung tissues from animals vaccinated either with NILV-PanCoVac or NILV (control) were analyzed at the indicated time points (left graph). The cumulative results are also shown (right graph). Error bars represent the mean ± SEM; ***P < 0.001; **P < 0.01; *P < 0.05, unpaired t-test. One animal in the control group (Hamster No. 8) scheduled for the analysis at day 7 dpi died at 4 dpi. The corresponding lung tissue was analyzed together with the probes scheduled for 5 dpi resulting in 4 measured values at this time point.

induced antibodies contribute to the immune response against SARS-CoV-2. Altogether, PanCoVac-encoded conserved T cell epitopes could generate cross-reactive T cells in vaccinated humans that act as a first layer of defense. In accordance, T cells in the respiratory tract of a large proportion of unexposed individuals cross-react with SARS-CoV-2 and may enable rapid antiviral immune responses (86, 144, 145).

Vaccination with a single-low dose of NILV-PanCoVac did not prevent infection of the oropharynx, the site of SARS-CoV-2 entry. However, sterilizing immunity with prevention of virus transmission is difficult to achieve by single vaccination i.n. and requires vaccine boosts (122). Indeed, the protective effect of i.n. immunization can be enhanced if combined with systemic priming (prime-boost regime). For example, systemic priming and i.n. boost with NILV expressing S protein in the Syrian hamster model resulted in strong vaccine efficacy and only limited lung damage after challenge with SARS-CoV-2 (97). Similarly, prime and i.n. boost with adenoviral vector expressing both the S protein and N protein resulted in complete protection against SARS-CoV-2 (146). Moreover, Syrian hamsters immunized *via* the i.n. route with the S protein linked to outer membrane vesicles from *Neisseria meningitides* were protected from weight loss and viral replication in the lungs (147). In a mouse model of COVID-19, boosting mice i.n. with non-replicating adenovirus vectoring S protein after priming with lipid nanoparticles (LNPs) containing S protein-mRNA (heterologous prime-boost regime) improved SARS-CoV-2 immunity in the lung (148). Finally, a heterologous prime-boost regime using an i.n. unadjuvanted S protein boost after intramuscular priming with LNPs containing S protein-mRNA induces neutralizing immunoglobulin A at the respiratory mucosa and simultaneously increases systemic immunity, which protects from lethal SARS-CoV-2 infection (149). Intriguingly, i.n. boosting with a divergent S protein from SARS-CoV-2 induces mucosal immunity against diverse sarbecovirus clades (149).

The NILV vaccine platform has the advantage that vaccines get access to non-proliferating cells including DCs, which are located in the mucosa of the respiratory tract. NILV-transduced DCs show strong and reliable expression of the vectored protein (150–153). Importantly, DCs play a pivotal role in successful vaccinations (154). Firstly, they transport vaccine-encoded antigen to the T cell areas of lymphoid organs. Secondly, they efficiently process and present this antigen as peptides bound to MHC molecules to activate antigen-specific T cells. There are possible advantages of using NILV as a vaccine platform as compared to adenoviral vectors. For example, immunization with lentiviral vectors generates highly multifunctional CD8+ T cells and primes development of CD8+ T cells with central memory phenotype (155). In contrast to adenoviral vector, the problem of pre-existing immunity to the vector, which can prevent successful vaccination, does not exist for NILV due to pseudotyping with VSV-G. Thus, after i.n. immunization NILV-PanCoVac could induce a long-lasting, multi-functional T cell immunity against SARS-CoV-2.

Our study has several limitations. First of all, PanCoVac was designed for binding to a broad range of common human MHC molecules, which are highly polymorphic. Although not characterized, it is likely that the MHC molecules of dwarf hamster are less diverse and have different peptide binding traits when compared to human molecules. This suggests that only a single or very few PanCoVac-encoded epitopes bind to MHC molecules of Roborovski dwarf hamsters. Secondly, PanCoVac was codon optimized for expression in human cells. Thus, it is unlikely that PanCoVac-based vaccines develop their full protective potential in the Roborovski dwarf hamster model of COVID-19. Thirdly, we did not prime *via* systemic injection of a PanCoVac-based vaccine, which provides broader mucosal protection against SARS-CoV-2 after i.n. boosting (97, 149). Fourthly, we used a single-low dose of NILV particles ($1 \times 10^{5)}$ i.n. whereas a recent study, which analyzed the protective effect of NILV expressing S protein in the Syrian hamster model of COVID-19, primed systemically and boosted with a high dose of NILV particles ($1 \times 10^{8}$) i.n (97). Moreover, we challenged vaccinated dwarf hamster only with the ancestral strain of SARS-CoV- 2 but not against currently circulating VOCs. However, T cell epitopes are very resistant to antigenic evolution of SARS-CoV-2 as compared to epitopes recognized by neutralizing antibodies (60, 68, 69, 156). Thus, PanCoVac is most likely also protective against SARS-CoV-2 variants and subvariants. Finally, we did not study T cell responses because the necessary tools and reagents for studying specific T cell responses in Roborovski dwarf hamsters are not available.

In summary, we generated a universal vaccine (PanCoVac) encoding cross-reactive T cell epitopes that are highly conserved across structural proteins of human coronaviruses and bind to common human MHC molecules. Despite of the huge differences between human and hamster MHC molecules a single-low dose of a PanCoVac-based vaccine i.n. induced an early protective effect in Roborovski dwarf hamsters independently of neutralizing antibodies. The use of (HLA-) humanized animal models will allow for further efficacy studies of PanCoVac-based vaccines *in vivo*. In humans, PanCoVac could induce broad T cell responses that prevent severe disease courses leading to hospitalizations and death.

## Data availability statement

The original contributions presented in the study are included in the article/Supplementary Material. Further inquiries can be directed to the corresponding authors.

## Ethics statement

The animal experiments were reviewed and approved by the Landesamt für Gesundheit und Soziales (LAGeSo) in Berlin, Germany (permit number 0086/20). They were performed in compliance with relevant national and international guidelines for responsible care and humane use of animals in the BSL-3 facility at the Institute of Virology, Free University Berlin, Germany.

## Author contributions

MA and MR designed experiments, performed experiments, analyzed results, and co-wrote the article. JW, OB, RE, JK, DV, JA, TF, AV, AG, LH, IFM, FM-M, GW and NE conducted experiments and data analysis. JT and GS directed the project, designed experiments, interpreted results, and wrote the article. All authors contributed to the article and approved the submitted version.

## Funding

This work was supported by the SPARK-Validation Track II program of the Berlin Institute of Health. NE was funded by a full scholarship from the Ministry of Higher Education from the Arab Republic of Egypt.

## Acknowledgments

We would like to thank Dr. Azza Abdelgawad for excellent technical assistance. We are grateful to Prof. Dr. P. Steinberger, Vienna, for making the HPV E6-specific reporter T cell line available to us. The authors apologize that many research articles with relevance to the field were not included in this study due to space limitations.

## Conflict of interest

MA, MR and GS hold a patent EP4176898 related to the PanCoVac vaccine described herein.

The remaining authors declare that the research was conducted in the absence of any commercial or financial relationships that could be construed as a potential conflict of interest.

## Publisher's note



## Supplementary material

The Supplementary Material for this article can be found online at: https://www.frontiersin.org/articles/10.3389/fimmu.2023.1166765/full#supplementary-material

SUPPLEMENTARY FIGURE 1
(Alignment of PanCoVac with SARS-CoV-2 variants).

SUPPLEMENTARY FIGURE 2
(Western blot analysis of FLAG tagged PanCoVac).

SUPPLEMENTARY FIGURE 3
(Histopathological scoring of tissue).

SUPPLEMENTARY TABLE 1
(Sex distribution of Roborovski dwarf hamsters).

SUPPLEMENTARY TABLE 2
(HLA-I alleles presenting PanCoVac-encoded peptides).

SUPPLEMENTARY TABLE 3
(HLA-II alleles presenting PanCoVac-encoded peptides).

## References

1. Gorbalenya AE, Baker SC, Baric RS, de Groot RJ, Drosten C, Gulyaeva AA, et al. The species severe acute respiratory syndrome-related coronavirus: classifying 2019-nCoV and naming it SARS-CoV-2. *Nat Microbiol* (2020) 5:536–44. doi: 10.1038/s41564-020-0695-z

2. Menachery VD, Yount BLJr., Debbink K, Agnihothram S, Gralinski LE, Plante JA, et al. A SARS-like cluster of circulating bat coronaviruses shows potential for human emergence. *Nat Med* (2015) 21:1508–13. doi: 10.1038/nm.3985

3. Ruiz-Aravena M, McKee C, Gamble A, Lunn T, Morris A, Snedden CE, et al. Ecology, evolution and spillover of coronaviruses from bats. *Nat Rev Microbiol* (2022) 20:299–314. doi: 10.1038/s41579-021-00652-2

4. Cherry JD, Krogstad P. SARS: the first pandemic of the 21st century. *Pediatr Res* (2004) 56:1–5. doi: 10.1203/01.PDR.0000129184.87042.FC

5. Arabi YM, Balkhy HH, Hayden FG, Bouchama A, Luke T, Baillie JK, et al. Middle East respiratory syndrome. *N Engl J Med* (2017) 376:584–94. doi: 10.1056/NEJMsr1408795

6. Lee N, Hui D, Wu A, Chan P, Cameron P, Joynt GM, et al. A major outbreak of severe acute respiratory syndrome in Hong Kong. *N Engl J Med* (2003) 348:1986–94. doi: 10.1056/NEJMoa030685

7. de Groot RJ, Baker SC, Baric RS, Brown CS, Drosten C, Enjuanes L, et al. Middle East respiratory syndrome coronavirus (MERS-CoV): announcement of the coronavirus study group. *J Virol* (2013) 87:7790–2. doi: 10.1128/JVI.01244-13

8. Larkin HD. Global COVID-19 death toll may be triple the reported deaths. *JAMA* (2022) 327:1438–8. doi: 10.1001/jama.2022.4767

9. Abou Ghayda R, Lee KH, Han YJ, Ryu S, Hong SH, Yoon S, et al. The global case fatality rate of coronavirus disease 2019 by continents and national income: a meta-analysis. *J Med Virol* (2022) 94:2402–13. doi: 10.1002/jmv.27610

10. Delaune D, Hul V, Karlsson EA, Hassanin A, Ou TP, Baidaliuk A, et al. A novel SARS-CoV-2 related coronavirus in bats from Cambodia. *Nat Commun* (2021) 12:6563. doi: 10.1038/s41467-021-26809-4

11. Mallapaty S. Closest known relatives of virus behind COVID-19 found in Laos. *Nature* (2021) 597:603. doi: 10.1038/d41586-021-02596-2

12. Temmam S, Vongphayloth K, Salazar EB, Munier S, Bonomi M, Regnault B, et al. Bat coronaviruses related to SARS-CoV-2 and infectious for human cells. *Nature* (2022) 604:330–6. doi: 10.1038/s41586-022-04532-4

13. Zhou H, Ji J, Chen X, Bi Y, Li J, Wang Q, et al. Identification of novel bat coronaviruses sheds light on the evolutionary origins of SARS-CoV-2 and related viruses. *Cell* (2021) 184:4380–4391.e14. doi: 10.1016/j.cell.2021.06.008

14. Sánchez CA, Li H, Phelps KL, Zambrana-Torrelio C, Wang L-F, Zhou P, et al. A strategy to assess spillover risk of bat SARS-related coronaviruses in southeast Asia. *Nat Commun* (2022) 13:4380–0. doi: 10.1038/s41467-022-31860-w

15. Altmann DM, Boyton RJ. COVID-19 vaccination: the road ahead. *Science* (2022) 375:1127–32. doi: 10.1126/science.abn1755

16. Cohen J. The dream vaccine. *Science* (2021) 372:227–31. doi: 10.1126/science.372.6539.227

17. Giurgea LT, Han A, Memoli MJ. Universal coronavirus vaccines: the time to start is now. *NPJ Vaccines* (2020) 5:43. doi: 10.1038/s41541-020-0198-1

18. Morens DM, Taubenberger JK, Fauci AS. Universal coronavirus vaccines - an urgent need. *N Engl J Med* (2022) 386:297–9. doi: 10.1056/NEJMp2118468

19. Zhao F, Zai X, Zhang Z, Xu J, Chen W. Challenges and developments in universal vaccine design against SARS-CoV-2 variants. *NPJ Vaccines* (2022) 7:167. doi: 10.1038/s41541-022-00597-4

20. Kirtipal N, Bharadwaj S, Kang SG. From SARS to SARS-CoV-2, insights on structure, pathogenicity and immunity aspects of pandemic human coronaviruses. *Infect Genet Evol* (2020) 85:104502. doi: 10.1016/j.meegid.2020.104502

21. Li M, Wang H, Tian L, Pang Z, Yang Q, Huang T, et al. COVID-19 vaccine development: milestones, lessons and prospects. *Signal Transduct Targeted Ther* (2022) 7:146. doi: 10.1038/s41392-022-00996-y

22. Watson OJ, Barnsley G, Toor J, Hogan AB, Winskill P, Ghani AC. Global impact of the first year of COVID-19 vaccination: a mathematical modelling study. *Lancet Infect Dis* (2022) 22:1293–302. doi: 10.1016/S1473-3099(22)00320-6

23. Goldberg Y, Mandel M, Bar-On YM, Bodenheimer O, Freedman L, Haas EJ, et al. Waning immunity after the BNT162b2 vaccine in Israel. *New Engl J Med* (2021) 385:e85. doi: 10.1056/NEJMoa2114228

24. Naaber P, Tserel L, Kangro K, Sepp E, Jürjenson V, Adamson A, et al. Dynamics of antibody response to BNT162b2 vaccine after six months: a longitudinal prospective study. *Lancet Reg Health - Europe* (2021) 10:100208. doi: 10.1016/j.lanepe.2021.100208

25. Alu A, Chen L, Lei H, Wei Y, Tian X, Wei X. Intranasal COVID-19 vaccines: from bench to bed. *eBioMedicine* (2022) 76:103841. doi: 10.1016/j.ebiom.2022.103841

26. Carabelli AM, Peacock TP, Thorne LG, Harvey WT, Hughes J, de Silva TI, et al. SARS-CoV-2 variant biology: immune escape, transmission and fitness. *Nat Rev Microbiol* (2023) 21:162–77. doi: 10.1038/s41579-022-00841-7

27. Dejnirattisai W, Huo J, Zhou D, Zahradník J, Supasa P, Liu C, et al. SARS-CoV-2 omicron-B.1.1.529 leads to widespread escape from neutralizing antibody responses. *Cell* (2022) 185:467–484.e15. doi: 10.1016/j.cell.2021.12.046

28. Harvey WT, Carabelli AM, Jackson B, Gupta RK, Thomson EC, Harrison EM, et al. SARS-CoV-2 variants, spike mutations and immune escape. *Nat Rev Microbiol* (2021) 19:409–24. doi: 10.1038/s41579-021-00573-0

29. Mittal A, Khattri A, Verma V. Structural and antigenic variations in the spike protein of emerging SARS-CoV-2 variants. *PloS Pathog* (2022) 18:e1010260. doi: 10.1371/journal.ppat.1010260

30. Schmidt F, Muecksch F, Weisblum Y, Da Silva J, Bednarski E, Cho A, et al. Plasma neutralization of the SARS-CoV-2 omicron variant. *New Engl J Med* (2021) 386:599–601. doi: 10.1056/NEJMc2119641

31. Chemaitelly H, Tang P, Hasan MR, AlMukdad S, Yassine HM, Benslimane FM, et al. Waning of BNT162b2 vaccine protection against SARS-CoV-2 infection in Qatar. *New Engl J Med* (2021) 385:e83. doi: 10.1056/NEJMoa2114114

32. Cohn BA, Cirillo PM, Murphy CC, Krigbaum NY, Wallace AW. SARS-CoV-2 vaccine protection and deaths among US veterans during 2021. *Science* (2022) 375:331–6. doi: 10.1126/science.abm0620

33. Zhang Z, Mateus J, Coelho CH, Dan JM, Moderbacher CR, Gálvez RI, et al. Humoral and cellular immune memory to four COVID-19 vaccines. *Cell* (2022) 185:2434–2451.e17. doi: 10.1016/j.cell.2022.05.022

34. Miller JF. Immunological function of the thymus. *Lancet* (1961) 2:748–9. doi: 10.1016/S0140-6736(61)90693-6

35. Doherty PC, Topham DJ, Tripp RA, Cardin RD, Brooks JW, Stevenson PG. Effector CD4+ and CD8+ T-cell mechanisms in the control of respiratory virus infections. *Immunol Rev* (1997) 159:105–17. doi: 10.1111/j.1600-065X.1997.tb01010.x

36. Ahrends T, Busselaar J, Severson TM, Bąbała N, de Vries E, Bovens A, et al. CD4 (+) T cell help creates memory CD8(+) T cells with innate and help-independent recall capacities. *Nat Commun* (2019) 10:5531. doi: 10.1038/s41467-019-13438-1

37. Castellino F, Germain RN. Cooperation between CD4+ and CD8+ T cells: when, where, and how. *Annu Rev Immunol* (2006) 24:519–40. doi: 10.1146/annurev.immunol.23.021704.115825

38. Chandran A, Rosenheim J, Nageswaran G, Swadling L, Pollara G, Gupta RK, et al. Rapid synchronous type 1 IFN and virus-specific T cell responses characterize first wave non-severe SARS-CoV-2 infections. *Cell Rep Med* (2022) 3:100557. doi: 10.1016/j.xcrm.2022.100557

39. Bertoletti A, Le Bert N, Tan AT. SARS-CoV-2-specific T cells in the changing landscape of the COVID-19 pandemic. *Immunity* (2022) 55:1764–78. doi: 10.1016/j.immuni.2022.08.008

40. Kedzierska K, Thomas PG. Count on us: T cells in SARS-CoV-2 infection and vaccination. *Cell Rep Med* (2022) 3:100562. doi: 10.1016/j.xcrm.2022.100562

41. Moss P. The T cell immune response against SARS-CoV-2. *Nat Immunol* (2022) 23:186–93. doi: 10.1038/s41590-021-01122-w

42. Sette A, Sidney J, Crotty S. T Cell responses to SARS-CoV-2. *Annu Rev Immunol* (2023) 41:343–73. doi: 10.1146/annurev-immunol-101721-061120

43. Vardhana S, Baldo L, Morice WG, Wherry EJ. Understanding T cell responses to COVID-19 is essential for informing public health strategies. *Sci Immunol* (2022) 7: eabo1303. doi: 10.1126/sciimmunol.abo1303

44. Iannetta M, Landi D, Cola G, Malagnino V, Teti E, Fraboni D, et al. T-Cell responses to SARS-CoV-2 in multiple sclerosis patients treated with ocrelizumab healed from COVID-19 with absent or low anti-spike antibody titers. *Multiple Sclerosis Related Disord* (2021) 55:103157. doi: 10.1016/j.msard.2021.103157

45. Soresina A, Moratto D, Chiarini M, Paolillo C, Baresi G, Focà E, et al. Two X-linked agammaglobulinemia patients develop pneumonia as COVID-19 manifestation but recover. *Pediatr Allergy Immunol* (2020) 31:565–9. doi: 10.1111/pai.13263

46. Wurm H, Attfield K, Iversen AK, Gold R, Fugger L, Haghikia A. Recovery from COVID-19 in a b-cell-depleted multiple sclerosis patient. *Multiple sclerosis (Houndmills Basingstoke England)* (2020) 26:1261–4. doi: 10.1177/1352458520943791

47. McMahan K, Yu J, Mercado NB, Loos C, Tostanoski LH, Chandrashekar A, et al. Correlates of protection against SARS-CoV-2 in rhesus macaques. *Nature* (2021) 590:630–4. doi: 10.1038/s41586-020-03041-6

48. Matchett WE, Joag V, Stolley JM, Shepherd FK, Quarnstrom CF, Mickelson CK, et al. Cutting edge: nucleocapsid vaccine elicits spike-independent SARS-CoV-2 protective immunity. *J Immunol* (2021) 207:376–9. doi: 10.4049/jimmunol.2100421

49. Bilich T, Nelde A, Heitmann JS, Maringer Y, Roerden M, Bauer J, et al. T Cell and antibody kinetics delineate SARS-CoV-2 peptides mediating long-term immune responses in COVID-19 convalescent individuals. *Sci Trans Med* (2021) 13:eabf7517. doi: 10.1126/scitranslmed.abf7517

50. Fan Y-Y, Huang Z-T, Li L, Wu M-H, Yu T, Koup RA, et al. Characterization of SARS-CoV-specific memory T cells from recovered individuals 4 years after infection. *Arch Virol* (2009) 154:1093–9. doi: 10.1007/s00705-009-0409-6

51. Le Bert N, Tan AT, Kunasegaran K, Tham CYL, Hafezi M, Chia A, et al. SARS-CoV-2-specific T cell immunity in cases of COVID-19 and SARS, and uninfected controls. *Nature* (2020) 584:457–62. doi: 10.1038/s41586-020-2550-z

52. Ng OW, Chia A, Tan AT, Jadi RS, Leong HN, Bertoletti A, et al. Memory T cell responses targeting the SARS coronavirus persist up to 11 years post-infection. *Vaccine* (2016) 34:2008–14. doi: 10.1016/j.vaccine.2016.02.063

53. Oh H-LJ, Chia A, Chang CXL, Leong HN, Ling KL, Grotenbreg GM, et al. Engineering T cells specific for a dominant severe acute respiratory syndrome coronavirus CD8 T cell epitope. *J Virol* (2011) 85:10464–71. doi: 10.1128/JVI.05039-11

54. Rodda LB, Netland J, Shehata L, Pruner KB, Morawski PA, Thouvenel CD, et al. Functional SARS-CoV-2-Specific immune memory persists after mild COVID-19. *Cell* (2021) 184:169–183.e17. doi: 10.1016/j.cell.2020.11.029

55. Sette A, Crotty S. Immunological memory to SARS-CoV-2 infection and COVID-19 vaccines. *Immunol Rev* (2022) 310:27–46. doi: 10.1111/imr.13089

56. Tang F, Quan Y, Xin Z-T, Wrammert J, Ma M-J, Lv H, et al. Lack of peripheral memory b cell responses in recovered patients with severe acute respiratory syndrome: a six-year follow-up study. *J Immunol* (2011) 186:7264–8. doi: 10.4049/jimmunol.0903490

57. Zuo J, Dowell AC, Pearce H, Verma K, Long HM, Begum J, et al. Robust SARS-CoV-2-specific T cell immunity is maintained at 6 months following primary infection. *Nat Immunol* (2021) 22:620–6. doi: 10.1038/s41590-021-00902-8

58. De Marco L, D'Orso S, Pirronello M, Verdiani A, Termine A, Fabrizio C, et al. Assessment of T-cell reactivity to the SARS-CoV-2 omicron variant by immunized individuals. *JAMA Netw Open* (2022) 5:e2210871–e2210871. doi: 10.1001/jamanetworkopen.2022.10871

59. Gao Y, Cai C, Grifoni A, Müller TR, Niessl J, Olofsson A, et al. Ancestral SARS-CoV-2-specific T cells cross-recognize the omicron variant. *Nat Med* (2022) 28:472–6. doi: 10.1038/s41591-022-01700-x

60. Geers D, Shamier MC, Bogers S, den Hartog G, Gommers L, Nieuwkoop NN, et al. SARS-CoV-2 variants of concern partially escape humoral but not T cell responses in COVID-19 convalescent donors and vaccine recipients. *Sci Immunol* (2021) 6: eabj1750. doi: 10.1126/sciimmunol.abj1750

61. GeurtsvanKessel Corine H, Geers D, Schmitz Katharina S, Mykytyn Anna Z, Lamers Mart M, Bogers S, et al. Divergent SARS CoV-2 omicron-reactive T- and b cell responses in COVID-19 vaccine recipients. *Sci Immunol* (2022) 7:eabo2202. doi: 10.1126/sciimmunol.abo2202

62. Guo L, Wang G, Wang Y, Zhang Q, Ren L, Gu X, et al. SARS-CoV-2-specific antibody and T-cell responses 1 year after infection in people recovered from COVID-19: a longitudinal cohort study. *Lancet Microbe* (2022) 3:e348–56. doi: 10.1016/S2666-5247(22)00036-2

63. Keeton R, Tincho MB, Ngomti A, Baguma R, Benede N, Suzuki A, et al. T Cell responses to SARS-CoV-2 spike cross-recognize omicron. *Nature* (2022) 603:488–92. doi: 10.1038/s41586-022-04460-3

64. Liu J, Chandrashekar A, Sellers D, Barrett J, Jacob-Dolan C, Lifton M, et al. Vaccines elicit highly conserved cellular immunity to SARS-CoV-2 omicron. *Nature* (2022) 603:493–6. doi: 10.1038/s41586-022-04465-y

65. Madelon N, Heikkilä N, Sabater Royo I, Fontannaz P, Breville G, Lauper K, et al. Omicron-specific cytotoxic T-cell responses after a third dose of mRNA COVID-19 vaccine among patients with multiple sclerosis treated with ocrelizumab. *JAMA Neurol* (2022) 79:399–404. doi: 10.1001/jamaneurol.2022.0245

66. Maringer Y, Nelde A, Schroeder SM, Schuhmacher J, Hörber S, Peter A, et al. Durable spike-specific T cell responses after different COVID-19 vaccination regimens are not further enhanced by booster vaccination. *Sci Immunol* (2022) 7:eadd3899. doi: 10.1126/sciimmunol.add3899

67. Redd AD, Nardin A, Kared H, Bloch EM, Abel B, Pekosz A, et al. Minimal cross-over between mutations associated with omicron variant of SARS-CoV-2 and CD8+ T cell epitopes identified in COVID-19 convalescent individuals. *mBio* (2022) 3(2): e0361721. doi: 10.1128/mbio.03617-21

68. Skelly DT, Harding AC, Gilbert-Jaramillo J, Knight ML, Longet S, Brown A, et al. Two doses of SARS-CoV-2 vaccination induce robust immune responses to emerging SARS-CoV-2 variants of concern. *Nat Commun* (2021) 12:5061. doi: 10.1038/s41467-021-25167-5

69. Tarke A, Sidney J, Methot N, Yu ED, Zhang Y, Dan JM, et al. Impact of SARS-CoV-2 variants on the total CD4+ and CD8+ T cell reactivity in infected or vaccinated individuals. *Cell Rep Med* (2021) 2:100355. doi: 10.1016/j.xcrm.2021.100355

70. Tarke A, Coelho CH, Zhang Z, Dan JM, Yu ED, Methot N, et al. SARS-CoV-2 vaccination induces immunological T cell memory able to cross-recognize variants from alpha to omicron. *Cell* (2022) 185:847–859.e11. doi: 10.1016/j.cell.2022.01.015

71. Almendro-Vázquez P, Laguna-Goya R, Paz-Artal E. Defending against SARS-CoV-2: the T cell perspective. *Front Immunol* (2023) 14:1107803. doi: 10.3389/fimmu.2023.1107803

72. Braun J, Loyal L, Frentsch M, Wendisch D, Georg P, Kurth F, et al. SARS-CoV-2-reactive T cells in healthy donors and patients with COVID-19. *Nature* (2020) 587:270–4. doi: 10.1038/s41586-020-2598-9

73. Grifoni A, Weiskopf D, Ramirez SI, Mateus J, Dan JM, Moderbacher CR, et al. Targets of T cell responses to SARS-CoV-2 coronavirus in humans with COVID-19 disease and unexposed individuals. *Cell* (2020) 181:1489–1501. e15. doi: 10.1016/j.cell.2020.05.015

74. Mateus J, Grifoni A, Tarke A, Sidney J, Ramirez SI, Dan JM, et al. Selective and cross-reactive SARS-CoV-2 T cell epitopes in unexposed humans. *Science* (2020) 370:89–94. doi: 10.1126/science.abd3871

75. Nelde A, Bilich T, Heitmann JS, Maringer Y, Salih HR, Roerden M, et al. SARS-CoV-2-derived peptides define heterologous and COVID-19-induced T cell recognition. *Nat Immunol* (2021) 22:74–85. doi: 10.1038/s41590-020-00808-x

76. Sekine T, Perez-Potti A, Rivera-Ballesteros O, Strålin K, Gorin J-B, Olsson A, et al. Robust T cell immunity in convalescent individuals with asymptomatic or mild COVID-19. *Cell* (2020) 183:158–168.e14. doi: 10.1016/j.cell.2020.08.017

77. Weiskopf D, Schmitz KS, Raadsen MP, Grifoni A, Okba NMA, Endeman H, et al. Phenotype and kinetics of SARS-CoV-2–specific T cells in COVID-19 patients with acute respiratory distress syndrome. *Sci Immunol* (2020) 5:eabd2071. doi: 10.1126/sciimmunol.abd2071

78. Grifoni A, Sidney J, Vita R, Peters B, Crotty S, Weiskopf D, et al. SARS-CoV-2 human T cell epitopes: adaptive immune response against COVID-19. *Cell Host Microbe* (2021) 29:1076–92. doi: 10.1016/j.chom.2021.05.010

79. Schulien I, Kemming J, Oberhardt V, Wild K, Seidel LM, Killmer S, et al. Characterization of pre-existing and induced SARS-CoV-2-specific CD8+ T cells. *Nat Med* (2021) 27:78–85. doi: 10.1038/s41591-020-01143-2

80. Sette A, Crotty S. Pre-existing immunity to SARS-CoV-2: the knowns and unknowns. *Nat Rev Immunol* (2020) 20:457–8. doi: 10.1038/s41577-020-0389-z

81. Kundu R, Narean JS, Wang L, Fenn J, Pillay T, Fernandez ND, et al. Cross-reactive memory T cells associate with protection against SARS-CoV-2 infection in COVID-19 contacts. *Nat Commun* (2022) 13:80. doi: 10.1038/s41467-021-27674-x

82. Loyal L, Braun J, Henze L, Kruse B, Dingeldey M, Reimer U, et al. Cross-reactive CD4+ T cells enhance SARS-CoV-2 immune responses upon infection and vaccination. *Science* (2021) 374:eabh1823. doi: 10.1126/science.abh1823

83. Mateus J, Dan JM, Zhang Z, Rydyznski Moderbacher C, Lammers M, Goodwin B, et al. Low-dose mRNA-1273 COVID-19 vaccine generates durable memory enhanced by cross-reactive T cells. *Science* (2021) 374:eabj9853. doi: 10.1126/science.abj9853

84. Meyer-Arndt L, Schwarz T, Loyal L, Henze L, Kruse B, Dingeldey M, et al. Cutting edge: serum but not mucosal antibody responses are associated with pre-existing SARS-CoV-2 spike cross-reactive CD4+ T cells following BNT162b2 vaccination in the elderly. *J Immunol* (2022) 208:1001–5. doi: 10.4049/jimmunol.2100990

85. Moore SC, Kronsteiner B, Longet S, Adele S, Deeks AS, Liu C, et al. Evolution of long-term vaccine-induced and hybrid immunity in healthcare workers after different

COVID-19 vaccine regimens. *Med* (2023) 4:191–215.e9. doi: 10.1016/j.medj.2023.02.004

86. Niessl J, Sekine T, Lange J, Konya V, Forkel M, Maric J, et al. Identification of resident memory CD8(+) T cells with functional specificity for SARS-CoV-2 in unexposed oropharyngeal lymphoid tissue. *Sci Immunol* (2021) 6:eabk0894. doi: 10.1126/sciimmunol.abk0894

87. Ogbe A, Kronsteiner B, Skelly DT, Pace M, Brown A, Adland E, et al. T Cell assays differentiate clinical and subclinical SARS-CoV-2 infections from cross-reactive antiviral responses. *Nat Commun* (2021) 12:2055. doi: 10.1038/s41467-021-21856-3

88. Swadling L, Diniz MO, Schmidt NM, Amin OE, Chandran A, Shaw E, et al. Pre-existing polymerase-specific T cells expand in abortive seronegative SARS-CoV-2. *Nature* (2022) 601:110–7. doi: 10.1038/s41586-021-04186-8

89. Prakash S, Srivastava R, Coulon PG, Dhanushkodi NR, Chentoufi AA, Tifrea DF, et al. Genome-wide b cell, CD4(+), and CD8(+) T cell epitopes that are highly conserved between human and animal coronaviruses, identified from SARS-CoV-2 as targets for preemptive pan-coronavirus vaccines. *J Immunol* (2021) 206:2566–82. doi: 10.4049/jimmunol.2001438

90. Becerra-Artiles A, Calvo-Calle JM, Co MD, Nanaware PP, Cruz J, Weaver GC, et al. Broadly recognized, cross-reactive SARS-CoV-2 CD4 T cell epitopes are highly conserved across human coronaviruses and presented by common HLA alleles. *Cell Rep* (2022) 39:110952. doi: 10.1016/j.celrep.2022.110952

91. Fraser R, Orta-Resendiz A, Mazein A, Dockrell DH. Upper respiratory tract mucosal immunity for SARS-CoV-2 vaccines. *Trends Mol Med* (2023) 29:255–67. doi: 10.1016/j.molmed.2023.01.003

92. Reynisson B, Alvarez B, Paul S, Peters B, Nielsen M. NetMHCpan-4.1 and NetMHCIIpan-4.0: improved predictions of MHC antigen presentation by concurrent motif deconvolution and integration of MS MHC eluted ligand data. *Nucleic Acids Res* (2020) 48:W449–w454. doi: 10.1093/nar/gkaa379

93. Doytchinova IA, Flower DR. VaxiJen: a server for prediction of protective antigens, tumour antigens and subunit vaccines. *BMC Bioinf* (2007) 8:4. doi: 10.1186/1471-2105-8-4

94. Nguyen MN, Krutz NL, Limviphuvadh V, Lopata AL, Gerberick GF, Maurer-Stroh S. AllerCatPro 2.0: a web server for predicting protein allergenicity potential. *Nucleic Acids Res* (2022) 50:W36–43. doi: 10.1093/nar/gkac446

95. Gupta S, Kapoor P, Chaudhary K, Gautam A, Kumar ROpen Source Drug Discovery C, et al. In silico approach for predicting toxicity of peptides and proteins. *PloS One* (2013) 8:e73957. doi: 10.1371/journal.pone.0073957

96. Weber K, Bartsch U, Stocking C, Fehse B. A multicolor panel of novel lentiviral "gene ontology" (LeGO) vectors for functional gene analysis. *Mol Ther* (2008) 16:698–706. doi: 10.1038/mt.2008.6

97. Ku M-W, Bourgine M, Authié P, Lopez J, Nemirov K, Moncoq F, et al. Intranasal vaccination with a lentiviral vector protects against SARS-CoV-2 in preclinical animal models. *Cell Host Microbe* (2021) 29:236–249.e6. doi: 10.1016/j.chom.2020.12.010

98. Shaw A, Cornetta K. Design and potential of non-integrating lentiviral vectors. *Biomedicines* (2014) 2:14–35. doi: 10.3390/biomedicines2010014

99. Dull T, Zufferey R, Kelly M, Mandel RJ, Nguyen M, Trono D, et al. A third-generation lentivirus vector with a conditional packaging system. *J Virol* (1998) 72:8463–71. doi: 10.1128/JVI.72.11.8463-8471.1998

100. Geraerts M, Willems S, Baekelandt V, Debyser Z, Gijsbers R. Comparison of lentiviral vector titration methods. *BMC Biotechnol* (2006) 6:34. doi: 10.1186/1472-6750-6-34

101. Abdelaziz MO, Ossmann S, Kaufmann AM, Leitner J, Steinberger P, Willimsky G, et al. Development of a human cytomegalovirus (HCMV)-based therapeutic cancer vaccine uncovers a previously unsuspected viral block of MHC class I antigen presentation. *Front Immunol* (2019) 10:1776–6. doi: 10.3389/fimmu.2019.01776

102. Ressing ME, Sette A, Brandt RM, Ruppert J, Wentworth PA, Hartman M, et al. Human CTL epitopes encoded by human papillomavirus type 16 E6 and E7 identified through *in vivo* and *in vitro* immunogenicity studies of HLA-A*0201-binding peptides. *J Immunol* (1995) 154:5934–43. doi: 10.4049/jimmunol.154.11.5934

103. Jutz S, Hennig A, Paster W, Asrak Ö, Dijanovic D, Kellner F, et al. A cellular platform for the evaluation of immune checkpoint molecules. *Oncotarget* (2017) 8:64892–906. doi: 10.18632/oncotarget.17615

104. Trimpert J, Vladimirova D, Dietert K, Abdelgawad A, Kunec D, Dökel S, et al. The roborovski dwarf hamster is a highly susceptible model for a rapid and fatal course of SARS-CoV-2 infection. *Cell Rep* (2020) 33:108488. doi: 10.1016/j.celrep.2020.108488

105. Corman VM, Landt O, Kaiser M, Molenkamp R, Meijer A, Chu DK, et al. Detection of 2019 novel coronavirus (2019-nCoV) by real-time RT-PCR. *Euro surveillance Bull Europeen sur les maladies transmissibles = Eur communicable Dis Bull* (2020) 25:2000045. doi: 10.2807/1560-7917.ES.2020.25.3.2000045

106. Osterrieder N, Bertzbach LD, Dietert K, Abdelgawad A, Vladimirova D, Kunec D, et al. Age-dependent progression of SARS-CoV-2 infection in Syrian hamsters. *Viruses* (2020) 12:779. doi: 10.3390/v12070779

107. Trimpert J, Herwig S, Stein J, Vladimirova D, Adler JM, Abdelgawad A, et al. Deciphering the role of humoral and cellular immune responses in different COVID-19 vaccines-a comparison of vaccine candidate genes in roborovski dwarf hamsters. *Viruses* (2021) 13:2290. doi: 10.3390/v13112290

108. Neefjes J, Jongsma MLM, Paul P, Bakke O. Towards a systems understanding of MHC class I and MHC class II antigen presentation. *Nat Rev Immunol* (2011) 11:823–36. doi: 10.1038/nri3084

109. Sidney J, Peters B, Frahm N, Brander C, Sette A. HLA class I supertypes: a revised and updated classification. *BMC Immunol* (2008) 9:1. doi: 10.1186/1471-2172-9-1

110. Foix A, López D, Díez-Fuertes F, McConnell MJ, Martín-Galiano AJ. Predicted impact of the viral mutational landscape on the cytotoxic response against SARS-CoV-2. *PloS Comput Biol* (2022) 18:e1009726. doi: 10.1371/journal.pcbi.1009726

111. Tarke A, Sidney J, Kidd CK, Dan JM, Ramirez SI, Yu ED, et al. Comprehensive analysis of T cell immunodominance and immunoprevalence of SARS-CoV-2 epitopes in COVID-19 cases. *Cell Rep Med* (2021) 2:100204. doi: 10.1016/j.xcrm.2021.100204:100204

112. Del Val M, Schlicht HJ, Ruppert T, Reddehase MJ, Koszinowski UH. Efficient processing of an antigenic sequence for presentation by MHC class I molecules depends on its neighboring residues in the protein. *Cell* (1991) 66:1145–53. doi: 10.1016/0092-8674(91)90037-Y

113. Eggers M, Boes-Fabian B, Ruppert T, Kloetzel PM, Koszinowski UH. The cleavage preference of the proteasome governs the yield of antigenic peptides. *J Exp Med* (1995) 182:1865–70. doi: 10.1084/jem.182.6.1865

114. Thomas G. Furin at the cutting edge: from protein traffic to embryogenesis and disease. *Nat Rev Mol Cell Biol* (2002) 3:753–66. doi: 10.1038/nrm934

115. Gil-Torregrosa BC, Castaño AR, López D, Del Val M. Generation of MHC class I peptide antigens by protein processing in the secretory route by furin. *Traffic* (2000) 1:641–51. doi: 10.1034/j.1600-0854.2000.010808.x

116. Lázaro S, Gamarra D, Del Val M. Proteolytic enzymes involved in MHC class I antigen processing: a guerrilla army that partners with the proteasome. *Mol Immunol* (2015) 68:72–6. doi: 10.1016/j.molimm.2015.04.014

117. Oliveira CC, van Hall T. Alternative antigen processing for MHC class I: multiple roads lead to Rome. *Front Immunol* (2015) 6:298–8. doi: 10.3389/fimmu.2015.00298

118. Yan J, Yoon H, Kumar S, Ramanathan MP, Corbitt N, Kutzler M, et al. Enhanced cellular immune responses elicited by an engineered HIV-1 subtype b consensus-based envelope DNA vaccine. *Mol Ther* (2007) 15:411–21. doi: 10.1038/sj.mt.6300036

119. Trimpert J, Adler JM, Eschke K, Abdelgawad A, Firsching TC, Ebert N, et al. Live attenuated virus vaccine protects against SARS-CoV-2 variants of concern B.1.1.7 (Alpha) and B.1.351 (Beta). *Sci Adv* (2021) 7:eabk0172. doi: 10.1126/sciadv.abk0172

120. Bricker TL, Darling TL, Hassan AO, Harastani HH, Soung A, Jiang X, et al. A single intranasal or intramuscular immunization with chimpanzee adenovirus-vectored SARS-CoV-2 vaccine protects against pneumonia in hamsters. *Cell Rep* (2021) 36:109400. doi: 10.1016/j.celrep.2021.109400

121. Dhama K, Dhawan M, Tiwari R, Emran TB, Mitra S, Rabaan AA, et al. COVID-19 intranasal vaccines: current progress, advantages, prospects, and challenges. *Hum Vaccin Immunother* (2022) 18:2045853. doi: 10.1080/21645515.2022.2045853

122. Wahl I, Wardemann H. Sterilizing immunity: understanding COVID-19. *Immunity* (2022) 55:2231–5. doi: 10.1016/j.immuni.2022.10.017

123. Lineburg KE, Grant EJ, Swaminathan S, Chatzileontiadou DSM, Szeto C, Sloane H, et al. CD8(+) T cells specific for an immunodominant SARS-CoV-2 nucleocapsid epitope cross-react with selective seasonal coronaviruses. *Immunity* (2021) 54:1055–1065.e5. doi: 10.1016/j.immuni.2021.04.006

124. Meyerholz DK, Perlman S. Does common cold coronavirus infection protect against severe SARS-CoV-2 disease? *J Clin Invest* (2021) 131:e144807. doi: 10.1172/JCI144807

125. Murray SM, Ansari AM, Frater J, Klenerman P, Dunachie S, Barnes E, et al. The impact of pre-existing cross-reactive immunity on SARS-CoV-2 infection and vaccine responses. *Nat Rev Immunol* (2022) 23:304–16. doi: 10.1038/s41577-022-00809-x

126. Sagar M, Reifler K, Rossi M, Miller NS, Sinha P, White LF, et al. Recent endemic coronavirus infection is associated with less-severe COVID-19. *J Clin Invest* (2021) 131:e143380. doi: 10.1172/JCI143380

127. Aran D, Beachler DC, Lanes S, Overhage JM. Prior presumed coronavirus infection reduces COVID-19 risk: a cohort study. *J Infect* (2020) 81:923–30. doi: 10.1016/j.jinf.2020.10.023

128. Gallais F, Velay A, Nazon C, Wendling M-J, Partisani M, Sibilia J, et al. Intrafamilial exposure to SARS-CoV-2 associated with cellular immune response without seroconversion, France. *Emerg Infect Dis* (2021) 27:113–21. doi: 10.3201/eid2701.203611

129. Kingstad-Bakke B, Lee W, Chandrasekar SS, Gasper DJ, Salas-Quinchucua C, Cleven T, et al. Vaccine-induced systemic and mucosal T cell immunity to SARS-CoV-2 viral variants. *Proc Natl Acad Sci* (2022) 119:e2118312119. doi: 10.1073/pnas.2118312119

130. Humbert M, Olofsson A, Wullimann D, Niessl J, Hodcroft EB, Cai C, et al. Functional SARS-CoV-2 cross-reactive CD4+ T cells established in early childhood decline with age. *Proc Natl Acad Sci* (2023) 120:e2220320120. doi: 10.1073/pnas.2220320120

131. Saletti G, Gerlach T, Jansen JM, Molle A, Elbahesh H, Ludlow M, et al. Older adults lack SARS CoV-2 cross-reactive T lymphocytes directed to human coronaviruses OC43 and NL63. *Sci Rep* (2020) 10:21447. doi: 10.1038/s41598-020-78506-9

132. Russell CD, Lone NI, Baillie JK. Comorbidities, multimorbidity and COVID-19. *Nat Med* (2023) 29:334–43. doi: 10.1038/s41591-022-02156-9

133. Mallajosyula V, Ganjavi C, Chakraborty S, McSween Alana M, Pavlovitch-Bedzyk Ana J, Wilhelmy J, et al. CD8+ T cells specific for conserved coronavirus epitopes correlate with milder disease in patients with COVID-19. *Sci Immunol* (2021) 6:eabg5669. doi: 10.1126/sciimmunol.abg5669

134. Mettelman RC, Allen EK, Thomas PG. Mucosal immune responses to infection and vaccination in the respiratory tract. *Immunity* (2022) 55:749–80. doi: 10.1016/j.immuni.2022.04.013

135. King RG, Silva-Sanchez A, Peel JN, Botta D, Dickson AM, Pinto AK, et al. Single-dose intranasal administration of AdCOVID elicits systemic and mucosal immunity against SARS-CoV-2 and fully protects mice from lethal challenge. *Vaccines (Basel)* (2021) 9:881. doi: 10.3390/vaccines9080881

136. Schultz MD, Suschak JJ, Botta D, Silva-Sanchez A, King RG, Detchemendy TW, et al. A single intranasal administration of AdCOVID protects against SARS-CoV-2 infection in the upper and lower respiratory tracts. *Hum Vaccines Immunother* (2022) 18:2127292. doi: 10.1080/21645515.2022.2127292

137. Afkhami S, D'Agostino MR, Zhang A, Stacey HD, Marzok A, Kang A, et al. Respiratory mucosal delivery of next-generation COVID-19 vaccine provides robust protection against both ancestral and variant strains of SARS-CoV-2. *Cell* (2022) 185:896–915.e19. doi: 10.1016/j.cell.2022.02.005

138. Ishii H, Nomura T, Yamamoto H, Nishizawa M, Thu Hau TT, Harada S, et al. Neutralizing-antibody-independent SARS-CoV-2 control correlated with intranasal-vaccine-induced CD8+ T cell responses. *Cell Rep Med* (2022) 3:100520. doi: 10.1016/j.xcrm.2022.100520

139. Zhao J, Zhao J, Mangalam Ashutosh K, Channappanavar R, Fett C, Meyerholz David K, et al. Airway memory CD4+ T cells mediate protective immunity against emerging respiratory coronaviruses. *Immunity* (2016) 44:1379–91. doi: 10.1016/j.immuni.2016.05.006

140. Channappanavar R, Fett C, Zhao J, Meyerholz DK, Perlman S. Virus-specific memory CD8 T cells provide substantial protection from lethal severe acute respiratory syndrome coronavirus infection. *J Virol* (2014) 88:11034–44. doi: 10.1128/JVI.01505-14

141. Pardieck IN, van der Sluis TC, van der Gracht ETI, Veerkamp DMB, Behr FM, van Duikeren S, et al. A third vaccination with a single T cell epitope confers protection in a murine model of SARS-CoV-2 infection. *Nat Commun* (2022) 13:3966. doi: 10.1038/s41467-022-31721-6

142. Zhuang Z, Lai X, Sun J, Chen Z, Zhang Z, Dai J, et al. Mapping and role of T cell response in SARS-CoV-2-infected mice. *J Exp Med* (2021) 218:e20202187. doi: 10.1084/jem.20202187

143. Sette A, Saphire EO. Inducing broad-based immunity against viruses with pandemic potential. *Immunity* (2022) 55:738–48. doi: 10.1016/j.immuni.2022.04.010

144. Diniz MO, Mitsi E, Swadling L, Rylance J, Johnson M, Goldblatt D, et al. Airway-resident T cells from unexposed individuals cross-recognize SARS-CoV-2. *Nat Immunol* (2022) 23:1324–9. doi: 10.1038/s41590-022-01292-1

145. Flemming A. Cross-reactive tissue-resident CD8(+) T cells may provide first line of defence against SARS-CoV-2. *Nat Rev Immunol* (2021) 21:693. doi: 10.1038/s41577-021-00638-4

146. Lapuente D, Fuchs J, Willar J, Vieira Antão A, Eberlein V, Uhlig N, et al. Protective mucosal immunity against SARS-CoV-2 after heterologous systemic prime-mucosal boost immunization. *Nat Commun* (2021) 12:6871. doi: 10.1038/s41467-021-27063-4

147. van der Ley PA, Zariri A, van Riet E, Oosterhoff D, Kruiswijk CP. An intranasal OMV-based vaccine induces high mucosal and systemic protecting immunity against a SARS-CoV-2 infection. *Front Immunol* (2021) 12:781280. doi: 10.3389/fimmu.2021.781280

148. Tang J, Zeng C, Cox TM, Li C, Son YM, Cheon IS, et al. Respiratory mucosal immunity against SARS-CoV-2 after mRNA vaccination. *Sci Immunol* (2022) 7:eadd4853. doi: 10.1126/sciimmunol.add4853

149. Mao T, Israelow B, Peña-Hernández MA, Suberi A, Zhou L, Luyten S, et al. Unadjuvanted intranasal spike vaccine elicits protective mucosal immunity against sarbecoviruses. *Science* (2022) 378:eabo2523. doi: 10.1126/science.abo2523

150. Dullaers M, Thielemans K. From pathogen to medicine: HIV-1-derived lentiviral vectors as vehicles for dendritic cell based cancer immunotherapy. *J Gene Med* (2006) 8:3–17. doi: 10.1002/jgm.846

151. Esslinger C, Romero P, MacDonald HR. Efficient transduction of dendritic cells and induction of a T-cell response by third-generation lentivectors. *Hum Gene Ther* (2002) 13:1091–100. doi: 10.1089/104303402753812494

152. Hu B, Dai B, Wang P. Vaccines delivered by integration-deficient lentiviral vectors targeting dendritic cells induces strong antigen-specific immunity. *Vaccine* (2010) 28:6675–83. doi: 10.1016/j.vaccine.2010.08.012

153. Schroers R, Chen S-Y. Lentiviral transduction of human dendritic cells. In: Heiser WC, editor. *Gene delivery to mammalian cells: volume 2: viral gene transfer techniques*. Totowa, NJ: Humana Press (2004). p. 451–9. doi: 10.1385/1-59259-650-9:451

154. Steinman RM. Dendritic cells and vaccines. *Proc (Baylor Univ Med Center)* (2008) 21:3–8. doi: 10.1080/08998280.2008.11928346

155. Ku MW, Authié P, Nevo F, Souque P, Bourgine M, Romano M, et al. Lentiviral vector induces high-quality memory T cells *via* dendritic cells transduction. *Commun Biol* (2021) 4:713. doi: 10.1038/s42003-021-02251-6

156. Heitmann JS, Bilich T, Tandler C, Nelde A, Maringer Y, Marconato M, et al. A COVID-19 peptide vaccine for the induction of SARS-CoV-2 T cell immunity. *Nature* (2022) 601:617–22. doi: 10.1038/s41586-021-04232-5

# Frontiers in Immunology

**Explores novel approaches and diagnoses to treat immune disorders.**

The official journal of the International Union of Immunological Societies (IUIS) and the most cited in its field, leading the way for research across basic, translational and clinical immunology.

## Discover the latest Research Topics

See more →


**Frontiers**

Avenue du Tribunal-Fédéral 34
1005 Lausanne, Switzerland
frontiersin.org

**Contact us**

+41 (0)21 510 17 00
frontiersin.org/about/contact